



**BIOTECHNOLOGICAL ROUTES  
FOR THE DEVELOPMENT OF  
ANTIMICROBIAL NANO-METAL  
BASED POLYHYDROXYALKANOATES  
FOR ACTIVE FOOD  
PACKAGING APPLICATIONS**

**Jinneth Lorena Castro Mayorga**

**Supervised by: Jose María Lagarón  
María José Fabra**



**Valencia, Mayo de 2017**



**UNIVERSITAT  
POLITÈCNICA  
DE VALÈNCIA**





**INSTITUTO DE AGROQUÍMICA Y TECNOLOGIA DE ALIMENTOS**  
Grupo de Nuevos Materiales y Nanotecnología para Aplicaciones Alimentarias

**Universidad Politécnica de Valencia**

Doctorado en Biotecnología

Tesis Doctoral Internacional

**BIOTECHNOLOGICAL ROUTES FOR THE DEVELOPMENT OF  
ANTIMICROBIAL NANOMETAL-BASED  
POLYHYDROXYALKANOATES FOR ACTIVE FOOD  
PACKAGING APPLICATIONS**

**RUTAS BIOTECNOLÓGICAS PARA EL DESARROLLO DE  
POLIHIDROXIALCANOATOS ANTIMICROBIANOS BASADOS  
EN NANOMETALES PARA APLICACIONES DE ENVASADO  
ACTIVO DE ALIMENTOS**

**Jinneth Lorena Castro Mayorga**

Dirigida por:

**Dr. José María Lagarón**

**Dra. María José Fabra**



Dr. José María Lagarón, Investigador Científico del Consejo Superior de Investigaciones Científicas en el Instituto de Agroquímica y Tecnología de Alimentos y Dra María José Fabra, Investigadora Ramón y Cajal en el mismo instituto

#### CERTIFICAN

Que la presente memoria titulada “**Biotechnological routes for the development of antimicrobial nanometal-based polyhydroxyalkanoates for active food packaging applications**” que para aspirar al grado de Doctor, presenta **Jinneth Lorena Castro Mayorga**, realizada bajo su dirección en el Instituto de Agroquímica y Tecnología de Alimentos (IATA-CSIC), reúne las condiciones adecuadas para su presentación como tesis doctoral, por lo que **AUTORIZAN** al interesado a su **presentación**. Asimismo, certifican haber dirigido y supervisado tanto los distintos aspectos del trabajo como la redacción.

Y para que así conste a los efectos oportunos, firmamos la presente en Valencia a 19 de Junio de 2017.



Fdo. José María Lagarón.



Fdo. María José Fabra



## AGRADECIMIENTOS

Un día como hoy, después de una deliciosa paella valenciana en el IATA, con olor a leña y en la soledad de la biblioteca, encuentro el momento perfecto para escribir estas sentidas líneas. Hoy, cuando me siento enteramente agradecida por esta experiencia de hacerme doctora, por contar con gente con el corazón grande, gente que ha estado ahí, de cerca, apoyándome, dándome su mano para aprender y crecer, para alimentar el alma de bellos sentimientos, de enseñanza, de vida y de CIENCIA. Mil y mil gracias por hacer de estos unos años inolvidables. Gracias porque con cada experiencia he aprendido a querer esta profesión desde dentro, con los “ojos del alma”, desde la mirada utópica que nos adentra en un mundo curioso, desconocido, expectante por ser descubierto, ese, donde las cosas más perfectas son invisibles, donde descubrimos la esencia de la vida, de nuestra propia humanidad. Estaré eternamente agradecida por esta oportunidad de la vida para ser lo que yo soñaba ser desde pequeña, CIENTÍFICA. Esta profesión grandiosa, con la que empecé a soñar desde que estaba en primaria, cuando mi profe de ciencias, me decía “la científica Jinneth”, que luego me llenó de orgullo cuando mi padre, al entrar en el laboratorio de mi queridísima Universidad Nacional de Colombia, se vio reflejado en mí. Una profesión en la que aún me queda mucho por recorrer, pero que me ha llevado por un camino del cual me siento orgullosa

Han sido momentos de risas, de lágrimas, de sacrificios, pero también de recompensas y bonitas vivencias, años que han puesto a prueba mi capacidad de empezar de nuevo, de persistir en la causa, de mucha paciencia, de levantarme una y otra vez repitiendo en la mañana “Si Lorena, tú puedes, levanta la cabeza y sigue adelante”, de momentos de soledad y distintas compañías, de gente que viene y va dejándote un mensaje a su paso, de ver el cielo azul despejado de esta hermosa ciudad

y sentir que al final no estás ni tan lejos de casa, de sentir que el amor y la pasión por lo que haces son capaces de traspasar fronteras.

Son tantas las personas que han pasado por mi vida en estos últimos años, que quienes me conocen de cerca, saben que sería imposible para mí recordar a cada una (ya saben cómo tengo la cabeza), pero tengo, eso sí, la certeza de en que cada momento, intenté recoger lo mejor de ellas para mis recuerdos. Agradecer a mis directores, a Chema por creer en mí y proporcionarme los medios, a Maria José por su perseverancia y amable disponibilidad en todo momento, a Maria Reis, Filomena y Auxi, por su hospitalidad, cordialidad y guía durante mis estancias en Portugal y Madrid, dos experiencias muy enriquecedoras desde el punto de vista profesional, que me hicieron sentir de nuevo ingeniera y admirar el valor de las cosas bien hechas.

A toda la gente del IATA y de la UJI por aportar su granito de arena a la consecución de esta meta; un sincero agradecimiento a las personas más cercanas, a Ampí por su energía positiva, a Gloria y a Deni por sus aportes y por su cercanía, a Laura por su buen ánimo y carisma, a mi gran amigo Jesús por sus “cúchames” y dichos que me sacaron unas cuantas risas, aún en sus momentos de enojo y por el diseño de la portada de esta tesis. A los chicos de prácticas, a Alejo en especial por su dedicación y entusiasmo. A Sabina por los sustos, por sus caminatas a la montaña a primera hora de la mañana y por las idas a la playa junto a su cocodrila.

Agradecer la compañía de las “Naciones Unidas” durante los primeros meses de mi llegada a Valencia, por las cañas, los viajes y los karaokes; a los “latinos en Valencia”, gente amable con la que compartí alegres momentos falleros y al “Colombian (and Brasileán) Team” que hizo más llevadero el estrés de estos últimos meses. A mis compis de piso, que más que eso son grandes amigos, especialmente a Lidia y Fayna, con sus familias incluidas, por su cariñosa acogida y por acercarme a la cultura española desde el calor de sus hogares, a Andresito por sus palabras y abrazos

oportunos, a las chicas “Colciencias” por sus charlas profundas en la bodega de los viejitos, a Natalia que desde Madrid siempre me mostró su apoyo y su sincera amistad. A mi hermana Yamile, por su compañía a la mitad de este camino, por su alegría y por compartir conmigo un poco más de cerca esta etapa de mi vida.

Y por supuesto agradecer y dedicar este trabajo a MIS PADRES a quienes han hecho de mí lo que soy, a quienes quiero y adoro con el alma, a mis hermanitos Yamile, Sonia y Miguelito; a los “mochis” y a mi tía Amparo, a mi abuelita Leo y mi abuelo Alejo, por ser personas serviciales e inspiradoras; a toda mi familia y amigos, por sus abrazos y manifestaciones de cariño, por compartir conmigo esta alegría desde la distancia. A toda mi gente chuntivera, porque aún desconociendo este entorno, me han manifestado su aprecio y me han recibido siempre con los brazos abiertos haciéndome sentir en mi casa, a pesar de que la distancia y las diferencias se hayan hecho cada vez más grandes, por recordarme siempre el valor de la humildad, la constancia y la “berraquera”. A esa, mi patria, mi Colombia querida, el país del sagrado corazón, donde prima la ley del más “vivo”, esa que me quita el sueño porque no logro entender, esa que quiere la paz y quiere la guerra, esa en la que tuve la suerte de nacer y que me motiva a luchar cada día.

## Abstract

---

The development of novel bio-based materials with antimicrobial properties for active packaging applications is a topic of significant interest. The current PhD thesis deals with the development of biotechnologically derived polyhydroxyalkanoates (PHAs) based on nanometals for antimicrobial active food packaging applications. Initially, silver nanoparticles (AgNPs) were produced by chemical reduction and stabilized *in situ* within unpurified poly(hydroxybutyrate-co-hydroxyvalerate), PHBV18 (18 mol% valerate) suspensions previously obtained from mixed microbial cultures. The stabilized AgNPs were subsequently used to develop PHAs-AgNPs nanocomposites following two different strategies: 1) a direct melt-blending process where the AgNPs were added to the PHBV3 (3% mol valerate) from a highly dispersed and distributed enriched masterbatch form and, 2) as an annealed electrospun coating of PHBV3/PHBV18/AgNPs over compression molded PHBV3. The implementation of both strategies resulted in active nanocomposites with strong antimicrobial activity against food-borne pathogens, being the electrospinning coating technique the most efficient one in reducing the bacterial and virus population, even at very low AgNPs loading (from 0.002 to 0.04% wt.).

As an alternative route, an integrated bioprocess for the biological synthesis of AgNPs and polyhydroxybutyrate (PHB) from the fermentation process with *Cupriavidus necator* was also carried out. Interestingly, this work demonstrated for the first time, the inherent capacity of *C. necator* to reduce silver nitrate and produce AgNPs without the need for adding a reducing agent. The process was successfully optimized and scaled-up to a fully automated 10 liters bioreactor.

Finally, because of the limitations of the use of AgNPs in food applications, antimicrobial PHAs films based on zinc oxide (ZnO) and copper oxide (CuO)

nanoparticles were prepared according to the previously developed strategies but in this case, a melt-mixing process of preincorporated ZnO into unpurified PHBV18 fiber mats made by electrospinning was also carried out to stabilize the metal nanoparticles. The effect of ZnO nanoparticles morphology and the method of ZnO/CuO incorporation on the morphological, optical, thermal, mechanical and barrier properties of the resulting active films as well as their influence on the antimicrobial (bactericide and virucidal) performance were studied.

Thus, this PhD thesis represents a significant step forward in the understanding of the antimicrobial efficacy of highly dispersed and distributed nanometals and highlights the suitability of the developed PHAs/nanometals materials for antimicrobial applications and in particular for antimicrobial active food packaging applications.

## Resumen

---

El desarrollo de nuevos biomateriales con propiedades antimicrobianas para aplicaciones de envasado activo resulta un tema de gran interés en la actualidad. La presente tesis doctoral estudia el desarrollo por vía biotecnológica de polihidroxialcanoatos (PHAs) conteniendo nanometales para aplicaciones de envasado activo antimicrobiano de alimentos. En primer lugar, se produjeron nanopartículas de plata (AgNPs) por reducción química y se estabilizaron *in situ* en una suspensión de poli (hidroxibutirato-co-hidroxivalerato) no purificado, PHBV18 (18% en moles de valerato), obtenido previamente a partir de cultivos mixtos microbianos. Posteriormente, las AgNPs estabilizadas se utilizaron para desarrollar nanocompuestos de PHAs-AgNPs siguiendo dos estrategias diferentes: 1) un proceso de mezclado-fundido en donde las AgNPs se añadieron al PHBV3 (3% mol de valerato) a partir de un masterbatch de nanopartículas altamente dispersas y distribuidas y, 2) como una estructura bicapa formada por un recubrimiento a base de PHBV/PHBV18/AgNPs depositado sobre un film de PHBV3 obtenido por moldeo por compresión. La aplicación de ambas estrategias dio lugar a nanocompuestos activos con una fuerte actividad antimicrobiana frente a patógenos transmitidos por los alimentos, siendo la estructura bicapa la más eficaz en la reducción de la población bacteriana y viral, incluso a una carga muy baja de AgNPs (de 0.002 a 0.04% en peso).

Como ruta alternativa, también se llevó a cabo un proceso integrado de fermentación con *Cupriavidus necator* para la síntesis biológica de AgNPs y polihidroxibutirato (PHB). En este trabajo se demostró, por primera vez, la capacidad inherente de *C. necator* para reducir nitrato de plata y producir AgNPs sin la necesidad de añadir un agente reductor. El proceso fue optimizado y escalado satisfactoriamente a un biorreactor automatizado de 10 litros.

Finalmente, debido a las limitaciones del uso de AgNPs en aplicaciones alimentarias, se prepararon films antimicrobianos de PHAs basados en nanopartículas de óxido de zinc (ZnO) y óxido de cobre (CuO) de acuerdo con las estrategias previamente desarrolladas. Adicionalmente, ambas estrategias se compararon con una tercera basada en la preincorporación de ZnO en fibras de PHBV18 no purificado y su posterior mezclado-fundido con polímero virgen. Se estudió el efecto de la morfología de las nanopartículas de ZnO y del método de incorporación de ZnO/CuO sobre las propiedades morfológicas, ópticas, térmicas, mecánicas y de barrera de los films activos resultantes, así como su influencia en el comportamiento antimicrobiano (bactericida y virucida).

Por lo tanto, esta tesis doctoral representa un avance significativo en la comprensión de la eficacia antimicrobiana de nanometales altamente dispersos y distribuidos y destaca la idoneidad de los materiales desarrollados a base de PHAs y nanometales para aplicaciones antimicrobianas y, en particular, para aplicaciones de envasado de alimentos activos antimicrobianos.

## Resum

---

El desenvolupament de nous materials d'origen biològic amb propietats antimicrobianes per a aplicacions d'envasament actiu és un tema d'interès significatiu. La tesi doctoral actual s'ocupa del desenvolupament de polihidroxialcanoats (PHA) reforçats amb nanometals per via biotecnològicament per a aplicacions d'envasament actiu antimicrobià d'aliments. Inicialment, les nanopartícules de plata (AgNPs) van ser produïdes per reducció química i estabilitzades *in situ* dins en suspensions de poli(hidroxi-butirato-co-hidroxi-valerato) sense purificar, PHBV18 (18 mol% de valerato), prèviament obtinguts a partir de cultius mixtes microbians. Les AgNPs estabilitzades es van usar posteriorment per a desenvolupar nanocompostos de PHA's- AgNPs seguint dues estratègies diferents: 1) Procés directe de barreja en fusió que no utilitza dissolvents orgànics o estabilitzants addicionals i on es van afegir les AgNPs al PHBV3 (3% mol valerato) a partir d'un masterbath on estaven perfectament disperses i distribuïdes 2) com una estructura bicapa formada per un recobriment de PHBV3 / PHBV18/AgNPs que es deposita sobre un film de PHBV3 obtingut per modelat per compressió. L'aplicació d'ambdues estratègies va donar lloc a nanocompostos actius amb una forta activitat antibacteriana enfront de patògens transmesos pels aliments, sent l'estructura de doble capa la més eficaç en la reducció de la població bacteriana i viral, fins i tot a una càrrega molt baixa de AgNPs (de 0.002-0.04% en pes).

Com ruta alternativa, també es va dur a terme un procés integrat de fermentació amb *Cupriavidus necator* per a la síntesi biològica de AgNPs i polihidroxi-butirato (PHB). En aquest treball es demostra, per primera vegada, la capacitat inherent de *C. necator* per reduir la sal de plata i produir AgNPs sense la necessitat d'afegir un agent reductor. El procés va ser optimitzat i escalat satisfactòriament a un bioreactor de 10 litres.

Finalment, a causa de les limitacions de l'ús de nanopartícules de plata en aplicacions alimentàries, es van preparar films antimicrobians de PHA que incorporessin nanopartícules d'òxid de zinc (ZnO) i òxid de coure (CuO) d'acord amb les estratègies prèviament desenvolupades. Les dues estratègies es van comparar amb una tercera basada en la preincorporació de ZnO en fibres de PHBV18 no purificat i aquestes fibres es van barrejar posteriorment amb polímer verge. Es va estudiar l'efecte de la morfologia de les nanopartícules de ZnO i el mètode de la incorporació de ZnO/CuO sobre les propietats morfològiques, òptiques, tèrmiques, mecàniques i de barrera dels films actius resultants, així com la seva influència en el comportament antimicrobià (bactericida i virucida).

Per tant, aquesta tesi doctoral representa un pas endavant significatiu en la comprensió de l'eficàcia antimicrobiana de nanometalles altament dispersos i distribuïts i posa en relleu la idoneïtat dels materials desenvolupats basats en PHAs i nanometalles per a aplicacions antimicrobianes i, en particular, per a aplicacions d'envasat d'aliments actius antimicrobians.

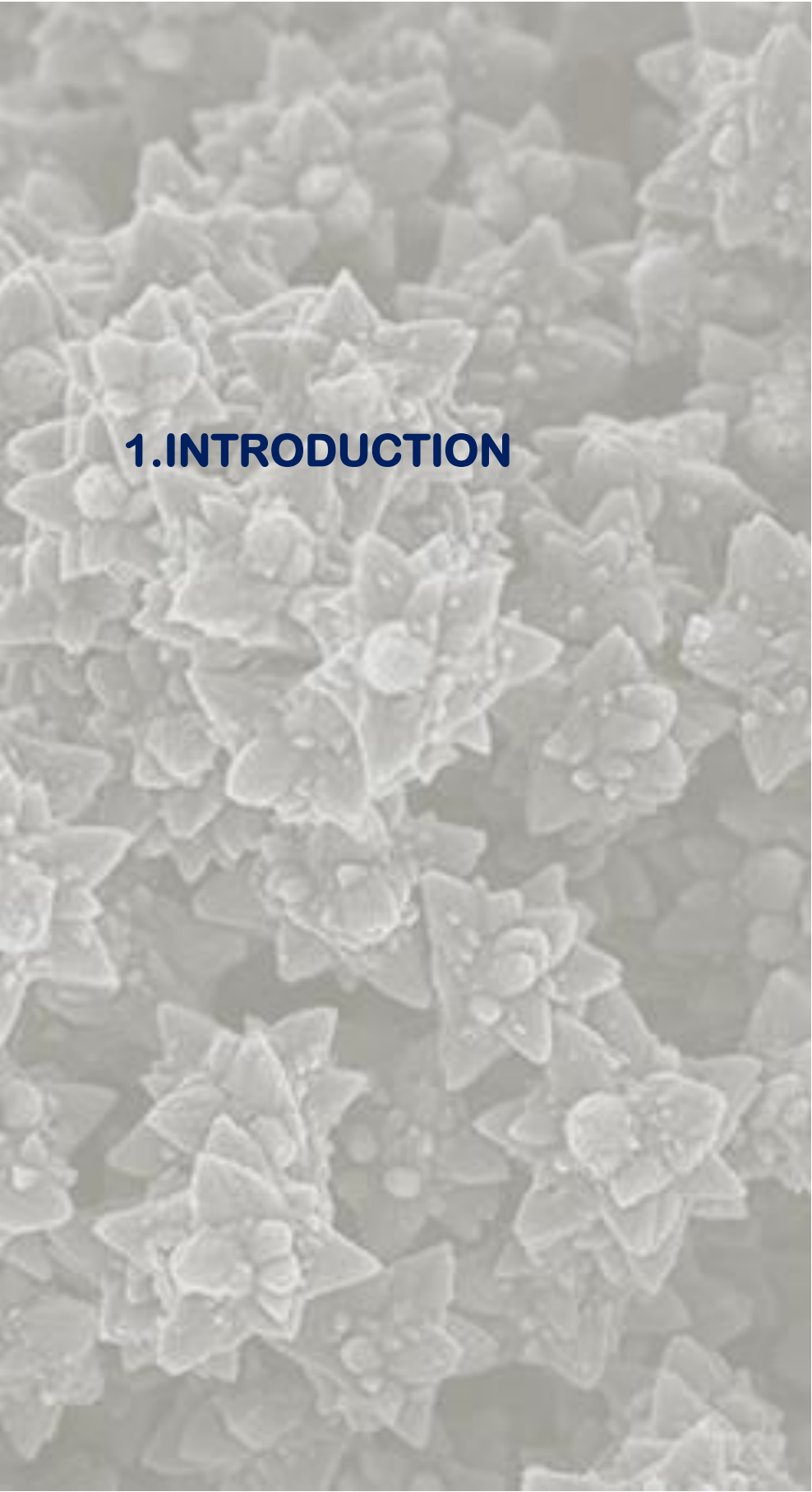
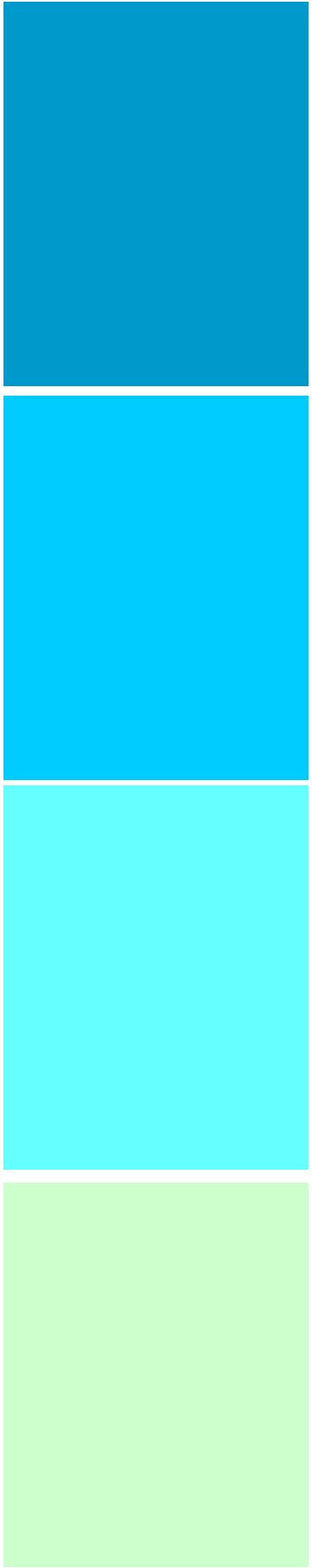
# Index

---

<b>1. Introduction.....</b>	<b>1</b>
1.1 Bio-based food packaging.....	3
1.2 Polyhydroxyalkanoates: microbial biopolyesters.....	6
1.3 Antimicrobial active packaging.....	9
1.4 Metal nanoparticles as antimicrobial agents in food packaging.....	11
1.4.1 Silver nanoparticles.....	12
1.4.2 Zinc oxide nanoparticles.....	13
1.4.3 Copper oxide nanoparticles.....	15
1.5 Electrospinning as an emerging processing technology in food packaging.....	16
<b>2. General and specific aims.....</b>	<b>27</b>
<b>3. Results.....</b>	<b>33</b>
<b>Chapter I:</b> Stabilization of antimicrobial silver nanoparticles by a polyhydroxyalkanoate obtained from mixed bacterial culture.....	37
<b>Chapter II:</b> Stabilized nanosilver based antimicrobial poly(3-hydroxybutyrate-co-3-hydroxyvalerate) nanocomposites of interest in active food packaging.....	67
<b>Chapter III:</b> On the use of the electrospinning coating technique to produce antimicrobial polyhydroxyalkanoate materials containing <i>in situ</i> stabilized silver nanoparticles.....	105
<b>Chapter IV:</b> Antiviral properties of silver nanoparticles against norovirus surrogates and their efficacy in coated polyhydroxyalkanoates systems.....	133

<b>Chapter V:</b> Optimization and scaling up of the biosynthesis of silver nanoparticles and polyhydroxybutyrate nanocomposites of interest in antimicrobial applications.....	155
<b>Chapter VI:</b> The impact of zinc oxide particle morphology as an antimicrobial and when incorporated in Poly(3-hydroxybutyrate-co-3-hydroxyvalerate) films for food packaging and food contact surfaces applications.....	185
<b>Chapter VII:</b> Antimicrobial Nanocomposites and Electrospun Coatings Based on Poly(3-hydroxybutyrate-co-3-hydroxyvalerate) and Copper Oxide Nanoparticles for Active Packaging and Coating Applications.....	225
<b>4. General discussion.....</b>	<b>259</b>
<b>5. Conclusions.....</b>	<b>271</b>
<b>6. Annexes.....</b>	<b>277</b>
<b>Annex A:</b> List of publications.....	279
<b>Annex B:</b> Additional works.....	285





# 1.INTRODUCTION



## **1. Introduction**

### **1.1 Bio-based food packaging**

---

Packaging has been developed as an essential preservation technology for the manufacturing and marketing of foodstuffs to provide, by maintaining or even increasing, the required levels of product quality and safety. Most foods are deteriorated during their transport, processing and storage through contamination by growing of microorganisms, the chemical reactions and the physical changes, being considered the microbial spoilage and the oxidative reactions as the greatest limitants of the life of perishable products [1-3]. Therefore, the main roles of food packaging are protecting food products from outside influence and damage, containing the food, and providing consumers with ingredient and nutritional information. Traceability, convenience, and tamper indication are also secondary functions of increasing importance. The goal of food packaging is containing food in a cost-effective way that satisfies industry requirements and consumer needs, keeping food safe and minimizing environmental impact [4].

Although a huge and broad amount of materials, such as glass, metals, paper and cardboard have been traditionally used in food packaging; plastic materials are nowadays one of the most powerful industrial sectors, with a worldwide production of 322 million tons per year. In Europe, the packaging applications represent almost 40% of the plastics market (Figure 1), with the greatest contribution corresponding to the food sector [5]. The commercial success of plastics as packaging product is due to a combination of flexibility (from film to rigid applications), strength, lightness, stability, low cost and ease of sterilization. Moreover, many plastics are heat sealable,

## Introduction

easy to print, and can be integrated into production processes where the package is formed, filled, and sealed in the same production line.



**Figure 1.** European plastics demand by segment in 2015. Source: PlasticsEurope [5].

Plastics, in contrast to more traditional packaging materials like glass and metal, (1) are permeable to the exchange of low molecular weight compounds such as gases and vapors, (2) undergo sorption, so-called scalping, of packaged food constituents, and (3) are amenable to migration into foodstuffs of packaging constituents [6]. To overcome these problems, high barrier polymers and multilayer structures have been developed over time. These multilayer systems are usually formed by an inner layer which must be chemically inert, thermosealable and often water and/or grease barrier and several outer layers which should provide mechanical resistance, a certain barrier to gases and organic vapours as well as printability [6, 7]. Furthermore, the combination of the multilayer approach and nanotechnology has recently emerged as a very interesting alternative to improve the properties of packaging materials by incorporating nanostructured additives into polymer matrices [8].

The other major disadvantage of plastics is that most of them are still made from petroleum; a non-renewable resource. These petroleum-based polymers are extremely

resistant to natural decomposition. Consequently, after using, they are accumulated and negatively affect the environment and the ecosystem. The lack of biodegradability and the environmental concerns have prompted worldwide research seeking to biodegradable and renewable alternatives to petroleum-based plastics.

It is important to emphasize that the term “biodegradable polymers” is used to define those materials which are able to undergo decomposition into carbon dioxide, methane, water inorganic compounds or biomass as a result of being exposed to the enzymatic action of microorganism (ASTM D996-10A). The terms bio-based polymers or biopolymers refer to those polymers obtained from renewable resources. Most of these bio-based polymers are biodegradable, biodegradable polymers are not strictly bio-based though; for instance, caprolactone, poly(vinyl alcohol) and ethylene vinyl alcohol copolymers are petroleum-based polymers which can biodegrade under certain conditions [9]. Figure 2 shows a scheme of the classification of biodegradable polymers according to their origin.

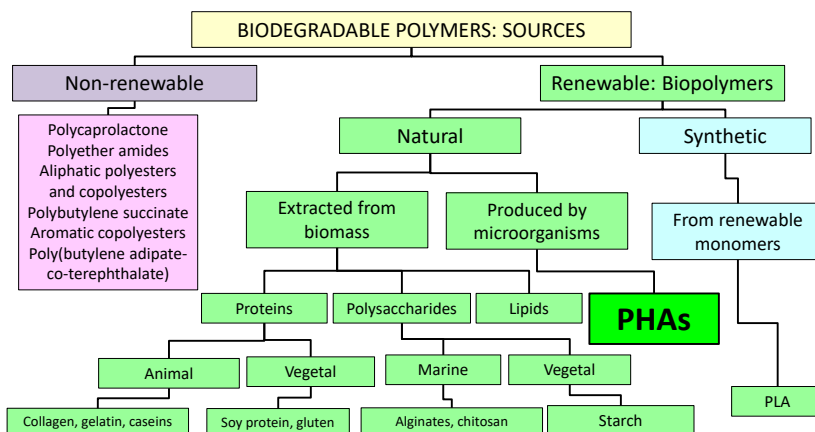


**Figure 2.** Classification of biopolymers according to their origin

The bioplastics, which are more viable from a commercial point of view, are some biodegradable polyester, such us poly(lactic acid) (PLA) and polyhydroxyalkanotes

## ***Introduction***

(PHAs), which can be processed by conventional processing equipment and formed into films or molded into objects [10]. However, the main drawbacks in terms of commercial applications of these biopolymers in the food packaging area are their higher cost and lower performance in regard to thermal, mechanical and barrier properties than their oil-based counterparts [11]. Thus, it is of significant relevance to enhance the gas barrier properties and overall functionalities of thermoplastic biopolyesters to make them more adequate for food packaging applications.

## **1.2 Polyhydroxyalkanoates: microbial biopolyesters**

---

As previously mentioned, among the different types of biopolymers, PHAs have recently attracted much attention as an alternative to petroleum-based materials. The main advantages of PHAs are their biodegradable nature, biocompatibility and film forming capacity with properties similar to polypropylene. Moreover, these materials can be drawn into films and blow moulded into various forms [12].

PHAs are polyesters of R-3-hydroxyalkanoic acids with the general structural formula shown in Figure 3, which are synthesized by a wide range of microorganisms as energy reserve materials. In general, bacteria that are used to produce PHAs can be divided into two groups based on the culture conditions required for PHAs synthesis. The first group of bacteria requires the limitation of an essential nutrient such as nitrogen, phosphorous, magnesium or sulphur for the synthesis of PHAs from an excess carbon source. The bacteria included in this group are *Cupriavidus necator*, *Protomonas extorquens*, and *Protomonas oleovorans*. The second group of bacteria, which include *Alcaligenes latus*, a mutant strain of *Azotobacter vinelandii*, and recombinant

*E. coli*, does not require nutrient limitation for PHAs synthesis and can accumulate polymer during their growth [13].

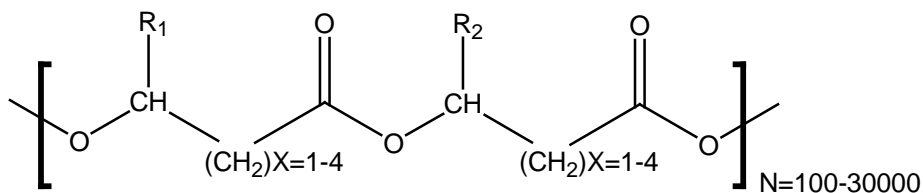


**Figure 3.** General structure of polyhydroxyalkanoates. R<sub>1</sub> and R<sub>2</sub> are alkyl groups (C<sub>1</sub>–C<sub>13</sub>).

The bacteria *Cupriavidus necator* (also called *Ralstonia eutropha*, *Wautersia eutropha*,) has been studied most extensively due to its ability to accumulate a large quantity of PHAs from simple carbon sources, for example, glucose, fructose and acetic acid. High productivity can be obtained by fed-batch fermentation. For fed-batch culture of *C. necator*, a two-step cultivation method is most often used. A high concentration of biomass is obtained without nutrient limitation in the first stage after which an essential nutrient is kept in a limited concentration in the second stage to allow efficient PHB synthesis. *C. necator* accumulates a large amount of polymer (up to 80% of dry cell weight) when nitrogen or phosphorous is completely depleted [14].

Depending on the selected microorganisms and the cultivation conditions, homo- or co-polyesters of hydroxyalkanoic acids are obtained, being the homopolymer polyhydroxybutyrate (PHB) and its copolymers with hydroxyvalerate (PHBV) the most interesting ones for commercial purposes, having the last one several advantages over the PHB in terms of processability [15]. The use of the homopolymer PHB has been limited not only because of its production costs, but also due to its brittleness and low thermal stability when melted, resulting in a narrow melt processing window [16, 17]. The PHBVs partially counteract the previous drawbacks as they have lower melting temperature and, thus, a larger melt processing window [15]. On the other

## *Introduction*

hand, they present lower crystallization rates, lower elongation at break but also lower barrier properties for certain food-related applications [18-20]. In order to tailor the performance of biopolymers, the most widely explored strategies have been blending, multilayer systems and nanocomposites.

In economic terms, PHAs have still some shortcomings that limit their use. The major drawbacks of PHAs production are the high cost of raw materials (mainly carbon source), low yield, low productivity and the high cost of the down-stream process [21, 22]. Therefore, attempts have been made to develop more cost-effective processes. Reducing the cost of the carbon substrates (e.g., using wastes) and increasing the efficiency of production technologies (including both fermentation and downstream extraction and recovery) are the most relevant attempts.

PHAs production processes based on mixed microbial cultures (MMC) are being investigated as a possible technology to decrease production costs, since no sterilization is required and bacteria can adapt quite well to the complex substrates [23]. MMC are microbial populations operating in open biological systems, whose composition directly depends on operational conditions imposed through the open bioreactor. The fermentation process with MMC is mostly based on using volatile fatty acids (VFA) as the main carbon source for PHAs accumulation, which has as additional advantage the fact that a wide range of no-cost/low cost waste feedstocks can be easily transformed into VFA-rich streams by anaerobic acidogenic fermentation. Hence, MMC based PHAs production can also make it easier to use complex substrates of undefined composition, such as industrial or agro-industrial waste effluents [24].

## **1.3 Antimicrobial active packaging**

---

Traditionally, food packaging has been designed as a passive barrier to delay the adverse effect of the environment over the packaged product. However, the current tendencies include the development of packaging materials that interact with the environment and with the food, playing an active role in its preservation. These new food-packaging systems have been developed as a response to trends in consumer preferences towards mildly preserved, fresh, tasty and convenient food products with an extended shelf-life. In addition, changes in retail practices such as globalization of markets resulting in longer distribution distances, present major challenges to the food packaging industry to develop packaging concepts that extend shelf-life while maintaining the safety and quality of the packaged food.

Active packaging is an innovative solution to meet the continuous changes in current consumer demands and market trends because it changes the condition of the packaged food in order to extend the quality and safety. Some examples of active-packaging systems are O<sub>2</sub> scavengers, CO<sub>2</sub> emitters, ethylene absorbers, moisture regulators, taint removal systems, ethanol emitters and antimicrobial-releasing systems [25].

In particular, because of the incidence of pathogenic bacteria (Table 1) and human norovirus (120 million cases per year) [26], which are responsible for many food-borne outbreaks, and in order to effectively prevent the food-borne diseases, the antimicrobial active packaging is attracting increased attention from the food and packaging industry.

## Introduction

**Table 1.** Reported hospitalisation and case-fatality rates due to zoonoses in confirmed human cases in the EU, 2013. Source: European Food Safety Authority. ©EFSA/ECDC, 2015.

Disease	Number of confirmed <sup>(a)</sup> human cases	Deaths	
		Reported deaths	Case-fatality rate (%)
Campylobacteriosis	214779	56	0,05
Salmonellosis	82694	59	0,14
Yersiniosis	6471	2	0,05
VTEC infections	6043	13	0,36
Listeriosis	1763	191	15,6
Echinococcosis	794	2	0,88
Q fever	648	2	0,61
Brucellosis	357	1	0,99
Tularaemia	279	0	0
West Nile fever <sup>(a)</sup>	250	16	3,4
Trichinellosis	217	1	0,56
Rabies	1	1	100

(a) For West Nile fever the total number of cases were included.

The incorporation of antimicrobial agents into polymeric films allows the industry to combine the preservative functions of antimicrobials with the protective functions of the pre-existing packaging concepts [27]. Antimicrobial activity in food packaging can be achieved by (1) including pads containing volatile antimicrobial agents into packages, (2) incorporating antimicrobial agents directly into polymers, coating antimicrobials onto polymer surfaces, (3) immobilizing antimicrobials by chemical grafting or (4) using polymers that are antimicrobial by themselves [28]. A wide variety of natural and synthetic compounds with strong antimicrobial properties have been investigated. These mainly include organic acids and their salts, bacteriocins, antimicrobial peptides, metals, fatty acid esters, and plant essential oils [29]. Antimicrobial agents have to be selected taking account factors such as stability during polymers processing, kinetics of release, mechanism of action, antimicrobial spectrum, minimal impact on food quality and cost effectiveness [6, 30]. Moreover, it

should be taken into account, and hence under control, the fact that antimicrobial agents incorporated in packaging are an intended source of migration into foods.

## **1.4 Metal nanoparticles as antimicrobial agents in food packaging**

---

Metal nanoparticles can be used as antimicrobial agents because they have numerous advantages over other antimicrobials. Their broad spectrum against food-borne pathogens (even at very low concentration) [31] as well as their improved stability and low volatility in comparison with organic antimicrobial agents [32], make them promising materials for food packaging and food contact surfaces applications. It has been demonstrated that the bactericidal effect of nanoparticles depends on their shape, size, size distribution, morphology, surface functionalization, and their stability [33].

Although there are chemical, physical and biological methods for the metal nanoparticles synthesis, the chemical reduction methods are the most commonly used ones. This process involves the chemical reduction of suitable metal ions in a solution with borohydride [34], citrate [35] or carbohydrates [36]. After reducing metal ions, the synthesized nanoparticles are often stabilized by coating them with capping agents. The stability of metallic nanoparticles can be provided by steric or electrostatic repulsion. The use of surface active agents such as polymers (e.g. polyethylene glycol, poly(vinylalcohol), poly(vinylpyrrolidone)) and non-ionic surfactants (e.g. Tween, Triton X-100) ensures steric stabilization. Electrostatic protection of nanoparticles can be achieved by addition of ionic surfactant (e.g. sodium dodecyl sulfate, cetyltrimethylammonium bromide). However, the preparation of a dispersed system

## ***Introduction***

with the required stability in time and resistance to the action of external factors remains to be the main challenge.

### **1.4.1 Silver nanoparticles**

Silver has been attributed antimicrobial properties since ancient times. It has been used as antimicrobial agent in food packaging because it has numerous advantages over other antimicrobials. It has a strong antimicrobial effect against a wide range of food-borne pathogens including bacteria, fungi and some viruses even at very low concentration [37, 38] with, according to some authors, negligible toxicity towards human cells at the same concentration range.

Recently, silver nanoparticles (AgNPs) have attracted increasing interest due to their unique physical-chemical properties compared to their macro-scaled counterparts. AgNPs have a higher antimicrobial effect than ionic silver because they can insert within cell membrane due to their small size and kill bacteria by direct lesion and/or release silver ions locally from the nanoparticles [39, 40] causing damage to bacterial enzymes. Furthermore, it is known that the antimicrobial activity of AgNPs could be related to the induction of oxidative stress which may cause damage in the respiratory chain and cell division machinery [33]. The effectiveness of AgNPs as antimicrobial agents and, hence, their possible use in active packaging systems, has been demonstrated in various *in vitro* experiments as summarized by Kuorwel et al. (2015)[41]. Several research works have investigated the effect of incorporating silver and nanosilver into different biopolymer matrices such as poly(vinyl alcohol) [42-44] and poly(lactic acid) [45] but these AgNPs were not synthesized and stabilized into the matrices, thus causing significant changes in the optical properties and reducing the antimicrobial efficiency.

Because the rediscovery of the use of silver as antimicrobial purposes in nanoparticles format is relatively new, there is no yet a full understanding as to its safety in regard to the environment or human health. Therefore, it still remains a topic of debate among the different legislative bodies in Europe, the United States, Japan, or Australia, becoming even contradictory in some cases. In the food area, only silver nitrate is regulated with a maximum limit of 0.017 mg/kg in treated bottled water [46]. As far as AgNPs are concerned, colloidal solutions are accepted in the United States and commercialized as nutrition supplements (e.g. Mesosilver), claiming to have important benefits on human health ([www.mesosilver.com](http://www.mesosilver.com)). The confrontation between past and present circumstances is best noticed in European law. The European Food Safety Authority (EFSA) provisionally accepts the use of silver in food-contact materials with a maximum of 5% silver in the form of silver containing zeolites or silver containing zirconium phosphate glasses until an official evaluation of their safety is stated. Migration is restricted to a maximum 0.05 mg/kg in food for the whole group [47]. Silver hydrosols are not included in the list of food additives or supplements “because of the lack of appropriate information about silver bioavailability” from them [48]. Paradoxically, under Directive 94/36/EC, still in force, silver is considered a colouring agent used in confectionery without any restriction limits (European Parliament and Council Directive 94/69/EC). Other countries, like Australia, have totally banned the use of silver in foodstuffs or food-contact materials.

### **1.4.2 Zinc oxide nanoparticles**

In contrast to other metals, zinc oxide (ZnO) is one of the five zinc compounds listed as a Generally Recognized as Safe (GRAS) materials by the US Food and Drug Administration [49]. As a food additive, it is the most commonly used zinc source in the fortification of cereal-based foods. Because of its antimicrobial properties, ZnO has

## ***Introduction***

been incorporated into the linings of food cans in packages for meat, fish, corn, and peas to preserve colors and to prevent spoilage [50]. Nano-sized particles of ZnO have more pronounced antimicrobial activities than large particles, since the small size and high surface-to-volume ratio of nanoparticles allow for better interaction with bacteria. Recent studies have shown that these nanoparticles have selective toxicity to bacteria but exhibit minimal effects on human cells [51]. ZnO nanoparticles have been shown to have a wide range of antibacterial activities against both Gram-positive and Gram-negative bacteria, including major foodborne pathogens like *Escherichia coli* O157:H7, *Salmonella*, *Listeria monocytogenes*, and *Staphylococcus aureus* [52, 53].

The antimicrobial mechanisms of zinc oxide are not completely understood. Besides the release of Zn<sup>2+</sup> ions, several mechanisms about the antimicrobial activity of ZnO have been described in the literature, such as the cell wall damage, the generation of ROS (like superoxide anions, hydroxyl radicals, hydrogen peroxide) as well as the penetration of the cell envelop, among others [54].

So far, in the food packaging area, ZnO nanoparticles have been mostly added to petroleum-derived polymers such as low density polyethylene (LDPE) [55], polypropylene (PP), polyurethane (PU) or polyethylene (PET) using conventional incorporation methods such as melt mixing or solvent casting. Nevertheless, in accordance with Espitia et al. (2012) [56], the use of these nanoparticles in biodegradable polymeric matrices allows for the improvement of packaging properties such as mechanical strength, barrier properties and stability [56].

### 1.4.3 Copper oxide nanoparticles

Copper oxide (CuO) has attracted particular importance because of it is the simplest member of the family of copper compounds and exhibits a range of potential useful catalytic, optical, electrical and antifungal/antibacterial applications. Moreover, CuO is cheaper than silver, easily mixed with polar liquids and relatively stable in terms of both chemical and physical properties. Reports on the preparation and characterization of nanocrystalline CuO are few in comparison to those of some other transition metal oxides, such as zinc oxide, titanium dioxide, tin dioxide and iron oxide. Some methods for the preparation of CuO nanoparticles have been reported such as the sonochemical method [57], sol-gel technique [58], one-step solid state reaction method at room temperature [59], electrochemical method [60] and thermal decomposition of precursors [61]. Even more limited information on the antimicrobial effect of CuO nanoparticles is available. The studies of CuO nanoparticles showed their antibacterial effect against Gram-positive bacteria (*Staphylococcus aureus* and *Bacillus subtilis*) and Gram-negative bacteria (*Pseudomonas aeruginosa* and *Escherichia coli*). It is believed that, as with other metal nanoparticles, the antimicrobial effect of copper probably results to a large extent from: 1) Release of copper cations from the metal surface, 2) its tendency to alternate between its cuprous [Cu(I)] and cupric [Cu(II)] oxidation states causing membrane damages, and 3) accumulation of copper in cells, with some degree of oxidative stress and DNA damage [62].

Regarding legislation, the US Environmental Protection Agency (EPA) has approved the registration of copper as an antimicrobial agent which is able to reduce the viability of specific harmful bacteria linked to potentially deadly microbial infections (European Copper Institute, 2008) [63]. In addition, so far it has never been reported the existence of bacteria able to develop immunity to copper as they often do with antibiotics.

## 1.5 Electrospinning as an emerging processing technology in food packaging

---

A recent approach to develop multilayer structures combining biopolymers and nanofabrication has been possible through the electrospinning technique. Electrospinning is a versatile method to produce continuous polymer fibers with diameters in the sub-micron range through the action of an external electric field applied between two electrodes and imposed onto a polymer solution or melt. A typical set up of electrospinning apparatus is shown in Figure 3. Basically, an electrospinning equipment consists on an injection pump, a syringe, a spinneret (e.g., a pipette tip or a needle), a high voltage power supply and a grounded collector plate (usually a metal screen, plate, or rotating mandrel) and utilizes a high voltage source to inject charge of a certain polarity into a polymer solution or melt, which is then accelerated towards a collector of opposite polarity [64, 65]. When the electrical force at the interface of the polymer solution exceeds the surface tension forces, a charged jet is formed. The jet initially extends in a straight line, then undergoes a vigorous whipping motion caused by the electro-hydrodynamic bending instabilities. As the solvent in the jet solution evaporates, the polymer is collected onto a grounded substrate to form a non-woven mat of fibers [66, 67]. Electrospun mats have shown unique functionalities from the very large surface-to-volume ratios of the fibers that promote self-adhesive properties and their capacity to effectively encapsulate active and bioactive components.

In the last decade, the electrospinning technique has received substantial attention for the fabrication of polymer nanofibers in a wide range of applications that demand high performance fibers. The functional electrospun mats can be used, for example, as reinforcing materials to enhance the physical properties of plastics and bioplastics, as

transparent interlayers with improved gas and vapours barrier, an even as an emerging technology to design active packaging with antimicrobial protection or delivery of nutraceuticals to foods [68, 69].

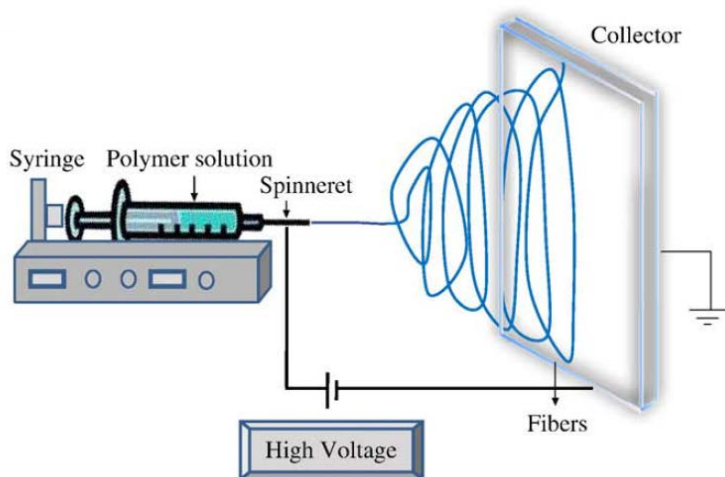


**Figure 3.** Schematic diagram of horizontal set up of electrospinning apparatus. Adapted from Bhardwaj et al. [67]

Concerning antimicrobial active packaging, two approaches have been considered in the generation of biocide systems using electrospinning. The first one consists on the use of inherent antimicrobial polymers such as chitosan [70] and the second one is based on the incorporation of exogenous biocides inside the fibers. Either way, the obtained mats can be used directly as packaging materials or as coating systems to prevent the growth of food-borne and spoilage microorganisms.

In the case of nanoadditives, electrospinning further allows the incorporation of these into packaging polymers with a high level of dispersion and distribution inside the polymer matrix. For instance, nanocrystals of cellulose and other nanoparticles have been finely dispersed to obtain enriched masterbatches that can be later diluted into packaging polymers by conventional melt blending strategies [18]

## 1.6 References

---

1. A. L. Brody, E. R. Strupinsky and L. R. Kline, "Introduction," in *Active Packaging for Food Applications*, Ed., CRC Press, 2001.
2. R. Ahvenainen, "2 - Active and intelligent packaging: An introduction," in *Novel Food Packaging Techniques*, Ed., pp. 5-21, Woodhead Publishing, 2003.
3. C. Ho Lee, D. Soon An, S. Cheol Lee, H. Jin Park and D. Sun Lee, "A coating for use as an antimicrobial and antioxidative packaging material incorporating nisin and  $\alpha$ -tocopherol," *Journal of Food Engineering*, vol. 62, no. 4, pp. 323-329, 2004.
4. Coles R, McDowell D and Kirwan MJ, "Introduction," in *Food packaging technology*, Coles R, McDowell D and Kirwan MJ, Ed., pp. 1-31, CRC Press, London, U.K, 2003.
5. P. E. Association of Plastics Manufacturers, "Plastics-the Facts 2014/2015. An analysis of European plastics production, demand and waste data," Ed.
6. J. M. Lagarón, M. J. Ocio and A. López-Rubio, "Antimicrobial Packaging Polymers. A General Introduction," in *Antimicrobial Polymers*, Ed., pp. 1-22, John Wiley & Sons, Inc., 2011.
7. M. J. Fabra, M. A. Busolo, A. Lopez-Rubio and J. M. Lagaron, "Nanostructured biolayers in food packaging," *Trends in Food Science and Technology*, vol. 31, no. 1, pp. 79-87, 2013.
8. Y. Echegoyen and C. Nerín, "Nanoparticle release from nano-silver antimicrobial food containers," *Food and Chemical Toxicology*, vol. 62, no. 0, pp. 16-22, 2013.
9. O. Betty Lucy López, G. Amanda Inés Mejía and G. Ligia Sierra, "Biodegradability of poly(vinyl alcohol)," *Polymer Engineering and Science*, vol. 39, no. 8, pp. 1346-1352, 1999.
10. S. Khanna and A. K. Srivastava, "Recent advances in microbial polyhydroxyalkanoates," *Process Biochemistry*, vol. 40, no. 2, pp. 607-619, 2005.

11. M. D. Sanchez-Garcia and J. M. Lagaron, "On the use of plant cellulose nanowhiskers to enhance the barrier properties of polylactic acid," *Cellulose*, vol. 17, no. 5, pp. 987-1004, 2010.
12. S. V. N. Vijayendra and T. R. Shamala, "Film forming microbial biopolymers for commercial applications—A review," *Critical Reviews in Biotechnology*, vol. 34, no. 4, pp. 338-357, 2014.
13. M. G. E. Albuquerque, C. A. V. Torres and M. A. M. Reis, "Polyhydroxyalkanoate (PHA) production by a mixed microbial culture using sugar molasses: Effect of the influent substrate concentration on culture selection," *Water Research*, vol. 44, no. 11, pp. 3419-3433, 2010.
14. B. S. Kim, S. C. Lee, S. Y. Lee, H. N. Chang, Y. K. Chang and S. I. Woo, "Production of poly(3-hydroxybutyric acid) by fed-batch culture of *Alcaligenes eutrophus* with glucose concentration control," *Biotechnol Bioeng*, vol. 43, no. 9, pp. 892-898, 1994.
15. D. Plackett and I. Siró, "Polyhydroxyalkanoates (phas) for food packaging," in *Multifunctional and Nanoreinforced Polymers for Food Packaging*, Ed., pp. 498-526, 2011.
16. M. Erceg, T. Kovačić and I. Klarić, "Thermal degradation of poly(3-hydroxybutyrate) plasticized with acetyl tributyl citrate," *Polymer Degradation and Stability*, vol. 90, no. 2, pp. 313-318, 2005.
17. E. Bugnicourt, P. Cinelli, A. Lazzeri and V. Alvarez, "Polyhydroxyalkanoate (PHA): Review of synthesis, characteristics, processing and potential applications in packaging," *Express Polymer Letters*, vol. 8, no. 11, pp. 791-808, 2014.
18. M. Martínez-Sanz, A. Lopez-Rubio, M. Villano, C. S. S. Oliveira, M. Majone, M. Reis and J. M. Lagaron, "Production of bacterial nanobiocomposites of polyhydroxyalkanoates derived from waste and bacterial nanocellulose by the electrospinning enabling melt compounding method," *Journal of Applied Polymer Science*, 2015.
19. M. J. Fabra, A. Lopez-Rubio and J. M. Lagaron, "High barrier polyhydroxyalkanoate food packaging film by means of nanostructured electrospun interlayers of zein," *Food Hydrocolloids*, vol. 32, no. 1, pp. 106-114, 2013.

## ***Introduction***

20. A. Martínez-Abad, L. Cabedo, C. S. S. Oliveira, L. Hilliou, M. Reis and J. M. Lagarón, "Characterization of polyhydroxyalkanoate blends incorporating unpurified biosustainably produced poly(3-hydroxybutyrate-co-3-hydroxyvalerate)," *Journal of Applied Polymer Science*, 2015.
21. D. Heinrich, M. H. Madkour, M. A. Al-Ghamdi, I. I. Shabbaj and A. Steinbüchel, "Large scale extraction of poly(3-hydroxybutyrate) from *Ralstonia eutropha* H16 using sodium hypochlorite," *AMB Express*, vol. 2, no. 1, 2012.
22. N. Gurieff and P. Lant, "Comparative life cycle assessment and financial analysis of mixed culture polyhydroxyalkanoate production," *Bioresource Technology*, vol. 98, no. 17, pp. 3393-3403, 2007.
23. J. M. L. Dias, P. C. Lemos, L. S. Serafim, C. Oliveira, M. Eiroa, M. G. E. Albuquerque, A. M. Ramos, R. Oliveira and M. A. M. Reis, "Recent advances in polyhydroxyalkanoate production by mixed aerobic cultures: From the substrate to the final product," *Macromolecular Bioscience*, vol. 6, no. 11, pp. 885-906, 2006.
24. M. Majone and M. Reis, "Editorial," *New Biotechnology*, vol. 31, no. 4, pp. 255-256, 2014.
25. A. López-Rubio, E. Almenar, P. Hernandez-Muñoz, J. M. Lagarón, R. Catalá and R. Gavara, "Overview of active polymer-based packaging technologies for food applications," *Food Reviews International*, vol. 20, no. 4, pp. 357-387, 2004.
26. WHO, "WHO Estimates of the Global Burden of Foodborne Diseases: Foodborne Disease Burden Epidemiology Reference Group 2007-2015. ," Ed., World Health Organization, 2015.
27. P. Appendini and J. H. Hotchkiss, "Review of antimicrobial food packaging," *Innovative Food Science and Emerging Technologies*, vol. 3, no. 2, pp. 113-126, 2002.
28. B. Malhotra, A. Keshwani and H. Kharkwal, "Antimicrobial food packaging: potential and pitfalls," *Frontiers in Microbiology*, vol. 6, pp. 611, 2015.

29. D. P. Karumathil, A. Upadhyay and K. Venkitanarayanan, "Chapter 19 - Antimicrobial Packaging for Poultry A2 - Barros-Velázquez, Jorge," in *Antimicrobial Food Packaging*, Ed., pp. 257-268, Academic Press, San Diego, 2016.
30. J. H. Han, "Antimicrobial Food Packaging," *Food Technology*, vol. 54, no. 3, pp. 56-65, 2000.
31. A. Llorens, E. Lloret, P. A. Picouet, R. Trbojevich and A. Fernandez, "Metallic-based micro and nanocomposites in food contact materials and active food packaging," *Trends in Food Science & Technology*, vol. 24, no. 1, pp. 19-29, 2012.
32. R. K. Dutta, B. P. Nenavathu, M. K. Gangishetty and A. V. R. Reddy, "Studies on antibacterial activity of ZnO nanoparticles by ROS induced lipid peroxidation," *Colloids and Surfaces B: Biointerfaces*, vol. 94, no. 0, pp. 143-150, 2012.
33. M. Moritz and M. Geszke-Moritz, "The newest achievements in synthesis, immobilization and practical applications of antibacterial nanoparticles," *Chemical Engineering Journal*, vol. 228, pp. 596-613, 2013.
34. S. Lee, K. Song and B. Lee, "Antibacterial activity of silver nanoparticles prepared by a chemical reduction method," *Korean Journal of Chemical Engineering*, vol. 27, no. 2, pp. 688-692, 2010.
35. R. J. Pinto, S. C. Fernandes, C. S. Freire, P. Sadocco, J. Causio, C. P. Neto and T. Trindade, "Antibacterial activity of optically transparent nanocomposite films based on chitosan or its derivatives and silver nanoparticles," *Carbohydr Res*, vol. 348, pp. 77-83, 2012.
36. M. Valodkar, S. Modi, A. Pal and S. Thakore, "Synthesis and anti-bacterial activity of Cu, Ag and Cu-Ag alloy nanoparticles: A green approach," *Materials Research Bulletin*, vol. 46, no. 3, pp. 384-389, 2011.
37. H. H. Lara, N. V. Ayala-Nuñez, L. Ixtapan-Turrent and C. Rodriguez-Padilla, "Mode of antiviral action of silver nanoparticles against HIV-1," *Journal of Nanobiotechnology*, vol. 8, 2010.

## ***Introduction***

38. M. Nocchetti, A. Donnadio, V. Ambrogi, P. Andreani, M. Bastianini, D. Pietrella and L. Latterini, "Ag/AgCl nanoparticle decorated layered double hydroxides: synthesis, characterization and antimicrobial properties," *Journal of Materials Chemistry B*, vol. 1, no. 18, pp. 2383-2393, 2013.
39. C. Marambio-Jones and E. M. V. Hoek, "A review of the antibacterial effects of silver nanomaterials and potential implications for human health and the environment," *Journal of Nanoparticle Research*, vol. 12, no. 5, pp. 1531-1551, 2010.
40. A. Grigor'Eva, I. Saranina, N. Tikunova, A. Safonov, N. Timoshenko, A. Rebrov and E. Ryabchikova, "Fine mechanisms of the interaction of silver nanoparticles with the cells of *Salmonella typhimurium* and *Staphylococcus aureus*," *BioMetals*, vol. 26, no. 3, pp. 479-488, 2013.
41. K. K. Kuorwel, M. J. Cran, J. D. Orbell, S. Buddhadasa and S. W. Bigger, "Review of Mechanical Properties, Migration, and Potential Applications in Active Food Packaging Systems Containing Nanoclays and Nanosilver," *Comprehensive Reviews in Food Science and Food Safety*, vol. 14, no. 4, pp. 411-430, 2015.
42. E. Fortunati, F. Luzi, D. Puglia, A. Terenzi, M. Vercellino, L. Visai, C. Santulli, L. Torre and J. M. Kenny, "Ternary PVA nanocomposites containing cellulose nanocrystals from different sources and silver particles: Part II," *Carbohydrate Polymers*, vol. 97, no. 2, pp. 837-848, 2013.
43. A. N. Krklješ, M. T. Marinović-Cincović, Z. M. Kačarević-Popović and J. M. Nedeljković, "Dynamic thermogravimetric degradation of gamma radiolytically synthesized Ag-PVA nanocomposites," *Thermochimica Acta*, vol. 460, no. 1-2, pp. 28-34, 2007.
44. Z. H. Mbhele, M. G. Salemane, C. G. C. E. Van Sittert, J. M. Nedeljković, V. Djoković and A. S. Luyt, "Fabrication and Characterization of Silver-Polyvinyl Alcohol Nanocomposites," *Chemistry of Materials*, vol. 15, no. 26, pp. 5019-5024, 2003.
45. A. Martínez-Abad, J. M. Lagarón and M. J. Ocio, "Characterization of transparent silver loaded poly(L-lactide) films produced by melt-compounding for the sustained release of antimicrobial silver ions in food applications," *Food Control*, vol. 43, no. 0, pp. 238-244, 2014.

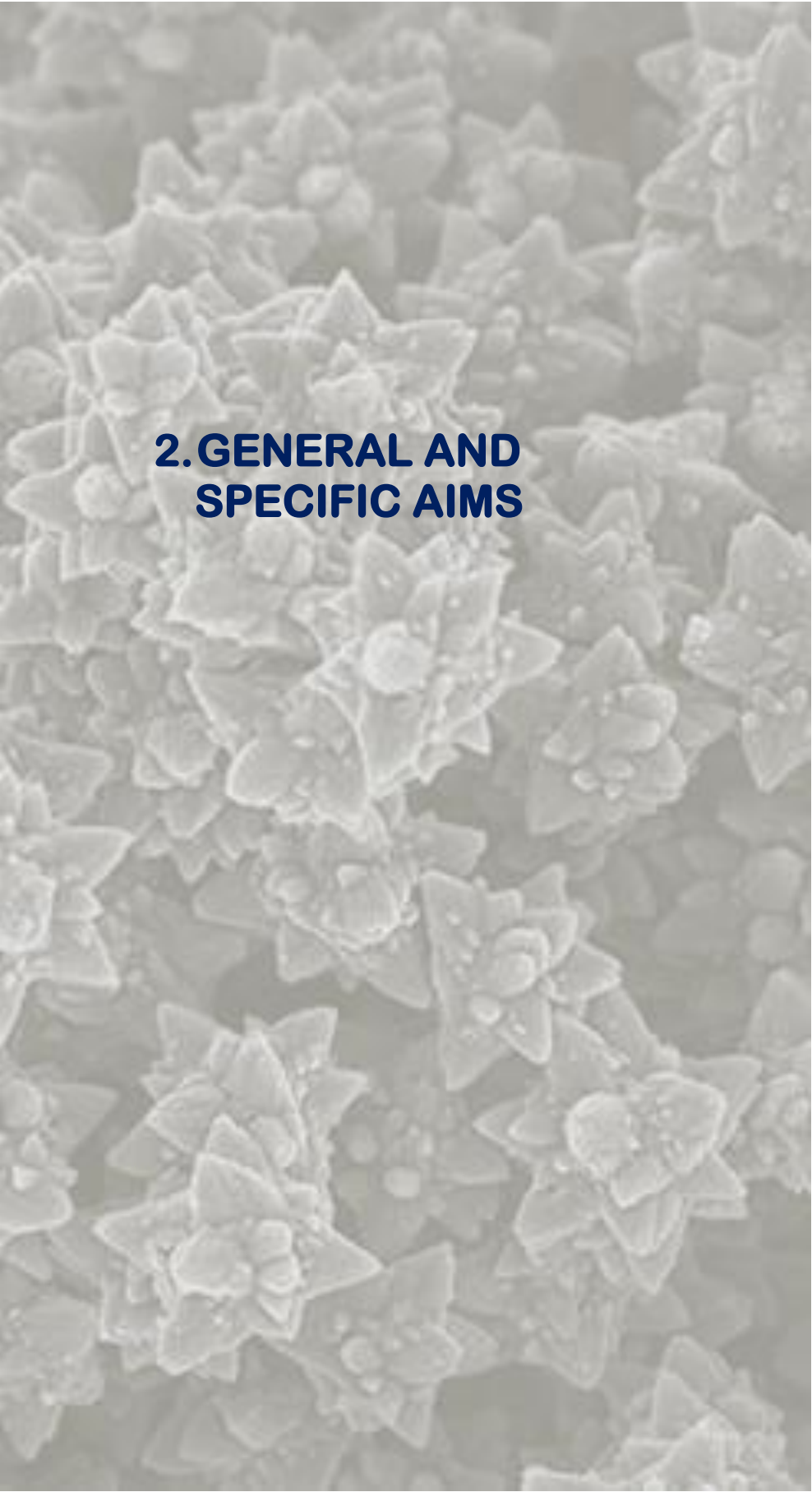
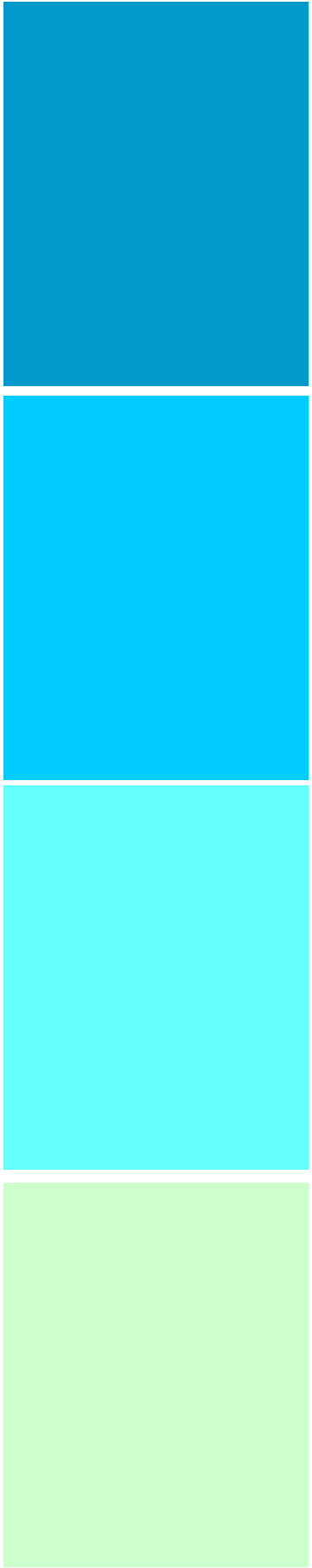
46. U. FDA/CFSAN, "Listing of food additive status: silver nitrate," Ed., pp. 172-167, Food and Drug Administration/ Center for Food Safety and Applied Nutrition, 2010.
47. EFSA, "Opinion of the Scientific Panel on food additives, flavourings, processing aids and materials in contact with food (AFC) on a request related to a 12th list of substances for food contact materials," Ed., pp. 1-21, European Food Safety Authority, 2006.
48. EFSA, "EFSA, 2008. Inability to assess the safety of a silver hydrosol added for nutritional purposes as a source of silver in food supplements and the bioavailability of silver from this source based on the supporting dossier. Scientific statement of the panel on food additives and nutrient sources added to food (ANS): question No EFSA-Q-2005-169. EFSA J. 884, 1-3," Ed., pp. 1-3, European Food Safety Authority 2008.
49. FDA, "PART 182—SUBSTANCES GENERALLY RECOGNIZED AS SAFE," Ed., Food and Drug Administration, 2011.
50. Y. Xie, Y. He, P. L. Irwin, T. Jin and X. Shi, "Antibacterial Activity and Mechanism of Action of Zinc Oxide Nanoparticles against *Campylobacter jejuni*," *Applied and Environmental Microbiology*, vol. 77, no. 7, pp. 2325-2331, 2011.
51. K. M. Reddy, K. Feris, J. Bell, D. G. Wingett, C. Hanley and A. Punnoose, "Selective toxicity of zinc oxide nanoparticles to prokaryotic and eukaryotic systems," *Appl Phys Lett*, vol. 90, no. 213902, pp. 2139021-2139023, 2007.
52. N. Jones, B. Ray, K. T. Ranjit and A. C. Manna, "Antibacterial activity of ZnO nanoparticle suspensions on a broad spectrum of microorganisms," *FEMS Microbiology Letters*, vol. 279, no. 1, pp. 71-76, 2008.
53. Y. Liu, L. He, A. Mustapha, H. Li, Z. Q. Hu and M. Lin, "Antibacterial activities of zinc oxide nanoparticles against *Escherichia coli* O157:H7," *J Appl Microbiol*, vol. 107, no. 4, pp. 1193-1201, 2009.
54. M. Arakha, M. Saleem, B. C. Mallick and S. Jha, "The effects of interfacial potential on antimicrobial propensity of ZnO nanoparticle," *Sci. Rep.*, vol. 5, 2015.

## ***Introduction***

55. A. Emamifar, M. Kadivar, M. Shahedi and S. Soleimanian-Zad, "Evaluation of nanocomposite packaging containing Ag and ZnO on shelf life of fresh orange juice," *Innovative Food Science & Emerging Technologies*, vol. 11, no. 4, pp. 742-748, 2010.
56. P. Espitia, N. d. Soares, J. d. Coimbra, N. de Andrade, R. Cruz and E. Medeiros, "Zinc Oxide Nanoparticles: Synthesis, Antimicrobial Activity and Food Packaging Applications," *Food and Bioprocess Technology*, vol. 5, no. 5, pp. 1447-1464, 2012.
57. R. Vijaya Kumar, Y. Diamant and A. Gedanken, "Sonochemical synthesis and characterization of nanometer-size transition metal oxides from metal acetates," *Chemistry of Materials*, vol. 12, no. 8, pp. 2301-2305, 2000.
58. A. A. Eliseev, A. V. Lukashin, A. A. Vertegel, L. I. Heifets, A. I. Zhironov and Y. D. Tretyakov, "Complexes of Cu(II) with polyvinyl alcohol as precursors for the preparation of CuO/SiO<sub>2</sub> nanocomposites," *Materials Research Innovations*, vol. 3, no. 5, pp. 308-312, 2000.
59. J. F. Xu, W. Ji, Z. X. Shen, S. H. Tang, X. R. Ye, D. Z. Jia and X. Q. Xin, "Preparation and Characterization of CuO Nanocrystals," *Journal of Solid State Chemistry*, vol. 147, no. 2, pp. 516-519, 1999.
60. K. Borgohain, J. B. Singh, M. V. Rama Rao, T. Shripathi and S. Mahamuni, "Quantum size effects in CuO nanoparticles," *Physical Review B - Condensed Matter and Materials Physics*, vol. 61, no. 16, pp. 11093-11096, 2000.
61. M. Salavati-Niasari and F. Davar, "Synthesis of copper and copper(I) oxide nanoparticles by thermal decomposition of a new precursor," *Materials Letters*, vol. 63, no. 3-4, pp. 441-443, 2009.
62. M. Vincent, P. Hartemann and M. Engels-Deutsch, "Antimicrobial applications of copper," *International Journal of Hygiene and Environmental Health*, vol. 219, no. 7, Part A, pp. 585-591, 2016.
63. G. Grass, C. Rensing and M. Solioz, "Metallic Copper as an Antimicrobial Surface," *Applied and Environmental Microbiology*, vol. 77, no. 5, pp. 1541-1547, 2011.

64. D. Liang, B. S. Hsiao and B. Chu, "Functional electrospun nanofibrous scaffolds for biomedical applications," *Advanced Drug Delivery Reviews*, vol. 59, no. 14, pp. 1392-1412, 2007.
65. T. J. Sill and H. A. von Recum, "Electrospinning: Applications in drug delivery and tissue engineering," *Biomaterials*, vol. 29, no. 13, pp. 1989-2006, 2008.
66. K. J. Kim, Y. Doi and H. Abe, "Effects of residual metal compounds and chain-end structure on thermal degradation of poly(3-hydroxybutyric acid)," *Polymer Degradation and Stability*, vol. 91, no. 4, pp. 769-777, 2006.
67. N. Bhardwaj and S. C. Kundu, "Electrospinning: A fascinating fiber fabrication technique," *Biotechnology Advances*, vol. 28, no. 3, pp. 325-347, 2010.
68. S. Torres-Giner, "Electrospun nanofibers for food packaging applications," in *Multifunctional and Nanoreinforced Polymers for Food Packaging*, Ed., pp. 108-125, 2011.
69. Y. Echegoyen, M. J. Fabra, J. L. Castro-Mayorga, A. Cherpinski and J. M. Lagaron, "High throughput electro-hydrodynamic processing in food encapsulation and food packaging applications: Viewpoint," *Trends in Food Science and Technology*, vol. 60, pp. 71-79, 2017.
70. S. Torres-Giner, M. J. Ocio and J. M. Lagaron, "Development of Active Antimicrobial Fiber-Based Chitosan Polysaccharide Nanostructures using Electrospinning," *Engineering in Life Sciences*, vol. 8, no. 3, pp. 303-314, 2008.





## **2. GENERAL AND SPECIFIC AIMS**



## 2. General and specific aims

---

As outlined in the introduction section, the interest in bio-based food packaging materials with adequate properties and functionalities to guarantee food quality and safety has increased considerably over the last years. Antimicrobial packaging is one of the most widely researched technologies in the so called active packaging area. In this context, the proper dispersion and distribution of antimicrobial agents in the nanorange into biopolyesters allows to combine the preservative functions of the antimicrobials with the inherent protective functions of these biopackaging materials. Therefore, the main goal of this PhD thesis was aimed at:

*“The development of biotechnological routes for the synthesis of polyhydroxyalkanoates based on nanometals -silver, zinc oxide and copper oxide- for antimicrobial active food packaging applications”*

To achieve this goal, several milestones had to be sequentially accomplished. Although the incorporation of metals as antimicrobial agents, mainly ionic silver, have been previously explored, silver ions are physically and chemically unstable, being reduced to elemental silver or silver nanoparticles by weak reducing treatments, such as the use of some solvents, UV-light, thermal treatments, ligands, etc. which radically diminish the nanoparticles dispersion and subsequently impair the optical properties of materials and their antimicrobial performance. Thus, the first milestone of this work consisted on the **study of the ability of a microbial derived**

**polyhydroxyalkanoate to stabilize silver nanoparticles** produced by chemical reduction and **the assessment of their antimicrobial performance.**

Once the silver nanoparticles were successfully stabilized, the next milestone involved **the incorporation of silver nanoparticles into polyhydroxyalkanoate matrices.** Along this process, several strategies were used for the incorporation of the nanoparticles into poly(3-hydroxybutyrate-co-3-hydroxyvalerate) by melt compounding and electrospinning. The effect of silver loading and dispersion on the antibacterial and antiviral activity of the developed materials as well as the physicochemical properties were also evaluated.

The following challenge was **the development of a simple bioprocess for the biological synthesis of silver nanoparticles and polyhydroxyalkanoates.** With that purpose in mind, a comparative study of the chemical and biological synthesis of silver nanoparticles during the polyhydroxyalkanoates fermentation was carried out and then optimized and scaled-up to fully-automated laboratory-scale bioreactor.

As an alternative to silver-based antimicrobials, given the restrictive legislation frames for the application of the silver ions or nanoparticles in food contact, zinc oxide and copper oxide nanocomposites were developed. The fourth milestone was then the **study of the effect of zinc oxide nanoparticles size and morphology on their antimicrobial activity and the evaluation of different methods for their incorporation into polyhydroxyalkanoates matrices.** In this case, the already developed strategies for the incorporation of silver nanoparticles into polyhydroxyalkanoates, i.e. melt compounding and electrospinning, were also used

for the development of the zinc oxide-based nanocomposites, which were also characterized in terms of barrier, thermal and antibacterial properties.

Finally, based on the strategies previously developed for the incorporation of metal nanoparticles into polyhydroxyalkanoates, the last milestone of the work was **the development of copper oxide-polyhydroxyalkanoates nanocomposites with high antibacterial and antiviral performance**. In addition, the **assessment of the biodegradation of the materials during composting** was carried out.



The background of the slide is a grayscale scanning electron micrograph (SEM) showing a highly textured surface. The texture consists of a dense, repeating pattern of small, star-shaped or floral motifs. Each motif appears to have a central, rounded part with several pointed, petal-like extensions radiating outwards. The overall appearance is that of a micro-structured material, possibly a polymer or ceramic coating. The lighting in the SEM image creates highlights and shadows that emphasize the three-dimensional nature of the surface features.

### **3.RESULTS**



### 3. Results

---

This PhD thesis is a compilation of works focused on the development of biotechnologically derived polyhydroxyalkanoates based on nanometals -silver, zinc oxide and copper oxide for antimicrobial active food packaging applications. Each chapter deals with one of the specific milestones defined above and correspond to specific journal papers already published or being currently submitted.

#### Chapter I:

J. L. Castro-Mayorga, A. Martínez-Abad, M. J. Fabra, C. Olivera, M. Reis and J. M. Lagarón, "Stabilization of antimicrobial silver nanoparticles by a polyhydroxyalkanoate obtained from mixed bacterial culture". *International Journal of Biological Macromolecules*, vol. 71, pp. 103-110, 2014.

#### Chapter II:

J. L. Castro-Mayorga, M. J. Fabra and J. M. Lagaron, "Stabilized nanosilver based antimicrobial poly(3-hydroxybutyrate-co-3-hydroxyvalerate) nanocomposites of interest in active food packaging". *Innovative Food Science and Emerging Technologies*, vol. 33, pp. 524-533, 2016.

#### Chapter III:

J. L. Castro-Mayorga, M. J. Fabra, L. Cabedo and J. M. Lagaron. "On the use of the electrospinning coating technique to produce antimicrobial polyhydroxyalkanoate materials containing *in situ* stabilized silver nanoparticles". *Nanomaterials*, vol. 7, no. 1, 2017.

## *Results*

### **Chapter IV:**

J. L. Castro-Mayorga, W. Randazzo, M.J. Fabra, J. M. Lagaron, R. Aznar and G. Sánchez. **“Antiviral properties of silver nanoparticles against norovirus surrogates and their efficacy in coated polyhydroxyalkanoates systems”**. *LWT - Food Science and Technology*, vol. 79, pp. 503-510, 2017.

### **Chapter V:**

J.L. Castro-Mayorga, F. Freitas, M. Reis, A. Prieto, J.M. Lagaron. **“Biosynthesis of silver nanoparticles and polyhydroxybutyrate nanocomposites of interest in antimicrobial applications”**. To be submitted.

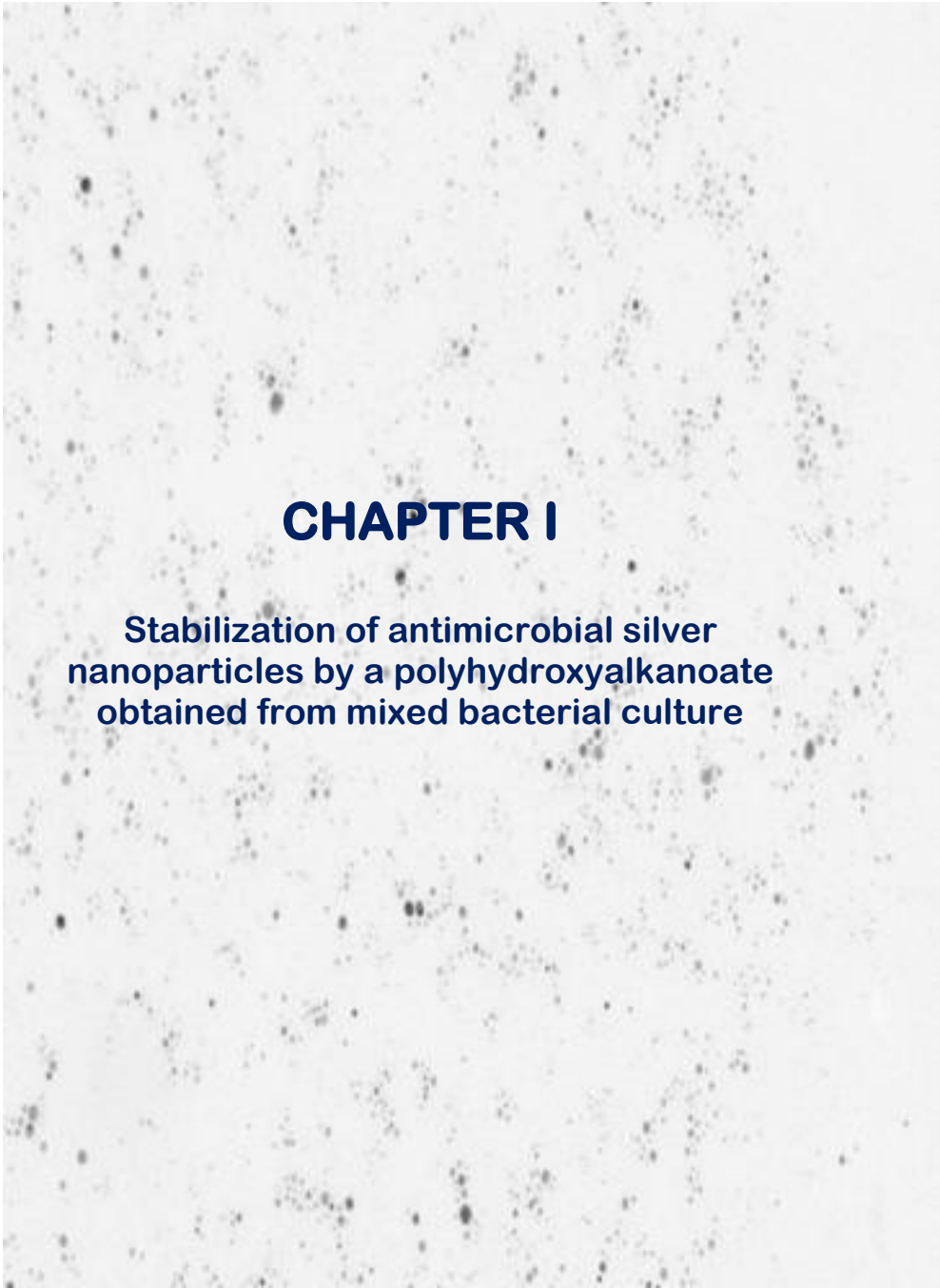
### **Chapter VI:**

Castro-Mayorga, J. L. Castro Mayorga, M. J. Fabra, A.M. Pourrahimi, R. Olsson . **“The impact of zinc oxide particle morphology as an antimicrobial and when incorporated in Poly(3-hydroxybutyrate-co-3-hydroxyvalerate) films for food packaging and food contact surfaces applications”**. *Food and Bioproducts Processing*, vol. 101, pp. 32-44, 2017.

### **Chapter VII:**

J. L. Castro-Mayorga, M. J. Fabra, L. Cabedo, G. Sanchez and J. M. Lagaron. **“Antimicrobial nanocomposites and electrospun coatings based on Poly(3-hydroxybutyrate-co-3-hydroxyvalerate) and copper oxide nanoparticles for active packaging and coating applications ”**. To be submitted.

A general discussion was included in the next section in order to highlight the most relevant results and explain how they can be interpreted from a holistic perspective within the PhD thesis.

A transmission electron micrograph (TEM) showing numerous small, dark, spherical silver nanoparticles of varying sizes, some appearing as individual particles and others as small clusters, distributed across a light gray background.

## CHAPTER I

### **Stabilization of antimicrobial silver nanoparticles by a polyhydroxyalkanoate obtained from mixed bacterial culture**

J. L. Castro-Mayorga, A. Martínez-Abad, M. J. Fabra, C. Oliveira, M. Reis and J. M. Lagarón, "Stabilization of antimicrobial silver nanoparticles by a polyhydroxyalkanoate obtained from mixed bacterial culture". *International Journal of Biological Macromolecules*, vol. 71, pp. 103-110, 2014



## Abstract

---

The incorporation of antimicrobials into polymer matrices is a promising technology in the food packaging and biomedical areas. Among the most widely used antimicrobials, silver nanoparticles (AgNPs) have emerged as one of the most researched technologies to prevent microbial outbreaks. However, it is known that AgNPs are rather unstable and present patterns of agglomeration that might limit their application. In this work, AgNPs were produced by chemical reduction in suspensions of an unpurified poly (3-hydroxybutyrate-co-3-hydroxyvalerate (PHBV) which was previously obtained from a mixed culture fermentation using a synthetic medium mimicking fermented cheese whey. The synthesis of AgNPs was carried out within the unpurified PHBV suspension (*in situ*) and by physical mixing (*mix*). The stability of crystalline and spherical nanoparticles ( $11 \pm 5.6$  nm) obtained *in situ* was found to be stable during at least 40 days. The results suggest that the unpurified PHBV appears to be a very efficient capping agent, preventing agglomeration and, thereby, stabilizing successfully the silver nanoparticles. The *in situ* obtained AgNP-PHBV materials were also found to exhibit a strong antibacterial activity against *Salmonella enterica* at low concentration (0.1 - 1 ppm).

## Keywords

---

Polyhydroxyalkanoates, silver nanoparticles, antimicrobial properties.

## **1. Introduction**

---

Polyhydroxyalkanoates (PHA's) are a family of naturally occurring storage biopolyesters synthesized by more than 300 species of Gram-positive and Gram-negative bacteria [1]. Among the various biodegradable polymers, PHA's provide a good alternative to fossil-fuel based plastics as they possess thermoplastic properties similar to conventional polyolefins, such as polypropylene, with the advantage of being 100% biodegradable and compostable and being produced from renewable resources [2-5]. Production of PHA's usually involves fermentation, isolation and purification processes, which imply higher production costs as compared to polyolefins. Therefore, much efforts and improvements have been developed to reduce the costs of the fermentation and downstream processes [4, 6]. As an example, the use of open mixed cultures avoids the need for sterility in the reactor and makes easier the use of low cost agricultural or industrial waste feedstock in the production of PHA's [4, 7]. Gurieff and Lant performed a lifecycle assessment and financial analysis and proved that PHA production by mixed cultures from renewable resources is financially and environmentally attractive. Moreover, it is a greener alternative to the pure culture processes since less CO<sub>2</sub> is produced [8].

The good biocompatibility and slow hydrolytic degradation of PHA's have prompted their implementation in packaging as well as in medical applications [9]. In the areas of food and cosmetic packaging, PHA's are already commercialized as cosmetic containers, shampoo bottles, covers, milk cartons and films, moisture barriers in nappies and sanitary towels, pens, and combs, among others (reviewed by [10]). More recently, attention has been also focused on the medical applications of PHA's, such as in bone plates, surgical sutures and blood vessel replacements [5, 11],

or as biodegradable carriers for long-term dosage of drugs, medicines, hormones, insecticides and herbicides [5, 12].

In this sense, the incorporation of antimicrobial substances into PHA's might allow the production of biodegradable materials which could be used for the targeted release of the antimicrobials in active food packaging, food contact surfaces or medical applications.

Silver nanoparticles (AgNPs) are highly effective against a wide spectrum of bacteria, fungi and viruses, possess anti-inflammatory properties and promote epithelisation and scarring [13-16]. Owing to the growing concern about resistance to antibiotics, the incorporation of silver nanoparticles into different matrices has emerged as an effective way of producing materials with long-term wide spectrum antimicrobial properties either for packaging, medical or other applications [16]. One of the main challenges in producing this kind of antimicrobials is the synthesis of stable nanoparticles, as their antimicrobial effectiveness greatly depends on their size, size distribution and agglomeration state [11, 17]. In this sense, several biological organisms, as well as different organic substances from natural sources have been used for the production of nanoparticles [18-21]

Some authors have shown that the fermentation residues [22, 23] greatly affects the PHA's degradation. However, Serafim et al. [24] stated that the presence of the impurities did not modify the glass transition temperature ( $T_g$ ) of PHA's materials produced by bacterial mixed cultures although the melting behavior (melting temperature and melting enthalpy) of the obtained materials were modified. The effect that the residual organic matter has on the PHA's degradation is unknown and it is therefore one of the objectives of this paper to ascertain its role in the stabilization of silver nanoparticles, there are no studies in the literature reporting about the use of poly (3-hydroxybutyrate-co-3-hydroxyvalerate (PHBV) obtained from mixed cultures

## *Chapter I*

as capping agent to stabilize AgNPs, neither detailed information involving the nanoparticles atomic organization or the biocide effect of AgNPs synthesized within polymer suspensions.

In the present paper, silver nanoparticles were produced by chemical reduction in PHBV suspensions. The stability of the nanoparticles in the polymer suspension was compared with that of AgNPs physically mixed with the polymer suspension and with aqueous AgNPs suspensions without polymer. The materials were characterized in terms of chemical composition, morphology, atomic organization, total silver content and antimicrobial performance against the food-borne pathogen *Salmonella enterica*.

## **2. Materials and methods**

---

### **2.1 Synthesis and characterization of the PHBV**

The PHBV was obtained from a mixed bacterial culture grown under small scale laboratory conditions. For the production of the PHBV, one fed-batch test was carried out in a 5 L reactor (BioStat® B plus, Sartorius) in order to produce a poly (3-hydroxybutyrate-co-3-hydroxyvalerate) copolymer using a mixed microbial culture enriched in PHA-accumulating microorganisms and synthetic volatile fatty acids (VFA) as precursors for PHA production. The mixed microbial culture was selected in a 20 L sequencing batch reactor (SBR) fed with a synthetic VFA mixture mimicking fermented cheese whey (% mol basis: 77 acetate, 12 propionate, 9 butyrate, and 2 valerate), supplemented with nutrients ( $\text{NH}_4\text{Cl}$  and  $\text{KH}_2\text{PO}_4$ , at a ratio C/N/P of 100/10/1), and operated at 12 h cycles (four discrete phases: influent filling - 5min; aeration - 675 min; settling - 30 min; and withdrawal of the exhausted effluent

- 10 min), an organic loading rate (OLR) of 25.4 mM days<sup>-1</sup>, hydraulic retention time (HRT) of 1 day, and sludge retention time (SRT) of 4 days.

The fed-batch reactor was inoculated with 2.5 L concentrated mixed liquor (12.1 g L<sup>-1</sup> volatile suspended solids) and pulse fed with a synthetic VFA mixture of 65.5 g VFA L<sup>-1</sup> (0.7M), with a composition in % mol basis: 91 butyrate, and 9 valerate. VFA synthetic solution pH was adjusted to 7.5 with the addition of 5M NaOH and pH was not controlled during the production assay, varying between 7.5 and 8.2. No nitrogen or phosphorus sources were supplied in order to maximize the PHBV storage response. The reactor was continuously mixed and aerated at 300 rpm and 4 L min<sup>-1</sup>, respectively, and working at room temperature (20-23°C). The PHBV accumulation experiments were carried by feeding the synthetic VFA mixture pulse-wise (12.2 mM), controlled by dissolved oxygen response. A new pulse of synthetic mixture was always injected when the dissolved oxygen concentration increased. This procedure was repeated until no dissolved oxygen response was observed indicating PHBV storage saturation, which took ca. 10 h, after the injection of 7 pulses (0.4 L of synthetic VFA mixture).

In order to recover the polymer, a quenching step (by adding ca. 2 M HCl until a pH of 2-3 was attained) was performed directly on the mixed liquor, followed by a 3 h reaction at room temperature (20-23°C) with NaClO (1% Cl<sub>2</sub>) at a ratio of 1 g NaClO per g cells, in order to degrade the cellular material, then the polymeric material was recovered by centrifugation (20 min x 6850 rpm), washed once with ca. 10 L distilled water, and lyophilized for 72 h. No further purification steps were followed to eliminate cell debris or other organic material from the polymer, this material was called unpurified PHBV throughout the manuscript.

The polymer composition, referred to the hydroxybutyrate (HB) and hydroxyvalerate (HV) content, and the purity were determined by gas

## *Chapter I*

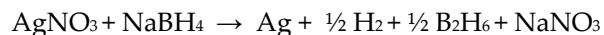
chromatography (GC) using a method adapted from Serafim et al. [3]. The average molecular weight (Mw), the number average molecular weight (Mn) and the polydispersity index (PDI =Mw/Mn) were estimated using a size exclusion chromatography (SEC) apparatus (Waters) as described by Serafim et al. [24].

The unpurified PHBV was dissolved in chloroform (3% w/v) at 60°C and precipitated by adding it drop by drop to a 10-fold excess ice-cold methanol solution under stirring. Once all the solution was added to the cold methanol and after 1 h under stirring, the precipitated was separated by vacuum filtration using a filter of ca. 3 µm pore size. The filtrate was removed and the solid fraction was dried at 60°C overnight.

The protein quantification of both purified and unpurified PHBV, was carried out by suspending a certain amount (varying between 2- 5 mg) of the material in 1 mL of distilled water under vigorous mixing, promoting the proteins solubilization, Then the protein concentration in the solution was spectrophotometrically quantified at 750 nm by using the Folin phenol reagent [29].

### **2.2 Synthesis and characterization of the PHBV-AgNP materials**

Silver nanoparticles (AgNPs) were synthesized by chemical reduction of silver nitrate (Sigma, Germany) with sodium borohydride (Panreac, Spain) according with the following reaction:



Three different suspensions of unpurified PHBV and AgNPs were prepared. First, the produced unpurified PHBV was suspended (0.08 wt.-%) in ultrapure MilliQ® water (Millipore Corporation Co., USA) in a 250 mL Erlenmeyer flask. The assembly was

placed into an ice bath and stirred using a magnetic stirrer. Sodium borohydride was added first to the suspension to get 1 mM, 2 mM or 4 mM concentration and the volume was adjusted to 30 mL. After 20 min, 10 mL of desirable silver nitrate solution were added dropwise to the suspension to generate the nanoparticles. This suspension was labeled as PHBV-AgNP *in situ*. A silver nanoparticles colloid, labeled as “aqueous AgNPs” was prepared analogously but without polymer. The third suspension was prepared by physically mixing the AgNP colloid with the unpurified PHBV suspension (PHBV-AgNP *mix*).

The stability of the silver nanoparticles in the produced PHBV-AgNP suspensions was routinely monitored by visual inspection as well as by Ultraviolet visible (UV-VIS) spectroscopy with a UV-VIS Spectrum system 8453 (Agilent Technologies Waldbronn, Germany) from 1 hour after the synthesis (as synthesized) and throughout 40 days at room temperature and 100% of relative humidity (RH).

The morphology, atomic order, chemical identification and size distribution of the silver nanoparticles formed into the unpurified PHBV suspension were examined using a High Resolution Transmission Electron Microscopy (HR-TEM) at an accelerating voltage of 200 kV. The HR-TEM instrument is equipped with a camera CCD GATAN and “Digital Micrograph” Software for image acquisition and treatment, which allows the obtaining of the electron diffraction patterns and spectroscopic techniques such as energy dispersive X-ray analysis (EDX) for chemical identification. A sample of freshly synthesized PHBV-AgNP and aqueous suspensions were prepared by drying a small drop over a carbon-coated copper grid.

The PHBV-AgNP suspensions were centrifuged at 17 387 g for 30 min and the precipitate was dried at 40°C under vacuum for 24 h. The dried materials were digested with 2 mL nitric acid, dried and filtered. The silver content of final supernant

## *Chapter I*

was measured by Inductively Coupled Plasma-Mass Spectroscopy (ICP-MS) (Agilent Technologies 7500CX, Tokyo, Japan)

Attenuated Total Reflectance Fourier Transform Infrared (FTIR) spectroscopic analysis of the purified as well as the unpurified PHBV-AgNPs were made with a ATR-FTIR tensor 37 equipment (Bruker, Rheinstetten, Germany) using KBr pellets prepared by dispersing the solid material into KBr and compressing to form a disc as described elsewhere [25].

### **2.3 Antimicrobial activity of the unpurified PHBV-AgNP**

The antimicrobial test was performed for *Salmonella enterica* because it is one of the most frequent food-borne pathogen [26-28]. A pathogenic microorganism, *Salmonella enterica* CECT554 strain was obtained from the Spanish Type Culture Collection (CECT: Valencia, Spain) and stored in phosphate buffered saline (PBS) with 10 wt.-% tryptic soy broth (TSB, Conda Laboratories, Madrid, Spain) and 10 wt.-% glycerol at -80°C until needed. For experimental use, the stock culture was maintained by regular subculture to Triptone Soybean Agar (TSA, Conda Laboratories, Madrid, Spain) slants at 4°C and transferred monthly. Previous to each study, a loopful of bacteria was transferred to 10 mL of TSB and incubated at 37°C overnight. A 100 µL aliquot from the overnight culture was again transferred to TSB and grown at 37°C to the mid-exponential phase of growth. An approximate count of about  $3 \times 10^5$  CFU/mL was reproducibly obtained in the test tubes by inoculation of 0.1 mL of a culture having an absorbance value of 0.20 as determined by optical density at 600 nm (Agilent 8453 UV-visible spectrum system, Germany) into 10 mL growth medium.

Antimicrobial performance of the materials was evaluated by using a macrodillution technique as described in the clinical and Laboratory Standards Institute (M26-A). Briefly, a small amount of the PHBV-AgNP material was

introduced in M9 Minimal Salts medium (Sigma-Aldrich, St. Louis, USA) as to achieve concentrations of 0.1, 0.5 and 1 ppm and inoculated with *S. enterica*. Control experiments with the dried polymer without AgNPs were performed under the same conditions. All samples were incubated at 37°C for 24 h. Afterwards, 0.1 mL of each one was cultivated in TSA plates and incubated for 24 h at 37°C. The biocide activity of the unpurified AgNP-PHBV powder was evaluated as synthesized (0 days) and after 40 days aging at ambient conditions. Three replicate experiments were performed for each of the samples.

The collected control and AgNPs treated cells were fixed with 2.5% glutaraldehyde and 2% osmium tetroxide for 2 h at room temperature. After eliminating the remaining glutaraldehyde and osmium tetroxide, the dehydration process was conducted with 30%, 70%, 90% and 100% of alcohol. The fixed cells were embedded with LR-White resin, and small blocks of bacteria in the resin were cut with an ultramicrotome (Leica UC6). Ultrathin sections were then positively stained with uranylacetate and lead citrate for TEM observation in a transmission electron microscope, Jeol 1010 (Hitachi) instrument, equipped with a digital Bioscan (Gatan) image acquisition system at 80 kV.

## **3. Results and discussion**

---

### **3.1 Synthesis and characterization of the PHBV**

The polymer produced from bacterial mixed culture was identify as PHBV, with a PHBV cell content of 40% (wt.-%) and a valerate and butyrate content of 18% and 82%, respectively. The amount of PHBV in the unpurified form was estimated to be 70% and it was calculated as the ratio between the total amount of HB and HV, which was

## *Chapter I*

previously determined by GC, and the total mass of the unpurified PHBV. The purity of the purified PHBV was determined to be 97%. The purified and unpurified PHBV had similar Mw and PDI values which were found to be  $\sim 3.6 \times 10^5 \text{ g mol}^{-1}$  and  $\sim 1.7$ , respectively. The protein content of unpurified and purified PHBV was 5.6% (wt.-%) and 1.7% (wt.-%) respectively.

In order to identify structural differences among the purified and the unpurified PHBV used, and how these may affect the formation and stabilization of silver nanoparticles, the unpurified and purified PHBV extracted from microbial mixed cultures were both further analyzed by FTIR (cf. Fig. 1). A characteristic strong absorption band at  $1725 \text{ cm}^{-1}$  represents the ester carbonyl C=O stretching mode. This band was somewhat more intense in the unpurified PHBV as compared to the purified PHBV, suggesting a possible interaction between amide linkage and C=O stretching band of the unpurified polymer. In fact, the FTIR spectrum of unpurified materials showed the stretching amide I band at  $1650 \text{ cm}^{-1}$ , the CN stretching and NH bending band at  $1280 \text{ cm}^{-1}$  and the stretching band of amine groups at  $3300 - 3500 \text{ cm}^{-1}$ . A similar spectrum was obtained for PHBV-AgNP materials, but the peptide linkage signals were significantly reduced in the purified PHBV. Therefore, the structural differences can be attributed to the presence of impurities from the fermentation process and are not related to the AgNPs (see the PHVB-AgNP samples of Fig. 1). Albeit the FTIR characterization, along the higher protein content measured by Lowry method's [29] support the idea that the proteins are the responsible factor for the AgNP stabilization within the polymer suspension, other components such as lipids, mineral and broth media residual components may also be present in the unpurified samples. It was not possible to identify those elements or to relate them to stabilization of silver from the existing literature, which on the other hand is relatively abundant in regard to silver -protein interactions [19, 30, 31]. It is worth to note that

the characteristic bands of the valerate copolymer were located at  $1085\text{ cm}^{-1}$  and  $1008\text{ cm}^{-1}$  in both unpurified and purified samples [32].

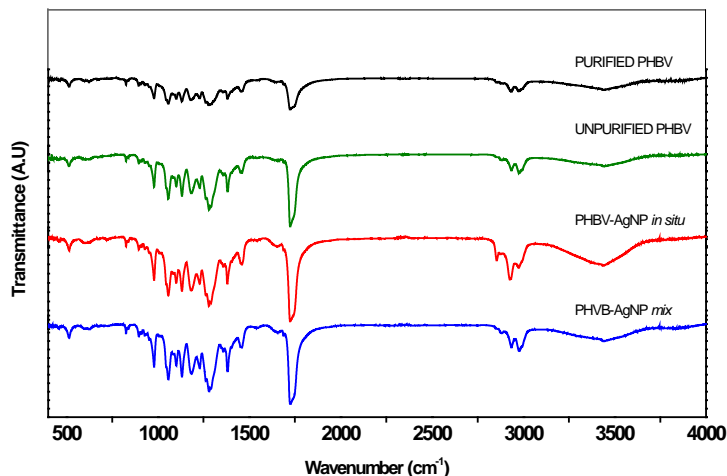


**Figure 1.** FTIR spectra of the purified and unpurified PHBV and PHBV-AgNP samples. The spectra have been shifted along the Y axis for comparative purposes.

### 3.2 Synthesis and stability of the unpurified the PHVB-AgNPs.

To analyze the effect of silver nitrate and sodium borohydride content on the silver nanoparticles synthesis, three different  $\text{AgNO}_3$ :  $\text{NaBH}_4$  ratios were used onto the same PHBV suspension:  $0.5\text{mM}$ :  $1\text{mM}$ ,  $1\text{mM}$ :  $2\text{mM}$  and  $2\text{mM}$ :  $4\text{mM}$ . The UV-VIS spectrum of these suspensions showed the characteristic silver surface plasmon resonance band with an absorption peak at  $400\text{-}420\text{ nm}$  (cf. Fig 2a, 2b). The characteristic surface resonance patterns of metal particles are known to be associated with the particle size, stabilizing molecules, surface of adsorbed particles and dielectric constant of the medium [33]. The band has been reported to shift to higher wavelengths with increased particle size [34], accompanied with a change in the colour of the suspension. Additionally, the presence of a single surface plasmon

## Chapter 1

resonance band is ascribed to spherical nanoparticles while the presence of several bands corresponds to anisotropic molecules [19]. Accordingly, monitoring the appearance, position and thickness of this band constitutes a very useful tool to roughly estimate the yield, size and size distribution.

As seen in the Fig. 2a, the intensity of the silver plasmon resonance band was found to be the highest for the AgNPs with a 2mM: 4mM ratio, which implies that the UV-visible absorption is more intense when increasing the silver nitrate and reducing agent content. However, the plasmon resonance bands of ratio 2mM: 4mM were relatively broader than those of the suspension with the ratio 1mM: 2mM, indicating agglomeration of AgNPs and/or the formation of anisotropic particles at the higher ratio. Therefore, suspensions with a 1mM: 2mM were selected to produce the unpurified PHBV-AgNP.

The stability of the silver nanoparticles in the unpurified PHBV-AgNP *in situ*, in the unpurified PHBV-AgNP *mix* suspensions as well as in the aqueous AgNPs suspensions was subsequently monitored by visual observation and using UV-VIS spectral analysis throughout 40 days., where the characteristic plasmon resonance band of the AgNPs was clearly remained over the storage time. The stability of the synthesized PHBV-AgNPs *in situ* suspensions with 1mM:2mM ratio was measured by UV-VIS after six months and no changes in absorbance or shapes of peaks was noticed (data not shown).

When the UV-VIS spectra of the PHBV-AgNPs was analyzed, slight changes in the intensity of the plasmon resonance band were observed in the PHBV-AgNP *in situ* sample before and after this aging time (cf. Fig 2b). On the contrary, PHBV-AgNP *mix* and aqueous AgNPs showed a drastic flattening of the plasmon resonance band. This indicates that the AgNPs were notably more stable when they were synthesized *in situ* within the polymer suspension, suggesting again that the unpurified PHBV may be acting as a capping agent, preventing agglomeration [21].

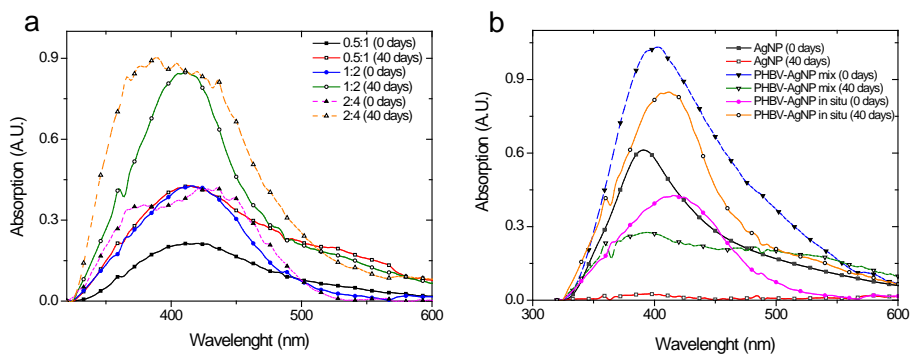


**Figure 2.** **a)** UV-VIS spectra of colloidal PHBV suspensions with AgNPs generated *in situ* as synthesized (0 days) and after 40 days aging (40 days) with different molar ratios of silver and sodium borohydride, **b)** UV-VIS spectra of colloidal PHBV-AgNP *in situ*, PHBV-AgNP mix and aqueous AgNPs.

The photographs of the suspensions showed the appearance of yellowish to brown colors that suggest the formation of AgNP both in the PHBV-AgNP *in situ*, mix and in the aqueous suspensions. After 40 days, the suspensions presented changes in their color patterns clearly associated with the stability of the AgNPs. A significant difference between AgNP *in situ*, AgNP mix and aqueous AgNPs samples was noted (cf. Fig. 3b). While the *in situ* suspensions showed a yellow color throughout the aging, the mix and aqueous AgNPs samples presented a dark yellow to brownish color. The turbidity of these suspensions gradually decreased with aging, especially in the aqueous AgNPs samples and a dark grey precipitate was formed at the bottom of the test tubes. This was clearly signaling agglomeration, followed by precipitation of silver (cf. Fig. 3c), as previously suggested by the UV-VIS results.

It has been reported that the carbonyl group from amino acid residues in proteins has a strong ability to bind metals, suggesting that the proteins and the biopolymer intermixed with them could form a solid layer capping the silver nanoparticles, thus

## Chapter 1

preventing agglomeration and, thereby, stabilizing the silver nanoparticles [35-37]. Therefore, it may be possible that the presence of cell residues or proteins present in the unpurified PHBV samples from the fermentation process may be strongly contributing to the stabilization of the AgNPs. Eliminating the residues by purification by using organic solvents may also affect the solubility of the polymer and hence its ability to stabilize AgNPs in a water suspension.

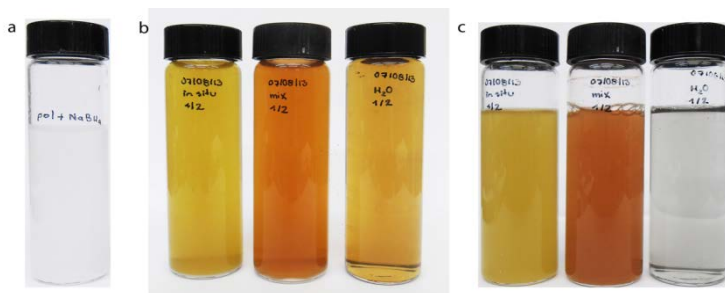


**Figure 3.** Photographs of the PHBV-AgNPs suspensions. **a)** the polymeric suspension without silver, and (from left to right) PHBV-AgNP *in situ*, PHBV-AgNP *mix* and aqueous AgNP **b)** as synthesized and **c)** after 40 days aging.

### 3.3 Characterization of the unpurified PHBV-AgNPs materials

The morphology of the PHBV-AgNPs suspensions was investigated by HR-TEM. As shown in Fig.4, spherical nanoparticles of different sizes were found in all samples. However, the particles in the *in situ* samples were considerably smaller and better distributed along the polymer matrix (cf. Fig. 4a) than in the *mix* (cf. Fig. 4b) and aqueous AgNP samples (cf. Fig. 4c). Additionally, a great amount of bigger and aggregated AgNPs in *mix* samples were observed, suggesting that mere physical mixing is not adequate to procure efficient capping of the nanoparticles by the polymer (cf. Fig. 4b). The HR-TEM images of the *in situ* samples (cf. inset Fig. 4a) showed the presence of small crystalline particles with an electron lighter, amorphous edge of about 2nm, which is ascribed to the biopolymer capping. Additionally, bigger

particles exhibiting dislocations and other defects in the crystal lattice were detected by HR-TEM in the *mix* samples (c.f Fig. 4b). In the case of AgNPs synthesized without the polymer (aqueous AgNPs), bigger agglomerates of AgNPs were found (cf. Fig. 4c). This would again support the higher stability of the nanoparticles in the *in situ* samples in accordance with the UV analysis.

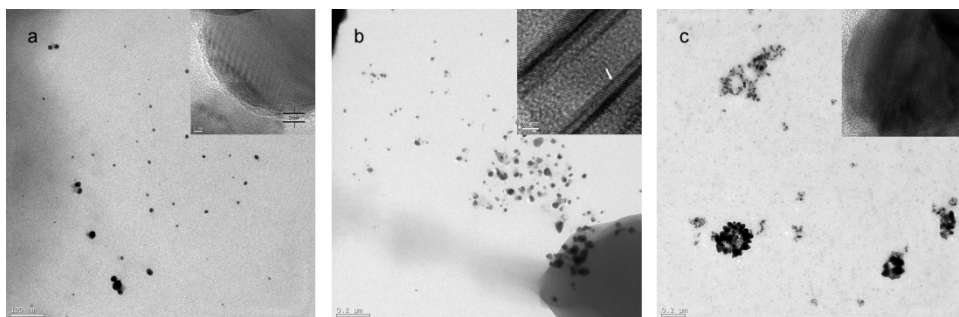


**Figure 4.** HR-TEM images of PHBV-AgNP and AgNPs suspensions. **a)** PHBV-AgNP *in situ*, **b)** PHBV-AgNP *mix* and **c)** aqueous AgNPs. The insets show a higher magnification highlighting the atomic organization. Inset in (a) displays an electron lighter, amorphous edge of about 2nm in the *in situ* sample. Arrow in the inset in (b) indicates the dislocation of lattice plane fringes in the *mix* sample.

Energy-dispersive X-Ray Spectroscopy (EDX) analysis coupled to HR-TEM indicated silver as the component in the nanoparticles. In the crystals was possible to calculate the experimental lattice constant ( $a$ ), see Table 1, and to observe the lattice plane fringes (cf. Fig. 5). The fringe spacing corresponds well with that of the (1 1 1) and (2 0 0) lattice spacing of Ag and suggests a face centered cubic structure (FCC) as expected. These results are in agreement with the Standard Powder Diffraction card of Joint Committee on Powder Diffraction Standard (JCPDS), silver file No. 04-783 ( $a=4.086\text{\AA}$ ) and in line with previous experimental reports [38, 39]. For instance, Theivasanthi and Alagar reported similar crystalline structures using silver

## Chapter 1

nanopowder made by electrolytic synthesis [40]. Similar results were found by Kalpana et al. working with AgNPs obtained from *Klebsiella pneumoniae* [19].

**Table 1.** Experimental crystal lattice parameters of AgNP materials.

h k l	Sample	d-spacing (nm)	Lattice parameter (a) Å
(1 1 1)	PHBV-AgNP <i>in situ</i>	0.235 ± 0.002	4.08
	PHBV-AgNP <i>mix</i>	0.235 ± 0.004	4.07
	Aqueous AgNP	0.236 ± 0.004	4.07
(2 0 0)	PHBV-AgNP <i>in situ</i>	0.203 ± 0.001	4.06
	PHBV-AgNP <i>mix</i>	0.203 ± 0.004	4.06
	Aqueous AgNP	0.204 ± 0.002	4.08

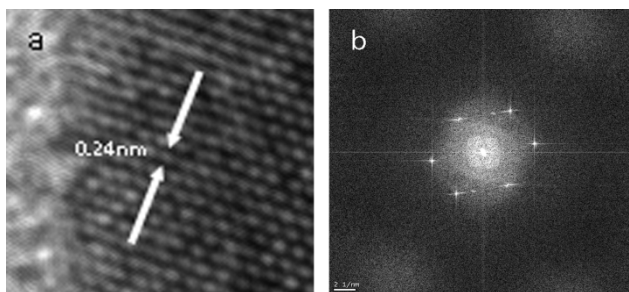


**Figure 5.** HR-TEM image of a synthesized AgNPs, **a)** Image of the lattice plane fringe with spacing of 0.24nm and **b)** of the corresponding diffractogram.

As mentioned before, the AgNPs in the *mix* and aqueous suspensions were found to be more heterogeneous in size and they were clearly more agglomerated than in the *in situ* samples. These changes are reflected in the size distribution of the particles (cf. Fig. 6). The mean particle diameter of the PHBV-AgNP *in situ*, PHBV-AgNP *mix* and aqueous AgNPs suspension were  $11 \pm 5.6$  nm,  $23 \pm 10.2$  nm and  $17 \pm 14.4$  nm, respectively. A narrower size distribution was observed in the *in situ* samples, with a maximum frequency at around 5nm. This is notably different as compared to the size distribution of nanoparticles in PHBV-AgNP *mix* and aqueous AgNPs suspension, where bigger particles and greater mean diameter standard deviations were found.

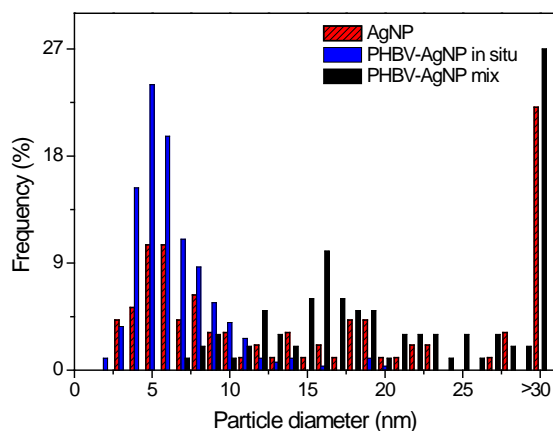


**Figure 6.** Size distribution of AgNPs, PHBV-AgNP *in situ* and PHBV-AgNP *mix*.

The total silver content retained within the biopolymers, after centrifugation and drying was analyzed by ICP-MS. A silver content of 226 mg Kg<sup>-1</sup> and 73.5 mg Kg<sup>-1</sup> was reported for the *in situ* and *mix* preparations, respectively. These results further confirm the excellent capacity of unpurified PHBV to retain and to stabilize the silver nanoparticles, especially when they were synthesized within the polymer suspension. Although scarce literature is found about the incorporation of silver nanoparticles into PHA's, recent reports have shown that hydrophobic PHA obtained from *Bacillus circulans* (MTCC 8167) can stabilize silver nanoparticles for 30 days, providing an anchoring surface for their immobilization [21]. In this regard, in addition to PHA's, several surfactants like cetyltrimethylammoniumbromide (CTAB) [41], Tween [42], or SDS [43], among others have been used to stabilize nanoparticles in suspension. Additionally, other natural and synthetic polymers, mostly water soluble, such as, polyvinyl alcohol (PVOH) [44], chitosan [45] [46], cellulose [47], etc, have also been reported to cap and stabilize silver nanoparticles or even act as reducing agents.

The stability of AgNPs in unpurified PHBV matrix during the analyzed aging time was higher or similar than other reported stabilizing agents. For instance,

## Chapter I

Bankura et. al [48] and Mukherjee and Mahapatra [42] observed that AgNP were successfully stabilized for 30 days in dextran and Tween matrices, respectively. More recently, the synthesis of AgNP in water-soluble polysaccharide matrices extracted from four marine macro-algae as reducing agents for silver ions as well as stabilizing agents for the synthesized AgNP has been reported by El-Rafie [35]. They observed that AgNP were stabilized in these polysaccharide matrices for six months.

It is worth to note that one of the most advantages of synthesizing AgNPs within the unpurified PHBV suspension (*in situ*) is that it can be subjected to the temperature typical for polymeric materials processing methods even at high temperatures. Furthermore, the so-prepared materials have a homogeneous distribution of the small nanoparticles within the polymeric matrix that can provide it a strong and durable antibacterial or antibiofilm properties. The immobilization of the AgNPs onto PHBV can prevent any movement of the nanoparticles, not only decreasing the effects of agglomeration and but also increasing the material's biocompatibility, specially due to the biopolymer layer that might be acting as capping agent, which might reduce the cytotoxicity of AgNP for human cells and for the environment. Therefore, all these additional features can promote the application of AgNP in several industrial fields.

### 3.4 Antimicrobial activity of PHBV-AgNPs

As mentioned before, one of the key areas of implementation of metal-based antimicrobial biopolymers is in the active food packaging. The incorporation of stable AgNPs within the polymeric matrix can make the polymers processing easier, while at the same time it can provide a powerful biocide effect against the growth of pathogenic and spoilage microorganism, preventing and/or indicating the migration of contaminants while maintaining or even improving their nutritional quality and ensuring food safety [49]. Between food-borne pathogens, *Salmonella spp.* is one of the

most common and widely distributed microorganisms, with ten millions of human Salmonellosis cases occurring worldwide every year [26-28] and with high levels of multi-drug resistance [50].

The antimicrobial activity of unpurified PHBV-AgNPs against *Salmonella enterica* was found to be dependent not only on the type of suspension where the nanoparticles were synthesized but also on the unpurified PHBV-AgNPs content. Furthermore, significant differences in efficacy were noted in some samples when the materials were tested after 40 days of aging. When the materials were tested after the synthesis, a substantial reduction (>99%) of the bacterial population was registered in all samples having unpurified PHBV-AgNPs content of 0.5 and 1 ppm (cf. Fig. 7). When 0.1 ppm of the unpurified PHBV-AgNPs was added, only the *in situ* samples showed antibacterial performance (>90% reduction in bacterial viability), whereas in *mix* samples no significant differences were found as compared to the controls without silver.

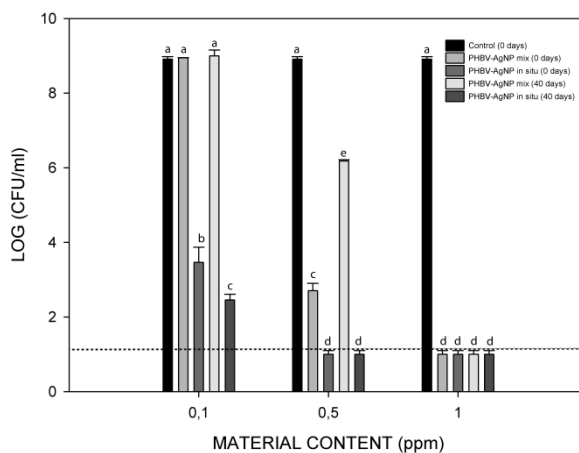


**Figure 7.** Antimicrobial activity of as synthesized (0 days) and 40 days aged PHBV-AgNP powder against *Salmonella enterica* CECT 554 after 24h exposure. The dashed line depicts the detection limit. Mean values with different letters represent significant differences ( $p < 0.05$ ) among the samples as determined with a one-way analysis of variance (ANOVA) and Tukey's multiple comparison tests.

## Chapter 1

After 40 days of aging, the antimicrobial performance of the unpurified PHBV-AgNP *in situ* samples was not significantly reduced for any of the tested concentrations. However, 0.5 ppm of the aged unpurified PHBV-AgNP mix samples showed significantly lower antibacterial performance as compared to readily prepared material. This fact supports the idea that the polymer suspension may contribute to further stabilize the AgNPs when they are produced *in situ* within the polymer matrix.

The unpurified PHBV-AgNPs, displayed a higher antimicrobial performance so far in the literature reports; only 1 ppm of the polymer powder containing AgNP (with 22.6 wt.-% of silver) inhibited completely the growth of *Salmonella enterica*, even at lower concentration. For instance, De Faria et al. [51] achieved a completed inhibition of *S. typhimurium* with 2.0 ppm using graphene oxide and AgNPs hybrid material. Kalpana et al. [19] synthesized AgNPs from *Klebsiella pneumoniae* grown in a complex simulated microgravity system and found bactericidal effect against *Salmonella enterica* at range of 50-100 ppm. Noh et al. [52] prepared AgNPs employing carbohydrate as sialyllactose sucrose, and trehalose to increase the stability of silver nanoparticles. They obtained a minimum inhibitory concentration of 16 ppm for *Salmonella typhimurium*.

It is known that the size and shape of the silver nanoparticles plays an important role in their antimicrobial activity. Several mechanisms have been proposed to explain the biocide properties of silver, being generally accepted that the antimicrobial activity of AgNPs increases with decreasing particle size, on the grounds that smaller sized particles can easily pass through the bacterial membrane pores and interact with cell membrane components [32, 53]. This feature gives them a strong protein binding capability to inactivate enzymes of the respiratory chain and cell division machinery [54].

The biocide effect of most metal nanoparticles has been reported to depend on their stability and resistance to agglomeration and aggregation [17, 55]. Considering these issues, the increase in the antimicrobial activity of the *in situ* samples may be related with (1) the silver content within polymer, which was three times higher according to ICP-MS analysis, (2) the smaller size of nanoparticles as reflected by HR-TEM analysis and (3) a better stability of surface plasmon resonance band during the aging time in comparison with the mix samples as observed from the UV-Vis results. The combination of these factors might explain the greater and more prolonged antimicrobial performance of *in situ* samples as compared with mix samples and other AgNP preparation reported in the literature.

Some studies report that a better surface stabilization is in direct relation to the observed highest antibacterial activity, as the AgNPs could be separated from each other by the polymer chains. Therefore, the non-aggregated particles could strongly interact with the cell wall because of their high surface energy and mobility that are not lowered by the formation of aggregates [43].

The morphological changes in *Salmonella enterica* after 24 h exposure to 0.1ppm of unpurified PHBV-AgNP *in situ* was further examined using TEM. Untreated bacterial cells retained their original shape and seemed to have regular morphology (cf. Fig. 8a). In contrast, cells treated with unpurified PHBV-AgNP *in situ* were completely lysed and broken (cf. Fig. 8b). An electron-light region appeared in the center of the treated cells (indicated by asterisk in Fig. 8b) which was not present in the untreated cells. This may be related to lysis of the cell components within cytoplasm as reported by Grigor'eva [54]. These significant morphological changes are in line with previous reports involving TEM analysis of bacteria damaged by AgNPs [9, 54, 56, 57].

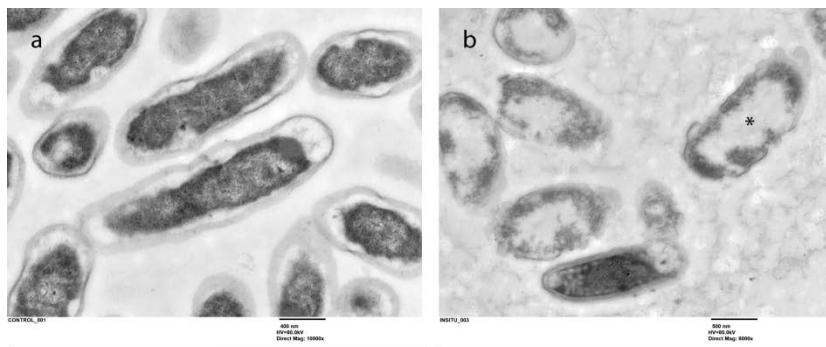


**Figure 8.** TEM image of *Salmonella enterica* treated after 24h of incubation. **a)** Untreated cells, **b)** Cells treated with 0.1ppm of PHBV-AgNP *in situ*, **c)** Cells treated with 0.1ppm of PHBV-AgNP *mix*. The electron light region in the center is highlighted with an asterisk, **d)** Detail of detachment and rupture of the membrane cell and small aggregation of silver nanoparticles was seen on the outer membrane (indicated with an arrow).

## 4. Conclusions

---

The unique capacity of PHBV from mixed cultures to stabilize silver nanoparticles prepared *in situ* within the biopolymer suspensions was demonstrated. A renewable material containing well dispersed and distributed crystalline and small AgNPs were obtained by a simple method. The nanoparticles stability was ascribed to the presence of protein residues within the biopolymer. Moreover, the biopolymer stabilized AgNPs exhibited a very strong antimicrobial activity that is of great promise in the design of antibacterial surfaces in various applications.

## 5. Acknowledgements

---

The authors wish to thank the Spanish Ministry of Economy and competitiveness (MAT2012-38947-C02-01) and to the Fundação para a Ciência e a Tecnologia (SFRH/BPD/88817/2012) for financial support. J.L. Castro-Mayorga was supported by the Departamento Administrativo de Ciencia, Tecnología e Innovación (Colciencias) of Colombian Government. M. J. Fabra was recipient of a Juan de la Cierva contract from the Spanish Ministry of Economy and Competitiveness.

We would also like to thank the “Servicios Centrales de Soporte a la Investigación Experimental, Sección de Microscopia” from the University of Valencia for technical support. Dr. A. Lopez-Rubio is acknowledged for assistance in the preparation of the manuscript.

## 6. References

---

1. B. H. A. Rehm, "Polyester synthases: Natural catalysts for plastics," *Biochemical Journal*, vol. 376, no. 1, pp. 15-33, 2003.
2. M. A. M. Reis, L. S. Serafim, P. C. Lemos, A. M. Ramos, F. R. Aguiar and M. C. M. Van Loosdrecht, "Production of polyhydroxyalkanoates by mixed microbial cultures," *Bioprocess and Biosystems Engineering*, vol. 25, no. 6, pp. 377-385, 2003.
3. L. S. Serafim, P. C. Lemos, R. Oliveira and M. A. M. Reis, "Optimization of polyhydroxybutyrate production by mixed cultures submitted to aerobic dynamic feeding conditions," *Biotechnology and Bioengineering*, vol. 87, no. 2, pp. 145-160, 2004.
4. B. Laycock, P. Halley, S. Pratt, A. Werker and P. Lant, "The chemomechanical properties of microbial polyhydroxyalkanoates," *Progress in Polymer Science*, vol. 38, no. 3-4, pp. 536-583, 2013.

## Chapter I

5. S. Khanna and A. K. Srivastava, "Recent advances in microbial polyhydroxyalkanoates," *Process Biochemistry*, vol. 40, no. 2, pp. 607-619, 2005.
6. N. Jacquet, C.-W. Lo, Y.-H. Wei, H.-S. Wu and S. S. Wang, "Isolation and purification of bacterial poly(3-hydroxyalkanoates)," *Biochemical Engineering Journal*, vol. 39, no. 1, pp. 15-27, 2008.
7. M. G. E. Albuquerque, C. A. V. Torres and M. A. M. Reis, "Polyhydroxyalkanoate (PHA) production by a mixed microbial culture using sugar molasses: Effect of the influent substrate concentration on culture selection," *Water Research*, vol. 44, no. 11, pp. 3419-3433, 2010.
8. N. Guriëff and P. Lant, "Comparative life cycle assessment and financial analysis of mixed culture polyhydroxyalkanoate production," *Bioresource Technology*, vol. 98, no. 17, pp. 3393-3403, 2007.
9. W. K. Jung, H. C. Koo, K. W. Kim, S. Shin, S. H. Kim and Y. H. Park, "Antibacterial activity and mechanism of action of the silver ion in *Staphylococcus aureus* and *Escherichia coli*," *Appl Environ Microbiol*, vol. 74, no. 7, pp. 2171-2178, 2008.
10. T. Keshavarz and I. Roy, "Polyhydroxyalkanoates: bioplastics with a green agenda," *Current Opinion in Microbiology*, vol. 13, no. 3, pp. 321-326, 2010.
11. Z. C. Xing, W. P. Chae, J. Y. Baek, M. J. Choi, Y. Jung and I. K. Kang, "In vitro assessment of antibacterial activity and cytocompatibility of silver-containing phbv nanofibrous scaffolds for tissue engineering," *Biomacromolecules*, vol. 11, no. 5, pp. 1248-1253, 2010.
12. T. V. Ojumu, J. Yu and B. O. Solomon, "Production of Polyhydroxyalkanoates, a bacterial biodegradable polymer," *African Journal of Biotechnology*, vol. 3, no. 1, pp. 18-24, 2004.
13. A. D. Russell and W. B. Hugo, "7 Antimicrobial Activity and Action of Silver," Ed., pp. 351-370, 1994.
14. L. S. Nair and C. T. Laurencin, "Silver nanoparticles: Synthesis and therapeutic applications," *Journal of Biomedical Nanotechnology*, vol. 3, no. 4, pp. 301-316, 2007.
15. J. Tian, K. K. Y. Wong, C. M. Ho, C. N. Lok, W. Y. Yu, C. M. Che, J. F. Chiu and P. K. H. Tam, "Topical delivery of silver nanoparticles promotes wound healing," *ChemMedChem*, vol. 2, no. 1, pp. 129-136, 2007.
16. A. Martinez-Abad, "Silver- and nanosilver-based plastic technologies " in *Antimicrobial Polymers*, J. Lagarón, M. J. Ocio and A. Lopez-Rubio, Ed., pp. 287-316, John Wiley and sons inc., Hoboken, New jersey, 2010.

17. V. J. Schacht, L. V. Neumann, S. K. Sandhi, L. Chen, T. Henning, P. J. Klar, K. Theophel, S. Schnell and M. Bunge, "Effects of silver nanoparticles on microbial growth dynamics," *Journal of Applied Microbiology*, vol. 114, no. 1, pp. 25-35, 2013.
18. M. Rai, A. Yadav and A. Gade, "Silver nanoparticles as a new generation of antimicrobials," *Biotechnology Advances*, vol. 27, no. 1, pp. 76-83, 2009.
19. D. Kalpana and Y. S. Lee, "Synthesis and characterization of bactericidal silver nanoparticles using cultural filtrate of simulated microgravity grown *Klebsiella pneumoniae*," *Enzyme and Microbial Technology*, vol. 52, no. 3, pp. 151-156, 2013.
20. M. Moritz and M. Geszke-Moritz, "The newest achievements in synthesis, immobilization and practical applications of antibacterial nanoparticles," *Chemical Engineering Journal*, vol. 228, pp. 596-613, 2013.
21. P. Phukon, J. P. Saikia and B. K. Konwar, "Enhancing the stability of colloidal silver nanoparticles using polyhydroxyalkanoates (PHA) from *Bacillus circulans* (MTCC 8167) isolated from crude oil contaminated soil," *Colloids Surf B Biointerfaces*, vol. 86, no. 2, pp. 314-318, 2011.
22. F. D. Kopinke, M. Remmler and K. Mackenzie, "Thermal decomposition of biodegradable polyesters - I: Poly( $\beta$ -hydroxybutyric acid)," *Polymer Degradation and Stability*, vol. 52, no. 1, pp. 25-38, 1996.
23. K. J. Kim, Y. Doi and H. Abe, "Effects of residual metal compounds and chain-end structure on thermal degradation of poly(3-hydroxybutyric acid)," *Polymer Degradation and Stability*, vol. 91, no. 4, pp. 769-777, 2006.
24. L. S. Serafim, P. C. Lemos, C. Torres, M. A. M. Reis and A. M. Ramos, "The Influence of Process Parameters on the Characteristics of Polyhydroxyalkanoates Produced by Mixed Cultures," *Macromolecular Bioscience*, vol. 8, no. 4, pp. 355-366, 2008.
25. M. Martínez-Sanz, R. T. Olsson, A. Lopez-Rubio and J. M. Lagaron, "Development of bacterial cellulose nanowhiskers reinforced EVOH composites by electrospinning," *Journal of Applied Polymer Science*, vol. 124, no. 2, pp. 1398-1408, 2012.
26. World Health Organization. WHO Food Safety. Fact Sheet No. 139. August 2013. Available at <http://www.who.int/mediacentre/factsheets/fs139/en/> (accessed 15.05.2014).
27. European Food Safety Authority. National Food Institute Technical University of Denmark. S. Pares, L. De Knegt, T. Hald. July 2011. Available at [http://orbit.dtu.dk/fedora/objects/orbit:119559/datastreams/file\\_729eaa5a-b742-430d-883d-3429a840c73f/content](http://orbit.dtu.dk/fedora/objects/orbit:119559/datastreams/file_729eaa5a-b742-430d-883d-3429a840c73f/content) (accessed 15.05.2014).

## Chapter I

28. European Centre for Disease Prevention and Control, EFSA J. 12 (3) (2014) 3590, Available at <http://www.efsa.europa.eu/en/efsajournal/doc/3547.pdf> (accessed 15.05.2014).
29. O. H. Lowry, N. J. Rosebrough, A. L. Farr and R. J. Randall, "Protein measurement with the Folin phenol reagent," *The Journal of biological chemistry*, vol. 193, no. 1, pp. 265-275, 1951.
30. A. Martínez-Abad, M. J. Ocio, J. M. Lagarón and G. Sánchez, "Evaluation of silver-infused polylactide films for inactivation of Salmonella and feline calicivirus in vitro and on fresh-cut vegetables," *International Journal of Food Microbiology*, vol. 162, no. 1, pp. 89-94, 2013.
31. S. Gurunathan, K. Kalishwaralal, R. Vaidyanathan, D. Venkataraman, S. R. Pandian, J. Muniyandi, N. Hariharan and S. H. Eom, "Biosynthesis, purification and characterization of silver nanoparticles using Escherichia coli," *Colloids Surf B Biointerfaces*, vol. 74, no. 1, pp. 328-335, 2009.
32. T. M. Tolaymat, A. M. El Badawy, A. Genaidy, K. G. Scheckel, T. P. Luxton and M. Suidan, "An evidence-based environmental perspective of manufactured silver nanoparticle in syntheses and applications: A systematic review and critical appraisal of peer-reviewed scientific papers," *Science of The Total Environment*, vol. 408, no. 5, pp. 999-1006, 2010.
33. C. Krishnaraj, E. G. Jagan, S. Rajasekar, P. Selvakumar, P. T. Kalaichelvan and N. Mohan, "Synthesis of silver nanoparticles using Acalypha indica leaf extracts and its antibacterial activity against water borne pathogens," *Colloids and Surfaces B: Biointerfaces*, vol. 76, no. 1, pp. 50-56, 2010.
34. V. K. Sharma, R. A. Yngard and Y. Lin, "Silver nanoparticles: Green synthesis and their antimicrobial activities," *Advances in Colloid and Interface Science*, vol. 145, no. 1-2, pp. 83-96, 2009.
35. H. M. El-Rafie, M. H. El-Rafie and M. K. Zahran, "Green synthesis of silver nanoparticles using polysaccharides extracted from marine macro algae," *Carbohydr Polym*, vol. 96, no. 2, pp. 403-410, 2013.
36. A. Kanchana, I. Agarwal, S. Sunkar, J. Nellore and K. Namasivayam, "Biogenic silver nanoparticles from Spinacia oleracea and Lactuca sativa and their potential antimicrobial activity," *Digest Journal of Nanomaterials and Biostructures*, vol. 6, no. 4, pp. 1741-1750, 2011.
37. T. Mochochoko, O. S. Oluwafemi, D. N. Jumbam and S. P. Songca, "Green synthesis of silver nanoparticles using cellulose extracted from an aquatic weed; water hyacinth," *Carbohydr Polym*, vol. 98, no. 1, pp. 290-294, 2013.

38. G. Jiang, M. Wang, X. Gu, T. Chen, Y. Shang, Y. Tang, G. Jiang and Y. Shi, "Synthesis, structure and characterization of Fe<sub>6</sub> molecular clusters with peripheral sulfur atom-capped silver nanoparticles," *CrystEngComm*, vol. 16, no. 3, pp. 472-478, 2014.
39. H. Hofmeister, G. L. Tan and M. Dubiel, "Shape and internal structure of silver nanoparticles embedded in glass," *Journal of Materials Research*, vol. 20, no. 6, pp. 1551-1562, 2005.
40. T. Theivasanthi and M. Alagar, "Electrolytic synthesis and characterization of silver nanopowder," *Nano Biomedicine and Engineering*, vol. 4, no. 2, pp. 58-65, 2012.
41. S. A. Al-Thabaiti, F. M. Al-Nowaiser, A. Y. Obaid, A. O. Al-Youbi and Z. Khan, "Formation and characterization of surfactant stabilized silver nanoparticles: A kinetic study," *Colloids and Surfaces B: Biointerfaces*, vol. 67, no. 2, pp. 230-237, 2008.
42. M. Mukherjee and A. Mahapatra, "Catalytic effect of silver nanoparticle on electron transfer reaction: Reduction of [Co(NH<sub>3</sub>)<sub>5</sub>Cl](NO<sub>3</sub>)<sub>2</sub> by iron(II)," *Colloids and Surfaces A: Physicochemical and Engineering Aspects*, vol. 350, no. 1-3, pp. 1-7, 2009.
43. L. Kvítek, A. Panáček, J. Soukupová, M. Kolář, R. Večeřová, R. Prucek, M. Holecová and R. Zbořil, "Effect of surfactants and polymers on stability and antibacterial activity of silver nanoparticles (NPs)," *Journal of Physical Chemistry C*, vol. 112, no. 15, pp. 5825-5834, 2008.
44. R. Bryaskova, D. Pencheva, M. Kyulavska, D. Bozukova, A. Debuigne and C. Detrembleur, "Antibacterial activity of poly(vinyl alcohol)-b-poly(acrylonitrile) based micelles loaded with silver nanoparticles," *Journal of Colloid and Interface Science*, vol. 344, no. 2, pp. 424-428, 2010.
45. R. J. Pinto, S. C. Fernandes, C. S. Freire, P. Sadocco, J. Causio, C. P. Neto and T. Trindade, "Antibacterial activity of optically transparent nanocomposite films based on chitosan or its derivatives and silver nanoparticles," *Carbohydr Res*, vol. 348, pp. 77-83, 2012.
46. S. Boufi, M. R. Vilar, A. M. Ferraria and A. M. Botelho do Rego, "In situ photochemical generation of silver and gold nanoparticles on chitosan," *Colloids and Surfaces A: Physicochemical and Engineering Aspects*, vol. 439, no. 0, pp. 151-158, 2013.
47. E. Fortunati, S. Rinaldi, M. Peltzer, N. Bloise, L. Visai, I. Armentano, A. Jiménez, L. Latterini and J. M. Kenny, "Nano-biocomposite films with modified cellulose nanocrystals and synthesized silver nanoparticles," *Carbohydrate Polymers*, vol. 101, no. 0, pp. 1122-1133, 2014.
48. K. P. Bankura, D. Maity, M. M. R. Mollick, D. Mondal, B. Bhowmick, M. K. Bain, A. Chakraborty, J. Sarkar, K. Acharya and D. Chattopadhyay, "Synthesis,

## Chapter I

characterization and antimicrobial activity of dextran stabilized silver nanoparticles in aqueous medium," *Carbohydrate Polymers*, vol. 89, no. 4, pp. 1159-1165, 2012.

49. M. Ozdemir and J. D. Floros, "Active food packaging technologies," *Critical Reviews in Food Science and Nutrition*, vol. 44, no. 3, pp. 185-193, 2004.

50. C. f. D. C. a. Prevention.

51. A. F. De Faria, A. C. M. De Moraes, P. D. Marcato, D. S. T. Martinez, N. Durán, A. G. S. Filho, A. Brandelli and O. L. Alves, "Eco-friendly decoration of graphene oxide with biogenic silver nanoparticles: Antibacterial and antibiofilm activity," *Journal of Nanoparticle Research*, vol. 16, no. 2, 2014.

52. H. J. Noh, A. R. Im, H.-S. Kim, J. K. Sohng, C.-K. Kim, Y. S. Kim, S. Cho and Y. Park, "Antibacterial Activity and Increased Freeze-Drying Stability of Sialyllactose-Reduced Silver Nanoparticles Using Sucrose and Trehalose," *Journal of Nanoscience and Nanotechnology*, vol. 12, no. 5, pp. 3884-3895, 2012.

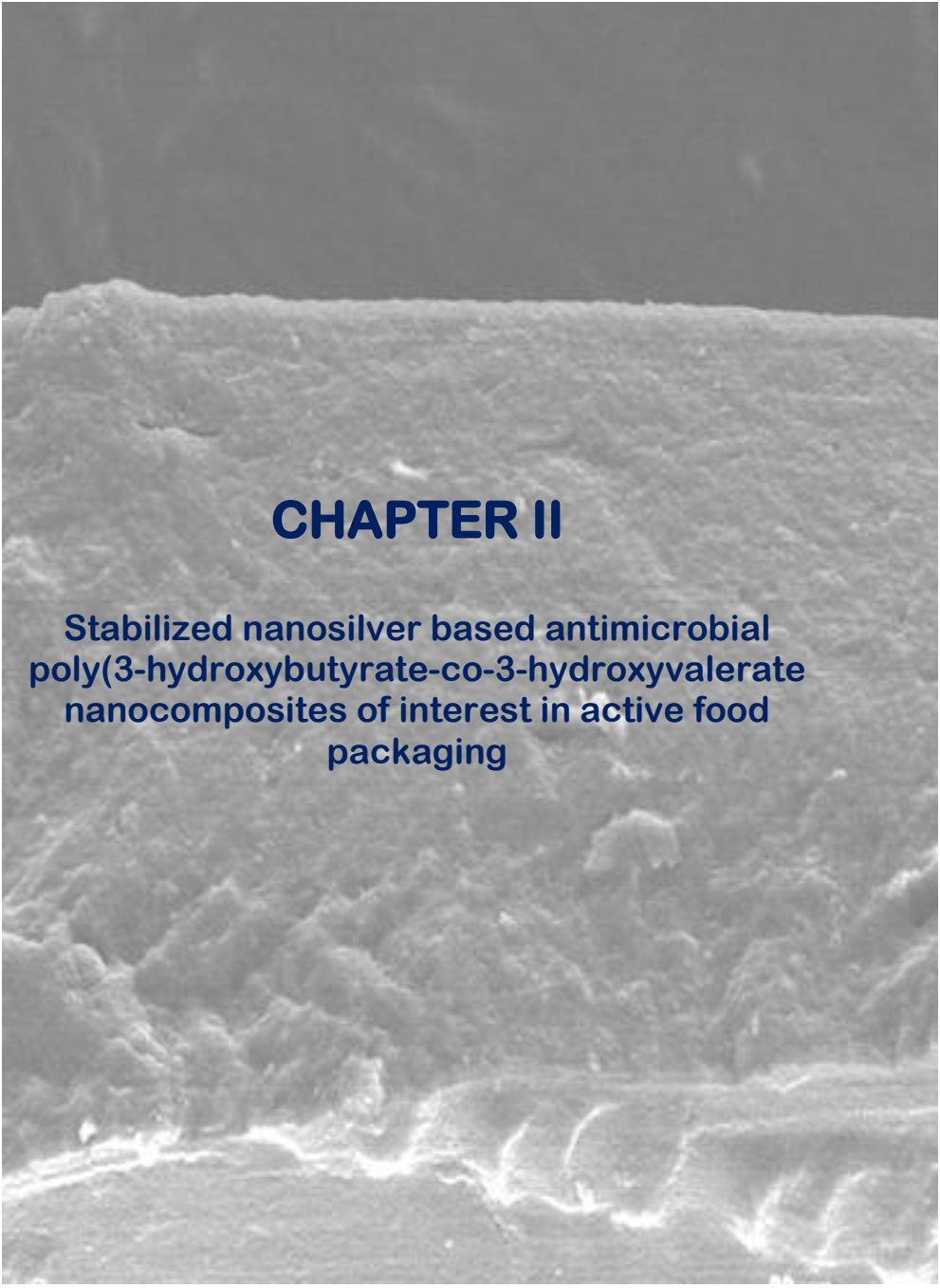
53. P. Kanmani and S. T. Lim, "Synthesis and structural characterization of silver nanoparticles using bacterial exopolysaccharide and its antimicrobial activity against food and multidrug resistant pathogens," *Process Biochemistry*, vol. 48, no. 7, pp. 1099-1106, 2013.

54. A. Grigor'Eva, I. Saranina, N. Tikunova, A. Safonov, N. Timoshenko, A. Rebrov and E. Ryabchikova, "Fine mechanisms of the interaction of silver nanoparticles with the cells of *Salmonella typhimurium* and *Staphylococcus aureus*," *BioMetals*, vol. 26, no. 3, pp. 479-488, 2013.

55. E. Bae, H.-J. Park, J. Lee, Y. Kim, J. Yoon, K. Park, K. Choi and J. Yi, "Bacterial cytotoxicity of the silver nanoparticle related to physicochemical metrics and agglomeration properties," *Environmental Toxicology and Chemistry*, vol. 29, no. 10, pp. 2154-2160, 2010.

56. Q. L. Feng, J. Wu, G. Q. Chen, F. Z. Cui, T. N. Kim and J. O. Kim, "A mechanistic study of the antibacterial effect of silver ions on *Escherichia coli* and *Staphylococcus aureus*," *Journal of Biomedical Materials Research*, vol. 52, no. 4, pp. 662-668, 2000.

57. J. Y. Kim, C. Lee, M. Cho and J. Yoon, "Enhanced inactivation of *E. coli* and MS-2 phage by silver ions combined with UV-A and visible light irradiation," *Water Res*, vol. 42, no. 1-2, pp. 356-362, 2008.

The background of the page is a grayscale scanning electron micrograph (SEM) showing a highly textured, porous surface. The texture consists of irregular, interconnected structures that resemble a sponge or a network of fibers. The lighting creates highlights and shadows, emphasizing the three-dimensional nature of the material. The overall appearance is that of a complex, porous nanocomposite structure.

## CHAPTER II

### Stabilized nanosilver based antimicrobial poly(3-hydroxybutyrate-co-3-hydroxyvalerate) nanocomposites of interest in active food packaging

J. L. Castro-Mayorga, M. J. Fabra and J. M. Lagaron, "Stabilized nanosilver based antimicrobial poly(3-hydroxybutyrate-co-3-hydroxyvalerate) nanocomposites of interest in active food packaging". *Innovative Food Science and Emerging Technologies*, vol. 33, pp. 524-533, 2016.



## Abstract

---

Antimicrobial silver based nanocomposites of poly(3-hydroxybutyrate-co-3-hydroxyvalerate) were successfully synthesized and characterized. For the synthesis, a masterbatch of *in situ* stabilized silver nanoparticles (AgNPs) produced into a mixed microbial cultures based poly(3-hydroxybutyrate-co-18 mol%- 3-hydroxyvalerate) (PHBV18) was used, which was diluted by melt compounding with a commercial poly(3-hydroxybutyrate-co-3 mol%- 3-hydroxyvalerate) (PHBV3) material. The incorporated AgNPs (0.04 wt.-%) led to a surprising oxygen permeability drop of *ca.* 56% compared to the neat polymer. The thermal stability and optical properties of the nanocomposites were not significantly modified as compared to the neat PHBV3. Moreover, the antimicrobial performance of the PHBVs-AgNPs films against two of the most common food borne pathogens, *Salmonella enterica* and *Listeria monocytogenes*, showed a strong and sustained (even after seven-months) antibacterial activity. This study provides an innovative route to generate fully renewable and biodegradable antimicrobial nanocomposites that could potentially be of interest in film and coating applications such as active food packaging.

## Keywords

---

Polyhydroxyalkanoates, Silver nanoparticles, Antimicrobials, Active packaging.

## **1. Introduction**

---

With a continuous growth for more than 50 years and a worldwide production of more than 250 million tonnes per year, plastics are the base of many products typically used, being packaging the largest sector of application for the plastics industry [1]. Most plastics are primarily synthesized from petroleum derived compounds. However, these finite petroleum reserves will progressively decline. The eventually growing gap between supply and demand as well as the greenhouse gas emissions, and the saturation of landfill sites with plastic waste has steered research toward the development of green polymeric materials.

Polyhydroxyalkanoates (PHA) have recently attracted much attention as an alternative to petroleum-based materials. PHA are polymers synthesized by a wide range of microorganisms as carbon storage material [2]. Nowadays, PHA have still economic shortcomings that limit their use. The major drawbacks of PHA production are the high cost of raw materials (mainly carbon source), low yield, low productivity and the high cost of the down-stream process [3, 4]. To reduce cost production, researchers have targeted the synthesis of PHA through fermentation from by-products and wastes. In fact, low cost processes, such as the use of mixed microbial cultures, have recently been developed. Their use offers several advantages compared with the pure-cultures fermentation, as sterile conditions are not required and cheap or even free substrates, like industrial waste material or by-products, may be used [5].

One of the most extensively studied polymers from the PHA group is poly(3-hydroxybutyrate), PHB. However, PHB is partially crystalline with a high melting temperature, high degree of crystallinity and high rigidity. To overcome these aspects, the copolymer obtained with the insertion of 3-hydroxyvalerate (HV) units, known as poly(3-hydroxybutyrate-co-3-hydroxyvalerate), PHBV, is usually used to improve

handling properties of PHB films. PHBV has greater flexibility and reduced melting temperature without reducing the thermal stability of the material, hence widening the processing window of the PHBV [6]. One of the main disadvantages arising from the use of PHBV is probably the fact that they are more permeable to low molecular weight compounds, thus allowing more freely the passage of gases, water vapour and aroma components that could compromise food quality and safety [7]. This negative aspect can be converted into a positive one for the development of active packaging technologies where controlled release migration is sought.

Scientific researchers have been focused lately on the development and characterization of active composites based on the addition of silver as antimicrobial agent into polymer matrices. There are different strategies to incorporate silver ions and silver nanoparticles (AgNPs) into polymeric matrices, either by adding them directly by solvent casting [8-12], melt-compounding [13-15] and injection moulding techniques [16] or by making a fibrous membrane containing the active agents [17, 18]. However, silver is a rather unstable metal that undergoes colour changes triggered by environmentally-induced reduction and/or agglomeration. Therefore, one of the major challenges is to prepare a dispersed system with the required stability and resistance to the action of external factors, such as the high processing temperatures usually required in conventional plastic processing machinery. Consequently, the addition of silver into polymeric materials imply a preliminary step in which the steric and electrostatic stabilization of the active agent will be guaranteed by coating them with surface active agents such as polymers (e.g. poly(vinyl alcohol), poly(ethylene glycol) and polyvinylpyrrolidone) and non-ionic surfactants (e.g. Tween and Triton X-100) or by incorporating ionic surfactants (e.g. sodium dodecyl sulfate, cetyltrimethylammonium bromide) [19].

AgNPs are emerging as common engineered nanomaterials to prevent microbial proliferation on food packaging systems or food contact surfaces because of the high

## Chapter 11

surface-to-volume ratio, nanosize diameter and enhanced surface reactivity, making them able to inactivate microorganisms more effectively than their micro- or macro-scale counterparts [19]. On the other hand, it should be noted that the content of silver in composites used for active food packaging applications must be kept as low as possible and below the maximum migration limits recommended for food contact materials established by legislation bodies such as European Food Safety Association (EFSA) or Food and Drug Administration (FDA) and this can be more effectively achieved by using low doses of stabilized AgNPs.

Although, it is presumed that AgNPs may promote enhanced barrier and antimicrobial properties to develop active materials, limited information concerning the effect of adding these nanoparticles to biopolymer matrices have been found in the literature. Some authors have reported the effect of incorporating silver fillers and nanofillers into different biopolymer matrices such as poly(vinyl alcohol) [9, 12, 20], poly(lactic acid) [21, 22], chitosan [10, 23], or cellulose [24, 25] but these silver particles were not synthesized and stabilized into the matrices, thus causing significant changes in the optical properties and reducing the antimicrobial efficiency [8, 26]. Regarding to PHBV matrices, Xing et al. stated that the addition of 1 wt.-% of AgNPs into PHBV matrices provided antibacterial activity and improved the *in vitro* cell compatibility of nanofibrous scaffolds for joint arthroplasty [27]. More recently, Min et al. [28] observed an improvement in thermal stability and an increase in crystallinity of PHBV composites containing AgNPs coated with oleic acid and n-propylamine. In a more recent work, Yu et al. [29] developed PHBV reinforced with different amounts of 1-15 wt.-% cellulose nanocrystal/silver nanohybrids in which the improvement in the nanocomposites performance was attributed to the synergistic effect of both nanofillers and AgNPs although it was hypothesized that the high cellulose nanocrystals content could be the responsible agent attributing the enhanced barrier and mechanical properties.

To the best of our knowledge, there is no existing literature on the formulation and characterization of PHA-AgNPs nanocomposites, where the AgNPs were previously synthesized and stabilized *in situ* in the presence of unpurified PHA. Furthermore, no data was found in the literature regarding oxygen and water vapour permeability improvements induced by AgNPs or on the long term stability and antimicrobial activity against food-borne pathogens. Therefore, the main goal of this paper was to develop and characterize an active antimicrobial food packaging nanocomposite of PHA containing AgNPs obtained by the industrially meaningful melt blending process which does not use organic solvent or additional stabilizers and where the AgNPs were added to the PHA in a highly dispersed and distributed enriched masterbatch form. The bases for the synthesis of the AgNPs were previously reported and consisted of *in situ* formation and stabilization of AgNPs in the presence of unpurified cheese whey derived PHBV [30].

## **2. Materials and methods**

---

### **2.1 Materials**

Two different PHA grades, with different valerate (HV) contents, were used throughout this study. PHBV3 (3 mol % valerate content) ENMAT Y1000P supplied by Tianan Biopolymer (Ningbo, China) and PHBV18 (18 mol % valerate content) synthesized from mixed microbial cultures as described by Castro-Mayorga, et al. 2014 [30] and without purification steps. Briefly, the biopolymer was produced in a multi-stage process consisting of lab-scale reactors, operating under feast and famine conditions and using enriched PHA-accumulating microorganism and cheese whey as feedstock [31]. Silver nitrate (>98% purity; Sigma-Aldrich, Germany) and sodium

## Chapter 11

borohydride (Panreac, Spain) was used for the AgNPs synthesis. Hiperpur nitric acid (HNO<sub>3</sub>) 69%, were purchased from Panreac (Barcelona, Spain).

### 2.2 Synthesis of silver nanoparticles in PHBV18 matrices

AgNPs were synthesized by chemical reduction into polymer suspensions on the bases of a previously reported method [30]. Briefly, 0.08 wt.-% of PHBV18 was suspended in ultrapure MilliQ© water (Millipore Corporation Co., USA) and the assembly was placed into an ice bath and stirred using a magnetic stirring. A sodium borohydride aqueous solution was added first to the suspension to get 2mM concentration and then silver nitrate aqueous solution (1mM) was added dropwise to generate *in situ* silver nanoparticles. Finally, the obtained product was separated by centrifugation and dried overnight in a vacuum oven at 40°C.

### 2.3 Preparation of nanocomposites

Nanocomposite PHBV films were prepared by melt compounding of the enriched masterbatch form of the AgNPs previously described and neat PHBV3. To this end, the PHBV18/AgNPs masterbatch was melt mixed with the required amount of virgin PHBV3 pellets to obtain blends having a final concentration of an 8% in weight (wt.-%) of the PHBV18/AgNPs. The PHBV blends were prepared in an internal mixer (Brabender Plastograph, Germany) during 5 minutes at 60 rpm and 180°C.

The batches were then subjected to a rapid cooling-down and they were subsequently compression moulded into films using a hot-plate hydraulic press (Carver 4122, USA) at 180°C and 1.2 MPa for 2 min. The so-obtained films had a thickness of about 100 µm as measured with a digital micrometer (Mitutoyo, Spain, ± 0.001 mm) by averaging four measurements on each sample. Neat PHBV3 and

PHBV3/PHBV18 samples were prepared and used as control for comparative purposes.

## **2.4 Determination of silver content in the nanocomposites**

To calculate the total Ag content within the films, 100 mg samples were subjected to acid digestion with 2 mL of HNO<sub>3</sub> at 80°C for 16 h. The resultant digestant was diluted to a final volume of 5 mL. The quantification of silver was carried out by inductively coupled plasma- optical emission spectroscopy (ICP-OES, Perkin-Elmer, USA) using a silver standard solution (traceable to SRM from NIST, AgNO<sub>3</sub> in HNO<sub>3</sub> 2-3 % 1000 mg/L Ag Certipur®, Merck, Germany) for calibration. All measurements were done, in triplicate

## **2.5 Scanning Electronic Microscopy (SEM)**

The morphology of the films was investigated by using electronic microscopy. The Scanning Electronic Microscopy (SEM) images were taken with a Hitachi S-4100 electron microscope at an accelerating voltage of 5 kV and a working distance of 8-10 mm. PHBV films cryo-fractured, after immersion in liquid nitrogen, were sputtered with a gold- palladium mixture under vacuum before their examination.

## **2.6 Transmission Electronic Microscopy (TEM)**

The morphology and distribution of silver nanoparticles was studied using a Jeol 1010 (Hitachi) transmission electronic microscope an accelerating voltage of 80 kV. Samples were previously ultra-microtomed (Leica EM UC6) and placed onto carbon carbon-coated copper grids. Estimation of the nanoparticles dimensions was done by

## Chapter 11

means of the Adobe Photoshop CS4 software from 300 nanoparticles at random from TEM images.

### 2.7 Optical properties

The transparency of the films was determined through the surface reflectance spectra in a spectrophotometer CM-3600d (Minolta Co., Tokyo, Japan) with a 10 mm illuminated sample area. Measurements were taken in triplicate for each sample by using both a white and a black background. Film transparency was evaluated through the internal transmittance ( $T_i$ ) (0–1, theoretical range) by applying the Kubelka–Munk theory for multiple scattering to the reflection data [32]. Internal transmittance ( $T_i$ ) of the films was quantified using equation (1). In this equation,  $R_0$  is the reflectance of the film on an ideal black background. Parameters  $a$  and  $b$  were calculated by equations (2) and (3), where  $R$  is the reflectance of the sample layer backed by a known reflectance  $R_g$ .

$$T_i = \sqrt{(a - R_0)^2 - b^2} \quad (1)$$

$$a = \frac{1}{2} \left( R + \frac{R_0 - R + R_g}{R_0 R_g} \right) \quad (2)$$

$$b = \sqrt{(a^2 - 1)} \quad (3)$$

### 2.8 Wide Angle X-Ray Diffraction Analysis

Wide angle x-ray diffraction (WAXD) measurements were performed using a Bruker AXS D4 Endeavour diffractometer. The samples were scanned at room temperature in reflection mode using incident Cu  $K\alpha$  radiation (1.54 Å), while the generator was set up at 40 kV and 40 mA. The data were collected over a range of

scattering angles ( $2\theta$ ) of 2–40°. Peak fitting was carried out using Igor Pro software package (Wavemetrics, Lake Oswego, Oregon). Gaussian function was used to fit the experimental diffraction profiles obtained. The crystallinity was taken as the ratio of the sum of areas under the crystalline diffraction peaks to the total area under the curve between  $2\theta = 5^\circ$  and  $40^\circ$ .

## 2.9 Differential Scanning Calorimetry (DSC)

Differential scanning calorimetry (DSC) of PHBV nanocomposites was performed on a Perkin-Elmer DSC 8000 thermal analysis system using  $N_2$  as the purging gas. The sample treatment consisted of a first heating step from  $0^\circ\text{C}$  to  $200^\circ$  followed by a subsequent cooling down to  $-50^\circ\text{C}$ . The heating and cooling rates for the runs were  $10^\circ\text{C}/\text{min}$  and the typical sample weight was  $\sim 3$  mg. Before evaluation, similar runs of an empty pan were subtracted from the thermograms. The DSC equipment was calibrated using indium as a standard. The crystallinity degree (%) was estimated from the corrected enthalpy for total PHBV content in the nanocomposites samples, using the ratio between the enthalpy of the studied material and the enthalpy of a perfect PHBV crystal as per Equation (4), where  $\Delta H_m^0$  is the melting enthalpy of an infinity PHBV crystal (109 J/g) [33]. The tests were done, at least, in triplicate.

$$X(\%) = \frac{\Delta H_m}{\Delta H_m^0} * 100 \quad (4)$$

## 2.10 Thermogravimetric Analysis (TGA)

Thermogravimetric analysis (TGA) was performed under nitrogen atmosphere in a Perkin Elmer Thermobalance TGA 7. TGA curves were obtained after conditioning the sample in the sensor for 5 min at  $30^\circ\text{C}$ . The samples were then heated from  $30^\circ\text{C}$

## ***Chapter 11***

to 600 °C at a heating rate of 10 °C/min. Derivative TGA curves (DTG) express the weight loss rate as the function of temperature and were obtained using TA analysis software. All tests were carried out in duplicate.

### **2.11 Mechanical properties**

Tensile tests were performed according to ASTM Standard D638 (ASTM 2010) in stamped dumbbell-shaped specimens of the samples. An Instron Testing Machine (Model 4469; Instron Corp., Canton, MA, USA) was used, with a crosshead speed of 10 mm/min, at ambient conditions of typically 24°C and 50% RH. Elastic Modulus (E), Tensile Strength (TS), and Elongation at Break (EAB) were determined from the stress-strain curves, estimated from force–distance data obtained for the different films. At least, four specimens of each film were tensile tested as to obtain statistically meaningful results.

### **2.12 Water Vapour Permeability (WVP)**

Water vapour permeability (WVP) was measured, in triplicate, according to the ASTM E96 (2011) gravimetric method, using Payne permeability cups (Elcometer SPRL, Hermelle/s Argenteau, Belgium). Distilled water was placed inside the cup to expose the film (the exposed area was  $9.6 \times 10^{-4} \text{ m}^2$ ) to 100% RH on one side. Once the films were secured, each cup was placed in an equilibrated relative humidity cabinet at 0% RH and 25°C. The cups were weighed periodically ( $\pm 0.0001 \text{ g}$ ). Cups with aluminium films were used as control samples to estimate solvent loss through the sealing. Water vapour permeation rate was calculated from the steady-state permeation slopes obtained from the regression analysis of weight loss data vs. time, and weight loss was calculated as the total cell loss minus the loss through the sealing.

Permeability was obtained by multiplying the permeance by the average film thickness.

### **2.13 Oxygen transmission rate (OTR) measurements**

The oxygen permeability coefficient was derived from oxygen transmission rate (OTR) measurements recorded using an Oxygen Permeation Analyser M8001 (Systech Illinois, UK). Experiments were carried out at 23°C and 80% RH. The samples were previously purged with nitrogen in the humidity equilibrated samples, before exposure to an oxygen flow of 10 mL min<sup>-1</sup>. The exposure area during the test was 5 cm<sup>2</sup> for each sample. In order to obtain the oxygen permeability, film thickness and gas partial pressure were considered in each case. The measurements were done in triplicate.

### **2.14 Water uptake**

The water uptake was estimating during sorption experiments at 24 ± 1°C and 100% RH by means of weight gain using a Mettler AE-240 (IET, USA) analytical balance. Saturation was considered when successive weight uptake measurements yielded same values.

### **2.15 Antimicrobial activity of nanocomposites**

The frequent food-borne pathogens, *Salmonella enterica* CECT 4300 and *Listeria monocytogenes* CECT 7467, strains were obtained from the Spanish Type Culture Collection (CECT: Valencia, Spain) and stored in Phosphate buffered saline (PBS, Sigma Aldrich, USA) with 10 wt.-% tryptic soy broth (TSB, Conda Laboratories, Madrid, Spain) and 10 wt.-% glycerol at -80°C until needed. Previous to each study, a

## *Chapter 11*

loopful of bacteria was transferred to 10 mL of TSB and incubated at 37°C overnight and an aliquot was again transferred to TSB and grown at 37°C and 120 rpm to the mid-exponential phase of growth having an absorbance value of 0.20 as determined by optical density at 600 nm (Agilent 8453 UV-visible spectrum system, Germany). This culture was used as inoculum for antimicrobial assays.

To evaluate the antimicrobial performance of the obtained films, a modification of the Japanese Industrial Standard JIS Z 2801 was used. Briefly, a microorganism suspension containing about  $5 \times 10^5$  CFU/mL was applied onto the test PHVB/AgNPs films of 3 x 3 cm and covered by an inert piece of Low-Density Polyethylene (LDPE) of 2.5 x 2.5 cm and 80  $\mu$ m of thickness. After incubation at 24°C and a relative humidity at least 95% for 24 h, bacteria were recovered with PBS, 10-fold serially diluted and incubated at 37°C for 24 h in order to quantify the number of viable bacteria by conventional plate count. PHBV films (without silver) were used as a negative control. The antimicrobial activity was evaluated as synthesized (0 days) and after seven months aging. The value of antimicrobial activity was calculated by determining  $\log_{10} (N_0/N_i)$ , where  $N_0$  is the average of the number of viable cells of bacteria on the untreated test piece after 24 h and  $N_i$  is average of the number of viable cells of bacteria on the antimicrobial test piece after 24 h. Three replicate experiments were performed for each of the samples.

### **2.16 Statistical analysis**

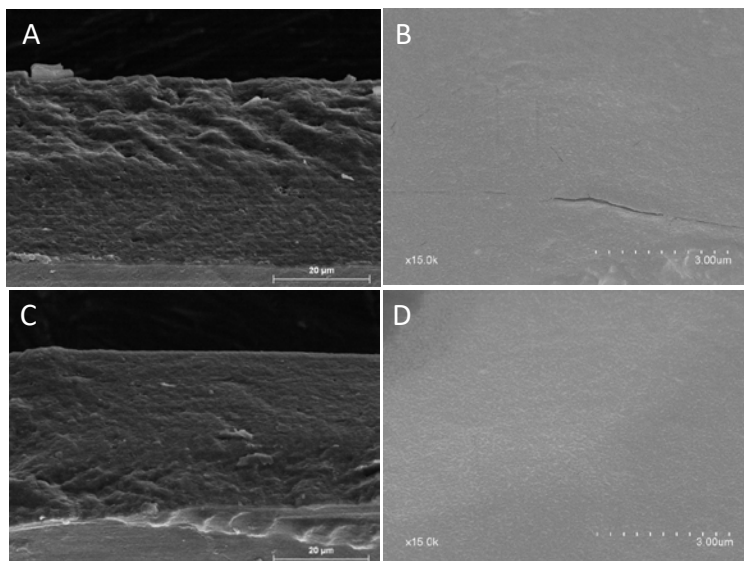
The statistical analysis of physicochemical and antimicrobial data was carried out by means of StatGraphics Plus version 5.1 (Statistical Graphics Corp.) through the analysis of variance (ANOVA). Tukey's Honestly Significant Difference (HSD) was used at the 95% confidence level for multiple comparison tests.

## 3. Results and discussion

---

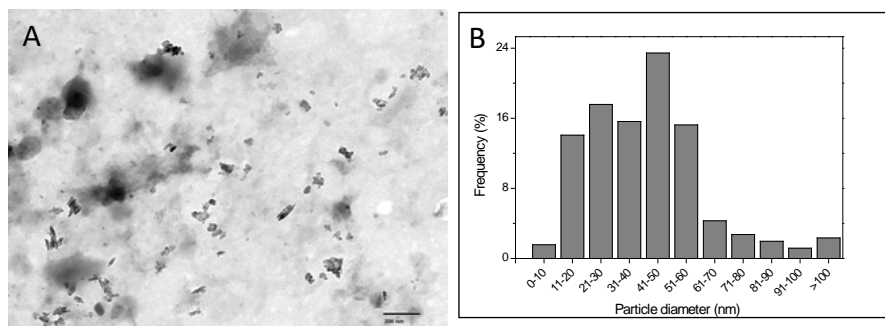
### 3.1 Morphology and optical properties

The morphology of the obtained PHBV3/PHBV18 nanocomposite films with and without AgNPs was qualitatively studied using both scanning electron microscopy (SEM) and transmission electron microscopy (TEM). Microstructural images yield information about the arrangement of the nanoparticles in the PHBV matrices, allowing a better understanding of the physicochemical and antimicrobial properties of the developed nanocomposite films. Firstly, to examine the morphology of the neat matrices (without AgNPs) and of the nanocomposite PHBV3/PHBV18/AgNPs films, the cross-section and surfaces of the developed nanocomposite films were examined by SEM (*cf.* Figure 1). As observed from this figure, smooth and uniform fractured surfaces were observed in all cases, suggesting good compatibility, dispersion and distribution of the PHBV18/AgNPs masterbatch within the PHBV3 matrix. It is worth noting that AgNPs were not easily observed by SEM either at the cross-section or at the surface, probably due to both reduced contrast and the size of the silver nanoparticles at the nanoscale.



**Figure 1.** SEM micrographs of the cryo-fractured sections (A and C) and surfaces (B and D) of the neat PHBV3/PHBV18 (A-B) and PHBV3/PHBV18/AgNPs nanocomposites (C-D).

Figure 2 displays a typical TEM image of the nanocomposite films containing AgNPs which provide more resolved information about the dispersion of AgNPs into the polymer matrix. As shown in Figure 2a, AgNPs appeared well dispersed and distributed into the PHBV matrices, having both spherical and cylindrical geometries as it can be observed in the ultrathin sections of the microtomed thin sheets of nanocomposite films containing AgNPs. The particles diameters of the AgNPs ranged between 10 and 60 nm, with a maximum frequency at around 41-50 nm (*cf.* Fig 2b) and with a small percentage rate of AgNPs agglomerates. Taking into account that after the masterbatch synthesis, the nanoparticles showed a spherical geometry with a mean diameter of around  $7\pm 3$  nm [30], the cylindrical geometry of AgNPs observed in the nanocomposite is ascribed to particles agglomeration along the flow direction during compounding and compression moulding steps.



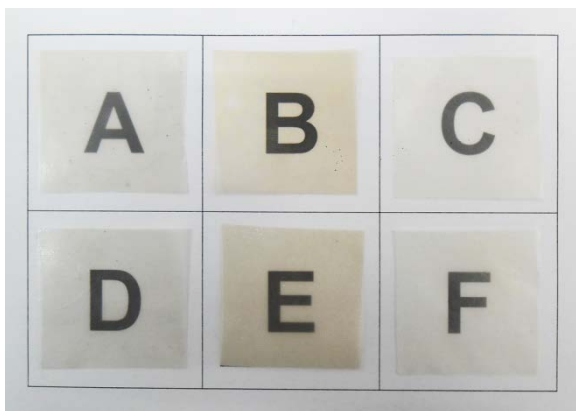
**Figure 2.** TEM typical image of the PHBV3/PHBV18/AgNPs sample (A) and size distribution of the AgNPs in the PHBV3/PHBV18/AgNPs film (B).

Figure 3 shows the contact transparency images of the PHBV3/PHBV18 film and of its nanocomposites containing AgNPs. As observed, both materials presented a relatively good contact transparency, which was not compromised by the incorporation of AgNPs and that can be explained by the good dispersion and distribution of the AgNPs in the PHBV matrices. It is worth noting that the presence of PHBV18 resulted in a somewhat yellowish colour in the films, which may be indicative of a certain degree of thermal degradation such as the degradation of cell debris or other organic residues of PHBV18 arising from the fermentation process. This is consistent with the TGA profiles of the developed PHBV3/PHBV18 films (*cf.* Table 2) which showed a slight reduction in the degradation temperature of nanocomposite films prepared with mixtures of both PHBVs, as will be shown later. It is worth noting that the yellowish colour was not seen in the presence of AgNPs, which could be ascribed to the higher thermal stability of these nanocomposite films promoted by the filler at the melt compounding temperature window. However, this differentiating effect in process stability was not picked up by the TGA measurements, where no significant differences were observed between PHBV3/PHBV18 films with and without AgNPs. This may be explained by the fact that the TGA analysis does not

## Chapter 11

match the environmental conditions during the actual melt processing, as they were carried out under nitrogen atmosphere, and that the colour changes must involve small degradation steps that occur without significant mass changes at the processing temperatures that are not picked up by the TGA measurements (see TGA results, Table 2).

As it has been widely reported, the thermal and photochemical reduction of residual  $\text{Ag}^+$  ions and the agglomeration of unstable AgNPs can considerably affect the physical appearance of silver containing polymer films [17, 34]. This is manifested by a colour change from light yellow to brown or black, which is an undesirable effect for most industrial applications, most especially for food packaging where transparency is a requirement for consumer acceptance. Interestingly, neither in freshly made nor in aged samples (aging was carried out by storing the samples at room temperature and 0% RH over a 7 months period), the incorporation of AgNPs resulted in marked differences in appearance or contact transparency of the nanocomposite films when compared to their counterparts prepared without AgNPs (*cf.* Figure 3). Therefore, it could be stated that no significant reduction of silver or agglomeration of AgNPs appears to occur during the melt-compounding, compression-moulding and film aging steps. This is a remarkable finding since typically melt compounding of silver containing compounds is very challenging and leads to strong dark colour developed during mixing and/or subsequent aging.



**Figure 3.** Contact transparency pictures of freshly made nanocomposites (0 days): PHBV3 (A), PHBV3/PHBV18 (B), and PHBV3/PHBV18/AgNPs (C); and after 210 days of aging: PHBV3 (D), PHBV3/PHBV18 (E), and PHBV3/PHBV18/AgNPs (F).

The transparency of nanocomposite films was quantitatively assessed by means of internal transmittance ( $T_i$ ) measurements. This parameter is directly related to the surface and the internal structure of the material and is greatly dependent on the morphology and particle size distribution. In fact, the tortuosity of the internal structure could affect the light transmission/dispersion behaviour of the nanocomposite films and, thus, its transparency-opacity ratio. It is generally assumed that an increase in  $T_i$  values is related to more homogeneous and transparent films, while a decrease in these values implies films matrices with greater opacity and thus more heterogeneous matrices. Over the wavelength range considered, a similar pattern was observed between nanocomposite films containing and not containing AgNPs, and only small differences were detected in the internal transmittance values (*cf.* Fig. 4). This slight decrease in transparency could be partially attributed to the presence of AgNPs resulting in somewhat different refractive index.

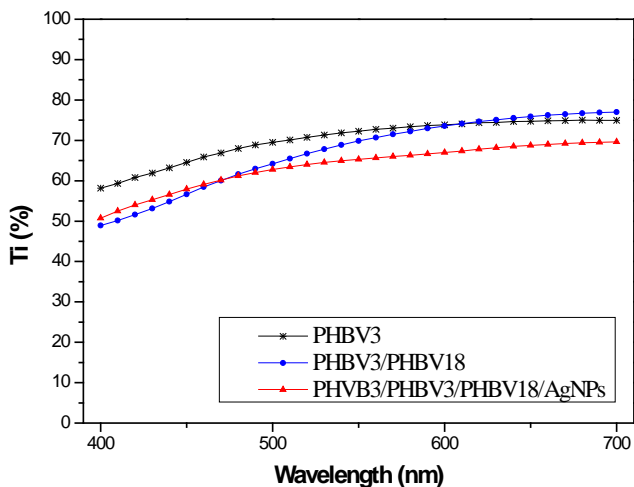


**Figure 4.** Spectral distribution of internal transmittance (Ti) of PHBV3, PHBV3/PHBV18 and PHBV3/PHBV18/AgNPs nanocomposites.

### 3.2 Crystal structure

WAXD experiments were carried out in order to study the crystalline structure of the PHBV nanocomposites. Figure 5 displays diffraction patterns of the neat PHBV3 and PHBV3/PHBV18 films and the corresponding nanocomposite films containing AgNPs. As observed from Figure 5, the characteristic peaks of PHBV appeared at  $13.7^\circ$ ,  $17.1^\circ$ ,  $20.4^\circ$ ,  $21.5^\circ$ ,  $22.7^\circ$ ,  $25.5^\circ$ ,  $26.9^\circ$ ,  $30.6^\circ$  which correspond to the typical (020), (110), (021), (101), (111), (121), (200) crystal planes for orthorhombic PHBV, respectively [35]. When PHBV18 was added to PHBV3 matrix, the intensity of the peak located at  $13.7^\circ$  decreased while those located at  $22.7^\circ$  increased, indicating that the PHBV crystals of the PHBVs mixtures were preferentially oriented along (111) plane instead of (020). This resulted in a lower crystallinity index of the overall PHBV3/PHBV18 containing or not containing AgNPs. This was expected since copolymers of hydroxybutyrate (HB) with hydroxyvalerate (HV), usually present

lower crystallinity for higher HV contents due to the HV units inhibiting crystallization through hydrogen bonding [36, 37].

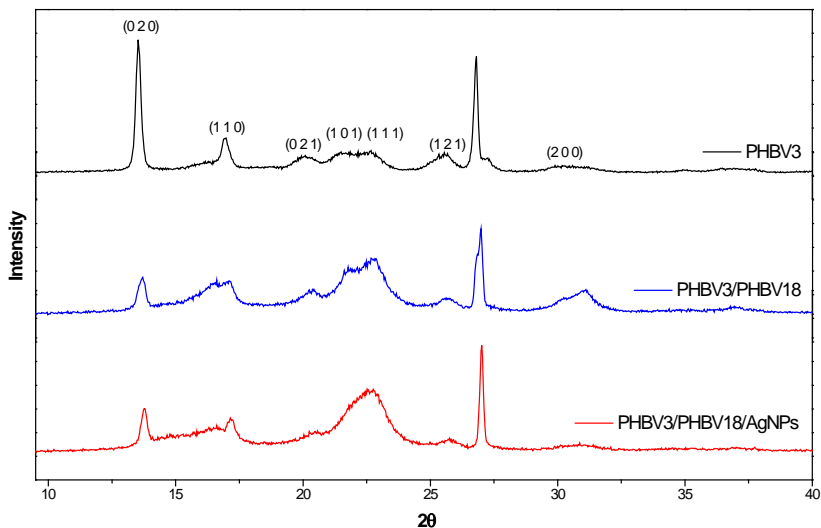


**Figure 5.** WAXD patterns of PHBV3, PHBV3/PHBV18 and PHBV3/PHBV18/AgNPs nanocomposites.

Interestingly, when the WAXD diffraction patterns of PHBV3/PHBV18 and PHBV3/PHBV18 films containing AgNPs were compared, the intensity of the peaks located at  $22.7^\circ$  and  $26.9^\circ$  increased and were sharper after AgNPs addition, which indicated that PHBV crystals were preferentially oriented in (040) and (111) directions. The fact that the intensity of these peaks became more intense after the incorporation of AgNPs into PHBV3/PHBV18 matrices may suggest that AgNPs can act as a nucleating agent, favouring the crystallization process of the PHBV matrices. In fact, the crystallinity index seemed to increase slightly, up to *ca.* 6%, in the nanocomposites containing AgNPs, as compared to their counterparts prepared without silver nanoparticles (*cf.* Table 1). These results are in good agreement with the existing literature [28, 29, 38, 39]. In this regard, it is worth noting that some authors reported

## Chapter 11

the appearance of Bragg reflections of the face-centered cubic crystal structure of silver located at  $2\theta = 37^\circ, 44^\circ, 64^\circ, 78^\circ$  and  $82^\circ$  and corresponding to the (111), (200), (220), (311) and (222) lattice plane [28, 40]. Most likely, the content of AgNPs in the developed nanocomposites was too low to impact the WAXD diffraction patterns.

### 3.3 Thermal properties and thermal stability

The thermal properties of the neat PHBV3 and PHBV3/PHBV18 films and the nanocomposite films containing AgNPs were investigated by DSC analysis. Table 1 gathers the melting temperature ( $T_m$ ), melting enthalpy ( $\Delta H_m$ ) and crystallinity index ( $X_c$ ) obtained from the first heating run. Both the neat PHBVs and nanocomposites presented a two-step melting behaviour, consisting of a sharp melting peak ( $\sim 169^\circ\text{C}$ ) followed by a melting shoulder ( $\sim 183^\circ\text{C}$ ) during the first heating run, which was consistent with results published earlier [6, 41]. Some authors hypothesized that the first melting peak corresponds to more defective or smaller crystals which are able to recrystallize during the run, thus forming more perfect crystals which subsequently melt at higher temperatures (second melting peak) [42]. However, other studies reported the existence of two different crystalline phases corresponding to HB-rich and HV-rich domains associated to the high and low temperature melting processes, respectively [43].

A decrease in the melting enthalpy was observed when PHBV18 was added to the PHBV3 matrix, being in accordance with the previous literature [6]. However, no significant differences in the melting enthalpy were observed between the neat PHBV3/PHBV18 and its counterpart prepared with AgNPs may be due to the low loading of AgNPs. The crystallinity degree obtained by the DSC method does not correspond to the crystallinity of the composite after processing since the crystallinity and crystalline morphology are thought to develop during the thermal run. This fact

may explain the discrepancy between the crystallinity values obtained by both methods. In any case, WAXD has been widely demonstrated to be a more adequate technique to assess crystallinity as compared to DSC [44].

**Table 1.** DSC melting point ( $T_m$ ), melting enthalpy ( $\Delta H_m$ ) and degree of crystallinity ( $X_c$ ) of PHBV3, PHBV3/PHBV18 and PHBV3/PHBV18/AgNPs nanocomposites, obtained from the first heating run. The degree of crystallinity obtained by means of WAXD is also included ( $X_c^*$ ).

Sample	$T_{m1}$ (°C)	$T_{m2}$ (°C)	$\Delta H_m$ (J/g)	$X_c$ (%)	$X_c^*$ (%)
PHBV3	168.7 ± 1.0 <sup>a</sup>	181.8 ± 0.2 <sup>a</sup>	72.3 ± 0.5 <sup>a</sup>	66.3 ± 0.5 <sup>a</sup>	70.4 ± 0.1 <sup>a</sup>
PHBV3/PHBV18	168.6 ± 0.3 <sup>a</sup>	182.3 ± 0.2 <sup>a</sup>	66.1 ± 1.2 <sup>b</sup>	60.7 ± 1.1 <sup>b</sup>	55.5 ± 1.0 <sup>b</sup>
PHBV3/PHBV18/AgNPs	170.1 ± 0.7 <sup>a</sup>	184.0 ± 1.1 <sup>a</sup>	66.8 ± 0.4 <sup>b</sup>	61.3 ± 0.7 <sup>b</sup>	61.7 ± 0.1 <sup>c</sup>

Mean values with different letters in the same column represent significant differences ( $p < 0.05$ ) among the samples according to ANOVA and Tukey's multiple comparison tests.

TGA analyses were also carried out to assess the thermal stability of the neat PHBVs, PHBV18/AgNPs masterbatch and of the nanocomposite films containing AgNPs. The DTG curves and decomposition temperatures ( $T_d$ ) are presented in Figure 6 and Table 2. It was demonstrated, in a previous work, that the increment of the HV content in a PHBV copolymer led to an increase in thermal stability, when PHBV3, PHBV9 and PHBV16 were compared [45]. However, in the present work, the incorporation of unpurified PHBV18 into the PHBV3 seemed to decrease slightly (not statistically significant thought) the decomposition temperature, as a consequence of the presence of some impurities in the PHBV18 which were close to 30 wt.-% [30]. This catalytic effect of fermentation residues was particularly significant when the neat PHBV18 was analysed. In that case a noticeable decrease, at around 45°C respect to PHBV3, in the decomposition temperature ( $T_d$ ) was observed. It is considered that the degradation mechanism in PHA begins with free radical formations at weak bonds and/or chain ends, followed by their transfer to adjacent chains via interchain

## Chapter 11

reactions [12] and this mechanism is accelerated by the presence of fermentation residues which can act in synergy with the compounds which are responsible for the catalysis of PHB [46].

**Table 2.** TGA decomposition temperatures ( $T_d$ ) for the neat PHBVs, the PHBV18/AgNPs masterbatch and their nanocomposites.

Sample	$T_d$ (°C)
PHBV3	$294.8 \pm 3.8^a$
PHBV18	$249.8 \pm 2.8^b$
PHBV18/AgNPs	$260.4 \pm 3.2^c$
PHBV3/PHBV18	$289.6 \pm 2.9^a$
PHBV3/PHBV18/AgNPs	$289.6 \pm 2.8^a$

Mean values with different letters in the same column represent significant differences ( $p < 0.05$ ) among the samples according to ANOVA and Tukey's multiple comparison tests.

On the other hand, the influence of the nanofiller in the thermal stability of the PHA is complex and reports, in the literature, sometimes conflict. Thus, the effect of the filler is mainly thought to depend on the type, content and the degree of dispersion of this into the polymer matrix [46, 47]. In the present work, no significant differences between the TGA of PHBV3/PHBV18 with and without AgNPs were observed probably due to the low loadings of the nanofiller and to the small changes in mass associated to the degradation mechanisms that occur across the selected processing window (see the inset of Fig. 6). However, at higher silver content, as in the PHBV18/AgNPs masterbatch, the thermal stability of the PHBV18 matrix was clearly enhanced. These results agreed with previous works in which the incorporation of AgNPs into poly(vinyl alcohol) [12] and PHBV matrices [28, 29] gave rise to more thermally stable nanocomposite films and this phenomenon was explained by the reduced mobility of the PHBVs chains in the nanocomposite films. This implied that

the chain transfer reaction would be suppressed to some extent, and consequently the degradation process would be slowed. Therefore, the decomposition in this case will take place at higher temperatures. In the present work, the amount of AgNPs in the nanocomposites is quite low which could minimise any significant impact in the TGA measurable thermal stability of the PHBV3/PHBV18 films. However, the stabilized AgNPs produced in this study clearly inhibited colour formation during processing as it was commented above (see Figure 3), which strongly suggests that the highly dispersed and distributed AgNPs stabilized the organic matter to which they are linked by amide linkage [30, 48], hence stabilizing the PHBV3/PHBV18 nanocomposites during at least the processing steps. This interaction appeared to minimize the expected Maillard reactions between amide groups and reducing sugars present in the unpurified PHBV18 that would have given rise to the browning of the sample.

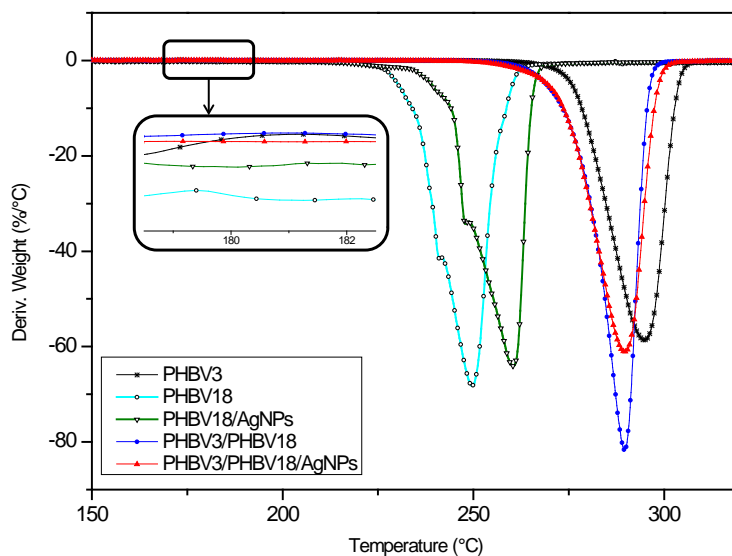


**Figure 6.** DTG curves of the neat PHBVs, the PHBV18/AgNPs masterbatch and their nanocomposites. The inset is an expanded view at the processing temperature range.

### 3.4 Mechanical properties

The typical mechanical parameters obtained during tensile tests of the neat PHBV (PHBV3 and PHBV3/PHBV18) matrices and the nanocomposites film containing AgNPs are summarized in Table 3. From the results, it can be deduced that the tensile parameters were not significantly affected by the incorporation of the PHBV18/AgNPs masterbatch into the PHBV3. This behaviour agrees with the one previously reported for PLA films loaded with 1%.-wt of silver salts obtained either by solvent casting [22] or by melt-compounding [13] techniques. However, there are some previous works based on PVA/cellulose nanocrystals [20] or methylcellulose [25] nanocomposite films containing silver nanoparticles in which the addition of cellulose nanofillers at higher loadings conferred them with a reinforcement effect, but they did not attribute any significant improvement to the presence of AgNPs. Furthermore, it has previously been reported that there is greater ductility as the hydroxyvalerate content increased in PHBV grades [6, 49, 50]. However, it seems that the amount of the PHBV18 in the PHBV3/PHBV18 blend or in the nanocomposites film was too low to induce any significant changes on the mechanical behaviour.

**Table 3.** Tensile parameters (E: Young's Modulus, TS: Tensile Strength and EAB: Elongation at Break) of PHBV3, PHBV3/PHBV18 and PHBV3/PHBV18/AgNPs nanocomposites.

Sample	E (GPa)	EAB (%)	TS (MPa)
PHBV3	2.6 ± 0.1 <sup>a</sup>	1.5 ± 0.2 <sup>a</sup>	33.9 ± 6.9 <sup>a</sup>
PHBV3/PHVB18	2.7 ± 0.1 <sup>a</sup>	1.7 ± 0.1 <sup>a</sup>	39.6 ± 1.7 <sup>a</sup>
PHBV3/PHBV18/AgNPs	2.7 ± 0.1 <sup>a</sup>	1.5 ± 0.1 <sup>a</sup>	34.0 ± 0.4 <sup>a</sup>

Mean values with different letters in the same column represent significant differences ( $p < 0.05$ ) among the samples according to ANOVA and Tukey's multiple comparison tests.

### 3.5 Water and oxygen barrier properties

Table 4 gathers water uptake, water vapour and oxygen permeability for the PHBV matrices and their nanocomposite films. From the results, a surprising small increase in water uptake, not statistically significant, was observed between the PHBV3 film and those containing PHBV18. Although the water uptake increase was very small or negligible, a higher water uptake was clearly expected from simple application of the rule of mixtures. Thus, it would have been expected that a higher water uptake should have taken place in the blend, since the blending element has a water uptake of *ca.* 32%. This inconsistency between the expected and the experimental results suggests that the blending element when confined into the less water sensitive matrix is restricted to swell. The same effect has already been reported for poly(lactic acid) [51], gelatin [52] and hydroxypropyl methylcellulose [53] reinforced with cellulose nanowhiskers or microcrystalline cellulose.

**Table 4.** Water vapor permeability measured at 100% RH and oxygen permeability measured at 80% RH for PHBV3, PHBV3/PHBV18 and PHBV3/PHBV18/AgNPs nanocomposites.

Sample	Water uptake (%)	WVP ( Kg m/ Pa. s. m <sup>2</sup> )	PO <sub>2</sub> (m <sup>3</sup> m/ m <sup>2</sup> . s. Pa) 80% RH
PHBV3	9.8 ± 0.6 <sup>a</sup>	1.10 ± 0.02 e <sup>-15</sup> <sup>a</sup>	2.06 ± 0.09 e <sup>-19</sup> <sup>a</sup>
PHBV18	32.1 ± 1.2 <sup>b</sup>	18.8 ± 0.26 e <sup>-15</sup> <sup>b</sup>	8.43 ± 0.44 e <sup>-19</sup> <sup>b</sup>
PHBV3/PHBV18	10.6 ± 0.1 <sup>a</sup> (11.58)*	1.85 ± 0.03 e <sup>-15</sup> <sup>c</sup> (2.52 e <sup>-15</sup> )*	2.23 ± 0.22 e <sup>-19</sup> <sup>a</sup> (2.56 e <sup>-19</sup> )*
PHBV3/PHBV18/AgNPs	10.1 ± 0.3 <sup>a</sup>	1.18 ± 0.03 e <sup>-15</sup> <sup>a</sup>	0.90 ± 0.08 e <sup>-19</sup> <sup>c</sup>

Mean values with different letters in the same column represent significant differences ( $p < 0.05$ ) among the samples according to ANOVA and Tukey's multiple comparison tests. Values between brackets represent calculations obtained by applying the simple rule of mixtures for the PHBV3/PHBV18 composites containing 92% of PHBV3 and 8% of PHBV18

## Chapter 11

The water permeability of the blend was, however, measurably impacted by addition of the PHBV18, and increased by *ca.* 68.2% compared to the matrix. Nevertheless, again, the rule of mixtures indicates that an even higher permeability would have been expected, hence supporting further the confinement argument of the minority phase. On the other hand, the addition of the stabilized AgNPs resulted in a positive barrier effect. Thus, it is remarkable to observe that the addition of such small quantity of AgNPs can lead to a significant reduction in the water vapour permeability of the PHBV3/PHBV18 nanocomposite films, which reached values similar to those obtained for the neat PHBV3 matrix. Therefore, the AgNPs contributed to mitigate the increase in the WVP produced by the stabilizing PHBV18.

A small increase in the oxygen permeability at 80% RH was seen in the blend, which is also somewhat smaller than would be expected by applying the rule of mixtures. This might be attributed to water molecules clustering rather than plasticizing the polymer and hence blocking the free volume sites for the oxygen molecules to sorb and diffuse. This phenomenon has been reported earlier in the literature for very hydrophilic or very hydrophobic glassy polymers, where the clustering of water molecules was inferred with increasing relative humidity [54, 55]. Laksmana et al., reported similar effects in glassy hydrophilic films. The authors stated that when the affinity of water towards the polymer is lower as compared to water cohesion, clustering of water molecules will occur and therefore, lower oxygen permeation will be obtained. The water clustering phenomenon is also supported by the confinement of the more hydrophilic phase experimentally measured in the water uptake and water permeability.

Interestingly, the addition of AgNPs reduced the oxygen permeability of the pure PHBV3 matrix by *ca.* 56.3% which is more likely to be explained by the additional tortuous path created by the highly dispersed and distributed AgNPs [56] since the crystallinity index of the PHBV3/PHBV18/AgNPs films was significantly lower than

that obtained for the neat PHBV3. When the barrier performance of the silver nanocomposite was compared to the one of the PHBV3/PHBV18 blend, an overall remarkable reduction in water and oxygen permeability of *ca.* 36.2% and 59.1% occurred, respectively. The latter results could also be ascribed to some extent to the observed increase in the crystallinity index and perhaps also to the changes in crystalline morphology. Permeability reductions were previously reported for zinc oxide nanoparticles added to PHBV [57] and poly(methyl methacrylate) [58], and for bifunctional cellulose nanocrystals/silver nano hybrids [29]. However, in the latter case the barrier effect was mainly ascribed to the presence of the cellulose nanocrystals as the carriers of silver.

### 3.6 Antimicrobial activity

The Japanese Industrial Standard (JIS) Z 2801:2000 is the most common method for assessing the antimicrobial activity of bacteria on the surface of antimicrobial products and it was used in the current study to determine the antibacterial activity of the PHBV3/PHBV18/AgNPs films (*cf.* Figure 7). After 24 h of exposure, no viable counts of *Salmonella enterica* and *Listeria monocytogenes* were recorded whether in the freshly made nanocomposites or in the aged samples after 7 months of storage. These results are of great interest since silver nanoparticles have demonstrated to have a biocide effect at very low concentrations  $0.040 \pm 0.002$  wt.-%, as it has been previously quantified by ICP-OES. Considering that the biocide effect of most metal nanoparticles has been reported to depend on their stability and resistance to agglomeration, the antimicrobial effect of AgNPs in the PHBV3/PHBV18 matrix is mainly ascribed to the fact that AgNPs were well-dispersed and stabilized in the polymer matrix over time. In this sense, nanocomposite films showed about 6.89 log CFU reduction for *Salmonella enterica* and 5.51 log CFU reduction for *Listeria*

## Chapter 11

*monocytogenes* as compared to the neat PHBV3/PHBV18 films (without AgNPs). In this particular case, the gram-positive bacterium *L. monocytogenes* appeared to be more tolerant to silver than gram-negative bacterium *S. enterica*. It has previously been reported that gram-positive bacteria are less susceptible to the antimicrobial activity of silver, which might be due to the differences in the cell wall structure. The cell wall of gram-positive bacteria contains multiple layers of peptidoglycan compared to the cell wall of gram-negative bacteria. Peptidoglycan is a complex structure and often contains teichoic acids or lipoteichoic acids which have a strong negative charge that may contribute to sequestration of free Ag ions. Thus, gram-positive bacteria may allow less silver molecules to reach the cytoplasmic membrane than gram-negative bacteria allow and may therefore be less susceptible [59, 60].

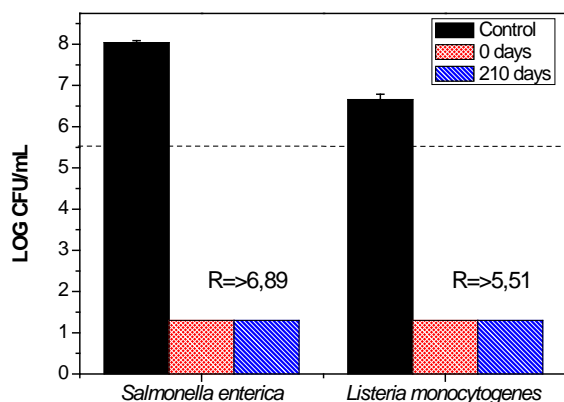


**Figure 7.** Antimicrobial activities of freshly made nanocomposites (0 days) and 210 days aged PHBV3/PHBV18/AgNPs nanocomposites against *Salmonella enterica* and *Listeria monocytogenes* after 24h exposure. The dashed line depicts the initial inoculum size of 5.6 log CFU. The detection limit was 20 CFU/mL.

It has been shown that the methodology followed in this work allows the development of antimicrobial and stable PHBV based nanocomposite films containing AgNPs at concentrations of up to twenty five times lower than when incorporated by

other methodologies (not *in situ* ones) as reported by Min et al. [28] or even fifty times lower than the silver modified nanocomposites based on PHBV and nanocrystals of cellulose developed by Yu et al. [29].

## 4. Conclusions

---

This study has demonstrated that the effective stabilization and dispersion of AgNPs in the obtained masterbatch avoided the use of surfactants or capping agents prior or during melt compounding with PHBV3 resulting in materials with excellent and stable upon aging optical properties. The work also demonstrated that AgNPs can act as both a nucleating agent promoting the crystallization of PHBV3/PHBV18 composites and a tortuosity enhancing element, effects both that lead to materials with higher barrier performance to oxygen and water vapour. Aside from the processability, optical properties and barrier advantages, the developed nanocomposites exhibited a strong and prolonged (even after seven months) antibacterial activity against pathogens such as *L. monocytogenes* and *S. enterica*. All of these features make the developed nanocomposites unique materials for active food packaging applications.

## 5. Acknowledgements

---

The authors gratefully thank Dr. Maria Reis from Universidade Nova de Lisboa, and Dr. Catarina Oliveira, from Centro de Quimica fina e Biotecnologia, for the synthesis of PHBV18 and Dr. Luis Cabedo, from Universitat Jaume I for his support with mechanical testing and WAXD analyses. This work was financially supported by

## Chapter 11

the Spanish Ministry of Economy and Competitiveness (MAT2012-38947-C02-01). J.L. Castro-Mayorga is supported by the Administrative Department of Science, Technology and Innovation (Colciencias) of Colombian Government. M. J. Fabra is recipient of a Juan de la Cierva contract from the Spanish Ministry of Economy and Competitiveness.

## 6. References

---

1. P. E. Association of Plastics Manufacturers, "Plastics-the Facts 2014/2015. An analysis of European plastics production, demand and waste data," Ed.
2. C. S. K. Reddy, R. Ghai, Rashmi and V. C. Kalia, "Polyhydroxyalkanoates: An overview," *Bioresource Technology*, vol. 87, no. 2, pp. 137-146, 2003.
3. P. Patwardhan and A. K. Srivastava, "Fed-batch cultivation of *Wautersia eutropha*," *Bioresour Technol*, vol. 99, no. 6, pp. 1787-1792, 2008.
4. D. Heinrich, M. H. Madkour, M. A. Al-Ghamdi, I. I. Shabbaj and A. Steinbüchel, "Large scale extraction of poly(3-hydroxybutyrate) from *Ralstonia eutropha* H16 using sodium hypochlorite," *AMB Express*, vol. 2, no. 1, 2012.
5. N. GuriEFF and P. Lant, "Comparative life cycle assessment and financial analysis of mixed culture polyhydroxyalkanoate production," *Bioresource Technology*, vol. 98, no. 17, pp. 3393-3403, 2007.
6. M. Martínez-Sanz, M. Villano, C. Oliveira, M. G. E. Albuquerque, M. Majone, M. Reis, A. Lopez-Rubio and J. M. Lagaron, "Characterization of polyhydroxyalkanoates synthesized from microbial mixed cultures and of their nanobiocomposites with bacterial cellulose nanowhiskers," *New Biotechnology*, vol. 31, no. 4, pp. 364-376, 2014.
7. D. Plackett and I. Siró, "Polyhydroxyalkanoates (phas) for food packaging," in *Multifunctional and Nanoreinforced Polymers for Food Packaging*, Ed., pp. 498-526, 2011.
8. A. Martínez-Abad, J. M. Lagaron and M. J. Ocio, "Development and characterization of silver-based antimicrobial ethylene-vinyl alcohol copolymer (EVOH) films for food-packaging applications," *Journal of Agricultural and Food Chemistry*, vol. 60, no. 21, pp. 5350-5359, 2012.
9. A. N. Krklješ, M. T. Marinović-Cincović, Z. M. Kačarević-Popović and J. M. Nedeljković, "Dynamic thermogravimetric degradation of gamma radiolytically

- synthesized Ag-PVA nanocomposites," *Thermochimica Acta*, vol. 460, no. 1-2, pp. 28-34, 2007.
10. R. J. Pinto, S. C. Fernandes, C. S. Freire, P. Sadocco, J. Causio, C. P. Neto and T. Trindade, "Antibacterial activity of optically transparent nanocomposite films based on chitosan or its derivatives and silver nanoparticles," *Carbohydr Res*, vol. 348, pp. 77-83, 2012.
  11. E. Fortunati, M. Peltzer, I. Armentano, A. Jiménez and J. M. Kenny, "Combined effects of cellulose nanocrystals and silver nanoparticles on the barrier and migration properties of PLA nano-biocomposites," *Journal of Food Engineering*, vol. 118, no. 1, pp. 117-124, 2013.
  12. Z. H. Mbhele, M. G. Salemane, C. G. C. E. van Sittert, J. M. Nedeljković, V. Djoković and A. S. Luyt, "Fabrication and Characterization of Silver-Polyvinyl Alcohol Nanocomposites," *Chemistry of Materials*, vol. 15, no. 26, pp. 5019-5024, 2003.
  13. A. Martínez-Abad, J. M. Lagarón and M. J. Ocio, "Characterization of transparent silver loaded poly(l-lactide) films produced by melt-compounding for the sustained release of antimicrobial silver ions in food applications," *Food Control*, vol. 43, no. 0, pp. 238-244, 2014.
  14. S. Jeong, S. Yeo and S. Yi, "The effect of filler particle size on the antibacterial properties of compounded polymer/silver fibers," *Journal of Materials Science*, vol. 40, no. 20, pp. 5407-5411, 2005.
  15. M. A. Busolo and J. M. Lagaron, "Antimicrobial biocomposites of melt-compounded polylactide films containing silver-based engineered clays," *Journal of Plastic Film and Sheeting*, vol. 29, no. 3, pp. 290-305, 2013.
  16. B. Panea, G. Ripoll, J. González, Á. Fernández-Cuello and P. Albertí, "Effect of nanocomposite packaging containing different proportions of ZnO and Ag on chicken breast meat quality," *Journal of Food Engineering*, vol. 123, no. 0, pp. 104-112, 2014.
  17. P.-o. Rujitanaroj, N. Pimpha and P. Supaphol, "Preparation, characterization, and antibacterial properties of electrospun polyacrylonitrile fibrous membranes containing silver nanoparticles," *Journal of Applied Polymer Science*, vol. 116, no. 4, pp. 1967-1976, 2010.
  18. H. J. Jeon, J. S. Kim, T. G. Kim, J. H. Kim, W.-R. Yu and J. H. Youk, "Preparation of poly( $\epsilon$ -caprolactone)-based polyurethane nanofibers containing silver nanoparticles," *Applied Surface Science*, vol. 254, no. 18, pp. 5886-5890, 2008.
  19. M. Moritz and M. Geszke-Moritz, "The newest achievements in synthesis, immobilization and practical applications of antibacterial nanoparticles," *Chemical Engineering Journal*, vol. 228, pp. 596-613, 2013.

## Chapter 11

20. E. Fortunati, F. Luzi, D. Puglia, A. Terenzi, M. Vercellino, L. Visai, C. Santulli, L. Torre and J. M. Kenny, "Ternary PVA nanocomposites containing cellulose nanocrystals from different sources and silver particles: Part II," *Carbohydrate Polymers*, vol. 97, no. 2, pp. 837-848, 2013.
21. A. Martínez-Abad, J. M. Lagarón and M. J. Ocio, "Characterization of transparent silver loaded poly(L-lactide) films produced by melt-compounding for the sustained release of antimicrobial silver ions in food applications," *Food Control*, vol. 43, pp. 238-244, 2014.
22. A. Martínez-Abad, M. J. Ocio and J. M. Lagaron, "Morphology, physical properties, silver release, and antimicrobial capacity of ionic silver-loaded poly(L-lactide) films of interest in food-coating applications," *Journal of Applied Polymer Science*, vol. 131, no. 21, 2014.
23. A. Travan, C. Pelillo, I. Donati, E. Marsich, M. Benincasa, T. Scarpa, S. Semeraro, G. Turco, R. Gennaro and S. Paoletti, "Non-cytotoxic silver nanoparticle-polysaccharide nanocomposites with antimicrobial activity," *Biomacromolecules*, vol. 10, no. 6, pp. 1429-1435, 2009.
24. S. Mahouche-Chergui, M. Guerrouache, B. Carbonnier and M. M. Chehimi, "Polymer-immobilized nanoparticles," *Colloids and Surfaces A: Physicochemical and Engineering Aspects*, vol. 439, pp. 43-68, 2013.
25. D. Maity, M. M. R. Mollick, D. Mondal, B. Bhowmick, M. K. Bain, K. Bankura, J. Sarkar, K. Acharya and D. Chattopadhyay, "Synthesis of methylcellulose-silver nanocomposite and investigation of mechanical and antimicrobial properties," *Carbohydrate Polymers*, vol. 90, no. 4, pp. 1818-1825, 2012.
26. A. Martínez-Abad, G. Sanchez, J. M. Lagaron and M. J. Ocio, "Influence of speciation in the release profiles and antimicrobial performance of electrospun ethylene vinyl alcohol copolymer (EVOH) fibers containing ionic silver ions and silver nanoparticles," *Colloid and Polymer Science*, vol. 291, no. 6, pp. 1381-1392, 2012.
27. Z. C. Xing, W. P. Chae, J. Y. Baek, M. J. Choi, Y. Jung and I. K. Kang, "In vitro assessment of antibacterial activity and cytocompatibility of silver-containing phbv nanofibrous scaffolds for tissue engineering," *Biomacromolecules*, vol. 11, no. 5, pp. 1248-1253, 2010.
28. M. Min, Y. Shi, H. Ma, H. Huang, J. Shi, X. Chen, Y. Liu and L. Wang, "Polymer-nanoparticle composites composed of poly(3-hydroxybutyrate-co-3-hydroxyvalerate) and coated silver nanoparticles," *Journal of Macromolecular Science, Part B: Physics*, vol. 54, no. 4, pp. 411-423, 2015.

29. H. Yu, B. Sun, D. Zhang, G. Chen, X. Yang and J. Yao, "Reinforcement of biodegradable poly(3-hydroxybutyrate-co-3-hydroxyvalerate) with cellulose nanocrystal/silver nanohybrids as bifunctional nanofillers," *Journal of Materials Chemistry B*, vol. 2, no. 48, pp. 8479-8489, 2014.
30. J. L. Castro-Mayorga, A. Martínez-Abad, M. J. Fabra, C. Olivera, M. Reis and J. M. Lagarón, "Stabilization of antimicrobial silver nanoparticles by a polyhydroxyalkanoate obtained from mixed bacterial culture," *International Journal of Biological Macromolecules*, vol. 71, pp. 103-110, 2014.
31. A. Martínez-Abad, L. Cabedo, C. S. S. Oliveira, L. Hilliou, M. Reis and J. M. Lagarón, "Characterization of polyhydroxyalkanoate blends incorporating unpurified biosustainably produced poly(3-hydroxybutyrate-co-3-hydroxyvalerate)," *Journal of Applied Polymer Science*, 2015.
32. M. J. Fabra, A. Lopez-Rubio and J. M. Lagaron, "High barrier polyhydroxyalkanoate food packaging film by means of nanostructured electrospun interlayers of zein," *Food Hydrocolloids*, vol. 32, no. 1, pp. 106-114, 2013.
33. M. Scandola, M. L. Focarete, G. Adamus, W. Sikorska, I. Baranowska, S. Świerczek, M. Gnatowski, M. Kowalczyk and Z. Jedliński, "Polymer Blends of Natural Poly(3-hydroxybutyrate-co-3-hydroxyvalerate) and a Synthetic Atactic Poly(3-hydroxybutyrate). Characterization and Biodegradation Studies," *Macromolecules*, vol. 30, no. 9, pp. 2568-2574, 1997.
34. A. Matsumoto, T. Ishikawa, T. Odani, H. Oikawa, S. Okada and H. Nakanishi, "An Organic/Inorganic Nanocomposite Consisting of Polymuconate and Silver Nanoparticles," *Macromolecular Chemistry and Physics*, vol. 207, no. 4, pp. 361-369, 2006.
35. S. Vidhate, L. Innocentini-Mei and N. A. D'Souza, "Mechanical and electrical multifunctional poly(3-hydroxybutyrate-co-3-hydroxyvalerate)—multiwall carbon nanotube nanocomposites," *Polymer Engineering & Science*, vol. 52, no. 6, pp. 1367-1374, 2012.
36. L. S. Serafim, P. C. Lemos, C. Torres, M. A. M. Reis and A. M. Ramos, "The influence of process parameters on the characteristics of polyhydroxyalkanoates produced by mixed cultures," *Macromolecular Bioscience*, vol. 8, no. 4, pp. 355-366, 2008.
37. Y. Wang, S. Yamada, N. Asakawa, T. Yamane, N. Yoshie and Y. Inoue, "Comonomer Compositional Distribution and Thermal and Morphological Characteristics of Bacterial Poly(3-hydroxybutyrate-co-3-hydroxyvalerate)s with High 3-Hydroxyvalerate Content," *Biomacromolecules*, vol. 2, no. 4, pp. 1315-1323, 2001.
38. S. Manna, S. K. Batabyal and A. K. Nandi, "Preparation and Characterization of Silver–Poly(vinylidene fluoride) Nanocomposites: Formation of Piezoelectric

## Chapter 11

Polymorph of Poly(vinylidene fluoride)," *The Journal of Physical Chemistry B*, vol. 110, no. 25, pp. 12318-12326, 2006.

39. D. W. Chae, S. S. Hwang, S. M. Hong, S. P. Hong, B. G. Cho and B. C. Kim, "Influence of high contents of silver nanoparticles on the physical properties of poly(vinylidene fluoride)," *Molecular Crystals and Liquid Crystals*, vol. 464, no. 1, pp. 233-241, 2007.

40. N. Pramanik, A. Bhattacharyya and P. P. Kundu, "Spectroscopic analysis and catalytic application of biopolymer capped silver nanoparticle, an effective antimicrobial agent," *Journal of Applied Polymer Science*, vol. 132, no. 8, 2015.

41. B. Laycock, M. V. Arcos-Hernandez, A. Langford, S. Pratt, A. Werker, P. J. Halley and P. A. Lant, "Crystallisation and fractionation of selected polyhydroxyalkanoates produced from mixed cultures," *New Biotechnology*, vol. 31, no. 4, pp. 345-356, 2014.

42. E. Ten, J. Turtle, D. Bahr, L. Jiang and M. Wolcott, "Thermal and mechanical properties of poly(3-hydroxybutyrate-co-3-hydroxyvalerate)/cellulose nanowhiskers composites," *Polymer*, vol. 51, no. 12, pp. 2652-2660, 2010.

43. M. V. Arcos-Hernández, B. Laycock, B. C. Donose, S. Pratt, P. Halley, S. Al-Luaibi, A. Werker and P. A. Lant, "Physicochemical and mechanical properties of mixed culture polyhydroxyalkanoate (PHBV)," *European Polymer Journal*, vol. 49, no. 4, pp. 904-913, 2013.

44. M. F. S. Lima, M. A. Zen Vasconcellos and D. Samios, "Crystallinity changes in plastically deformed isotactic polypropylene evaluated by x-ray diffraction and differential scanning calorimetry methods," *Journal of Polymer Science, Part B: Polymer Physics*, vol. 40, no. 9, pp. 896-903, 2002.

45. M. Martínez-Sanz, A. Lopez-Rubio, M. Villano, C. S. S. Oliveira, M. Majone, M. Reis and J. M. Lagaron, "Production of bacterial nanobiocomposites of polyhydroxyalkanoates derived from waste and bacterial nanocellulose by the electrospinning enabling melt compounding method," *Journal of Applied Polymer Science*, 2015.

46. E. Hablot, P. Bordes, E. Pollet and L. Avérous, "Thermal and thermo-mechanical degradation of poly(3-hydroxybutyrate)-based multiphase systems," *Polymer Degradation and Stability*, vol. 93, no. 2, pp. 413-421, 2008.

47. P. Maiti, C. A. Batt and E. P. Giannelis, "New biodegradable polyhydroxybutyrate/layered silicate nanocomposites," *Biomacromolecules*, vol. 8, no. 11, pp. 3393-3400, 2007.

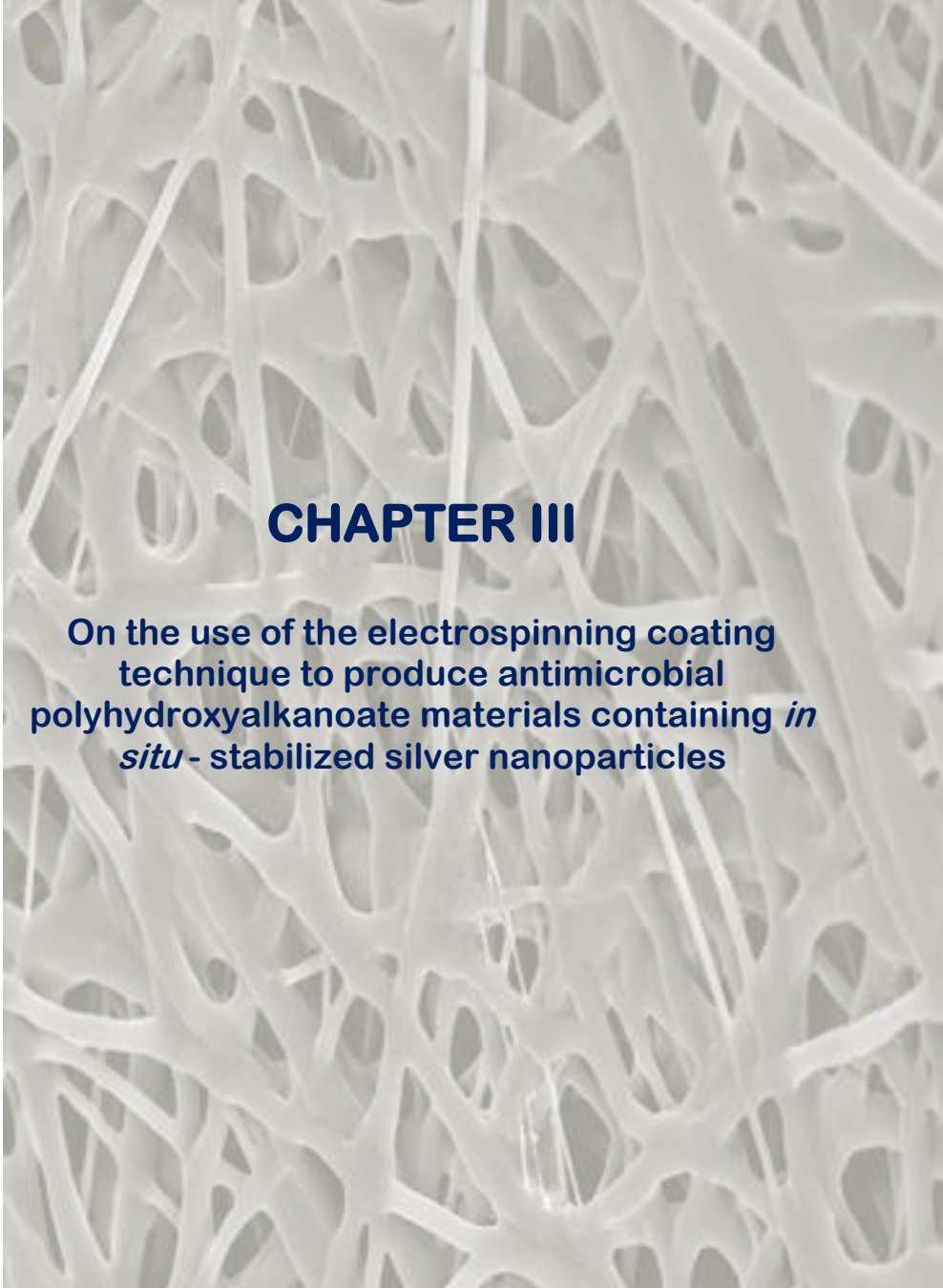
48. D. Kalpana and Y. S. Lee, "Synthesis and characterization of bactericidal silver nanoparticles using cultural filtrate of simulated microgravity grown *Klebsiella pneumoniae*," *Enzyme and Microbial Technology*, vol. 52, no. 3, pp. 151-156, 2013.
49. S. Modi, K. Koelling and Y. Vodovotz, "Assessment of PHB with varying hydroxyvalerate content for potential packaging applications," *European Polymer Journal*, vol. 47, no. 2, pp. 179-186, 2011.
50. L. Savenkova, Z. Gercberga, I. Bibers and M. Kalnin, "Effect of 3-hydroxy valerate content on some physical and mechanical properties of polyhydroxyalkanoates produced by *Azotobacter chroococcum*," *Process Biochemistry*, vol. 36, no. 5, pp. 445-450, 2000.
51. M. Martínez-Sanz, A. Lopez-Rubio and J. M. Lagaron, "Optimization of the dispersion of unmodified bacterial cellulose nanowhiskers into polylactide via melt compounding to significantly enhance barrier and mechanical properties," *Biomacromolecules*, vol. 13, no. 11, pp. 3887-3899, 2012.
52. J. George, K. V. Ramana, A. S. Bawa and Siddaramaiah, "Bacterial cellulose nanocrystals exhibiting high thermal stability and their polymer nanocomposites," *International Journal of Biological Macromolecules*, vol. 48, no. 1, pp. 50-57, 2011.
53. C. Bilbao-Sáinz, R. J. Avena-Bustillos, D. F. Wood, T. G. Williams and T. H. McHugh, "Composite edible films based on hydroxypropyl methylcellulose reinforced with microcrystalline cellulose nanoparticles," *Journal of Agricultural and Food Chemistry*, vol. 58, no. 6, pp. 3753-3760, 2010.
54. Q. T. Nguyen, E. Favre, Z. H. Ping and J. Néel, "Clustering of solvents in membranes and its influence on membrane transport properties," *Journal of Membrane Science*, vol. 113, no. 1, pp. 137-150, 1996.
55. F. L. Laksmanna, P. J. A. Hartman Kok, H. W. Frijlink, H. Vromans and K. Van Der Voort Maarschalk, "Gas permeation related to the moisture sorption in films of glassy hydrophilic polymers," *Journal of Applied Polymer Science*, vol. 116, no. 6, pp. 3310-3317, 2010.
56. S. D. F. Mihindukulasuriya and L. T. Lim, "Nanotechnology development in food packaging: A review," *Trends in Food Science and Technology*, vol. 40, no. 2, pp. 149-167, 2014.
57. A. M. Díez-Pascual and A. L. Díez-Vicente, "Poly(3-hydroxybutyrate)/ZnO bionanocomposites with improved mechanical, barrier and antibacterial properties," *International Journal of Molecular Sciences*, vol. 15, no. 6, pp. 10950-10973, 2014.
58. S. Hess, M. M. Demir, V. Yakutkin, S. Balushev and G. Wegner, "Investigation of oxygen permeation through composites of PMMA and surface-modified ZnO

## *Chapter II*

nanoparticles," *Macromolecular Rapid Communications*, vol. 30, no. 4-5, pp. 394-401, 2009.

59. J. S. Kim, E. Kuk, K. N. Yu, J.-H. Kim, S. J. Park, H. J. Lee, S. H. Kim, Y. K. Park, Y. H. Park, C.-Y. Hwang, Y.-K. Kim, Y.-S. Lee, D. H. Jeong and M.-H. Cho, "Antimicrobial effects of silver nanoparticles," *Nanomedicine: Nanotechnology, Biology and Medicine*, vol. 3, no. 1, pp. 95-101, 2007.

60. A. Grigor'Eva, I. Saranina, N. Tikunova, A. Safonov, N. Timoshenko, A. Rebrov and E. Ryabchikova, "Fine mechanisms of the interaction of silver nanoparticles with the cells of *Salmonella typhimurium* and *Staphylococcus aureus*," *BioMetals*, vol. 26, no. 3, pp. 479-488, 2013.



## CHAPTER III

On the use of the electrospinning coating technique to produce antimicrobial polyhydroxyalkanoate materials containing *in situ* - stabilized silver nanoparticles

J. L. Castro-Mayorga, M. J. Fabra, L. Cabedo and J. M. Lagaron.  
“On the use of the electrospinning coating technique to produce antimicrobial polyhydroxyalkanoate materials containing *in situ* stabilized silver nanoparticles”. *Nanomaterials*, vol. 7, no. 1, 2017.



## Abstract

---

Electro-hydrodynamic processing, comprising electrospraying and electrospinning techniques, has emerged as a versatile technology to produce nanostructured fiber-based and particle-based materials. In this work, an antimicrobial active multilayer system comprising a commercial polyhydroxyalkanoate substrate (PHA) and an electrospun PHA coating containing *in situ*-stabilized silver nanoparticles (AgNPs) was successfully developed and characterized in terms of morphology, thermal, mechanical, and barrier properties. The obtained materials reduced the bacterial population of *Salmonella enterica* below the detection limits at very low silver loading of  $0.002 \pm 0.0005$  wt %. As a result, this study provides an innovative route to generate fully renewable and biodegradable materials that could prevent microbial outbreaks in food packages and food contact surfaces.

## Keywords

---

Electro-hydrodynamic processing; foodborne pathogens; metal nanoparticles; biopolyesters

## **1. Introduction**

---

Electro-hydrodynamic processing comprising electrospinning and electrospraying techniques is a broadly used and efficient technology that uses electrical forces to produce ultrathin fibers and nanocapsules, respectively [1, 2]. Electrospinning has recently gained much attention not only because of its versatility in processing a wide range of polymer and biopolymer materials, but also because of its ability to produce fiber diameters within the submicro and nano range that is otherwise not viable to achieve by using conventional-generating technologies. The intrinsic characteristics of electrospun fibers, like very high specific surface and porosity [3] and the suitability of the technique to encapsulate active substances within the fibers, have prompted their use in a wide range of applications [4-8]. With the expansion of this technology, several researchers have used electrospinning to improve physicochemical and functional properties of biopolymer based materials by means of a controlled release of active compounds or by enhancing the dispersion of nano-additives into the biopolymer matrices [9-11].

Of particular interest is the generation of fiber-based systems for antimicrobial food packaging and food contact surface applications given that the direct application of biocide compounds onto the food surface can be inefficient because of their rapid diffusion within the bulk of food [12]. In this way, the incorporation of antimicrobial fiber-base mats as coating of the packaging material, leading to antimicrobial films, could improve their activity in maintaining an optimal effect during the food storage period. Furthermore, the high surface to volume ratio of electrospun mats could allow the efficient and prolonged delivery of previously loaded antibiotics [10].

Different antimicrobial compounds such as silver, ricinoleic acid [13], and others have been used to develop active food packaging materials either incorporated into

the polymer matrix or directly copolymerized with the electrospun fibers. Due to their strong antimicrobial properties and thermal stability, silver nanoparticles (AgNPs) have so far been one of the most researched nanomaterials. The most common methods for the preparation of antibacterial and antifungal polymeric films have been direct blending of the nanometal with the matrix [14-17] and solvent casting [18-21]. However, the main challenge today is the synthesis of stable nanoparticles in a polymer solution, as their antimicrobial effectiveness depends on their size distribution and agglomeration state [22]. In general, when antimicrobials are used in applications related to pharma or biomedicine, the cytotoxicity of the materials becomes very relevant. Thus, there is increasing interest in the biological impact of AgNPs on a large scale and the possible risks to the environment and health [23]. Recent studies suggest that free-standing nanometer-sized particles may enter cells of living organisms, potentially leading to various cell injuries [24]. In this regard, Chairuangkitti and colleagues showed that silver contents below 25 ppm did not affect either the cell viability or the reactive oxygen species (ROS) generation of human lung carcinoma (A549) cells [25]. Also, Składanowski and collaborators concluded that AgNPs can be used as an antibacterial agent, being that these harmless for eukaryotic cells [26]; Salama et al. reached similar conclusion [27]. In any case, it is very unlikely that silver nanoparticles will be released from polymeric films that do not dissolve or strongly plasticize in the contact media [28].

On the incorporation of AgNPs into ultrafine fibers based on polymers, there are only a small number of studies on electrospun polymer fibers containing silver, such as poly( $\epsilon$ -caprolactone) [29], ethylene vinyl alcohol [11], poly-(L-lactide) [30], polypropylene [15], or polyacrylonitrile [31]. Further, to date, only few studies have yet been published about the preparation of silver and PHA based electrospun fibers [32, 33], none of them analyzing the antimicrobial activity against foodborne pathogens. In a recent study, Castro-Mayorga et al. [34], demonstrated that the

## Chapter III

effective stabilization of AgNPs in an unpurified poly(3-hydroxybutyrate-co-18 mol % 3-hydroxyvalerate) (PHBV18) avoided the use of surfactants or capping agents prior to or during melt compounding with poly(3-hydroxybutyrate-co-3 mol % 3-hydroxyvalerate) (PHBV3). In that case, PHBV3/PHBV18 films, containing 0.04 wt % of AgNPs, showed a strong and sustained antibacterial activity against two of the most common foodborne pathogens, *Salmonella enterica* and *Listeria monocytogenes*. However, despite this progress, and especially considering that the application of these materials in the restrictive food legislation frames could be severely limited because of the use of AgNPs, the main goal of the present paper is the development of new strategies based on the coating design in order to reduce the AgNPs loading while keeping the antimicrobial performance.

The present work reports on the development and characterization of an antimicrobial multilayer system of polyhydroxyalkanoates (PHA) matrix and nanostructured silver-based coating obtained by means of the electrospinning technique. In particular, the active multilayer was characterized in terms of thermal, mechanical, and barrier properties and their antibacterial effectiveness against *S. enterica* and *L. monocytogenes* was also evaluated.

## 2. Materials and methods

---

### 2.1 Materials

In this work, two different PHA grades, with different valerate (HV) contents, were used. PHBV3 (3 mol % valerate content, ENMAT Y1000P) was purchased in a pellet form from Tianan Biopolymers (Ningbo, China) and PHBV18 (18 mol % valerate content) was produced in a fermentation multi-stage process with mixed

microbial culture and cheese whey industrial by-product as feed stock as it has been previously described by Martínez-Abad et al.[35].

## 2.2 Synthesis of silver nanoparticles in PHBV18 matrices

The AgNPs were synthesized according to the *in situ* method reported by Castro-Mayorga et al. [34]. Briefly, 0.08 wt % of unpurified PHBV18 was suspended in ultrapure MilliQ® water (Millipore Corporation Co., Billerica, MA, USA) and the assembly was placed into an ice bath and stirred using magnetic stirring. A sodium borohydride (Panreac, Barcelona, Spain) aqueous solution was added first to the suspension to get 2 mM concentration and then silver nitrate (>98% purity; Sigma-Aldrich, Hamburg, Germany) aqueous solution (1 mM) was added dropwise to generate AgNPs. Finally, the obtained product was separated by centrifugation and dried overnight in a vacuum oven at 40 °C.

## 2.3 Preparation of the multilayer systems

Multilayer films of PHBV3 and electrospun fibers with and without AgNPs were prepared as follows. The sample code and composition are summarized in Table 1.

**Table 1.** Sample code and composition of the developed materials.

Sample code	Composition
PHBV3	100% commercial PHBV3
PHBV <sub>s</sub>	92% commercial PHBV3 + 8% PHBV18
PHBV <sub>s</sub> /AgNPs	PHBV <sub>s</sub> + Silver nanoparticles
Multilayer	Substrate PHBV3 + PHBV <sub>s</sub> coating
Active Multilayer	Substrate PHBV3 + PHBV <sub>s</sub> /AgNPs coating

## **Chapter III**

### **2.3.1. Preparation of the PHBV3 Film**

PHBV3 films with a thickness of ca. 80  $\mu\text{m}$  were prepared by compression-molding using a hot plate hydraulic press (Carver 4122, Wabash, IN, USA) at 180  $^{\circ}\text{C}$  and 1.8 MPa for 5 min.

### **2.3.2. Preparation of the electrospun fibers**

For the PHBVs and PHBVs/AgNPs electrospun fiber preparation, polymer solutions containing a total solids content of 6 wt % was prepared as follows: First, the PHBV3 at 92 wt % was dissolved in 2,2,2-Trifluoroethanol (TFE,  $\geq 99$  wt %, Sigma Aldrich, Hamburg, Germany) under magnetic stirring for 4 h at 50  $^{\circ}\text{C}$  and cooled down at room temperature. Then, PHBV18 or stabilized PHBV18/AgNPs were incorporated at the remaining 8 wt % and stirred for 12 more hours. Thereafter, the solution was processed using a Fluidnatek<sup>®</sup> LE-500 pilot plant electrospinning setup manufactured by Bioinicia S.L., Valencia, Spain. The tool was operated under a steady flow-rate and made use of a motorized high throughput multinozzle injector, scanning vertically towards a metallic grid used as a collector. The distance between the needle and the collector was 20 cm, and the experiments were carried out at room temperature ( $23 \pm 2$   $^{\circ}\text{C}$ ) for 15 min. The voltages of the collector and injector were set at 24 kV and -18 kV, respectively. The flow rate was 80 mL/h. After electrospinning, the fiber mats were dried at 40  $^{\circ}\text{C}$  under vacuum overnight to completely remove the solvent and were subsequently used to prepare the coated systems.

### **2.3.3. Preparation of the multilayer films**

PHBV3 films were coated with PHBVs and PHBVs/AgNsP ultrathin fiber mats produced by means of electrospinning and an annealing step was applied. Fiber mats were placed onto PHBV3 films and the assembly was put in between hot plates

hydraulic press (Carver 4122, Wabash, IN, USA) at 160 °C for 2 min (without pressing). The total amount of electrospun coating ( $-0.71 \pm 0.01$  mg/cm<sup>2</sup>) was estimated by weighing the coated system before and after deposition of the electrospun material which corresponded to ~5 wt % of the coated systems.

## **2.4 Determination of silver content in the active multilayer systems**

The total Ag content within the active multilayer systems was determined by subjecting 100 mg samples to acid digestion with 2 mL of Hiperpur HNO<sub>3</sub> (Panreac, Barcelona, Spain) at 80 °C overnight. The resultant digestant was diluted to a final volume of 5 mL. The quantification of silver was carried out by inductively coupled plasma-optical emission spectroscopy (ICP-OES, Perkin-Elmer, Waltham, MA, USA) using a silver standard solution (traceable to SRM from NIST, AgNO<sub>3</sub> in HNO<sub>3</sub> 2–3%, 1000 mg/L, Ag Certipur®, Merck, Darmstadt, Germany) for calibration. All measurements were done, at least, in triplicate.

## **2.5 Transmission Electronic Microscopy (TEM)**

The morphology of the electrospun fibers and the active multilayer films was studied using a Jeol 1010 (Hitachi, Tokyo, Japan), transmission electronic microscope an accelerating voltage of 80 kV. Samples were previously ultra-microtomed (Leica EM UC6, Wetzlar, Germany) and placed onto carbon-coated copper grids.

## **2.6 Scanning Electronic Microscopy (SEM)**

SEM was conducted on a Hitachi S-4800 microscope (Hitachi, Chiyoda, Tokyo, Japan) at an accelerating voltage of 5 kV and a working distance of 8–10 mm. The active multilayer films were cryo-fractured after immersion in liquid nitrogen and

## *Chapter III*

subsequently sputtered with a gold-palladium mixture under vacuum before their examination. Estimation of the average fiber diameter was done by means of the Adobe Photoshop CS4 software from 300 fibers at random from SEM images.

### **2.7 Differential Scanning Calorimetry (DSC)**

Thermal properties of the neat electrospun fibers, PHBV3 films and the multilayer systems were evaluated by Differential Scanning Calorimetry (DSC) using a Perkin-Elmer DSC 8000 (Waltham, MA, USA) thermal analysis system under nitrogen atmosphere. The analysis was carried out on ~3 mg of each sample at a heating rate of 10 °C/min, from 0 °C to 200 °C, followed by a subsequent cooling down to -50 °C. The DSC equipment was calibrated with indium as a standard and the slope of the thermograms was corrected by subtracting similar scans of an empty pan. Tests were done, at least, in triplicate.

### **2.8 Mechanical properties**

Tensile tests of the neat PHBV3 and the multilayer systems were carried out in a universal testing machine (Shimadzu AGS-X 500N, Kyoto, Japan) at a crosshead rate of 10 mm/min at room temperature. All samples were allowed to reach the equilibrium under ambient conditions (25 °C and 50% R.H. for 24 h before the testing). Tests were performed according to ASTM D638 with dumb-bell samples die-cut from prepared films. Elastic Modulus (E), Tensile Strength (TS), and Elongation at Break (EAB) were determined from the stress-strain curves, estimated from force–distance data obtained for the different films.

## **2.9 Barrier properties**

### **2.9.1. Water Vapor Permeability (WVP)**

WVP was measured, in triplicate, according to the ASTM E96 gravimetric method, using Payne permeability cups (Elcometer SPRL, Ourpeye, Belgium). Distilled water was placed inside the cup to expose the film (the exposed area was  $9.6 \times 10^{-4} \text{ m}^2$ ) to 100% RH on one side. Once the films were secured, each cup was placed in an equilibrated relative humidity cabinet at 0% RH and room temperature. The cups were weighed periodically ( $\pm 0.0001 \text{ g}$ ). Water vapor permeation rate was calculated from the steady-state permeation slopes (eight points) obtained from the regression analysis of weight loss data vs. time, and weight loss was calculated as the total cell loss minus the loss through the sealing. Permeability was obtained by multiplying the permeance by the average film thickness.

### **2.9.2. Oxygen Permeability (PO<sub>2</sub>)**

The PO<sub>2</sub> was derived from oxygen transmission rate (OTR) measurements recorded using an Oxygen Permeation Analyzer M8001 (Systech Illinois, Thame, UK). Experiments were carried out at 23 °C and 80% RH. The samples were previously purged with nitrogen in the humidity equilibrated samples, before exposure to an oxygen flow of 10 mL/min. The exposure area during the test was 5 cm<sup>2</sup> for each sample. In order to obtain the oxygen permeability, film thickness and gas partial pressure were considered in each case. The measurements were done in triplicate.

### 2.10 Antimicrobial activity of coated systems

Gram negative, *Salmonella enterica* CECT 4300 and Gram positive *Listeria monocytogenes* CECT 7467 were used to determine the antimicrobial activity of the obtained films. The strains were purchased from the Spanish Type Culture Collection (CECT: Valencia, Spain) and stored in phosphate buffered saline (PBS, Sigma Aldrich, USA) with 10 wt % tryptic soy broth (TSB, Conda Laboratories, Madrid, Spain) and 10 wt % glycerol at  $-80\text{ }^{\circ}\text{C}$  until needed. For experimental use, a loopful of bacteria was transferred to 10 mL of TSB and incubated at  $37\text{ }^{\circ}\text{C}$  overnight and an aliquot was again transferred to TSB and grown at  $37\text{ }^{\circ}\text{C}$  and 120 rpm to the mid-exponential phase of growth having an absorbance value of 0.20 as determined by optical density at 600 nm (Agilent 8453 UV-visible spectrum system, Santa Clara, CA, USA). This culture served as inoculum for antimicrobial assays.

To perform the susceptibility study, a modification of the Japanese Industrial Standard JIS Z 2801 (ISO 22196) was used. Briefly, a microorganism suspension containing about  $5 \times 10^5$  CFU/mL was applied onto the active multilayers of  $3 \times 3$  cm and covered by an inert piece of Low-Density Polyethylene (LDPE) of  $2.5 \times 2.5$  cm and  $80\text{ }\mu\text{m}$  of thickness. After incubation at room temperature and a relative humidity of at least 95% for 24 h, bacteria were recovered with PBS, and the viable cells determined by the conventional plate count method. The multilayer film (without AgNPs) was used as a negative control. Three specimens of each sample were tested.

### 2.11 Statistical Analysis

Statistical analysis of physicochemical and antimicrobial data was performed through analysis of variance (ANOVA) using StatGraphics Plus for Windows version 5.1 (Statistical Graphics Corporation, NJ, USA). Homogeneous sample groups were

obtained by using Tukey's Honestly Significant Difference (HSD) (95% significant level). Data were reported as mean values  $\pm$  standard deviation.

## **3. Results and discussion**

---

### **3.1 Morphology**

It is well-known that efficient electrospinning depends on the solution properties (typically viscosity, surface tension, and conductivity). In this sense, stable electrospinning is often only achieved when the viscosity is high enough to produce the necessary polymer entanglements to form fibers and one of the most important factors which govern this aspect is the polymer concentration in the electrospinning solution. Based on screening studies dealing with the electrospinning of PHBVs, the concentration of the total polymer was adjusted to obtain stable electrospinning process avoiding the dripping of the solutions, the formation of beaded areas, or the formation of fibers in which the average diameters surpassed the micron size. Therefore, taking into account all these aspects, the concentration of the PHBVs was set to 6 wt %, as to obtain continuous fibers with no beads and in the submicron diameter range. For comparative purposes, the PHBV3/PHBV18 ratio was established at 92:8, according to the mixture used for highly efficient antibacterial nanocomposites recently reported by Castro-Mayorga et al.[36].

SEM micrographs of the PHBVs fibers with and without AgNPs and their corresponding average diameters are shown in Figure 1. The first clear observation is that the addition of AgNPs did not significantly modify the morphology of the fibers probably due to their low concentration in the PHBV mixture. In contrast, several authors have reported that the addition of silver ions or AgNPs greatly affected the

### Chapter III

diameter of the fibers, causing a significant reduction in the average diameter. However, in those cases, the additive was added in higher concentrations. They reported that the presence of silver, either in the form of ions or nanoparticles, increased the charge density and conductivity, which produces an increase in the stretching forces in the jet, consequently decreasing the fiber diameter [11, 37, 38].

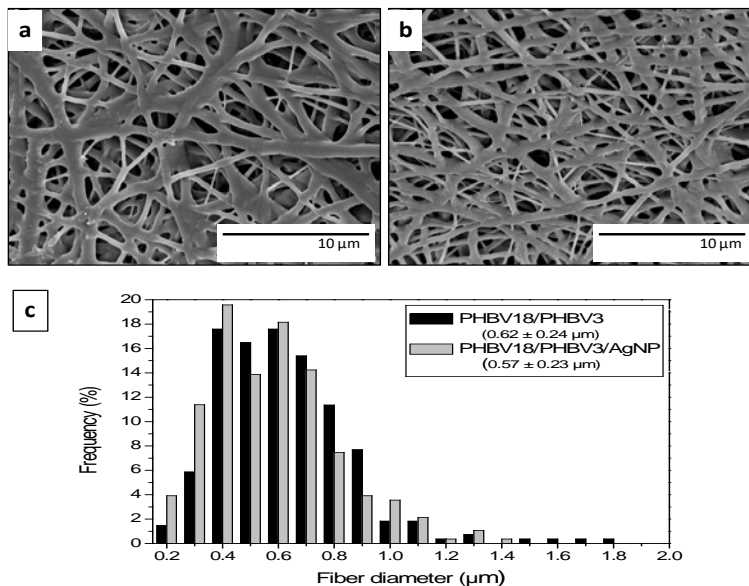


**Figure 1.** Scanning electron microscopy (SEM) images of the electrospun fibers: (a) PHBVs; (b) PHBVs/ silver nanoparticles (AgNPs); (c) size distribution of fibers.

In order to obtain more detailed information about the dispersion and distribution of individual AgNPs into the electrospun fibers and into the active multilayer system, these samples were ultra-microtomed and analyzed by TEM. Figure 2 shows the TEM micrographs of an ultrathin section of electrospun PHBVs/AgNPs fibers (Figure 2a) and microtomed thin sheets of the active multilayer (Figure 2b). It was clearly observed that AgNPs were well dispersed into the electrospun fibers and into the active multilayer, having an average particle diameter

of  $6 \pm 1$  nm. Since, by TEM observation, only the nanoparticles can be seen and not the fibers, it is interesting to note that the diameter enclosing the AgNPs observed in Figure 2a matches the actual electrospun fiber's diameter (ca.  $0.46 \mu\text{m}$ ), hence suggesting the AgNPs are well dispersed and distributed in the electrospun fibers. Thus, the PHBV18 clearly favored a proper entrapment of highly dispersed and distributed AgNPs. Compared with other PHBVs/AgNPs nanocomposites, the electrospinning process results in a lack of agglomeration that more easily occurs when processed by conventional melt compounding methods [15, 36, 39].

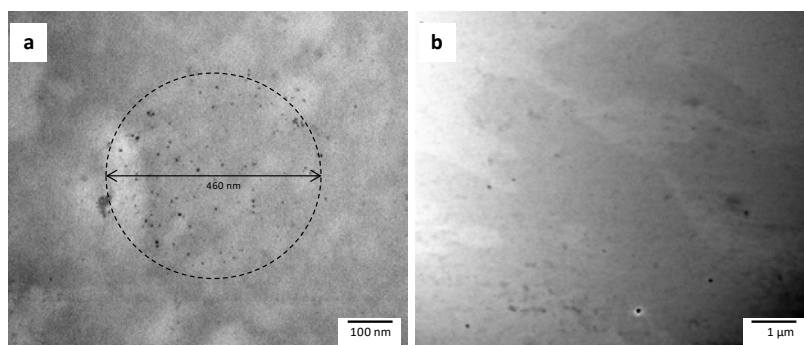


**Figure 2.** Transmission electron microscopy (TEM) micrographs of ultramicrotomed silver-containing materials: (a) in PHBVs/AgNPs; (b) in the active multilayer film. The dashed line in the Figure 2a shows a group of AgNPs whose diameter matches with the fiber's diameter of  $0.46 \mu\text{m}$ .

The morphology of the multilayer structures based on PHBV3 and PHBVs/AgNPs electrospun coatings were also examined by SEM and representative images are displayed in Figure 3. As it can be seen from this figure, after the annealing step, the active multilayer films exhibited a continuous and smooth surface from a top view ( Figure 3a), which is strongly adhered to the bottom layer in the cryo-fractured side view ( Figure 3b), revealing the excellent adhesion between the two layers after the annealing step.

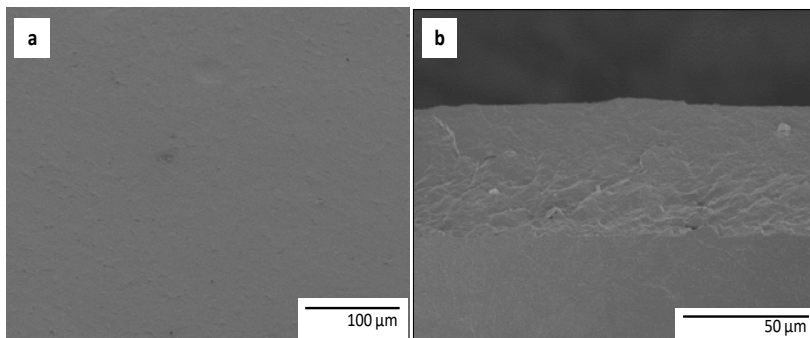


**Figure 3.** SEM micrographs of the active multilayer; (a) top view of the film; (b) side view of the cryo-fractured film section.

Figure 4 shows the overall contact transparency of the neat PHBV3 (Figure 4a) and of the multilayers prepared without and with AgNPs (Figure 4b,c, respectively). As observed, the coated systems preserved a good contact transparency and neither the multilayer nor the active multilayer induced significant differences in appearance in the internal transmittance of the films (data not shown). Therefore, it could be stated that no significant degradation of PHBV18 or silver reduction/agglomeration events occurred during the annealing step.

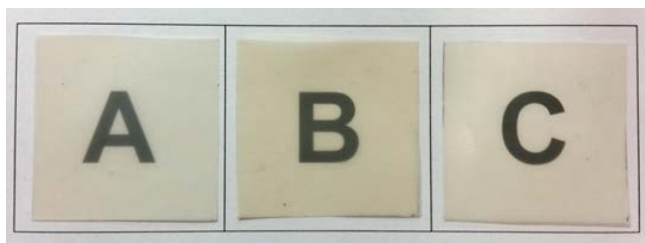


**Figure 4.** Contact transparency pictures of films. (A) poly(3-hydroxybutyrate-co-3 mol %-3-hydroxyvalerate) (PHBV3); (B) multilayer; (C) active multilayer.

### 3.2 Thermal properties

With the aim of investigating the effects of AgNPs addition and PHBV<sub>s</sub>/AgNPs electrospun coating on the thermal properties, differential scanning calorimetry (DSC) analyses of neat and silver-base fibers as well as PHBV<sub>3</sub> layer and bilayer systems with and without AgNPs were carried out ( Table 2 and Figure 5). The melting point ( $T_m$ ) and melting enthalpies ( $\Delta H_m$ ) were calculated from the maximum temperatures and peak area, respectively, of the peak associated with the melting process from the first heating runs. The crystallization temperature ( $T_c$ ) was also obtained from the cooling run. From Table 2, the presence of the silver nanoparticles seems to modify only slightly up the  $T_c$ , perhaps suggesting a small nucleation effect also reflected in the slightly increased melting enthalpy; albeit the changes are not statistically significant.

**Table 2.** Differential scanning calorimetry (DSC) parameters of the neat electrospun fibers and films and their silver-based coating system.

Sample	$T_{m1}$ (°C)	$T_{m2}$ (°C)	$T_c$ (°C)	$\Delta H_m$ (J/g)
PHBV <sub>s</sub>	173.7 ± 0.2 <sup>a</sup>	-	113.4 ± 0.5 <sup>a</sup>	61 ± 1 <sup>a</sup>
PHBV <sub>s</sub> /AgNPs	173.8 ± 0.1 <sup>a</sup>	-	114.9 ± 0.3 <sup>a</sup>	65 ± 1 <sup>a</sup>
PHBV <sub>3</sub>	168.7 ± 1.0 <sup>b</sup>	181.8 ± 0.2 <sup>a</sup>	114.7 ± 0.0 <sup>a</sup>	72 ± 1 <sup>b</sup>
Multilayer	168.5 ± 1.4 <sup>b</sup>	-	117.3 ± 0.1 <sup>b</sup>	73 ± 1 <sup>b</sup>
Active Multilayer	170.4 ± 0.8 <sup>a,b</sup>	184.8 ± 0.7 <sup>b</sup>	117.4 ± 0.6 <sup>b</sup>	74 ± 1 <sup>b</sup>

Mean values ± standard deviation. Mean values with different superscript letters in the same column represent significant differences ( $p < 0.05$ ) among the samples according to ANOVA and Tukey's multiple comparison tests.

However, from observation of Figure 5, it is clear that the formulation of the materials does have an effect in the shape of the melting endotherms of the different samples that is clearly related to the fact that electrospun fibers and electrospun coated films do have a different melting behavior during the DSC run. These variations can be ascribed to the morphology of the fibers which, during melting,

## Chapter III

seem to behave more homogeneously due to the high surface to volume ratio of the electrospun materials as compared to a thicker continuous film. The coated samples also show a different behavior as compared to the bulk PHBV3 compression molded film which suggests that the lower melting point of the coating alters the overall melting behavior of the bilayer. Thus, the observed multiple melting endotherms are here found to depend on how the samples were obtained and not on the actual intrinsic polymer composition. Therefore, the results above support that melting recrystallization phenomena during the DSC run could be at the origin of the multiple endotherms for this polymer as previously suggested in the literature [35, 36, 40, 41]

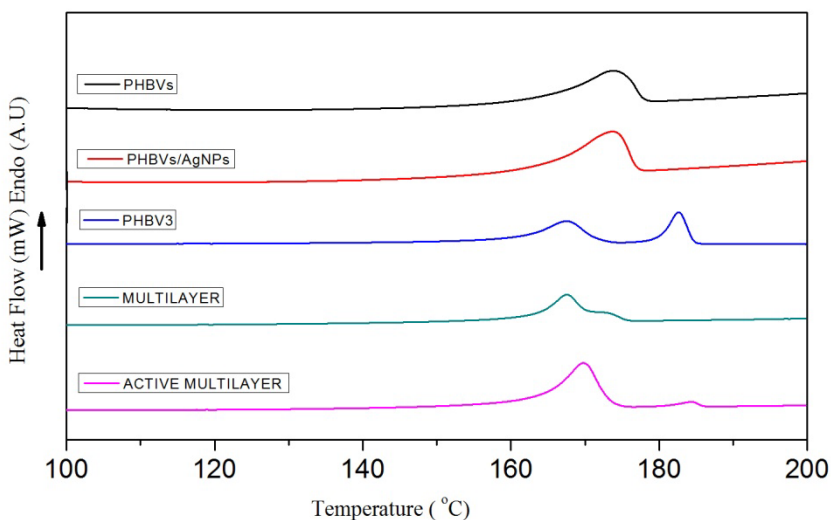


**Figure 5.** Differential scanning calorimetry (DSC) thermograms of first heating run of the neat electrospun fibers and films and their silver-based coating system.

### 3.3 Barrier properties

Table 3 gathers water vapor and oxygen permeability of the PHBV3 matrix and the coated systems with or without AgNPs. In general, the presence of the PHBV3 coatings did not significantly alter the barrier properties of the neat PHBV3 film.

Although the neat PHBV18 film has been reported to have higher oxygen and water vapor permeability values than the neat PHBV3 [36], its incorporation as a part of the electrospun coating did not significantly affect barrier properties of the PHBV3, probably due to the low concentration used. Contrary to that observed for nanocomposites prepared with PHBV3/PHBV18/AgNPs [36], the addition of the stabilized AgNPs did not result in a positive barrier effect on the active multilayer. These differences could be explained by the low AgNPs loading which was not enough to create a meaningful blocking tortuous path in the PHBV matrix. In contrast, Kanmani and Rhim [42] reported that the reduction in water vapor (WVP) of the gelatin-based nanocomposite films containing AgNPs was mainly due to nanofillers causing a more tortuous pathway for water vapor diffusion. This indicates that the barrier efficiency of nanocomposite films containing AgNPs, depends on having a sufficient quantity of nanoparticles since the spherical shape of this nanofiller is not thought to be as efficient in reducing diffusion as plate-like fillers such as clay minerals.

**Table 3.** Water vapor (WVP) and oxygen permeability ( $PO_2$ ) measurements of the neat PHBV3 and PHBVs films and the silver-based coating systems.

Sample	WVP (Kg m/Pa s m <sup>2</sup> )	PO <sub>2</sub> (m <sup>3</sup> m/m <sup>2</sup> s Pa) 80% RH
PHBV3	(1.10 ± 0.02) * 10 <sup>-15</sup> a	(2.06 ± 0.09) * 10 <sup>-19</sup> a
Multilayer	(1.25 ± 0.25) * 10 <sup>-15</sup> a	(2.13 ± 0.12) * 10 <sup>-19</sup> a
Active Multilayer	(1.59 ± 0.38) * 10 <sup>-15</sup> a	(2.17 ± 0.19) * 10 <sup>-19</sup> a

Mean values ± standard deviation. Mean values with different superscript letters in the same column represent significant differences ( $p < 0.05$ ) among the samples according to ANOVA and Tukey's multiple comparison tests.

### 3.4 Mechanical properties

The materials' Elastic Modulus (E), Elongation at Break (EAB) and Maximum Tensile Strength (TS) are presented in Table 4. The neat PHBV3 film presented an excellent rigidity and strength but an excessive brittleness. The mechanical

## Chapter III

performance of PHBV3 was not altered by the incorporation of electrospun PHBVs coating with or without AgNPs. The active multilayer seems to be somewhat more ductile than its counterparts prepared without AgNPs, although differences were not found significant. The lack of effect on mechanical properties in the coated systems was in line with the previous observations by Castro-Mayorga et al. [36] and Jeong et al. [15] in which highly dispersed AgNPs did not present a significant effect on PHBV melt compounded nanocomposites. However, once again, the AgNPs loading was perhaps too low to impact the mechanical performance of the neat polymer.

**Table 4.** Tensile parameters of the neat PHBV3 and PHBV films and the silver-based coating systems.

Sample	E (GPa)	EAB (%)	TS (MPa)
PHBV3	2.6 ± 0.1 <sup>a</sup>	1.5 ± 0.2 <sup>a</sup>	33.9 ± 6.9 <sup>a</sup>
Multilayer	2.6 ± 0.2 <sup>a</sup>	1.8 ± 0.2 <sup>a</sup>	37.1 ± 2.8 <sup>a</sup>
Active Multilayer	2.6 ± 0.1 <sup>a</sup>	2.4 ± 0.6 <sup>a</sup>	29.9 ± 3.5 <sup>a</sup>

Mean values ± standard deviation. Mean values with different superscript letters in the same column represent significant differences ( $p < 0.05$ ) among the samples according to ANOVA and Tukey's multiple comparison tests.

### 3.5 Antimicrobial Activity

To evaluate the antimicrobial activity of the coated systems containing AgNPs on the surface, a modification of the Japanese Industrial Standard JIS Z 2801:2000 (ISO 22196) was followed, the results are presented in Figure 6. The incubation temperature of  $23 \pm 2$  °C was chosen to mimic room temperature conditions of possible application of these plastics in food contact or other antimicrobial surfaces. The first observation to highlight is that, after 24 h of exposure, the active multilayer did not show any antibacterial effect against *Listeria monocytogenes*. In contrast, a surprising reduction of ca. 5 log CFU/mL of *Salmonella enterica* was recorded. These differences are in line with previous studies reporting a higher susceptibility of gram-negative as compared with gram-positive bacteria [43, 44] which related this finding with the presence of multiple

layers of peptidoglycan-containing teichoic acids or lipoteichoic acids with strong negative charge that may contribute to sequestration of free Ag ions needed to exert the antimicrobial effect.

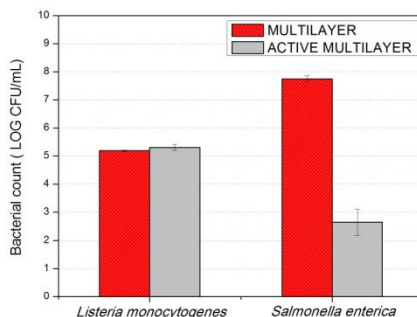


**Figure 6.** Antimicrobial activity of PHBV and PHBV/AgNP films against *Listeria monocytogenes* and *Salmonella enterica* after 24 h of exposure. The initial inoculum size was  $\sim 5$  log CFU/mL and the detection limit was 20 CFU/mL.

It should also be noted that, on the silver-based antimicrobial materials, Castro-Mayorga et al. [36] have recently demonstrated the bactericide effect of melt compounded nanocomposites containing  $0.040 \pm 0.002$  wt %, AgNPs against both *Listeria monocytogenes* and *Salmonella enterica*. However, in the present work, the total silver content was 20 times lower than the previously cited report (i.e., of only  $0.002 \pm 0.0005$  wt % as measured by ICP-OES) and even more than 50 times lower than other ones reporting silver loading between 0.1 and 5 wt % [14, 19, 32, 45]. This fact represents not only a significant reduction of silver concentration required to achieve a bactericide effect against *Salmonella enterica* but also an alternative way to satisfy the specific limit of migration established by the current legislation.

A similar set of samples used for the antimicrobial tests described above are currently being tested with regard to their cytotoxicity; the preliminary results (not shown) suggest that the materials do not provide cytotoxic effect when tested in direct

contact with colorectal carcinoma cells (HCT116) or with neonatal non-tumor fibroblasts cells (the study when completed will be published elsewhere).

## 4. Conclusions

---

The use of the electrospinning coating technique allows the development of packaging materials with unique properties. The present work successfully reports on the potential of the annealed electrospun coating process based on AgNPs and PHA as efficient antimicrobial materials, showing that the antimicrobial performance can be enhanced compared to the direct melt-compounded process previously reported. In fact, by means of the active electrospun coating, lower silver loadings are needed to achieve a bactericidal effect against *Salmonella enterica*. Furthermore, the physicochemical properties of the neat PHBV3 polymer were not detrimentally affected by the presence of the silver-based coating. Thus, the results of this work provide a new route to generate more efficient antimicrobial heterogeneous-across-thickness films that can be of relevance to develop active multilayer materials for food packaging and food contact surface applications.

## 5. Acknowledgements

---

This work was financially supported by the Spanish Ministry of Economy and Competitiveness (AGL2015-63855-C2-1-R). Jinneth Lorena Castro-Mayorga is supported by the Administrative Department of Science, Technology and Innovation (Colciencias) of the Colombian Government. Maria Jose Fabra is recipient of a Ramon y Cajal contract from the Spanish Ministry of Economy and Competitiveness. Maria

Reis from Universidade Nova de Lisboa, Lisbon, Portugal is acknowledged for supplying the PHBV18 material.

## 6. References

---

1. J. Anu Bhushani and C. Anandharamakrishnan, "Electrospinning and electrospaying techniques: Potential food based applications," *Trends in Food Science & Technology*, vol. 38, no. 1, pp. 21-33, 2014.
2. N. Bhardwaj and S. C. Kundu, "Electrospinning: A fascinating fiber fabrication technique," *Biotechnology Advances*, vol. 28, no. 3, pp. 325-347, 2010.
3. A. Frenot and I. S. Chronakis, "Polymer nanofibers assembled by electrospinning," *Current Opinion in Colloid and Interface Science*, vol. 8, no. 1-2, pp. 64-75, 2003.
4. M. Noruzi, "Electrospun nanofibres in agriculture and the food industry: a review," *Journal of the Science of Food and Agriculture*, pp. 4663-4678, 2016.
5. J. Quirós, K. Boltes and R. Rosal, "Bioactive Applications for Electrospun Fibers," *Polymer Reviews*, vol. 56, no. 4, pp. 631-667, 2016.
6. G. Sun, L. Sun, H. Xie and J. Liu, "Electrospinning of nanofibers for energy applications," *Nanomaterials*, vol. 6, no. 7, 2016.
7. P. J. Rivero, A. Urrutia, J. Goicoechea and F. J. Arregui, "Nanomaterials for Functional Textiles and Fibers," *Nanoscale Research Letters*, vol. 10, no. 1, pp. 1-22, 2015.
8. A. López-Rubio, E. Almenar, P. Hernandez-Muñoz, J. M. Lagarón, R. Catalá and R. Gavara, "Overview of active polymer-based packaging technologies for food applications," *Food Reviews International*, vol. 20, no. 4, pp. 357-387, 2004.
9. M. Martínez-Sanz, A. Lopez-Rubio and J. M. Lagaron, "Dispersing Bacterial Cellulose Nanowhiskers in Poly lactides via Electrohydrodynamic Processing," *Journal of Polymers and the Environment*, vol. 22, no. 1, pp. 27-40, 2014.
10. S. Torres-Giner, M. J. Ocio and J. M. Lagaron, "Development of Active Antimicrobial Fiber-Based Chitosan Polysaccharide Nanostructures using Electrospinning," *Engineering in Life Sciences*, vol. 8, no. 3, pp. 303-314, 2008.
11. A. Martínez-Abad, J. M. Lagaron and M. J. Ocio, "Development and characterization of silver-based antimicrobial ethylene-vinyl alcohol copolymer

### Chapter III

(EVOH) films for food-packaging applications," *Journal of Agricultural and Food Chemistry*, vol. 60, no. 21, pp. 5350-5359, 2012.

12. J. M. Lagarón, M. J. Ocio and A. López-Rubio, "Antimicrobial Packaging Polymers. A General Introduction," in *Antimicrobial Polymers*, Ed., pp. 1-22, John Wiley & Sons, Inc., 2011.

13. G. Totaro, L. Paltrinieri, G. Mazzola, M. Vannini, L. Sisti, C. Gualandi, A. Ballestrazzi, S. Valeri, A. Pollicino, A. Celli, D. Di Gioia and M. L. Focarete, "Electrospun Fibers Containing Bio-Based Ricinoleic Acid: Effect of Amount and Distribution of Ricinoleic Acid Unit on Antibacterial Properties," *Macromolecular Materials and Engineering*, vol. 300, no. 11, pp. 1085-1095, 2015.

14. M. Min, Y. Shi, H. Ma, H. Huang, J. Shi, X. Chen, Y. Liu and L. Wang, "Polymer-nanoparticle composites composed of poly(3-hydroxybutyrate-co-3-hydroxyvalerate) and coated silver nanoparticles," *Journal of Macromolecular Science, Part B: Physics*, vol. 54, no. 4, pp. 411-423, 2015.

15. S. Jeong, S. Yeo and S. Yi, "The effect of filler particle size on the antibacterial properties of compounded polymer/silver fibers," *Journal of Materials Science*, vol. 40, no. 20, pp. 5407-5411, 2005.

16. M. A. Busolo and J. M. Lagaron, "Antimicrobial biocomposites of melt-compounded polylactide films containing silver-based engineered clays," *Journal of Plastic Film and Sheeting*, vol. 29, no. 3, pp. 290-305, 2013.

17. A. Martínez-Abad, J. M. Lagarón and M. J. Ocio, "Characterization of transparent silver loaded poly(l-lactide) films produced by melt-compounding for the sustained release of antimicrobial silver ions in food applications," *Food Control*, vol. 43, no. 0, pp. 238-244, 2014.

18. S. Y. Yeo, W. L. Tan, M. Abu Bakar and J. Ismail, "Silver sulfide/poly(3-hydroxybutyrate) nanocomposites: Thermal stability and kinetic analysis of thermal degradation," *Polymer Degradation and Stability*, vol. 95, no. 8, pp. 1299-1304, 2010.

19. H. Yu, B. Sun, D. Zhang, G. Chen, X. Yang and J. Yao, "Reinforcement of biodegradable poly(3-hydroxybutyrate-co-3-hydroxyvalerate) with cellulose nanocrystal/silver nanohybrids as bifunctional nanofillers," *Journal of Materials Chemistry B*, vol. 2, no. 48, pp. 8479-8489, 2014.

20. E. Fortunati, M. Peltzer, I. Armentano, A. Jiménez and J. M. Kenny, "Combined effects of cellulose nanocrystals and silver nanoparticles on the barrier and migration properties of PLA nano-biocomposites," *Journal of Food Engineering*, vol. 118, no. 1, pp. 117-124, 2013.

21. A. N. Krklješ, M. T. Marinović-Cincović, Z. M. Kačarević-Popović and J. M. Nedeljković, "Dynamic thermogravimetric degradation of gamma radiolytically synthesized Ag-PVA nanocomposites," *Thermochimica Acta*, vol. 460, no. 1-2, pp. 28-34, 2007.
22. J. L. Castro-Mayorga, A. Martínez-Abad, M. F. Fabra, J. M. Lagarón, M. J. Ocio and G. Sánchez, "Chapter 32 - Silver-Based Antibacterial and Virucide Biopolymers: Usage and Potential in Antimicrobial Packaging A2 - Barros-Velázquez, Jorge," in *Antimicrobial Food Packaging*, Ed., pp. 407-416, Academic Press, San Diego, 2016.
23. R. de Lima, A. B. Seabra and N. Durán, "Silver nanoparticles: A brief review of cytotoxicity and genotoxicity of chemically and biogenically synthesized nanoparticles," *Journal of Applied Toxicology*, vol. 32, no. 11, pp. 867-879, 2012.
24. R. Liz, J.-C. Simard, L. B. A. Leonardi and D. Girard, "Silver nanoparticles rapidly induce atypical human neutrophil cell death by a process involving inflammatory caspases and reactive oxygen species and induce neutrophil extracellular traps release upon cell adhesion," *International Immunopharmacology*, vol. 28, no. 1, pp. 616-625, 2015.
25. P. Chairuangkitti, S. Lawanprasert, S. Roytrakul, S. Aueviriyavit, D. Phummiratch, K. Kulthong, P. Chanvorachote and R. Maniratanachote, "Silver nanoparticles induce toxicity in A549 cells via ROS-dependent and ROS-independent pathways," *Toxicology in Vitro*, vol. 27, no. 1, pp. 330-338, 2013.
26. M. Składanowski, P. Golinska, K. Rudnicka, H. Dahm and M. Rai, "Evaluation of cytotoxicity, immune compatibility and antibacterial activity of biogenic silver nanoparticles," *Medical Microbiology and Immunology*, vol. 205, no. 6, pp. 603-613, 2016.
27. H. E. Salama, G. R. Saad and M. W. Sabaa, "Synthesis, characterization, and biological activity of cross-linked chitosan biguanidine loaded with silver nanoparticles," *Journal of Biomaterials Science, Polymer Edition*, vol. 27, no. 18, pp. 1880-1898, 2016.
28. J. Bott, A. Störmer and R. Franz, "A Comprehensive Study into the Migration Potential of Nano Silver Particles from Food Contact Polyolefins," in *Chemistry of Food, Food Supplements, and Food Contact Materials: From Production to Plate*, Ed., pp. 51-70, American Chemical Society, 2014.
29. H. J. Jeon, J. S. Kim, T. G. Kim, J. H. Kim, W.-R. Yu and J. H. Youk, "Preparation of poly( $\epsilon$ -caprolactone)-based polyurethane nanofibers containing silver nanoparticles," *Applied Surface Science*, vol. 254, no. 18, pp. 5886-5890, 2008.
30. B. Munteanu, Z. Aytac, G. Pricope, T. Uyar and C. Vasile, "Polylactic acid (PLA)/Silver-NP/VitaminE bionanocomposite electrospun nanofibers with

### Chapter III

antibacterial and antioxidant activity," *Journal of Nanoparticle Research*, vol. 16, no. 10, pp. 1-12, 2014.

31. P.-o. Rujitanaroj, N. Pimpha and P. Supaphol, "Preparation, characterization, and antibacterial properties of electrospun polyacrylonitrile fibrous membranes containing silver nanoparticles," *Journal of Applied Polymer Science*, vol. 116, no. 4, pp. 1967-1976, 2010.

32. M. H. Min, Y. Y. Shi, X. X. Chen, J. G. Shi, H. Y. Ma, H. L. Huang and L. Wang, "Preparation and characteristics of electrospun silver-containing PHBV ultrafine fiber," in *Applied Mechanics and Materials*, Ed., pp. 34-37, 2014.

33. Z. C. Xing, W. P. Chae, J. Y. Baek, M. J. Choi, Y. Jung and I. K. Kang, "In vitro assessment of antibacterial activity and cytocompatibility of silver-containing phbv nanofibrous scaffolds for tissue engineering," *Biomacromolecules*, vol. 11, no. 5, pp. 1248-1253, 2010.

34. J. L. Castro-Mayorga, A. Martínez-Abad, M. J. Fabra, C. Olivera, M. Reis and J. M. Lagarón, "Stabilization of antimicrobial silver nanoparticles by a polyhydroxyalkanoate obtained from mixed bacterial culture," *International Journal of Biological Macromolecules*, vol. 71, pp. 103-110, 2014.

35. A. Martínez-Abad, L. Cabedo, C. S. S. Oliveira, L. Hilliou, M. Reis and J. M. Lagarón, "Characterization of polyhydroxyalkanoate blends incorporating unpurified biosustainably produced poly(3-hydroxybutyrate-co-3-hydroxyvalerate)," *Journal of Applied Polymer Science*, 2015.

36. J. L. Castro-Mayorga, M. J. Fabra and J. M. Lagarón, "Stabilized nanosilver based antimicrobial poly(3-hydroxybutyrate-co-3-hydroxyvalerate) nanocomposites of interest in active food packaging," *Innovative Food Science and Emerging Technologies*, vol. 33, pp. 524-533, 2016.

37. D. Zhang and H. Yang, "Facile synthesis of anisotropic silver nanoparticles and their surface-enhanced Raman scattering properties," *Journal of Molecular Structure*, vol. 1060, no. 0, pp. 1-5, 2014.

38. C. D. Saquing, J. L. Manasco and S. A. Khan, "Electrospun nanoparticle-nanofiber composites via a one-step synthesis," *Small*, vol. 5, no. 8, pp. 944-951, 2009.

39. C. Radheshkumar and H. Münstedt, "Morphology and mechanical properties of antimicrobial polyamide/silver composites," *Materials Letters*, vol. 59, no. 14-15, pp. 1949-1953, 2005.

40. M. Martínez-Sanz, M. Villano, C. Oliveira, M. G. E. Albuquerque, M. Majone, M. Reis, A. Lopez-Rubio and J. M. Lagarón, "Characterization of polyhydroxyalkanoates

synthesized from microbial mixed cultures and of their nanobiocomposites with bacterial cellulose nanowhiskers," *New Biotechnology*, vol. 31, no. 4, pp. 364-376, 2014.

41. J. Ambrosio-Martin, M. J. Fabra, A. López-Rubio, G. Gorrasi, A. Sorrentino and J. M. Lagaron, "Assessment of Ball Milling as a Compounding Technique to Develop Nanocomposites of Poly(3-Hydroxybutyrate-co-3-Hydroxyvalerate) and Bacterial Cellulose Nanowhiskers," *Journal of Polymers and the Environment*, vol. 24, no. 3, pp. 241-254, 2016.

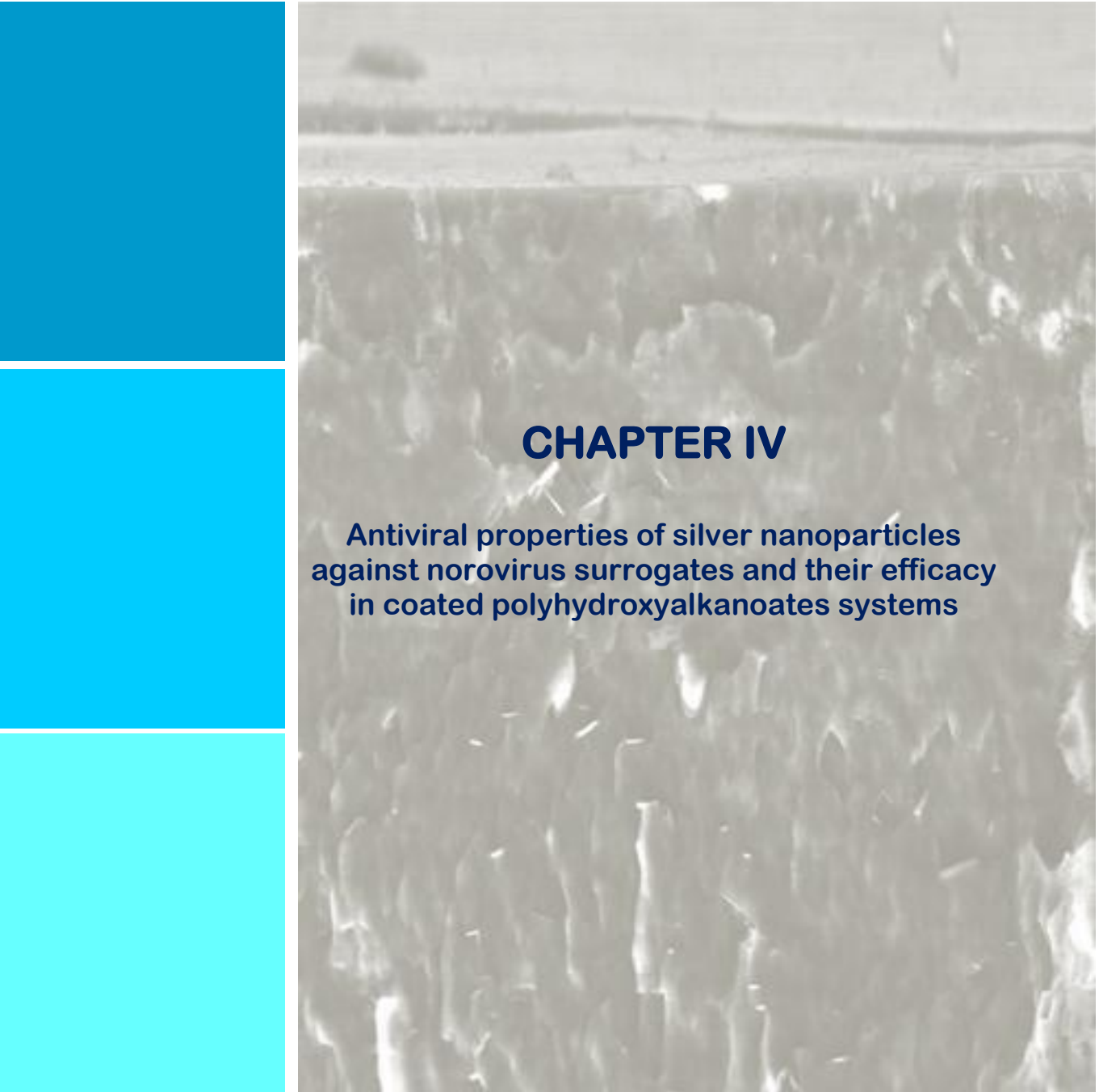
42. P. Kanmani and S. T. Lim, "Synthesis and structural characterization of silver nanoparticles using bacterial exopolysaccharide and its antimicrobial activity against food and multidrug resistant pathogens," *Process Biochemistry*, vol. 48, no. 7, pp. 1099-1106, 2013.

43. J. S. Kim, E. Kuk, K. N. Yu, J.-H. Kim, S. J. Park, H. J. Lee, S. H. Kim, Y. K. Park, Y. H. Park, C.-Y. Hwang, Y.-K. Kim, Y.-S. Lee, D. H. Jeong and M.-H. Cho, "Antimicrobial effects of silver nanoparticles," *Nanomedicine: Nanotechnology, Biology and Medicine*, vol. 3, no. 1, pp. 95-101, 2007.

44. A. Grigor'Eva, I. Saranina, N. Tikunova, A. Safonov, N. Timoshenko, A. Rebrov and E. Ryabchikova, "Fine mechanisms of the interaction of silver nanoparticles with the cells of *Salmonella typhimurium* and *Staphylococcus aureus*," *BioMetals*, vol. 26, no. 3, pp. 479-488, 2013.

45. Y. Echevoyen and C. Nerín, "Nanoparticle release from nano-silver antimicrobial food containers," *Food and Chemical Toxicology*, vol. 62, no. 0, pp. 16-22, 2013.





## CHAPTER IV

### Antiviral properties of silver nanoparticles against norovirus surrogates and their efficacy in coated polyhydroxyalkanoates systems

J. L. Castro-Mayorga, W. Randazzo, M.J. Fabra, J. M. Lagaron, R. Aznar and G. Sánchez. "Antiviral properties of silver nanoparticles against norovirus surrogates and their efficacy in coated polyhydroxyalkanoates systems". LWT - Food Science and Technology, vol. 79, pp. 503-510, 2017.



## Abstract

---

Silver nanoparticles (AgNP) have strong broad-spectrum antimicrobial activity and gained increased attention for the development of AgNP based products, including medical and food applications. Initially, the efficacy of AgNP and silver nitrate ( $\text{AgNO}_3$ ) was evaluated for inactivating norovirus surrogates, the feline calicivirus (FCV) and the murine norovirus (MNV). These norovirus surrogates were exposed to  $\text{AgNO}_3$  and AgNP solutions for 24 h at 25°C and then analyzed by cell-culture assays. Both AgNP and silver ions significantly decreased FCV and MNV infectivity in a dose-dependent manner between concentrations of 2.1 and 21 mg/L. Furthermore, poly (3-hydroxybutyrate-co-3-hydroxyvalerate) (PHBV) films were prepared by depositing a coating of thermally post-processed electrospun PHBV18 /AgNP fiber mats over compression moulded PHBV3 films. After 24 h exposure at 37°C and 100% RH, no infectious FCV were recovered when in contact with the AgNP films while MNV titers decreased by 0.86 log. The morphology of the PHBV18 and PHBV18/AgNP fibers studied by SEM showed smooth and continuous fibers in both cases and the EDAX analysis confirmed the homogeneously distribution of AgNP into the coating and onto the PHBV3/PHBV18 layer. This study showed, for the first time, the suitability of the PHBV18/AgNP electrospun coating for antiviral surfaces.

## Keywords

---

Noroviruses, Silver nanoparticles, Active packaging, Polyhydroxyalkanoates, Electrospinning.

## 1. Introduction

---

Human norovirus (family *Caliciviridae*) are reported as the leading causes of viral gastroenteritis in industrialized countries, and worldwide constituting a high public health concern. Norovirus gastroenteritis is self-limiting but extremely infectious with a low infectious dose (10-100 particles). This non-enveloped, single-stranded, positive-sense RNA virus is responsible for over 90% cases of non-bacterial and approximately half of all cases of gastroenteritis. Recently, the World Health Organization has estimated the global burden of foodborne diseases, reporting that infectious agents that cause diarrhoeal diseases accounted for the vast majority (550 million cases per year), in particular human norovirus (120 million cases per year) [1].

Moreover human norovirus is responsible for many outbreaks, especially in closed environments e.g. health-care facilities and cruise ships, whereas the contribution of contaminated surfaces in the spread of infection has a key role [2]. To effectively prevent norovirus outbreaks, the scientific community has been working to develop strategies for treating and preventing norovirus infection. The use of antimicrobial surfaces in food, clinical and community environments may help to reduce the spread of norovirus infection. Among them, the use of silver has emerged as a very efficient technology to prevent microbial proliferation on medical and food-contact surfaces [3] and, more concretely, silver nanoparticles (AgNP) have received considerable attention due to their attractive physico-chemical and antimicrobial properties [4 2009, 5] such as the high surface-to-volume ratio, nanosize diameter and enhanced surface reactivity, making them able to inactivate microorganisms more effectively than their micro- or macro- scale counterparts. For instance, Castro-Mayorga and collaborators [6 2016] have demonstrated that poly (3-hydroxybutyrate-co-3-hydroxyvalerate) (PHBV)-AgNP packaging materials exhibited a strong and

## Chapter IV

prolonged (even after seven months) antibacterial activity against *Listeria monocytogenes* and *Salmonella enterica* at very low AgNP loadings (0.4 g/kg). On the other hand, Martínez-Abad and collaborators [7] developed active renewable food packaging materials based on polylactic acid (PLA) and silver ions (from 0.1 to 10 g/kg) to control feline calicivirus (FCV) in vegetables. These packaging materials showed a remarkable potential for food-contact applications as well as active packaging to maintain or extend food quality and safety. However, the maximal antimicrobial potential can hardly be achieved in most cases because silver has low solubility or compatibility with the polymers matrices, leading to the agglomeration and blackening of the films, or simply because the amount of silver available in the film surface is insufficient to exert antimicrobial effect.

As an alternative, metal nanoparticles can be incorporated into sub-micro or nano fibers by means of electrospinning technique in order to generate masterbatches which are subsequently melt, mixed with polymers pellets, or even better, used as active coating over polymer surfaces [8]. The electrospun fibres lead the development of novel materials with useful features for antibacterial applications such as fibrous membranes for water filtration [9], wound dressings, implant materials or tissue engineering [10]. Concretely, in the area of active food packaging, the electrospinning technique successfully avoids the agglomerations of zinc oxide nanoparticles and greatly increases their antimicrobial activity [11].

Since human noroviruses cannot routinely be propagated by using cell-culture systems, cultivable surrogates such as FCV and murine norovirus (MNV) are commonly used as experimental models to study human norovirus infectivity and the efficacy of inactivation technologies [12]. Pioneering studies demonstrated the potential of silver ions and silver nanoparticles for enteric virus inactivation [13-18]. However, it is known that silver ions are easily inactivated by many different physical or chemical factors [19, 20]. For instance, thermal treatments or exposure to light or

UV can prompt the formation of sulphides or other silver complexes without antimicrobial properties and usually producing a strong brownish or blackish coloration of the materials [21]. Accordingly, the use of stabilized AgNP could not only improve the thermal stability, the visual appearance and optical properties of the active films but also enhance their antimicrobial performance. However, there is lack of information about the influence of storage time on their antiviral activity and its efficacy when incorporated into composites. Thus, silver nitrate and silver nanoparticles at different concentrations and with different aging time were investigated for their effect on norovirus surrogates. In the first part of this work, norovirus surrogates were exposed to different concentrations of silver nitrate and the virucidal activity was assessed using cell culture. In the second part, PHBV18/AgNP fiber mats were fabricated by electrospinning and used to coat PHBV3 films in order to develop virucidal biopolymers that may be suitable as active material, particularly in food and medical contact surfaces.

## 2. Materials and methods

---

### 2.1 Silver nitrate and silver nanoparticles

Stabilized AgNP were synthesized by chemical reduction into unpurified poly (3-hydroxybutyrate-co-18 mol%- 3-hydroxyvalerate) (PHBV18) suspension according to a previously reported method [22]. To this end, 500 mg/kg of PHBV18 was suspended in ultrapure Milli-Q® water (Millipore Corporation Co., USA) and then sodium borohydride was added to get 75.7 mg/L concentration. Thereafter, 10 mL of an aqueous AgNO<sub>3</sub> solution at 169.9 mg/L was added dropwise to generate *in situ* stabilized silver nanoparticles. The obtained PHBV18/AgNP suspension was

## *Chapter IV*

centrifuged at 17387×g for 15 min and the precipitate was dried at 40°C under vacuum for 24 h. The dried material was used as stock to evaluate the antiviral activity at three different concentrations (21, 10.5 and 2.1 mg/L). Analogous AgNO<sub>3</sub> solution (without PHBV18 and without sodium borohydride) was prepared to compare the antiviral activity of silver ions to AgNP.

### **2.2 Viral strains, cell lines and infections**

Murine norovirus (MNV-1 strain) was propagated and assayed in RAW 264.7 cells. Feline calicivirus (F9 strain, ATCC VR-782) was cultured in CRFK cells (ATCC CCL-94). Semi-purified viruses were obtained following three cycles of freeze-thawing infected cells and centrifugation at 660×g for 30 min. The supernatant was stored at -80°C until use. Infectious viruses were enumerated by determining the 50% tissue culture infectious dose (TCID<sub>50</sub>) with eight wells per dilution and 20 µL of inoculum per well using the Spearman-Kärber method [13].

### **2.3 Determination of antiviral activity**

Each silver solution was mixed with an equal volume of each virus suspension and further incubated at 25°C in a water-bath shaker at 150 rpm for 16 h (overnight). Then, infectious viruses were enumerated by cell culture assays as described above. Positive controls were virus suspensions added with water. Antiviral activity of silver was estimated by comparing the number of infectious viruses on suspensions without silver and on the silver-treated virus suspensions. Each treatment was performed in triplicate. The value of antiviral activity (Reduction, R) was calculated by determining  $\log_{10}(N_0/N_t)$ , where  $N_0$  is the number of infections viruses on the suspension without silver and  $N_t$  is the number of infections viruses on the suspension added with silver.

## 2.4 Preparation of AgNP based films

A coated structure was fabricated by coating the poly(3-hydroxybutyrate-co-3 mol%- 3-hydroxyvalerate) (PHBV3) films with PHBV18/AgNP fibers mat produced by means of the electrospinning technique. PHBV3 films used as matrix were compression molded using hot plates hydraulic press (Carver 4122, USA) at 180°C, 1.8 MPa during 5 min. The so-obtained films had a thickness of  $246 \pm 22 \mu\text{m}$  as measured with a digital micrometer (Mitutoyo, Spain,  $\pm 0.001 \text{ mm}$ ) by averaging four measurements on each sample.

To prepare the active coating, AgNP were firstly synthesized by chemical reduction into polymer suspensions on the bases of a previously reported method [22]. Then, PHBV18/AgNP masterbatch was dispersed in 2,2,2-Trifluoroethanol (TFE,  $\geq 99 \%$ , Sigma Aldrich) having a total solids content of 60 g/kg. The biopolymer solution was transferred to a 5 mL glass syringes, connected through polytetrafluoroethylene (PTFE) tubes to a stainless steel needle (0.9 mm of inner diameter) and processed using a Fluidnatek® LE-10 electrospinning equipment, trademark of the engineering division of Bioinicia S.L. (Valencia, Spain). Processed samples were collected on a stainless-steel plate connected to the cathode of the power supply and oriented perpendicular to the syringe. The distance between the needle and the plate was 12 cm and the voltage was maintained in the range 10-12 kV. All experiments were carried out at room temperature under a steady flow-rate of 7 mL/h. After electrospinning, the fiber mats were dried at 40°C under vacuum for 24 h to completely remove the solvent.

Finally, the coated structure was assembled placing 250-300 g/kg of fiber mat of about 100  $\mu\text{m}$  of thickness onto PHBV3 films. The resulting coated system was thermally post-processed in a hot press (Carver 4122, USA) at 150°C during 2 min (without pressing) to form a continuous film by fiber coalescence.

## *Chapter IV*

Neat PHBV3/PHBV18 films without silver were used as control for comparative purposes.

### **2.5 Scanning Electron Microscopy (SEM)**

The morphology of the PHBV18/AgNP electrospun fibers and bilayer films was analyzed using SEM. The SEM was conducted on a Hitachi microscope (Hitachi S-4800) at an accelerating voltage of 5 kV and a working distance of 8-10 mm before the examination, the films were cryo-fractured using liquid N<sub>2</sub> and sputtered with Au/Pd under vacuum. The microanalysis and elemental mapping were conducted by Energy Dispersive Analysis of X-rays (EDAX) from SEM images of carbon coated samples. Fibers thicknesses were measured by means of the of the Adobe Photoshop CS4 software from 300 fibers at random from SEM images.

### **2.6 Determination of virucidal activity of silver based films**

To test the virucidal activity of silver based films, a modification of the ISO 22196:2011 (Measurement of antibacterial activity on plastics and other non-porous surfaces) was used. Briefly, a suspension of viruses diluted in PBS buffer (4-6 log TCID<sub>50</sub>/mL) was placed onto the test films of 3×3 cm and covered by an inert piece of Low-Density Polyethylene (LDPE) of 2.5×2.5 cm and 10 μm thickness. Samples were incubated at 37 or 25°C overnight at 100% relative humidity (RH). Thereafter, the top film was lifted, and the virus droplet-exposed sides were recovered and 10-fold diluted with PBS. Lastly, the corresponding cell culture assays were performed to determine whether the silver films were effective in inactivating the tested viruses. A control film (without silver) was used as the negative control material.

Virucidal activity was calculated by comparing the number of infectious viruses on control films (without silver) and on the silver films. Each experimental condition was performed in triplicate.

## 2.7 Determination of silver content

The quantification of total silver content in the developed films was carried out by inductively coupled plasma- optical emission spectroscopy (ICP-OES, Perkin-Elmer, USA) using silver standard solution (traceable to SRM from NIST,  $\text{AgNO}_3$  in  $\text{HNO}_3$  2-3 % 1000 mg/L Ag Certipur®, Merck, Germany) for calibration. To this end, 100 mg of sample were subjected to acid digestion with 2 mL of  $\text{HNO}_3$  (69% for trace metal analysis, Panreac, Spain) at 80°C for 16 h. The resultant digestant was diluted to a final volume of 5 mL and analyzed. All measurements were done, at least, in triplicate.

## 2.8 Statistical analysis

The significance of differences among the mean numbers of viruses determined after the control and AgNP films to assess the antiviral effect was determined by Student's t test with a significance level of  $p < 0.05$ . The post-hoc Tukey's method ( $p < 0.05$ ) was used for pairwise comparison and to determine differences among silver nitrate and silver nanoparticles treatments on viruses (XLSTAT, Addinsoft SARL).

# 3. Results and discussion

.....

## 3.1 The effect of silver nitrate and silver nanoparticles on MNV and FCV

As shown in Fig.1 and 2, in all tested aging times, the exposition of norovirus surrogates, MNV and FCV, to silver ions or silver nanoparticles, produced a clear reduction in the virus titers. The results indicated that the antiviral activity of silver, in

## Chapter IV

any of its forms, is dose-dependent, where increasing concentrations of silver showed increased reduction in viral titers.

In the case of MNV, the silver nitrate suspension produced a higher reduction of MNV infectivity during the first 75 days of aging. However, the antiviral activity was significantly reduced after 150 days of storage probably due to the physical and chemical instability of silver ions (i.e. reduction and aggregation) as it has been previously reported [22]. Silver ions can be reduced to elemental silver or silver nanoparticles by weak reducing treatments, such as many solvents, UV-light, thermal treatment, ligands, etc. Since water was used as a solvent, external agents such as UV-light could compromise the stability of silver ions and the formation of elemental silver and silver nanoparticles in uncontrolled way forming particles with different forms and size which are not stabilized and can easily coalesce. In fact, one of the main problems which could compromise the final properties of an antimicrobial/antiviral packaging material is the stability of silver ions and the chemical environment where the material has to exert its effect and even the conditions to which the material will be exposed [23].

In contrast, the antiviral activity of silver nanoparticles at concentrations higher than 2.1 ppm increased or remained constant during all the time evaluated (150 days) (Fig.1). This effect can be ascribed to the nanosize diameter of AgNP ( $\sim 7 \pm 3$  nm) previously reported by Castro-Mayorga et al. (2014) [22] and the enhanced surface reactivity, making them able to affect more effectively the capsid of the viruses. Indeed, a synergic effect between silver ions release from the AgNP and AgNP themselves might enhance and extend the virucidal activity. The initial increase in the antiviral activity of the AgNP could be attributed to both the action of residual silver ions and the excess of reducing agent which could produce some more nanoparticles in the first days of the storage, increasing the virucidal efficacy. It is worth mentioning that the *in situ* synthesis of AgNP implied their stabilization in a biopolymer matrix

(PHBV18) which could also enhanced their virucidal activity preventing the aggregation of AgNP, as had been demonstrated by Castro-Mayorga et al. (2014) [22] for enhancing the antimicrobial activity. As a result, the AgNP suspensions exhibited a high and prolonged (even after 150 days) virucidal activity against MNV.

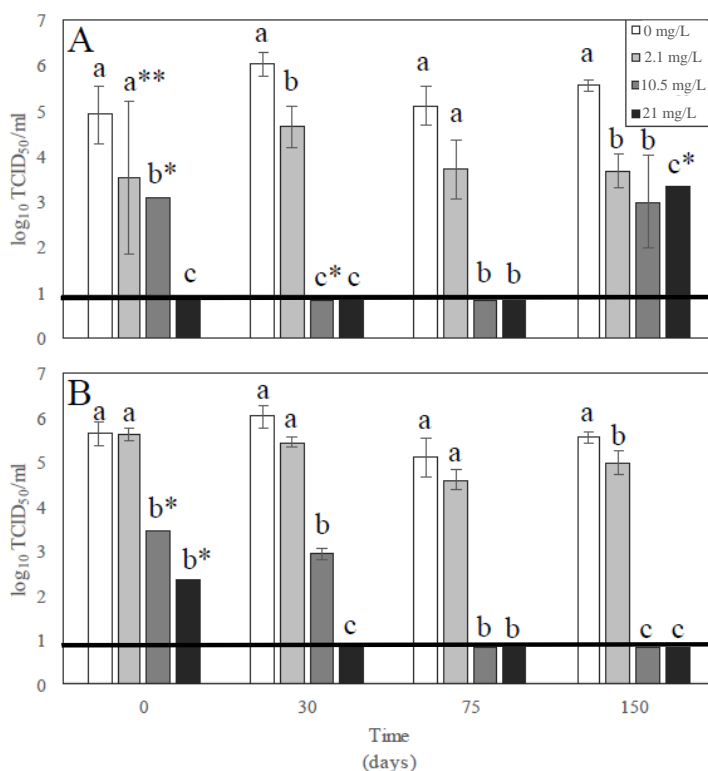


**Figure 1.** Effect of silver nitrate (A) and silver nanoparticles (B) on murine norovirus (MNV) over the storage time. Different letters denote significant differences between treatments ( $P < 0.05$ ). \*One negative samples out of three. \*\*Two negative samples out of three. Lines indicate the detection limit for the TCID<sub>50</sub> assay.

On the other hand, the FCV appeared more susceptible to the action of silver nitrate and the reduction in viral titers was higher than for their counterparts obtained for MNV (Fig.2). This appreciation leads to infer that the virucide effect of silver might depend to the differences in capsid structure and capsid composition of the treated

## Chapter IV

virus. Thus, for FCV, the silver nitrate suspension had a highest reduction of its infectivity. This fact could be a consequence of a combined effect between the high activity of soluble silver ions and the higher susceptibility of FCV at Ag<sup>0</sup> particles produced by uncontrolled reduction (having bigger size). Both, silver ions and the Ag<sup>0</sup> formed in the suspension could be able to disrupt the FCV capsid more easily than in the case of the MNV. AgNP suspensions followed a slight different pattern in FCV than in its counterparts prepared with MNV (Fig.2).

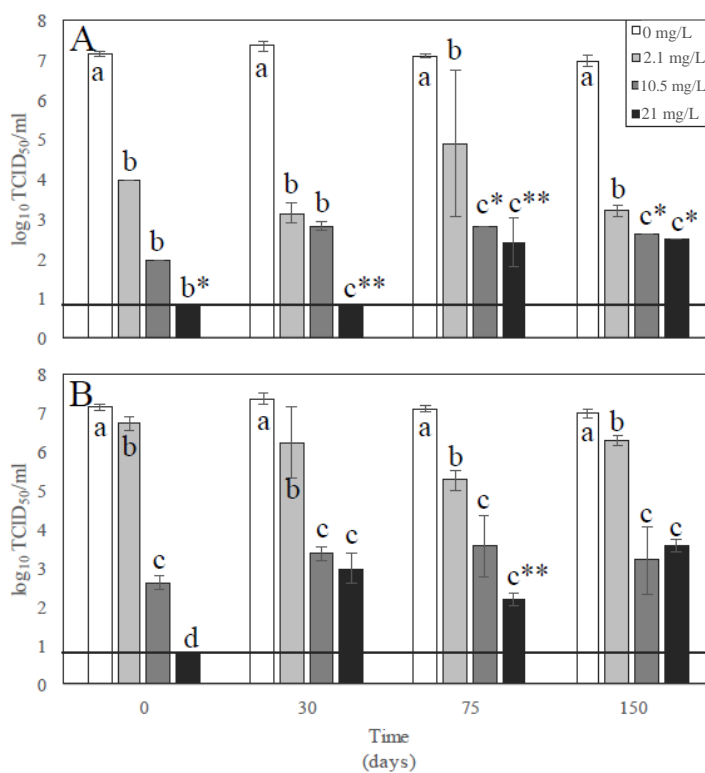


**Figure 2.** Effect of silver nitrate (A) and silver nanoparticles (B) on feline calicivirus (FCV) over the storage time. Different letters denote significant differences between treatments ( $P < 0.05$ ). \*One negative samples out of three. \*\*Two negative samples out of three. Lines indicate the detection limit for the TCID<sub>50</sub> assay.

To sum up, the results revealed that silver nitrate and AgNP were effective in reducing the titers of FCV and MNV. The differences found between the virucide activity of the two different silver forms and the two different viruses evaluated bring to light that might exist different mechanisms of action depending on the virus structure and composition [15]. In this respect, the efficacy of a micrometer-sized magnetic hybrid colloid (MHC) decorated with AgNP has recently been assessed on MNV. Park, et al. (2014) [24] reported that a suspension of AgNP with a size of 30 nm and a concentration of 400 ppm (Ag30-MHCs) had the highest antiviral activity, reporting about 6 log<sub>10</sub> reduction of MNV after exposure at 25°C for 6 h while Ag7-MHCs (corresponding to 57.5 mg/L and 7 nm) did not reduce the MNV infectivity. More recently, Bekele and collaborators [18] have reported the effect of the size (10, 75 and 110 nm) and dose (25, 50 and 100 mg/L) of AgNP on FCV, showing that only the smallest AgNP (10 nm) were effective in reducing the FCV titers. Therefore, comparing these results with those obtained in the present study (where the highest antiviral effect was achieved with AgNP of 7 ± 3 nm at 21 mg/L, it could be stated that the virucidal activity of AgNP is strongly dependent on their stabilization degree, size and concentration.

### **3.2 Fibers and films morphology**

The morphology of the PHBV18 and PHBV18/AgNP fibers obtained from electrospinning was studied by SEM and representative micrographs are shown in Fig. 3a and 3b, respectively. As it can be observed, smooth and continuous fibers without beads were attained in both cases. The electrospun fibers presented a diameter of 0.92 ± 0.36 and 1.1 ± 0.40 μm for PHBV18 and PHBV18/AgNP, respectively. Interestingly, the addition of AgNP did not result in a significant change in fiber diameter as it can be deduced from the SEM image and size distribution

## Chapter IV

(Fig.3c). However it has been previously reported that the addition of salts usually increases the charge density in the ejected jets and, thus, stronger elongation forces are imposed due to the self-repulsion of the excess charges under the electrical field, resulting in electrospun fibers having straighter shape and smaller diameter [25, 26]. In the present work, the low silver loading, the appropriate stabilization of AgNP into the polymer matrix and the electrospinning solution minimize the reduction of residual silver ion and the aggregation of AgNP or any significant impact on the fiber diameter.

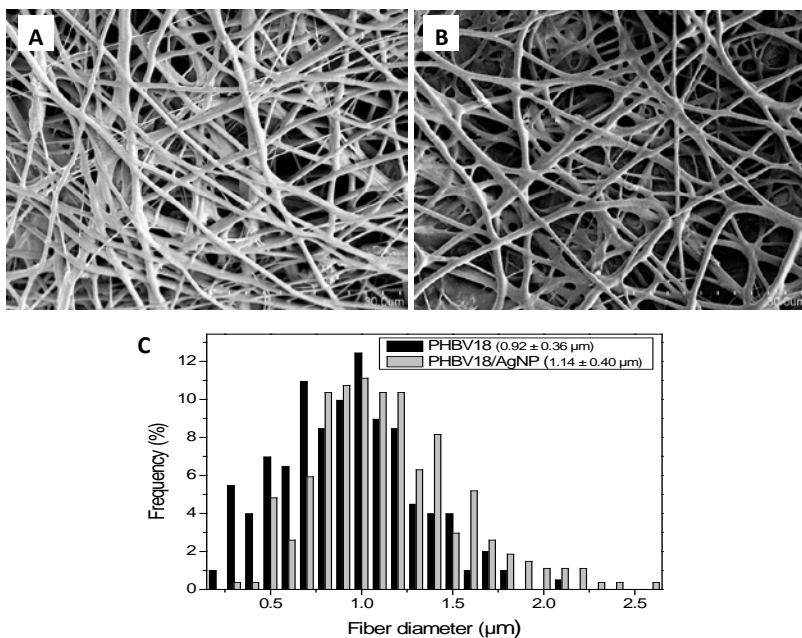


**Figure 3.** SEM images of electrospun fibers, A) without AgNP (PHBV18), B) with AgNP (PHBV18/ AgNP), and C) size distribution of fibers.

The surface and cross-section of the coated systems prepared with PHBV3 and PHBV18/AgNP was also analyzed by SEM. The coated system presented a uniform and smooth surface (Fig. 4a) formed by the continuous layer of annealed active fibers

whose thickness was not easily discerned, but it was measured to have a thickness of about  $60\mu\text{m}$  (Fig. 4b). The morphology of the coating layer suggests that a partial melting and contraction of fibers could take place during the annealing step, favoring the adhesion between the two layers. Furthermore, the presence of silver was confirmed by EDAX analysis (Fig.4c) and the AgNP distribution assessed by mapping from the SEM images. The elemental mapping image of the Fig.4d shows matched spatial distribution of silver, indicating that the AgNP are homogeneously distributed into the coating and onto the PHBV3/PHBV18 layer.

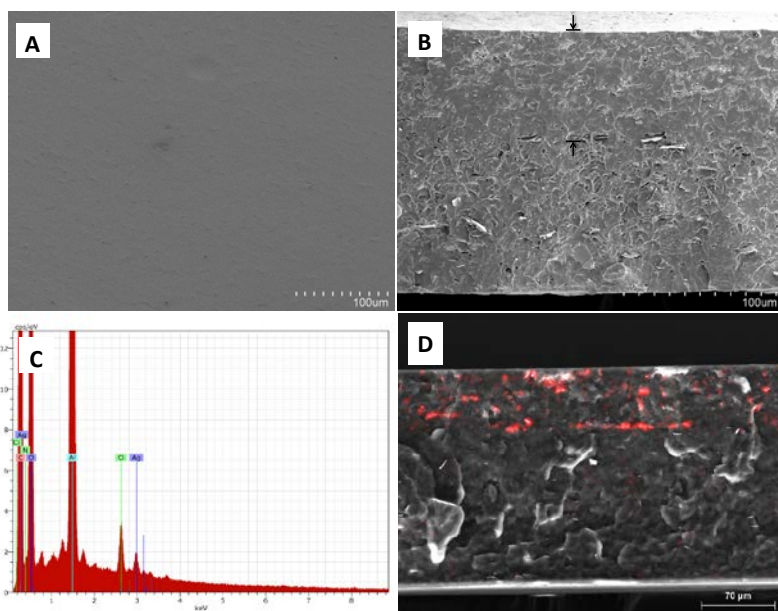


**Figure 4.** SEM micrographs and EDAX analysis of PHBV3/PHBV18/AgNP films. A) film surface, B) film cross-section, C) EDAX spectrum confirming the silver presence, D) Elemental mapping of coated system by EDAX from SEM image (silver in red).

Fig.5 shows the overall appearance images of the neat PHBV3 film and the coated systems containing or not AgNP. The first clear observation is that coated systems prepared without AgNP showed a darker yellowish coloration as compared to the

## Chapter IV

neat PHBV3. This effect could be ascribed to the presence of some impurities in the PHBV18 due to the fermentation process, which resulted in Maillard reactions during the thermal treatment [6]. In contrast, when the AgNP were added to the coating, the yellowish coloration disappeared and it turned light grey, thus indicating that both the thermal stability of the polymer matrix and the dispersion of nanoparticles were enhanced by means of this procedure.



**Figure 5.** Contact transparency pictures of PHBV3, PHBV3/PHBV18 and PHBV3/ PHBV18/AgNPs.

### 3.3 Antiviral effects of AgNP films

Taking into account the good performance of AgNP obtained in the first part of this work, PHBV3/PHBV18/AgNP coated systems were fabricated as described above and their antiviral activity was evaluated. The AgNP-films were inoculated with norovirus surrogates adapting the ISO 22196:2011 and incubated at 25°C and 100% RH. Table 1 shows that FCV and MNV titers decreased by 1.42 and 0.14 log TCID<sub>50</sub>/mL, respectively. However, the results were not found statistically significant ( $p > 0.05$ ). The effectiveness of AgNP-films was also evaluated at 37°C and 100% RH. After 24 h exposure, no infectious FCV were recovered when in contact with the AgNP films while MNV titers decreased by 0.86 log TCID<sub>50</sub>/mL (Table 1). As for other natural compounds AgNP-films exerted the strongest antiviral effect at 37°C [27].

**Table 1.** Antiviral effect of AgNP films on norovirus surrogates (MNV and FCV) after 24 h contact following the ISO 22196:2011 at different temperatures

Virus	Type of films	Temperature			
		25 °C		37 °C	
		Recovered titer (log <sub>10</sub> TCID <sub>50</sub> /ml)	Reduction	Recovered titer (log <sub>10</sub> TCID <sub>50</sub> /ml)	Reduction
MNV	Control	6.22 ± 0.15		4.45 ± 0.25	
	AgNP films	6.08 ± 0.17	0.14	3.59 ± 0.08	0.86
	p <sup>a</sup>	0.1725		0.0023	
FCV	Control	7.12 ± 0.19		3.41 ± 0.29	
	AgNP films	5.70 ± 1.59	1.42	<1.15	>2.26
	p <sup>a</sup>	0.0996		0.0033	

<sup>a</sup>p < 0.05 means values with different letters in the same column and same virus denote significant differences between treatments (P < 0.05).

In a similar work, an active renewable packaging material with virucide properties was synthesized by the incorporation of silver ions into PLA films by solvent casting technique. These films also showed antiviral activity on FCV. When FCV was exposed to PLA-silver films for 24 h at 25°C, FCV titers decreased by 2 log TCID<sub>50</sub>/mL when treated with PLA films at concentrations of 1 g/kg of silver, while in films containing 10 g/kg of silver, FCV infectivity was completely eliminated [7]. Likewise, Silvestry-Rodriguez et al. (2007) [14] evaluated the antiviral activity of active packaging, reporting that FCV titers were reduced by 5 log when in contact with plastic coupons impregnated with 100 g/kg silver–copper zeolites. In the present study, PHBV3/PHBV18/AgNP films containing a total silver concentration of 270 ± 10 mg/kg (as it was quantified by ICP-OES) demonstrated to have a higher antiviral activity against FCV than the above-mentioned publications. The highest antiviral activity observed for FCV as compared to MNV, could be due to the release of silver ions from the immobilized AgNP resulting in a final increased antiviral effect. Even if this assumption is in line with the higher sensitivity of FCV than MNV to

silver ions as reported in the suspension antiviral assay additional research on the migration of silver ions or silver nanoparticles are required to confirm this hypothesis.

## **4. Conclusions**

---

The effect of silver nitrate and silver nanoparticles on norovirus surrogates was investigated. It was found that both chemical forms (i.e. metallic and ionic silver) significantly decreased the MNV and FCV infectivity in a dose-dependent manner. Meanwhile, its effect depends on other factors, such as the aging time, the type of virus and the stabilization degree.

Furthermore, biopolymeric materials consisting of a matrix of poly(3-hydroxybutyrate-co-3-hydroxyvalerate) and AgNP-based coating obtained by means of electrospinning were also developed. Interestingly, the addition of very low loadings of stabilized AgNP into the electrospun coating provided a virucidal activity against norovirus surrogates and did not significantly modify the optical properties of films. The technology here proposed allows the design of custom made active adapted to the final intended use of packaging and contact surface industries.

## **5. Acknowledgements**

---

This work was supported by the Spanish Ministry of Economy and Competitiveness (MINECO) (RYC-2012-09950, RYC-2014-158, AGL2015-63855-C2-1-R and INIA grant RTA2014-00024-C04-03). GS and MJF were supported by the “Ramón y Cajal” Young Investigator from the MINECO. JLC-M was supported by the Administrative Department of Science, Technology and Innovation (Colciencias) of

Colombian Government. The authors thank Prof. H. W. Virgin (Washington University School of Medicine, USA) for kindly providing MNV-1 strain and RAW 264.7 cells.

## 6. References

---

1. WHO, "WHO Estimates of the Global Burden of Foodborne Diseases: Foodborne Disease Burden Epidemiology Reference Group 2007-2015. ," Ed., World Health Organization., 2015.
2. B. Lopman, P. Gastañaduy, G. W. Park, A. J. Hall, U. D. Parashar and J. Vinjé, "Environmental transmission of norovirus gastroenteritis," *Current Opinion in Virology*, vol. 2, no. 1, pp. 96-102, 2012.
3. K. K. Kuorwel, M. J. Cran, J. D. Orbell, S. Buddhadasa and S. W. Bigger, "Review of Mechanical Properties, Migration, and Potential Applications in Active Food Packaging Systems Containing Nanoclays and Nanosilver," *Comprehensive Reviews in Food Science and Food Safety*, vol. 14, no. 4, pp. 411-430, 2015.
4. M. Rai, A. Yadav and A. Gade, "Silver nanoparticles as a new generation of antimicrobials," *Biotechnology Advances*, vol. 27, no. 1, pp. 76-83, 2009.
5. M. Moritz and M. Geszke-Moritz, "The newest achievements in synthesis, immobilization and practical applications of antibacterial nanoparticles," *Chemical Engineering Journal*, vol. 228, pp. 596-613, 2013.
6. J. L. Castro-Mayorga, M. J. Fabra and J. M. Lagaron, "Stabilized nanosilver based antimicrobial poly(3-hydroxybutyrate-co-3-hydroxyvalerate) nanocomposites of interest in active food packaging," *Innovative Food Science and Emerging Technologies*, vol. 33, pp. 524-533, 2016.
7. A. Martínez-Abad, M. J. Ocio, J. M. Lagarón and G. Sánchez, "Evaluation of silver-infused polylactide films for inactivation of Salmonella and feline calicivirus in vitro and on fresh-cut vegetables," *International Journal of Food Microbiology*, vol. 162, no. 1, pp. 89-94, 2013.
8. T. Amna, J. Yang, K. S. Ryu and I. H. Hwang, "Electrospun antimicrobial hybrid mats: Innovative packaging material for meat and meat-products," *Journal of Food Science and Technology*, 2014.

## Chapter IV

9. M. Botes and T. E. Cloete, "The potential of nanofibers and nanobiocides in water purification," *Crit Rev Microbiol*, vol. 36, no. 1, pp. 68-81, 2010.
10. R. M. Navalakhe and T. D. Nandedkar, "Application of nanotechnology in biomedicine," *Indian J Exp Biol*, vol. 45, no. 2, pp. 160-165, 2007.
11. J. L. Castro-Mayorga, M. J. Fabra, A. M. Pourrahimi, R. T. Olsson and J. M. Lagaron, "The impact of zinc oxide particle morphology as an antimicrobial and when incorporated in poly(3-hydroxybutyrate-co-3-hydroxyvalerate) films for food packaging and food contact surfaces applications," *Food and Bioproducts Processing*, vol. 101, pp. 32-44, 2017.
12. D. H. D'Souza, "Phytochemicals for the control of human enteric viruses," *Current Opinion in Virology*, vol. 4, pp. 44-49, 2014.
13. F. X. Abad, R. M. Pinto, J. M. Diez and A. Bosch, "Disinfection of human enteric viruses in water by copper and silver in combination with low levels of chlorine," *Applied and Environmental Microbiology*, vol. 60, no. 7, pp. 2377-2383, 1994.
14. N. Silvestry-Rodriguez, E. E. Sicairos-Ruelas, C. P. Gerba and K. R. Bright, "Silver as a disinfectant," in *Reviews of Environmental Contamination and Toxicology*, Ed., pp. 23-45, 2007.
15. S. Galdiero, A. Falanga, M. Vitiello, M. Cantisani, V. Marra and M. Galdiero, "Silver nanoparticles as potential antiviral agents," *Molecules*, vol. 16, no. 10, pp. 8894-8918, 2011.
16. N. Khandelwal, G. Kaur, N. Kumar and A. Tiwari, "Application of silver nanoparticles in viral inhibition: A new hope for antivirals," *Digest Journal of Nanomaterials and Biostructures*, vol. 9, no. 1, pp. 175-186, 2014.
17. B. De Gusseme, L. Sintubin, L. Baert, E. Thibo, T. Hennebel, G. Vermeulen, M. Uyttendaele, W. Verstraete and N. Boon, "Biogenic silver for disinfection of water contaminated with viruses," *Applied and Environmental Microbiology*, vol. 76, no. 4, pp. 1082-1087, 2010.
18. A. Z. Bekele, K. Gokulan, K. M. Williams and S. Khare, "Dose and Size-Dependent Antiviral Effects of Silver Nanoparticles on Feline Calicivirus, a Human Norovirus Surrogate," *Foodborne Pathogens and Disease*, 2016.
19. Y. Ilg and J. Kreyenschmidt, "Effects of food components on the antimicrobial activity of polypropylene surfaces containing silver ions (Ag<sup>+</sup>)," *International Journal of Food Science and Technology*, vol. 46, no. 7, pp. 1469-1476, 2011.
20. J. L. Castro-Mayorga, A. Martínez-Abad, M. F. Fabra, J. M. Lagarón, M. J. Ocio and G. Sánchez, "Chapter 32 - Silver-Based Antibacterial and Virucide Biopolymers: Usage

and Potential in Antimicrobial Packaging A2 - Barros-Velázquez, Jorge," in *Antimicrobial Food Packaging*, Ed., pp. 407-416, Academic Press, San Diego, 2016.

21. N. C. Kasuga, R. Yoshikawa, Y. Sakai and K. Nomiya, "Syntheses, structures, and antimicrobial activities of remarkably light-stable and water-soluble silver complexes with amino acid derivatives, silver(I) N-acetylmethioninates," *Inorganic Chemistry*, vol. 51, no. 3, pp. 1640-1647, 2012.

22. J. L. Castro-Mayorga, A. Martínez-Abad, M. J. Fabra, C. Olivera, M. Reis and J. M. Lagarón, "Stabilization of antimicrobial silver nanoparticles by a polyhydroxyalkanoate obtained from mixed bacterial culture," *International Journal of Biological Macromolecules*, vol. 71, pp. 103-110, 2014.

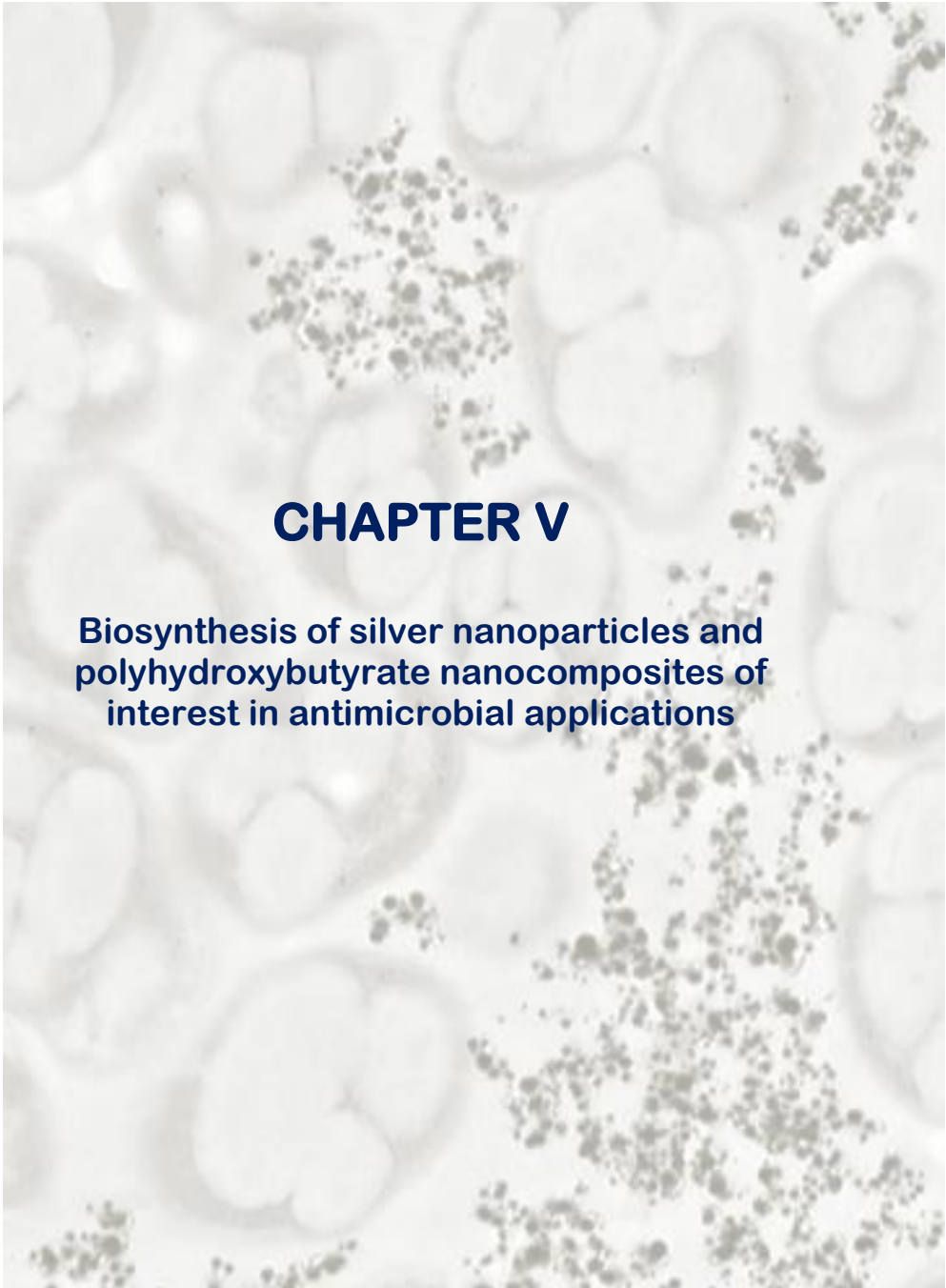
23. A. Martínez-Abad, J. M. Lagarón and M. J. Ocio, "Characterization of transparent silver loaded poly(L-lactide) films produced by melt-compounding for the sustained release of antimicrobial silver ions in food applications," *Food Control*, vol. 43, no. 0, pp. 238-244, 2014.

24. S. J. Park, H. H. Park, S. Y. Kim, S. J. Kim, K. Woo and G. Ko, "Antiviral properties of silver nanoparticles on a magnetic hybrid colloid," *Applied and Environmental Microbiology*, vol. 80, no. 8, pp. 2343-2350, 2014.

25. H. J. Jeon, J. S. Kim, T. G. Kim, J. H. Kim, W.-R. Yu and J. H. Youk, "Preparation of poly( $\epsilon$ -caprolactone)-based polyurethane nanofibers containing silver nanoparticles," *Applied Surface Science*, vol. 254, no. 18, pp. 5886-5890, 2008.

26. A. Martínez-Abad, G. Sanchez, J. M. Lagaron and M. J. Ocio, "Influence of speciation in the release profiles and antimicrobial performance of electrospun ethylene vinyl alcohol copolymer (EVOH) fibers containing ionic silver ions and silver nanoparticles," *Colloid and Polymer Science*, vol. 291, no. 6, pp. 1381-1392, 2012.

27. G. Sánchez and R. Aznar, "Evaluation of Natural Compounds of Plant Origin for Inactivation of Enteric Viruses," *Food and Environmental Virology*, vol. 7, no. 2, pp. 183-187, 2015.

A grayscale electron micrograph showing numerous oval-shaped cells, likely bacteria, with a granular texture. Scattered throughout the field are clusters of small, dark, spherical particles, which are silver nanoparticles. The background is a light gray, and the overall image has a slightly blurred appearance.

## CHAPTER V

### **Biosynthesis of silver nanoparticles and polyhydroxybutyrate nanocomposites of interest in antimicrobial applications**

J.L. Castro-Mayorga, F. Freitas, M. Reis, A. Prieto, J.M. Lagaron. "Biosynthesis of silver nanoparticles and polyhydroxybutyrate nanocomposites of interest in antimicrobial applications". To be submitted.



## Abstract

---

This study deals with the optimization and scaling up of the production of poly(3-hydroxybutyrate), PHB, nanocomposites containing biosynthesized silver nanoparticles (AgNPs) to generate materials with antimicrobial performance. First, a comparative study of the chemical and biological synthesis of AgNPs during the fermentation process of *Cupriavidus necator* at shake flask-scale was carried out. These experiments demonstrated the inherent capacity of *C. necator* to reduce the silver salt and produce AgNPs without the need for adding a reducing agent and, that the method of synthesis (with or without reducing agent) affects the dispersion of the AgNPs and their antimicrobial performance. Finally, the process was scaled-up to a 10 liters bioreactor and the relevant physical properties of the PHB-AgNPs nanocomposites pressed into films were determined. From the characterization work, the AgNPs were found to be well dispersed and distributed into the polymer matrix, having a maximum frequency of particles with average diameter of 76-95 nm. Moreover, the presence of AgNPs did not cause any effect on the thermal properties of the biopolymer, although a slight reduction in crystallinity was seen. The developed materials presented a strong antimicrobial activity against the food-borne pathogens *Salmonella enterica* and *Listeria monocytogenes*, which makes them potentially suitable for active coatings and packaging applications.

## Keywords

---

Polyhydroxyalkanoates, metal nanoparticles, antibacterial, films.

## 1. Introduction

---

Given the environmental concerns related to the massive use of petroleum-based plastics and their high demand in the packaging market, which was around 40% of the global plastic's consumption in 2014 [1], a great interest to develop biodegradable polymers obtained from renewable resources has emerged in the last decades. Among the most widely studied biopolymers, polyhydroxyalkanoates (PHAs) have attracted increased attention due to their thermoplastic, biodegradable, biocompatible and renewable nature [2].

PHAs are synthesized by many bacteria as intracellular carbon and energy storage granules. The bacterium *Cupriavidus necator* (before called *Ralstonia eutropha* and *Wautersia eutropha*) is an interesting candidate for the large-scale production of polyhydroxybutyrate (PHB). It provides all the necessary characteristics, which are required for a biotechnological production strain. Due to its metabolic versatility, it can convert a broad range of renewable carbon resources into diverse valuable compounds. Furthermore, this bacterium is accessible to engineering of its metabolism by genetic modification approaches [3].

The PHB produced by *C. necator* can be used for applications ranging from replacement of fossil resource-based bulk plastics to high-value special purpose polymers. In the packaging field, PHB has been used to make various biodegradable products, including films, coated paper and boards, compost bags, dispensable food service-ware, and molded products such as bottles and razors [4].

Particularly, packaged foods with enhanced quality and safety are demanded by consumers. In this context, the incorporation of antimicrobials into packaging materials allows the progressive diffusion of target bactericidal or bacteriostatic

## Chapter V

compounds into the packaging surface and from there also into the food matrix, thus reducing the use of high concentrations of antimicrobials in the food matrix to extend foods shelf-life [5].

Inorganic compounds in the nanosize range, i.e. below 100 nm, such as silver nanoparticles (AgNPs) have emerged as efficient tools to prevent microbial spoilage and microbial outbreaks in food contact plastics and surfaces. Traditionally, AgNPs are synthesized by chemical methods using different organic and inorganic reducing agents, such as sodium borohydride (NaBH<sub>4</sub>) [6, 7], sodium citrate [8], ascorbate [9], elemental hydrogen, Tollen's reagent, N,N-dimethyl formamide (DMF) and poly(ethylene glycol) block copolymers [10]. However, most chemicals used in this kind of synthesis are toxic and lead to non-eco-friendly by-products. To solve these problems, biological synthesis of nanomaterials using living organisms such as bacteria [11], fungi [12] or plant extracts [13] are currently being developed.

So far, there is only a study reported in the literature about the effects of AgNPs on *C. necator* growth dynamic, which indicates growth stimulation of this bacteria at certain AgNPs concentrations (40 µg/mL of AgNPs with primary particle size distribution D<sub>90</sub> < 15 nm and added after 12 hours of cultivation), as well as varying susceptibility to nanoparticles at different growth stages [14]. However, because it has been known and accepted that the silver susceptibility depends on the medium culture composition [15], it is necessary to make an analysis of the unbalanced growth conditions where PHB is produced. On the other hand, in a recent publication, the synthesis of AgNPs was carried out by using the cell-free supernatant of *Alkaliphilus oremlandii*, strain ohILA, culture. In that case, the synthesized AgNPs were subsequently stabilized by the extracted and purified biopolymer also produced by *A. oremlandii* [16].

The main goal of this study was to report the development, optimization and scaling up of a simple bioprocess for the simultaneous biosynthesis of PHB and AgNPs with antimicrobial properties. First, a comparative study of the chemical and biological synthesis of AgNPs during the fermentation process of *C. necator* at shake flask was carried out and then optimized and scale-up to fully-automated 10 liters bioreactor. Moreover, the physical properties and the antimicrobial performance of the developed nanocomposites, was determined.

## **2. Materials and methods**

---

### **2.1 Materials**

Silver nitrate (>98%; Silma-Aldrich, Germany), Sodium borohydride (96%, Panreac, Spain), chloroform stabilized with ethanol (Technical grade, Panreac, Spain), methanol (For analysis, ACS, ISO, Panreac, Spain), hiperpuric nitric acid (69%, Panreac, Spain), sulphuric acid in methanol solution (Sigma–Aldrich, HPLC grade) and benzoic acid in chloroform (1 g/L) (Sigma–Aldrich, HPLC grade) without further purification were used throughout the experiments.

### **2.2 Bacterial growth and media**

*Cupriavidus necator* strain H16 (DSM 428, Wilde 1962) was obtained from the German Collection of Microorganisms and Cell Cultures (DSMZ) and used in this study. The culture, cryopreserved in 20% (v/v) glycerol at -80 °C, was reactivated in solid Luria Bertani (LB) medium, at 30 °C for 24 h, and subsequently used as inoculum. The cultivation medium consisted of: MgSO<sub>4</sub>·7H<sub>2</sub>O, 0.39 mg/L; K<sub>2</sub>SO<sub>4</sub>, 0.45 mg/L; FeSO<sub>4</sub>·7H<sub>2</sub>O, 15 mg/L; NH<sub>4</sub>Cl, 0.01% (w/v); H<sub>3</sub>PO<sub>4</sub>, 1 M (12 mL/L); trace elements, 24 mL/L (CuSO<sub>4</sub>·5H<sub>2</sub>O, 20 mg/L; ZnSO<sub>4</sub>·6H<sub>2</sub>O, 100 mg/L; MnSO<sub>4</sub>·4H<sub>2</sub>O,

## Chapter V

100 mg/L; CaCl<sub>2</sub>·2H<sub>2</sub>O, 2.6g/L) and 1% (w/v) of sodium gluconate as sole carbon source.

### 2.3 Microbial synthesis of PHB and AgNPs

The biosynthesis of PHB and AgNPs was carried out in accordance with a proprietary methodology (Spanish Patent P201630829). First, the process was analyzed at shake flask scale and then optimized and scaled-up to 10 L capacity fully-automated laboratory-scale bioreactor.

#### 2.3.1 Synthesis at shake flask scale

Batch cultivation experiments of *C. necator* in shake flask were performed in order to investigate the AgNPs synthesis from silver nitrate. The inoculum for shake flasks experiments was prepared by inoculating a single *C. necator* colony into 200 mL of LB medium and incubation in an orbital shaker at 30° C and 200 rpm for 24 h. The cells were then harvested and resuspended in the culture medium described above (see 2.2 section) to reach an optical density of 0.3 at a wavelength of 600 nm. The cultivation was done in 2 L Erlenmeyer flask with an initial working of 800 mL, which were incubated at 30° C and 200 rpm for 24 h. Subsequently, the cultures were treated with 267 mL of silver nitrate solutions at 1 mM or 3.5 mM. The silver nitrate treatment was applied at the beginning and after 24 h of the cultivation and carried out both in presence and in absence of a reducing agent. For the experiments in the presence of the reducing agent, 8 mL of the culture broth were replaced by 8 mL a 0.1 M sodium borohydride solution to get 1 mM concentration and, after 20 min, the desirable silver nitrate solution were added dropwise During the addition of silver nitrate and sodium borohydride and for further 16 h, the cultures were kept under agitation (200rpm) and 30° C.

### 2.3.2 Scaled up synthesis to lab-scale bioreactor

Bioreactor cultivation experiments were performed in a 10 L bioreactor (BioStat B-Plus, Sartorius, Germany), with an initial working volume of 7 L. The inoculum was 10% (v/v) of the initial reactor working volume. It was prepared by inoculating a *C. necator* colony into LB medium and incubation in an orbital shaker, at 30° C and 200 rpm, for 24 hours. The culture thus obtained was then transferred into culture medium described above (see 2.2 section), further incubated for 48 h at the same agitation and temperature and used for the bioreactor experiments. The bioreactor was operated with controlled temperature (30 °C) and pH (7.0). The pH was controlled by the automated addition of HCl (1 M) and NH<sub>4</sub>OH (25% v/v, in the first 20 hours) which served also as nitrogen source, or NaOH (2 M, after 20 hours) to impose nitrogen-limitation conditions. The dissolved oxygen (DO) concentration was controlled at 30% by automatically adjusting the stirring rate (between 300 and 2000 rpm). The experiments comprised an initial batch phase of 20 h, followed by the fed-batch phase, wherein 1 L of sodium gluconate, at 1% (w/v) at 0.12 L/h was fed to stimulate the polymer accumulation. At the end of the cultivation runs, a sample of 10 mL was withdrawn from the bioreactor of broth was centrifuged at 4000 rpm for 15 min and the pellet washed with deionized water and lyophilized for the gravimetric the cell dry weight (CDW) quantification. In the bioreactor experiments the silver nitrate treatment was applied following the optimal parameters obtained in the shake flask cultivation.

### 2.4 Polymer extraction

The extraction of the polymer produced in the shake flask and bioreactor experiments was carried out by using organic solvents. To this end, the culture broth was centrifuged for 15 min at 4000rpm, the supernatant discarded and the biomass transferred to 300 mL a chloroform solution and left to form a suspension for a period

## Chapter V

of 20 h at 50 °C in a closed bottle with stirred with a magnetic bead. Subsequently, 300 mL of distilled water was added to the polymer rich solution. The mixture was separated in volumes of 50 mL, stirred in vortex for 1 min and centrifuged for 2 min at 2000 rpm to separate the organic phase. The resulting organic fraction was removed using glass Pasteur pipettes, and the polymer was then precipitated in ice-cold methanol (10-fold excess) with vigorous stirring. Finally, the precipitated polymer was separated by filtration and dried overnight in a vacuum oven at 60 °C. The PHB content in the biomass (% w/w) was calculated using the following equation (Equation 1):

$$\% PHA = \frac{\text{weight of extracted polymer}}{\text{cell dry weight}} \times 100 \quad (1).$$

The purity of the extracted polymer was determined by gas chromatography (GC) as described elsewhere [17, 18]. Briefly, 3-5 mg of the extracted polymer were hydrolyzed with 20% (v/v) sulfuric acid in methanol solution (1 mL) and benzoic acid (internal standard) in chloroform (1 mL), at 100 °C for 3.5 h. After the digestion, the methylated monomers were extracted and injected into a gas chromatograph (Varian CP-3800) coupled with a flame ionization detector (FID) (CTC Analytics, Switzerland) in a BR89342 WCOT fused silica column (60 m × 0.53 mm), using helium as carrier gas with a flow rate of 1 mL/min. The oven temperature program was as follows: 40 °C; 20 °C/min, until 100 °C; 3 °C/min, until 175 °C and, finally, 20 °C/min, until 220 °C. The injector and detector temperature were set at 280 °C and 250 °C, respectively. Pure copolymer solution (0.25-10 mg/L) containing poly(3-hydroxybutyrate-co-3-hydroxyvalerate), P(3HB-co-3HV) (Sigma-Aldrich), was used as standard.

## **2.5 Transmission electronic microscopy (TEM) of bacteria**

The size and morphology of AgNPs obtained from the shake flask experiments were characterized using a transmission electron microscope (JEOL 1010, Hitachi) equipped with a digital Bioscan (Gatan) image acquisition system at an accelerating voltage of 80 kV. The samples for TEM analysis were prepared by fixing the cells with 2.5% glutaraldehyde and 2% osmium tetroxide for 2 h at room temperature. The pellets were then washed three times with phosphate buffer saline (PBS) and dehydrated in ethanol series (30%, 70%, 90% and 100%). The specimens were further embedded in LR-White resin and cut with an ultramicrotome (Leica UC6). Ultrathin sections were then positively stained with uranylacetate and lead citrate and then placed onto carbon-coated copper grids for microscopic examination.

## **2.6 Preparation and characterization of films**

The polymer produced in the lab-scale reactor experiments was compression molded into films of 80  $\mu\text{m}$  of thickness using a hot-plate hydraulic press (Carver 4122, USA) at 180 °C and 1.8 MPa for 2 min and used for further characterization. Pure and silver containing films were prepared for comparative purposes. The morphology and size distribution of AgNPs into the film were analyzed through observation of ultramicrotomed cross sections by TEM using the same microscope that was used above (JEOL 1010, Hitachi). The particle diameters were estimated by means of Adobe Photoshop CS4 software from 300 particles at random.

### **2.6.1 Molecular weight determination**

The molecular weight of the pure and the silver containing polymer were determined using Gel Permeation Chromatography (GPC) as described elsewhere [19]. Briefly, a 10- $\mu\text{L}$  aliquot of 0.5 % w/v sample solution in chloroform was injected into the system operated at 35 °C with an eluent flow rate of 1 mL/min using a Spectra-

## Chapter V

Physics 8800 solvent delivery system with a set of two Mixed C Styragel columns and a Shodex SE 61 refractive index detector. Polystyrene standards with narrow molar mass dispersity were used to generate a universal calibration curve.

### 2.6.2 Thermal properties

The thermal properties of the polymers were determined by differential scanning calorimetry (DSC) and thermogravimetric analysis (TGA). DSC analysis were carried out using a Perkin-Elmer DSC 8000 with an intracooler (Intracooler 2 from Perkin Elmer). Samples were first heated from 0 °C to 200 °C, kept for 1 min at 200 °C and then cooled down to -50 °C. The heating and cooling rates for the runs were 10 °C/min and the typical sample weight was ~3 mg. The melting temperature ( $T_m$ ), melting enthalpy ( $\Delta H_m$ ), crystallization temperature ( $T_c$ ) and crystallization enthalpy ( $\Delta H_c$ ) were determined from the heating and cooling curves. The DSC instrument was calibrated with an indium standard before use. The tests were done in triplicate.

Thermal stability of the materials was analysed with a Perkin Elmer Thermobalance TGA 7 equipment operated under nitrogen atmosphere. After conditioning for 5 min at 30 °C, the sample was heated to 600 °C at a heating rate of 10 °C/min. Derivative TGA curves (DTG) represent the weight loss rate as function of temperature and the temperature of maximum rate of degradation ( $T_d$ ).

### 2.6.3. Wide Angle X-ray Diffraction analysis

Wide Angle X-ray Diffraction analysis (WAXD) measurements of the pure and silver containing films were recorded at room temperature using a Bruker AXSD4 Endeavour diffractometer with a Cu-K $\alpha$  source (wavelength = 1.54178 Å) and a generator at 40 kV and 40 mA. Peak fitting was carried out using IgorPro software package (Wavemetrics, Lake Oswego, Oregon). Gaussian function was used to fit the experimental diffracton profiles obtained. The crystallinity index ( $X_c$ ) was calculated by Equation (2).

$$X_c = \frac{\Sigma A_{Crystal}}{\Sigma A_{Total}} \times 100 \quad (2)$$

where  $\Sigma A_{Crystal}$  is the sum of the areas corresponding to crystalline peaks and  $\Sigma A_{Total}$  is the sum of the areas under all the diffraction peaks in the range of  $2\theta = 5^\circ$  and  $40^\circ$ .

#### 2.6.4 Determination of silver content

To estimate the total silver content within the films, ~100 mg of silver containing films were subjected to digestion with 2 mL of  $\text{HNO}_3$  at  $80^\circ\text{C}$  for 16 h. The silver concentration in the resultant digestant was determined by inductively coupled plasma-optical emission spectroscopy (ICP-OES, Perkin-Elmer, USA) using a silver standard solution (traceable to SRM from NIST,  $\text{AgNO}_3$  in  $\text{HNO}_3$  2-3 %, 1000 mg/L Ag Certipur®, Merck, Germany) for calibration. The measurements were done in triplicate.

### 2.7 Antimicrobial activity of PHB-AgNP films

The microorganisms used for the antimicrobial assays were the food-borne pathogens *Salmonella enterica* CECT 4300 and *Listeria monocytogenes* CECT 7467. The strains were obtained from the Spanish Type Culture Collection (CECT, Spain) and stored in phosphate buffered saline (PBS, Sigma Aldrich, U.S.) with 10 wt.% tryptic soy broth (TSB, Conda Laboratories, Spain) at  $-80^\circ\text{C}$  until used. Before antimicrobial activity test, an aliquot of bacteria stock was transferred twice to TSB and grown at  $37^\circ\text{C}$  to the mid-exponential phase. This culture served as inoculum for the susceptibility tests.

Antimicrobial activity was determined by using a modification of the Japanese industrial standard test (JIS Z 2801-ISO 22196). In brief, the test samples were placed in petri dishes and inoculated with  $10^5$  CFU/mL of bacterial culture. The inoculum was covered with a Low-Density Polyethylene film and incubated for 24 h at  $25^\circ\text{C}$  and

## Chapter V

>90% RH. After exposure, bacteria were then recovered with PBS, spread on TSA for plate counts after incubation at 37 °C overnight. The temperature of 25 °C was chosen as to mimic the room temperature condition of food storage and consumption. PHB films without silver were used as negative control. The bacterial reduction (R) was calculated as follows:  $R = \log_{10} (N_0/N_t)$ , where  $N_0$  is the average of the bacterial counts recovered from the PHB negative control film and  $N_t$  is average of the bacterial counts recovered from the PHB films loaded with silver.

### 2.8 Statistical analysis

The statistical analysis of data was carried out by means of OriginPro 8 (OriginLab Corporation, USA) with a one-way analysis of variance (ANOVA) and using the Tukey's multiple test at the 95% confidence level. Reported values of quantitative measurements were the means of triplicate data  $\pm$  standard deviation.

## 3. Results and discussion

---

### 3.1 Microbial synthesis of PHB-AgNPs in shake flasks

The addition of 1 mM or 3.5 mM silver nitrate solutions at the beginning and after 24 h of the *C. necator* cultivations resulted in a complete and irreversible cell growth inhibition, as no colony-forming units were detected in TSA plates (detection limit of 1.30 log CFU/mL). This result was likely expected due to the natural and well known antimicrobial effect of silver. Thus, in subsequent experiments the silver nitrate solutions were added after ca. 24 h of cultivation, when the *C. necator* achieved a concentration of cells achieved 8 log CFU-mL and an optical density of 6 at a wavelength of 600 nm.

### 3.1.1 Visual and microscopic observations

At the lower concentration of 1 mM, no visual changes in the colour of the reaction mixture with or without reducing agent were observed. However, a brown colour appeared in the reaction mixture incubated with the silver nitrate solution at 3.5 mM and the reducing agent (Fig. 1). These colour changes are associated with the synthesis of colloidal silver. Silver colloids show different colours due to light absorption and scattering in the visible region based on plasmon resonance, which depend on the shape and size of AgNPs and dielectric constant of the surrounding medium [20].

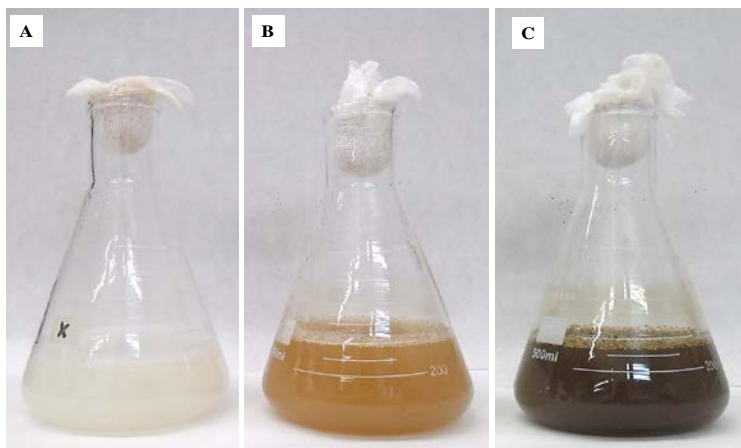


**Figure 1.** Visual aspect of *C. necator* cultures at shake flask-scale. (A) untreated bacteria, (B) bacteria treated with a silver nitrate solution at 3.5 mM in absence of the reducing agent, (C) bacteria treated with a silver nitrate solution at 3.5 mM in presence of the reducing agent.

A typical TEM image of untreated *C. necator* cells filled with large PHB granules is shown in the Fig. 2A. Interestingly, when the bacterial culture in stationary phase was treated with 1 mM of silver nitrate, spherical electron dense nanoparticles appeared inside and outside the cellular cytoplasm both in absence (Fig. 2B) and in presence of

## Chapter V

reducing agent (Fig. 2C). This finding confirms the inherent capacity of *C. necator* to reduce the silver salt and produce AgNPs. Furthermore, noticeable differences in the dispersion and the frequency of nanoparticles inside the cells were evidenced between the two preparations. Some bigger agglomerates and a higher number of particles located outside the cytoplasm were observed in the samples prepared in the presence of the reducing agent (Fig. 2C) as compared with those prepared without reducing agent. Incorporation of a reducing agent to the bacterial culture adds unnecessary reduction capacity to that already inherent within the biomass resulting in much stronger or in excess reduction power.

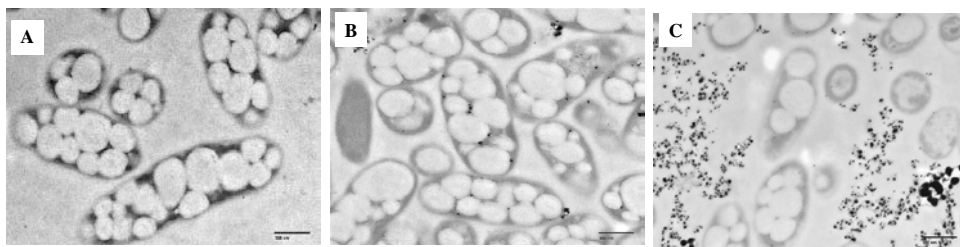


**Figure 2.** TEM micrographs of *C. necator* at 24 h of cultivation in shake flask. (A) untreated bacteria, (B) bacteria treated with a silver nitrate solution at 1 mM in absence of the reducing agent, (C) bacteria treated with a silver nitrate solution at 1 mM in presence of the reducing agent.

The discussed colour changes were also evident after polymer purification and compression moulding process, as deduced from the contact transparency pictures in Figure 3. In fact, the film prepared with the polymer obtained in the presence of at 1 mM silver nitrate (Fig. 3B) in the absence of the reducing agent presented a very slight colour difference from the neat PHB film (Fig. 3A). However, some visual dissimilarities were found for the material prepared with PHB synthesized at 1 mM silver nitrate in the presence of reducing agent (Fig. 3C) and those prepared at 3.5 mM

(Fig. 3D and 3E). In the case of materials prepared in the presence of the reducing agent, in both concentrations, small black particles were visually detected (see samples C and E of Fig. 3). It should be also noted that at 3.5 mM of silver nitrate concentration, the films showed a brown colour, which was more intense for those samples containing the reducing agent (see Fig. 3D and 3E). These findings could be explained by the excess of the reducing power and the AgNPs agglomeration discussed above, which is even more significant at the higher silver loading of 3.5 mM.

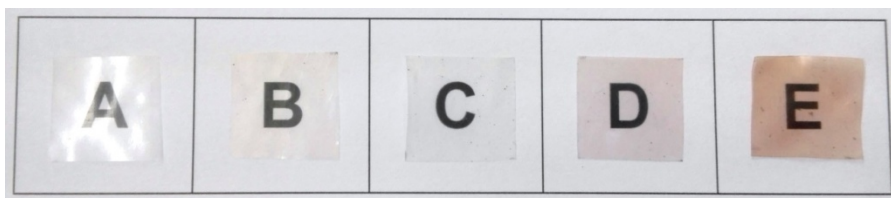


**Figure 3.** Contact transparency pictures of the pure PHB and the PHB-AgNPs films prepared with silver nitrate solutions at different concentrations. (A) pure PHB, (B) PHB-AgNPs film prepared with 1 mM silver nitrate solution and in absence of the reducing agent, (C) PHB-AgNPs film prepared at 1 mM in presence of the reducing agent, (D) PHB-AgNPs prepared at 3.5 mM in absence of the reducing agent, (E) PHB-AgNPs prepared at 3.5 mM in presence of the reducing agent.

### 3.1.2 Antimicrobial performance

The silver-based films developed at Erlenmeyer flask scale were tested against two of the most frequent food-borne pathogens, *Salmonella enterica* and *Listeria monocytogenes* (Table 1, Fig. 4). The Gram-negative bacterium *S. enterica* appeared to be more susceptible to the antimicrobial effect of silver nanoparticles than the Gram-positive bacterium *L. monocytogenes*, which can be explained by the differences on structural features of its cell envelope [21-23]. Furthermore, the active films showed dose-dependent antibacterial activity that directly increased with the silver concentration. This dose-dependent effect was particularly noticeable in the

## Chapter V

*L. monocytogenes* tests. No viable counts of *S. enterica* were recorded for both silver nitrate concentrations used for the biosynthesis, except for the one prepared in the presence of 1 mM silver nitrate, with reducing agent, which might be due to the lower dispersion, the bigger size and the higher agglomeration degree of AgNPs as compared to its counterpart prepared without reducing agent, as it has been previously observed by TEM (see Fig. 2). On the other hand, the PHB film obtained in the presence of a higher silver concentration of 3.5 mM was more effective to reduce the bacterial population of *L. monocytogenes* (by least 3 log CFU/mL, which is the minimal value to consider that the sample presents a relevant antimicrobial activity) [24, 25].

**Table 1.** Bacterial reduction of the PHB/AgNPs films prepared at shake flask-scale.

Sample	R	
	<i>S. enterica</i>	<i>L. monocytogenes</i>
1 mM without reducing agent	>6.59	2.21
1 mM with reducing agent	3.83	1.31
3.5 mM without reducing agent	>6.59	3.28
3.5 mM with reducing agent	>6.59	3.43

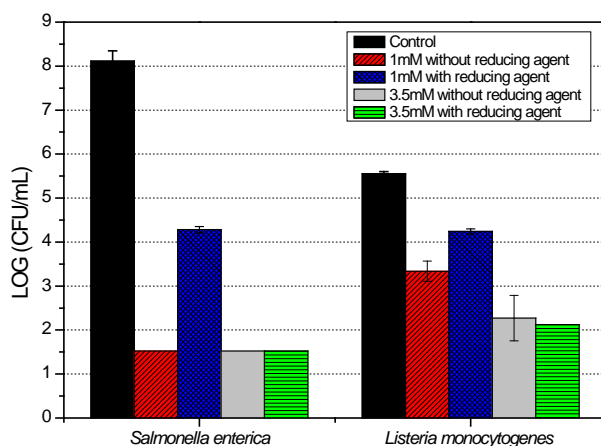


**Figure 4.** Antimicrobial activity of the PHB-AgNPs films prepared at shake flask-scale against *S. enterica* and *L. monocytogenes*. The initial inoculum size was 5 log CFU/mL and the detection limit was 1.30 log CFU/mL.

## 3.2 Microbial synthesis of PHB-AgNPs in 10 liters bioreactor

### 3.2.1 Fermentation process

In accordance with the results of the study at shake flask scale, fed-batch fermentations under controlled cultivation conditions at the 10-liter scale were carried out to obtain higher cell densities and higher polymer contents. In these experiments, the PHB production and the biological synthesis of AgNPs by using the intrinsic reducing power of the biomass were simultaneously performed. The silver nitrate concentration used in these experiments was 3.5 mM because of its effective antimicrobial activity against the two food-borne pathogens already described in the shake flask experiments.

The addition of silver nitrate in the bioreactor experiments was carried out 40 h after de cultivation, when the culture achieved a relative constant optical density of

## Chapter V

9-10 at a wavelength of 600 nm. At this point, a CDW of  $4.17 \pm 0.38$  g/L was obtained, which corresponded to a polymer production of  $3.38 \pm 0.65$  g/L and an overall volumetric productivity of  $2.03 \pm 0.39$  g/(L day). These values are significantly higher than the values obtained in the shake flask experiments (overall productivity  $0.50 \pm 0.04$  g/(L day) and in previous studies on PHB production from *C. necator* fed using virgin soybean oil, rapeseed oil, olive oil or glucose under batch flask mode [26, 27], but still much lower than those reported by Heinrich et. al (2012) [28] and Cruz et al. (2015) [29] for fed-batch and batch bioreactor cultivation of *C. necator* with used sodium gluconate and cooking oils, respectively. Nevertheless, the final polymer content of  $57.5 \pm 4.9$  wt. % obtained in the present work, was in the range of those reported in the literature [28, 30], although more studies are needed in order to gain a higher cell density and improve the productivity at large scale, but it is outside the scope of the present study.

### 3.2.2 Polymer characterization

As expected, the polymer produced by *C. necator* was the homopolymer poly(3-hydroxybutyrate), (PHB), which is in agreement with recent reports of PHB production from *C. necator* employing sodium gluconate as sole carbon source [28]. PHB purity after the recovery procedure was  $91.8 \pm 0.6$  wt. %, as measured by GC, without any significant variation after silver incorporation. The purity achieved with the present procedure was within the reported values (range of values?) for PHB extraction with similar procedures [26, 28, 31].

According to GPC results, there were no changes in the weight average molecular weight of PHB after silver addition, since the weight average molecular weight of the PHB and PHB/AgNPs films was  $1.12 \times 10^6$  g/mol. Similar values were reported for PHB synthesized by *C. necator* from used cooking oils under pulse feeding fermentation ( $2.0 \times 10^5 - 2 \times 10^6$  g/mol) [32].

### 3.2.3 Morphological properties of PHB-AgNPs films

Figure 5A shows a typical TEM micrograph of the ultramicrotomed cross section of the PHB containing AgNPs (hereinafter called PHB-AgNPs). The TEM results indicated that the particles are small, well dispersed and spherical in shape, having a maximum frequency of particles with an average diameter at 76-95 nm (Fig. 5B). Thus, the good dispersion of AgNPs into the PHB matrix led to macroscopically homogeneous films with a good contact and background transparency (Fig. 5C).

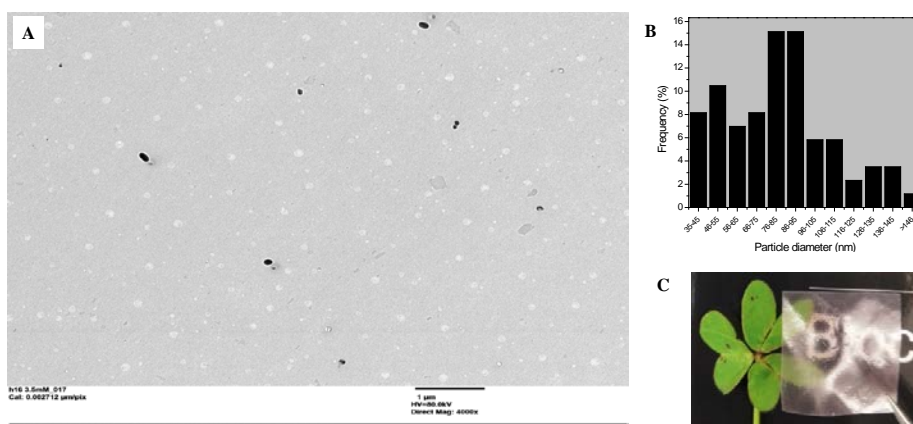


**Figure 5.** Morphological properties of the PHB-AgNPs films prepared at lab-scale bioreactor. (A) TEM micrograph of ultramicrotomed cross section of film, (B) Photograph of the film, (C) Particle size distribution of AgNPs into the film.

### 3.2.3 Thermal properties of PHB-AgNPs films

The thermal properties of the pure PHB and the PHB-AgNPs films were analyzed by TGA and DSC. The thermal degradation curves of the two materials exhibited a single weight loss with maximum decomposition temperature ( $T_d$ ) at 276 °C for PHB and 278 °C for PHB-AgNPs (Fig. 6). This result is in contrast with previous studies carried out with other PHA's materials, in which an improvement in the thermal

## Chapter V

stability of the composites were seen induced by the presence of metal nanoparticles [33-36]. Nevertheless, in the present work, the thermal stability was not seen to depend on the AgNPs loading since, in comparison with the previous studies, it was rather small to show any potential effect (i.e.  $0.015 \pm 0.001$  wt. %, as quantified by ICP-OES).

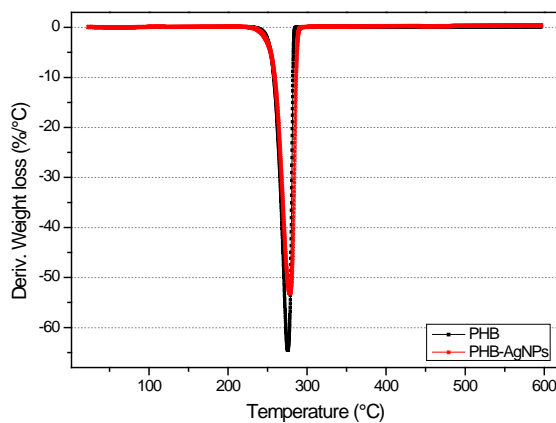


**Figure 6.** DTG curves of the pure PHB and PHB-AgNPs nanocomposites prepared at lab-scale bioreactor.

The DSC thermograms for heating and cooling of the neat and silver containing films are shown in Figure 7 and the resulting thermal properties are gathered in Table 2. A single melting peak was observed in the heating runs of both samples. Indeed, no significant or slight differences ( $p < 0.05$ ) were found between the melting temperature ( $T_m$ ) or melting enthalpy ( $\Delta H_m$ ) obtained from the heating step of the neat PHB and silver containing PHB. However, a measurable decrease in the crystallization temperature ( $T_c$ ) and crystallization enthalpy ( $\Delta H_c$ ) of PHB-AgNPs as compared to PHB was registered, suggesting an antinucleation effect in which the nanoparticles could be hindering the PHB crystallization [33, 37].

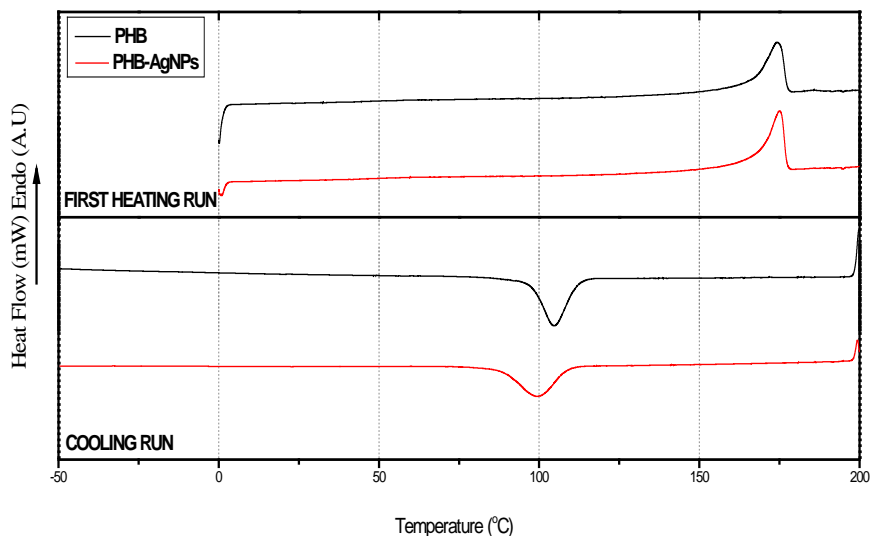


**Figure 7.** DSC thermograms of first heating and cooling run of the pure PHB and the PHB-AgNPs nanocomposites prepared at lab-scale bioreactor.

**Table 2.** DSC melting point ( $T_m$ ), melting enthalpy ( $\Delta H_m$ ), crystallization temperature ( $T_c$ ) and crystallization enthalpy ( $\Delta H_c$ ) of the pure PHB and the PHB-AgNPs nanocomposites prepared at lab-scale bioreactor.

Sample	$T_m$ (°C)	$\Delta H_m$ (J/g)	$T_c$	$\Delta H_c$ (J/g)
PHB	$175.3 \pm 1.1$ <sup>a</sup>	$80.5 \pm 0.7$ <sup>a</sup>	$103.7 \pm 1.5$ <sup>a</sup>	$76.5 \pm 1.8$ <sup>a</sup>
PHB-AgNPs	$175.0 \pm 0.4$ <sup>a</sup>	$83.1 \pm 0.6$ <sup>b</sup>	$98.8 \pm 1.8$ <sup>b</sup>	$68.9 \pm 0.6$ <sup>b</sup>

Mean values with different superscript letters in the same column represent significant differences ( $p < 0.05$ ) among the samples according to ANOVA and Tukey's multiple comparison tests

## Chapter V

The crystallinity of PHB and PHB AgNPs was assessed by Wide Angle X-Ray Diffraction (WAXD). Figure 8 shows the diffraction patterns and the crystallinity index calculated after curve fitting of the experimental WAXD patterns. It can be seen that when the silver is incorporated, the intensity of the sharp diffraction peaks between  $2\theta = 13\text{--}25^\circ$  decreases. This indicates a decrease in the crystallinity index, which can be explained by the antinucleant effect of AgNPs discussed above. It is worth mentioning that crystallinity was seen to decrease in the silver loaded sample while a heat of fusion drop was not observed by DSC. Both techniques seldom match one another, since DSC is a dynamic measurement and it is well known that PHAs develop crystallinity during the actual DSC run [34, 38, 39].

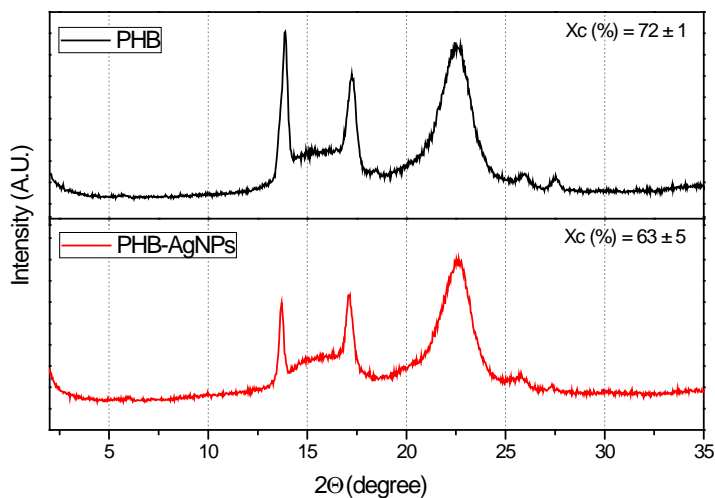


**Figure 8.** WAXD patterns of the pure PHB and the PHB-AgNPs nanocomposites prepared at lab-scale bioreactor. The crystallinity index ( $X_c$ ) was calculated from curve fitting by using the Eq. (2).

### 3.2.4 Antimicrobial activity of PHB-AgNPs films

The antibacterial capacity of the films developed at lab scale reactor was further confirmed (Table 3). As expected, in the PHB-AgNPs films, the bacterial population of *Salmonella enterica* was reduced below detection limit (1.30 log CFU/mL), while the viable cells of *Listeria monocytogenes* showed a reduction of 2.5 log units (99.8%) compared with the control. These results evidenced the great ability of PHB films loaded with very low amounts of silver, to exert a strong antimicrobial activity against food-borne pathogens.

**Table 3.** Antimicrobial activity of the PHB-AgNPs films prepared at lab-scale bioreactor against *S. enterica* and *L. monocytogenes*. The initial inoculum size was 5 log CFU/mL and the detection limit was 1.33 log CFU/mL.

Sample	LOG (CFU/mL)		R	
	<i>S. enterica</i>	<i>L. monocytogenes</i>	<i>S. enterica</i>	<i>L. monocytogenes</i>
PHB	8.11 ± 0.23	5.55 ± 0.05	-	-
PHB-AgNPs	<1.52	3.05 ± 0.05	>6.59	2.50

## 4. Conclusions

.....

A novel process for the biological synthesis of AgNPs and polyhydroxybutyrate (PHB) from the fermentation process with *Cupriavidus necator* was developed and scaled-up to fully automated 10 liters bioreactor. Interestingly, this work demonstrated for the first time, the inherent capacity of *C. necator* to reduce the silver salt and produce AgNPs without the need of adding a reducing agent. It was also observed that the method of AgNPs synthesis (with or without reducing agent) affected the dispersion of the nanoparticles and therefore their antimicrobial

## Chapter V

performance, being the biosynthesized ones the most effective in reducing the bacterial population of *S. enterica* and *L. monocytogenes*. Moreover, the incorporation of AgNPs by means of this method did not cause any detrimental effects on the thermal degradation and the optical properties of the polymer, although a slight reduction in crystallinity was seen. Thus, the procedure here developed allows the production of AgNPs- based polyhydroxyalkanotes, which are suitable for antimicrobial applications.

## 5. Acknowledgements

---

The authors would like to thank to the Active and intelligent fibre-based packaging - innovation and market introduction (ActInPak) COST Action FP1405 for the funding of the Short Term Scientific Mission, to Octavio Cedenilla from the Instituto de Ciencias Agrarias-CSIC for the ICP-OES analysis and to Dr. Luis Cabedo, from Universitat Jaume I for his support with mechanical testing and WAXD analyses. Research leading to these results has received funding from the Comunidad de Madrid (P2013/MIT2807) and the Spanish Ministerio de Economía y Competitividad, (BIO2013-44878-R and AGL2015-63855-C2-1-R). J. L. Castro-Mayorga is supported by the Administrative Department of Science, Technology and Innovation (Colciencias) of the Colombian Government.

## 6. References

---

1. P. E. Association of Plastics Manufacturers, "Plastics-the Facts 2014/2015. An analysis of European plastics production, demand and waste data," Ed.
2. D. Plackett and I. Siró, "Polyhydroxyalkanoates (phas) for food packaging," in *Multifunctional and Nanoreinforced Polymers for Food Packaging*, Ed., pp. 498-526, 2011.
3. A. Steinbüchel and T. Lütke-Eversloh, "Metabolic engineering and pathway construction for biotechnological production of relevant polyhydroxyalkanoates in microorganisms," *Biochemical Engineering Journal*, vol. 16, no. 2, pp. 81-96, 2003.
4. S. Khanna and A. K. Srivastava, "Recent advances in microbial polyhydroxyalkanoates," *Process Biochemistry*, vol. 40, no. 2, pp. 607-619, 2005.
5. P. Suppakul, J. Miltz, K. Sonneveld and S. W. Bigger, "Active Packaging Technologies with an Emphasis on Antimicrobial Packaging and its Applications," *Journal of Food Science*, vol. 68, no. 2, pp. 408-420, 2003.
6. S. Lee, K. Song and B. Lee, "Antibacterial activity of silver nanoparticles prepared by a chemical reduction method," *Korean Journal of Chemical Engineering*, vol. 27, no. 2, pp. 688-692, 2010.
7. J. L. Castro-Mayorga, A. Martínez-Abad, M. J. Fabra, C. Olivera, M. Reis and J. M. Lagarón, "Stabilization of antimicrobial silver nanoparticles by a polyhydroxyalkanoate obtained from mixed bacterial culture," *International Journal of Biological Macromolecules*, vol. 71, pp. 103-110, 2014.
8. R. J. Pinto, S. C. Fernandes, C. S. Freire, P. Sadocco, J. Causio, C. P. Neto and T. Trindade, "Antibacterial activity of optically transparent nanocomposite films based on chitosan or its derivatives and silver nanoparticles," *Carbohydr Res*, vol. 348, pp. 77-83, 2012.
9. M. Valodkar, S. Modi, A. Pal and S. Thakore, "Synthesis and anti-bacterial activity of Cu, Ag and Cu-Ag alloy nanoparticles: A green approach," *Materials Research Bulletin*, vol. 46, no. 3, pp. 384-389, 2011.
10. S. Iravani, H. Korbekandi, S. V. Mirmohammadi and B. Zolfaghari, "Synthesis of silver nanoparticles: chemical, physical and biological methods," *Research in Pharmaceutical Sciences*, vol. 9, no. 6, pp. 385-406, 2014.
11. S. Shivaji, S. Madhu and S. Singh, "Extracellular synthesis of antibacterial silver nanoparticles using psychrophilic bacteria," *Process Biochemistry*, vol. 46, no. 9, pp. 1800-1807, 2011.

## Chapter V

12. G. Rajakumar, A. A. Rahuman, S. M. Roopan, V. G. Khanna, G. Elango, C. Kamaraj, A. A. Zahir and K. Velayutham, "Fungus-mediated biosynthesis and characterization of TiO<sub>2</sub> nanoparticles and their activity against pathogenic bacteria," *Spectrochimica Acta Part A: Molecular and Biomolecular Spectroscopy*, vol. 91, pp. 23-29, 2012.
13. S. Ahmed, M. Ahmad, B. L. Swami and S. Ikram, "A review on plants extract mediated synthesis of silver nanoparticles for antimicrobial applications: A green expertise," *Journal of Advanced Research*, vol. 7, no. 1, pp. 17-28, 2016.
14. V. J. Schacht, L. V. Neumann, S. K. Sandhi, L. Chen, T. Henning, P. J. Klar, K. Theophel, S. Schnell and M. Bunge, "Effects of silver nanoparticles on microbial growth dynamics," *Journal of Applied Microbiology*, vol. 114, no. 1, pp. 25-35, 2013.
15. A. Martínez-Abad, G. Sánchez, J. M. Lagaron and M. J. Ocio, "On the different growth conditions affecting silver antimicrobial efficacy on *Listeria monocytogenes* and *Salmonella enterica*," *International Journal of Food Microbiology*, vol. 158, no. 2, pp. 147-154, 2012.
16. N. Pramanik, A. Bhattacharyya and P. P. Kundu, "Spectroscopic analysis and catalytic application of biopolymer capped silver nanoparticle, an effective antimicrobial agent," *Journal of Applied Polymer Science*, vol. 132, no. 8, 2015.
17. L. S. Serafim, P. C. Lemos, C. Torres, M. A. M. Reis and A. M. Ramos, "The influence of process parameters on the characteristics of polyhydroxyalkanoates produced by mixed cultures," *Macromolecular Bioscience*, vol. 8, no. 4, pp. 355-366, 2008.
18. G. Cárdenas, J. Díaz V, M. F. Meléndrez, C. Cruzat C and A. García Cancino, "Colloidal Cu nanoparticles/chitosan composite film obtained by microwave heating for food package applications," *Polymer Bulletin*, vol. 62, no. 4, pp. 511-524, 2009.
19. A. C. Mottin, E. Ayres, R. L. Oréface and J. J. D. Câmara, "What Changes in Poly(3-Hydroxybutyrate) (PHB) When Processed as Electrospun Nanofibers or Thermo-Compression Molded Film?," *Materials Research*, vol. 19, pp. 57-66, 2016.
20. A. Zielińska, E. Skwarek, A. Zaleska, M. Gazda and J. Hupka, "Preparation of silver nanoparticles with controlled particle size," *Procedia Chemistry*, vol. 1, no. 2, pp. 1560-1566, 2009.
21. J. L. Castro-Mayorga, M. J. Fabra, L. Cabedo and J. M. Lagaron, "On the use of the electrospinning coating technique to produce antimicrobial polyhydroxyalkanoate materials containing in situ-stabilized silver nanoparticles," *Nanomaterials*, vol. 7, no. 1, 2017.
22. J. S. Kim, E. Kuk, K. N. Yu, J.-H. Kim, S. J. Park, H. J. Lee, S. H. Kim, Y. K. Park, Y. H. Park, C.-Y. Hwang, Y.-K. Kim, Y.-S. Lee, D. H. Jeong and M.-H. Cho,

"Antimicrobial effects of silver nanoparticles," *Nanomedicine: Nanotechnology, Biology and Medicine*, vol. 3, no. 1, pp. 95-101, 2007.

23. A. Grigor'Eva, I. Saranina, N. Tikunova, A. Safonov, N. Timoshenko, A. Rebrov and E. Ryabchikova, "Fine mechanisms of the interaction of silver nanoparticles with the cells of *Salmonella typhimurium* and *Staphylococcus aureus*," *BioMetals*, vol. 26, no. 3, pp. 479-488, 2013.

24. G. A. Pankey and L. D. Sabath, "Clinical relevance of bacteriostatic versus bactericidal mechanisms of action in the treatment of gram-positive bacterial infections," *Clinical Infectious Diseases*, vol. 38, no. 6, pp. 864-870, 2004.

25. A. Felgentrager, T. Maisch, A. Spath, J. A. Schroder and W. Baumler, "Singlet oxygen generation in porphyrin-doped polymeric surface coating enables antimicrobial effects on *Staphylococcus aureus*," *Phys Chem Chem Phys*, vol. 16, no. 38, pp. 20598-20607, 2014.

26. L. Martino, M. V. Cruz, A. Scoma, F. Freitas, L. Bertin, M. Scandola and M. A. M. Reis, "Recovery of amorphous polyhydroxybutyrate granules from *Cupriavidus necator* cells grown on used cooking oil," *International Journal of Biological Macromolecules*, vol. 71, pp. 117-123, 2014.

27. V. U. Irorere, S. Bagheriasl, M. Blevins, Kwiecie, #x144, I. , A. Stamboulis and I. Radecka, "Electrospun Fibres of Polyhydroxybutyrate Synthesized by *Ralstonia eutropha* from Different Carbon Sources," *International Journal of Polymer Science*, vol. 2014, pp. 11, 2014.

28. D. Heinrich, M. H. Madkour, M. A. Al-Ghamdi, I. I. Shabbaj and A. Steinbüchel, "Large scale extraction of poly(3-hydroxybutyrate) from *Ralstonia eutropha* H16 using sodium hypochlorite," *AMB Express*, vol. 2, no. 1, 2012.

29. M. V. Cruz, M. C. Sarraguça, F. Freitas, J. A. Lopes and M. A. M. Reis, "Online monitoring of P(3HB) produced from used cooking oil with near-infrared spectroscopy," *Journal of Biotechnology*, vol. 194, pp. 1-9, 2015.

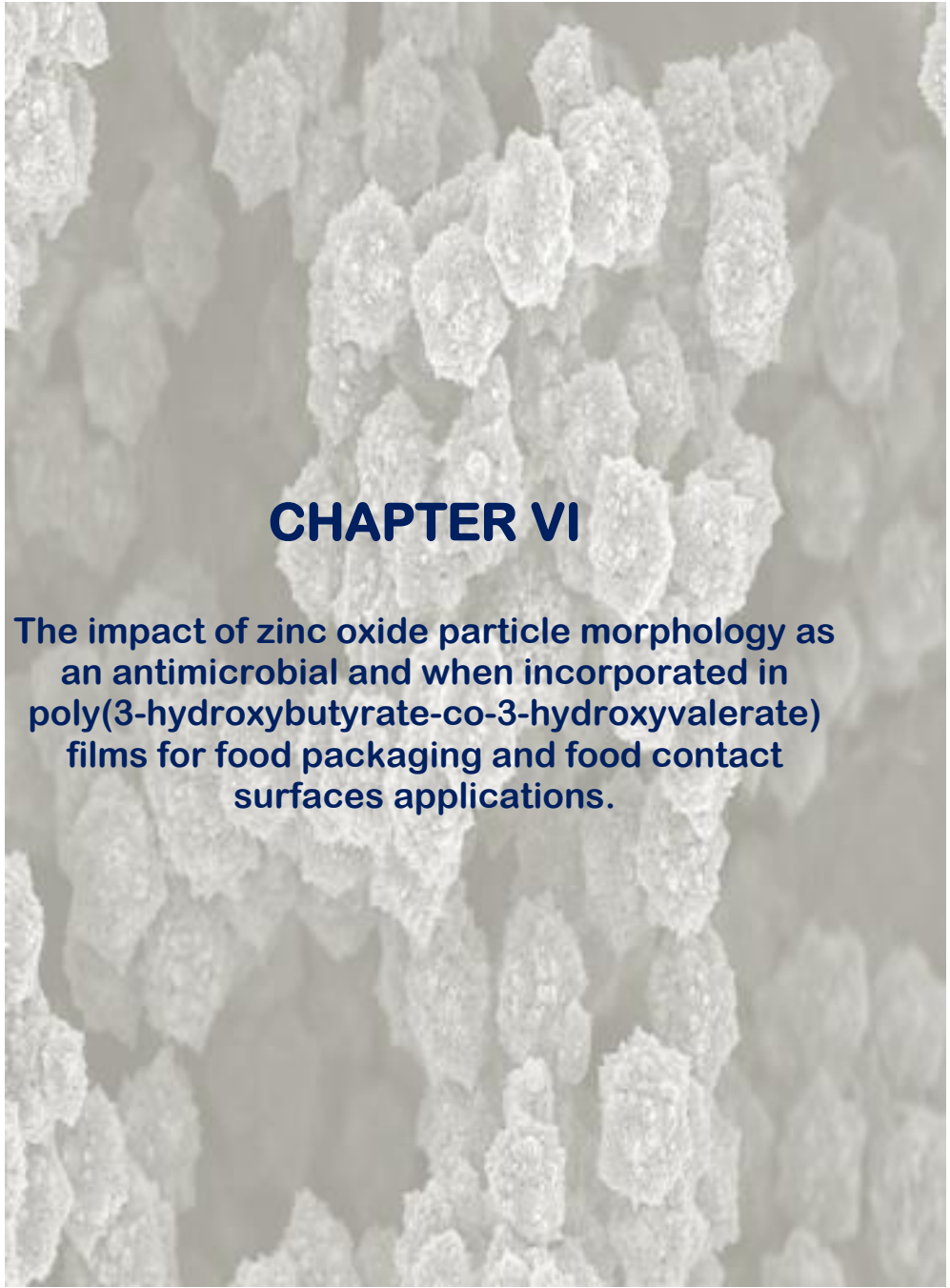
30. C.-C. Chien, L.-J. Wang and W.-R. Lin, "Polyhydroxybutyrate accumulation by a cadmium-resistant strain of *Cupriavidus taiwanensis*," *Journal of the Taiwan Institute of Chemical Engineers*, vol. 45, no. 4, pp. 1164-1169, 2014.

31. M. Kim, K. S. Cho, H. W. Ryu, E. G. Lee and Y. K. Chang, "Recovery of poly(3-hydroxybutyrate) from high cell density culture of *Ralstonia eutropha* by direct addition of sodium dodecyl sulfate," *Biotechnology Letters*, vol. 25, no. 1, pp. 55-59, 2003.

## Chapter V

32. R. A. J. Verlinden, D. J. Hill, M. A. Kenward, C. D. Williams, Z. Piotrowska-Seget and I. K. Radecka, "Production of polyhydroxyalkanoates from waste frying oil by *Cupriavidus necator*," *AMB Express*, vol. 1, no. 1, pp. 1-8, 2011.
33. J. L. Castro-Mayorga, M. J. Fabra, A. M. Pourrahimi, R. T. Olsson and J. M. Lagaron, "The impact of zinc oxide particle morphology as an antimicrobial and when incorporated in poly(3-hydroxybutyrate-co-3-hydroxyvalerate) films for food packaging and food contact surfaces applications," *Food and Bioproducts Processing*, vol. 101, pp. 32-44, 2017.
34. J. L. Castro-Mayorga, M. J. Fabra and J. M. Lagaron, "Stabilized nanosilver based antimicrobial poly(3-hydroxybutyrate-co-3-hydroxyvalerate) nanocomposites of interest in active food packaging," *Innovative Food Science and Emerging Technologies*, vol. 33, pp. 524-533, 2016.
35. M. Min, Y. Shi, H. Ma, H. Huang, J. Shi, X. Chen, Y. Liu and L. Wang, "Polymer-nanoparticle composites composed of poly(3-hydroxybutyrate-co-3-hydroxyvalerate) and coated silver nanoparticles," *Journal of Macromolecular Science, Part B: Physics*, vol. 54, no. 4, pp. 411-423, 2015.
36. H. Yu, B. Sun, D. Zhang, G. Chen, X. Yang and J. Yao, "Reinforcement of biodegradable poly(3-hydroxybutyrate-co-3-hydroxyvalerate) with cellulose nanocrystal/silver nanohybrids as bifunctional nanofillers," *Journal of Materials Chemistry B*, vol. 2, no. 48, pp. 8479-8489, 2014.
37. S. Y. Yeo, W. L. Tan, M. Abu Bakar and J. Ismail, "Silver sulfide/poly(3-hydroxybutyrate) nanocomposites: Thermal stability and kinetic analysis of thermal degradation," *Polymer Degradation and Stability*, vol. 95, no. 8, pp. 1299-1304, 2010.
38. M. Martínez-Sanz, M. Villano, C. Oliveira, M. G. E. Albuquerque, M. Majone, M. Reis, A. Lopez-Rubio and J. M. Lagaron, "Characterization of polyhydroxyalkanoates synthesized from microbial mixed cultures and of their nanobiocomposites with bacterial cellulose nanowhiskers," *New Biotechnology*, vol. 31, no. 4, pp. 364-376, 2014.
39. J. Ambrosio-Martin, M. J. Fabra, A. López-Rubio, G. Gorrasi, A. Sorrentino and J. M. Lagaron, "Assessment of Ball Milling as a Compounding Technique to Develop Nanocomposites of Poly(3-Hydroxybutyrate-co-3-Hydroxyvalerate) and Bacterial Cellulose Nanowhiskers," *Journal of Polymers and the Environment*, vol. 24, no. 3, pp. 241-254, 2016.



The background of the page is a scanning electron microscope (SEM) image showing numerous irregular, porous, and interconnected zinc oxide particles. The particles vary in size and shape, creating a complex, textured surface. The image is in grayscale, with the particles appearing as lighter, more detailed structures against a darker background.

## CHAPTER VI

**The impact of zinc oxide particle morphology as an antimicrobial and when incorporated in poly(3-hydroxybutyrate-co-3-hydroxyvalerate) films for food packaging and food contact surfaces applications.**

J. L. Castro Mayorga, M. J. Fabra, A.M. Pourrahimi, R. Olsson . "The impact of zinc oxide particle morphology as an antimicrobial and when incorporated in Poly(3-hydroxybutyrate-co-3-hydroxyvalerate) films for food packaging and food contact surfaces applications". Food and Bioproducts Processing, vol. 101, pp. 32-44, 2017.



## Abstract

---

In this work, zinc oxide (ZnO) micron and nano sized-particles with different morphologies were synthesized by aqueous precipitation and evaluated as antimicrobial agents against foodborne pathogens. The most effective bactericide system was selected to prepare active poly(3-hydroxybutyrate-co-3-hydroxyvalerate) (PHBV) films by three different methods: (i) direct melt-mixing, (ii) melt-mixing of preincorporated ZnO into PHBV18 (18 mol % valerate content) fiber mats made by electrospinning, and, (iii) as a coating of the annealed electrospun PHBV18/ZnO fiber mats over compression molded PHBV. Results showed that ZnO successfully improved the thermal stability of the PHBV18, being the preincorporation method the most efficient in mitigating the negative impact that the PHBV18 had on the thermal stability, barrier and optical properties of the PHBV films. Similar behavior was found for the coating structure although this film showed effective and prolonged antibacterial activity against *L. monocytogenes*. This study highlights the suitability of the PHBV/ZnO nanostructures for active food packaging and food contact surface applications.

## Keywords

---

ZnO, PHBV, Antimicrobial activity, Electrospinning, Active Packaging, Food contact surfaces.

## 1. Introduction

---

Over the last decades, polymer nanocomposites have become key materials in many nanotechnology applications. In this area, polymers reinforced by metal-based nanoparticles are advanced functional materials which have gained considerable attention specifically for the development of active materials containing metal-based nanoparticles. Active materials of particular interest in for instance food packaging involve components that release or absorb substances, from or into the packaged food, or the surrounding environment, thus extending the shelf life of foods (e.g. inhibiting the growth of pathogenic and spoilage microorganism), preventing and/or indicating the migration of contaminants while maintaining or even improving their nutritional quality and ensuring food safety [1]. Recently, the interest in antimicrobial packaging has been increased considerably owing to their ability to eliminate food borne pathogens and to reduce the risks of various food poisoning outbreaks and illnesses [2]. Inorganic agents, such as  $\text{TiO}_2$ ,  $\text{ZnO}$ ,  $\text{MgO}$  and  $\text{CaO}$  [3-6] in the form of bulk materials or nanoparticles are being applied in antimicrobial applications because they are not only stable under the high temperatures and pressures that may occur during plastic food packaging processing, but they are also generally regarded as safe for human beings and animals relative to organic compounds.

Among the inorganic antimicrobial agents, zinc oxide ( $\text{ZnO}$ ) nanostructures have emerged as very efficient tool to prevent microbial proliferation on food product due to their activity against a wide range of microorganism [7, 8]. The high surface to volume ratio of nanoparticles enhance their antibacterial effect at low concentrations and, additionally, provides exceptional chemical and physical properties as an additive for plastics for the UV-shielding, deodorizing, antiseptic, and so on.

## *Chapter VI*

However, the toxicity mechanism of ZnO particles is still not well understood and that is why the minimum inhibitory concentration (MIC) ranges from several to hundreds of ppm depending on the antimicrobial test conditions. According to this, it has been demonstrated that the chemical properties of the medium used in the antimicrobial test (pH, ionic composition, organic matter or ionic strength) can affect the aggregation, chemical form and surface charge of particles and therefore their antimicrobial performance [9, 10]. Although several studies have been carried out to better understand the antimicrobial activity of ZnO particles against different Gram-positive and Gram negative bacteria, the antibacterial mechanism of ZnO is still a matter of intensive research. Besides the release of  $Zn^{2+}$  ions, several mechanisms about the antimicrobial activity of ZnO has been described in the literature, such as the cell wall damage, the generation of ROS (like superoxide anions, hydroxyl radicals, hydrogen peroxide) as well as the penetration of the cell envelop, among others [11].

On another hand, it is important to highlight that, in contrast to other metals, ZnO is one of the five zinc compounds listed as a Generally Recognized as Safe (GRAS) materials by the US Food and Drug Administration (21CFR182.8991) [12], being most commonly used as supplement in the fortification of cereal-based foods. However, there are only few studies about the use of ZnO nanocomposites as an antimicrobial food packaging additive. So far, ZnO nanoparticles have been mostly added to petroleum-derived polymers such as low density polyethylene (LDPE) [13], polypropylene (PP), polyurethane (PU) or polyethylene (PET) using conventional incorporation methods as melt mixing or solvent casting. Nevertheless, in accordance to Espitia et al (2012) [8], the use of these nanoparticles in biodegradable polymeric matrices, although recent, will be expanded, since the incorporation of ZnO would improve the performance of the materials.

As renewable and biodegradable polymers, the polyhydroxyalkanoates (PHAs) have attracted interest for active packaging application. However, their usage has been limited by drawbacks such as the high cost of production, brittleness, low thermal stability in the molten state [14] as well as their relatively poor barrier properties that could compromise food quality and safety when intended for use in high demanding applications. Regardless of the above, the low barrier performance might convert into a positive aspect when applied for the development of active packaging technologies where controlled release migration is intended.

To the best of our knowledge, in the particular case of polyhydroxyalkanoates (PHA), there are only two works which reported the effect of the ZnO nanoparticles on the physicochemical properties and antimicrobial activity of poly(3-hydroxybutyrate) (PHB) [15] and poly(3-hydroxybutyrate-co-3-hydroxyvalerate) (PHBV) and ZnO composites prepared via solution casting [15]. In another work, Yu et al. (2010) [16] and Naphade and Jog (2012) [17] conducted pioneering research about the structural and optical properties of PHBV/ZnO nanofibers fabricated by the electrospinning technique. Nevertheless, neither the effect that the morphology of ZnO particles has on the antimicrobial properties against foodborne pathogens nor the effect that the incorporation method has on the physicochemical and antimicrobial properties of the PHBV nanocomposites and multilayer structures were reported. Therefore, the present work is focused on the development and characterization of antimicrobial structures of PHBV containing ZnO for active packaging applications. This work reports, for the first time, the effect of size, morphology and crystalline structure of the ZnO particles on their antimicrobial activity against the foodborne pathogens *Salmonella enterica* and *Listeria monocytogenes*. After selecting the more effective antimicrobial system, PHBV/ZnO nanocomposites of commercial PHBV3 (3% mol valerate) and mixed microbial culture derived PHBV18 (18%mol valerate) were prepared by three different methods: (i) direct melt-mixing, (ii) melt-mixing of

## Chapter VI

preincorporated ZnO into PHBV18 (18 mol % valerate) fiber mats made by electrospinning, and, (iii) as a coating of the annealed electrospun PHBV18/ZnO fiber mats over compression molded PHBV. The effect of the incorporation method and the PHBV18 / ZnO addition on the morphological, optical, thermal, mechanical and barrier properties of the resulting active films as well as their influence on the antimicrobial performance were studied in depth throughout this work.

## 2. Materials and methods

---

### 2.1 Materials

Zinc nitrate hexahydrate ( $\text{Zn}(\text{NO}_3)_2 \cdot 6 \text{H}_2\text{O}$ ,  $\geq 98$  wt.%, Sigma Aldrich), zinc acetate dihydrate ( $\text{Zn}(\text{CH}_3\text{COO})_2 \cdot 2 \text{H}_2\text{O}$ ,  $\geq 99$  %, Sigma Aldrich), sodium hydroxide ( $\geq 98$  wt.%, Sigma Aldrich), were used as received. High resistivity Milli-Q water ( $18.2 \text{ M}\Omega \text{ cm}$  at  $25^\circ\text{C}$ ) was used in all the aqueous reactions. PHBV3 (3 mol % valerate content) supplied by Tianan Biopolymer (Ningbo, China) and unpurified PHBV18 (18 mol % valerate ) synthesized from mixed microbial cultures fed with cheese whey, according to the method described by Martinez-Abad *et al.*, 2015 [18], were used as polymer matrix. 2,2,2-Trifluoroethanol (TFE,  $\geq 99$  wt.%, Sigma Aldrich) was used as a solvent for the PHBV18.

### 2.2 Synthesis of ZnO particles

The hexagonal-pyramid (P-ZnO), star (S-ZnO), rod (R-ZnO), and porous ball (B-ZnO) particles were synthesized by aqueous precipitation. ZnO nanoparticles with hexagonal-pyramid morphology were prepared by an aqueous precipitation method described by Pourrahimi *et al.* [19]. A 0.2 M zinc acetate aqueous solution (500 mL) was mixed with a 0.5 M NaOH aqueous solution (500 mL) under vigorous mechanical

stirring at 60 °C. For star and ball morphologies, 0.5 M and 1 M NaOH solution (250 mL) was added, respectively, to 0.067 M zinc nitrate solution (750 mL) at 60°C under vigorous stirring. For rod morphology, a 4 M NaOH solution was added to 0.067 M zinc nitrate solution at 80°C. The reaction time was set to 1h in all cases. The ZnO particles were purified thrice in Milli-Q water under ultrasonication, dried at 80 °C and normal pressure, ground to a fine powder with a pestle and mortar and finally dried at 60 °C and 20 kPa for 2 h.

## **2.3 Development of active PHBV films**

### **2.3.1 Preparation of nanocomposites**

Nanocomposites based on PHBV3 and hexagonal-pyramid ZnO nanoparticles (P-ZnO) were fabricated by two different methods. In the first method, PHBV3 pellet (70 wt.%), unpurified PHBV18 powder (24 wt.%) and the P-ZnO powder (6 wt.%) were directly melt mixing in an internal mixer (Brabender Plastograph, Germany) during 5 min at 60 rpm and 180°C (sample code: PHBVs-D). The second method involved the preincorporation of P-ZnO in PHBV18 electrospun fibers and subsequently the melt blended with PHBV3 pellets at the same mass ratio and processing parameters than the first method (sample code: PHBVs-P). For the PHBV18/ZnO ultrathin fiber mats preparation, polymer solutions contained a total solids content of 10 wt.% was prepared as follow: First, the unpurified PHBV18 at 80 wt.% was dissolved in TFE under magnetic stirring for 4 h at 50°C and cooled down at room temperature. Then, P-ZnO nanoparticles were incorporated at the remaining 20 wt. % and stirred for 12 more hours. Thereafter, the solution was transferred to a 5 mL glass syringes, connected through PTFE tubes to a stainless steel needle (0.9 mm of inner diameter) and processed using a Fluidnatek® LE-10 electrospinning equipment, trademark of the engineering division of Bioinicia S.L. (Valencia, Spain). Processed samples were collected on a stainless-steel plate

## *Chapter VI*

connected to the cathode of the power supply and oriented perpendicular to the syringe. The distance between the needle and the plate was 17 cm and the voltage was maintained in the range 10-12 kV. All experiments were carried out at room temperature under a steady flow-rate of 5 mL/h. After electrospinning, the fiber mats were dried at 60°C under vacuum for 24 h to completely remove the solvent and were subsequently used to prepare the nanocomposites.

The blends obtained by melt mixing were compression molded into films using hot plates hydraulic press (Carver 4122, USA) at 180 °C, 1.8 MPa during 5 min. All materials were oven dried at 60°C for at least 24 hours prior to the film preparation. The thickness of the films was measured with a digital micrometer (Mitutoyo, Spain, ± 0.001 mm) by averaging four measurements on each sample.

Neat PHBV3/PHBV18 blends prepared by melt mixing were used as control for comparative purposes (sample code: PHBVs).

### **2.3.2 Preparation of coating systems**

In a third approach, PHBV3 films were coated with PHBV18/ZnO ultrathin fiber mats produced by means of the electrospinning technique according to the above description (sample code: PHBVs-B). In this case, a post-annealing step was applied to form a continuous film by fiber coalescence. Fiber mats (30 wt%) of ca. 80 µm of thickness were placed onto PHBV3 films and the assembly was put in between hot plates hydraulic press (Carver 4122, USA) at 160 °C during 2 min (without pressing).

## **2.4 Characterization of ZnO particles and active PHBV films**

### **2.4.1 Surface morphology and surface area measurement**

A field emission scanning electron microscope (SEM; Hitachi S-4800) and a transmission electron microscope (TEM; Hitachi HT7700) were used to assess the particle shape and size (diameter) distributions. For the SEM analysis, powder

samples were coated with a thin conductive layer of Pt/Pd (60/40) by a 20 s sputtering using a current of 80 mA in a Cressington 208 HR. The size distribution of the particles was assessed by measuring 250 particles using ImageJ (National Institute of Health, Maryland, USA). For cross-section observations, films were cryofractured by immersion of the sample in liquid nitrogen and sputtered with a gold-palladium mixture under vacuum before their examination. Microanalysis and elemental mapping was conducted from SEM images with an EDAX detector.

The Brunauer–Emmett–Teller (BET) method based on nitrogen adsorption/desorption with a Micromeritics ASAP 2000 at 77 K was used to determine the specific surface area and pore size distribution.

#### 2.4.2 Optical properties

The transparency of the films was determined through the surface reflectance spectra in a spectrophotometer CM-3600d (Minolta Co., Tokyo, Japan) with a 10 mm illuminated sample area. Measurements were taken in triplicate for each sample by using both a white and a black background. Film transparency was evaluated through the internal transmittance ( $T_i$ ) (0–1, theoretical range) by applying the Kubelka–Munk theory for multiple scattering to the reflection data [20]. Internal transmittance ( $T_i$ ) of the films was quantified using eq. (1). In this equation,  $R_0$  is the reflectance of the film on an ideal black background. Parameters  $a$  and  $b$  were calculated by equations (2) and (3), where  $R$  is the reflectance of the sample layer backed by a known reflectance  $R_g$ .

$$T_i = \sqrt{(a - R_0)^2 - b^2} \quad (1)$$

$$a = \frac{1}{2} \left( R + \frac{R_0 - R + R_g}{R_0 R_g} \right) \quad (2)$$

$$b = \sqrt{(a^2 - 1)} \quad (3)$$

## Chapter VI

Moreover, CIE-L\* a\* b\* coordinates (CIE, 1986) were obtained by the infinite reflection spectra of the samples, using D65 illuminant/10 observer. Samples were evaluated per duplicate and three measurements were taken at random locations on each of the studied films.

### 2.4.3 Wide Angle X-Ray Diffraction Analysis

X-ray diffractograms of the powder samples were recorded at room temperature using a PANalytical X'pert Pro MPD diffractometer with a Cu-K $\alpha$  source (wavelength = 1.54178 Å) using a 2 $\theta$  step size of 0.017°.

### 2.4.4 Differential Scanning Calorimetry (DSC)

Thermal properties of PHBV and its nanocomposites with P-ZnO particles were evaluated by DSC using a Perkin-Elmer DSC 8000 thermal analysis system under nitrogen atmosphere. The sample treatment consisted of a first heating step from 0°C to 200°, a subsequent cooling down to -50°C and a second heating step up to 200°C. The heating and cooling rates for the runs were 10°C/min and the typical sample weight was ~3 mg. The first melting endotherm, and the controlled crystallization at 10°C/min from the melt, was analyzed. To ensure reliability of the data obtained, heat flow and temperature were calibrated using indium as a standard. The degree of crystallinity ( $X$ ) was estimated from the corrected enthalpy for total PHBV content in the nanocomposites samples, using the ratio between the enthalpy of the studied material and the enthalpy of a perfect PHBV crystal as expressed by eq. (4), where  $\Delta H_m$  is the melting enthalpy of the studied specimen,  $\Delta H_m^\circ$  is the melting enthalpy of a perfect PHBV crystal (109 J/g [21]) and  $w$  is the weight fraction of the filler. The tests were done, at least, in triplicate.

$$X = \frac{\Delta H_m}{\Delta H_m^\circ (1-w)} \quad (4)$$

#### **2.4.5 Thermogravimetric Analysis (TGA)**

Thermogravimetric analysis (TGA) was performed under nitrogen atmosphere in a Perkin Elmer Thermobalance TGA 7. The samples were heated from 30 °C to 600 °C at a heating rate of 10 °C/min. All tests were carried out in duplicate.

#### **2.4.6 Mechanical properties**

Tensile tests were performed according to ASTM Standard D638 (ASTM 2010) in stamped dumbbell-shaped specimens of the samples. An Instron Testing Machine (Model 4469; Instron Corp., Canton, MA, USA) was used, with a crosshead speed of 10 mm/min, at ambient conditions of typically 24°C and 50% RH. Elastic modulus, tensile strength, and elongation at break were determined from the stress-strain curves, estimated from force–distance data obtained for the different films. At least, three specimens of each film were tensile tested as to obtain statistically meaningful results.

#### **2.4.7 Water Vapour Permeability (WVP)**

Water vapour permeability (WVP) was determined according to the ASTM E96 (ASTM 2011) gravimetric method, using Payne permeability cups (Elcometer SPRL, Hermelle/s Argenteau, Belgium). Cells containing distillate water were placed inside a desiccator at 0% RH and 24°C and the water weight loss through a film area of 0.001 m<sup>2</sup> was monitored. WVP was calculated from the steady-state permeation slopes obtained from the regression analysis of weight loss data over time. All measurements were performed in triplicate.

#### **2.4.8 Oxygen transmission rate (OTR) measurements**

The oxygen permeability coefficient was derived from oxygen transmission rate (OTR) measurements recorded using an Oxygen Permeation Analyzer M8001 (Systech Illinois, UK). Experiments were carried out at 23°C and 80% RH. The samples were

## Chapter VI

previously purged with nitrogen in the humidity equilibrated samples, before exposure to an oxygen flow of 10 mL min<sup>-1</sup>. The exposure area during the test was 5 cm<sup>2</sup> for each sample. In order to obtain the oxygen permeability, film thickness and gas partial pressure were considered in each case. The measurements were done in triplicate.

### 2.5 Antimicrobial activity of ZnO particles and nanocomposites

The frequent foodborne pathogens, *Salmonella enterica* CECT 4300 and *Listeria monocytogenes* CECT 7467 were obtained from the Spanish Type Culture Collection (CECT: Valencia, Spain) and stored in phosphate buffered saline (PBS, Sigma Aldrich) with 10 wt.-% tryptic soy broth (TSB, Conda Laboratories) and 10 wt.-% glycerol at -80°C until needed. For experimental use, the stock culture was maintained by regular subculture to tryptone soy agar (TSA) slants at 4°C and transferred monthly. Previous to each antimicrobial assay, a loopful of bacteria was transferred to 10 mL of TSB and incubated at 37°C overnight and an aliquot was again transferred to TSB and grown at 37°C and 120 rpm to the mid-exponential phase of growth and this cultured was used as inoculum.

Firstly, susceptibility test were performed employing the macro-dilution method described by the Clinical and Laboratory Standard Institute (M26-A). To this end, four 1000 ppm stock suspensions (corresponding to the each of the four different ZnO particle morphologies) were prepared using Milli-Q water as solvent and the nonionic surfactant Tween 80 (20 wt.% respect to ZnO content) in order to facilitate the particles dispersion. Then, 7.5 mL of each ZnO suspensions were added into 2.5 mL TSB medium and subsequently inoculated with a bacterial suspension to achieve an initial inoculum size of ca. 5\*10<sup>5</sup> CFU/mL. The test tubes were incubated at 37°C for 24 h in a shaking bath at 100 rpm and samples were enumerated by conventional plate count on TSA.

Once the more effective ZnO particle was selected and incorporated into PHBV films, the antimicrobial activity of the films against *Listeria monocytogenes* was evaluated following the Japanese Industrial Standard JIS Z 2801. Briefly, a microorganism suspension containing about  $5 \times 10^5$  CFU/mL was inoculated onto the surface of the tested films with a square size of 3 x 3 cm and covered with an inert piece of Low-Density Polyethylene (LDPE) of 2.5 x 2.5 cm and 80  $\mu$ m of thickness. Then the samples were introduced into-Petri dishes and incubated at 24°C and at a relative humidity of at least 95% for 24 h. After the incubation time, the bacteria were recovered and enumerated by conventional plate count. The PHBV films (without ZnO) were used as a negative control. The value of the antimicrobial activity (R) was calculated by determining  $\log_{10} (N_0/N_t)$ , where  $N_0$  is the average of the number of viable cells of bacteria on the untreated test piece after 24 h and  $N_t$  is the average of the number of viable cells of bacteria on the antimicrobial test piece after 24 h. Three replicate experiments were performed for each sample.

The antimicrobial activity of the active PHBV films was determined as described above, both in freshly made films (0 washes) and after successive washes (5, 10 and 15 washes). The films were completely immersed in 5 mL of sterilized Milli-Q water during time intervals of 5 minutes and then inoculated in order to study the effect of washing on the availability of zinc in each methodology of incorporation (direct, preincorporation and coating structure).

The morphological changes in *L. monocytogenes* after 24 h exposure to 750 ppm of P-ZnO were further examined by TEM. To this purpose, untreated and P-ZnO treated bacteria were fixed, dehydrated and embedded into LR-White resin, following which were cut with an ultramicrotome (Leica UC6) and positively stained with uranylacetate and lead citrate. A Jeol 1010 microscope (Hitachi) equipped with a digital Bioscan (Gatan) image acquisition system at an accelerating voltage of 80 kV was used for the observation.

## **2.6 Determination of zinc content**

The estimation of Zn content in the washing water from successive washes was carried out by inductively coupled plasma- optical emission spectroscopy (ICP-OES, Perkin-Elmer, USA) using a zinc standard solution (traceable to SRM from NIST,  $\text{Zn}(\text{NO}_3)_2$  in  $\text{HNO}_3$  2-3 % 1000 mg/L Zn Certipur®, Merck, Germany) for calibration. All measurements were done, in triplicate.

## **2.7 Statistical analysis**

The statistical analysis of physico-chemical and antimicrobial data was carried out by means of StatGraphics Plus version 5.1 (Statistical Graphics Corp.) through the analysis of variance (ANOVA). Tukey's Honestly Significant Difference (HSD) was used at the 95% confidence level for multiple comparison tests.

# **3. Results and discussion**

---

## **3.1 Morphology of ZnO particles**

Fig. 1 presents the scanning electron micrographs of ZnO particles together with the crystal model of different planar terminations. The 25 nm acetate derived hexagonal-pyramid nanoparticles (P-ZnO) had surfaces (Fig. 1a) consisting of basal planes of zinc terminated (001) and zinc enriched {101} prismatic planes [19, 22], see Fig 1b. The particles have ca. 74 % of its surfaces terminated by zinc and the rest oxygen, considering the representation of the specific atoms in the prismatic crystal planes, which had a specific surface area of  $34 \text{ m}^2\text{g}^{-1}$  [23]

On the self-assembly of the prisms to star-shaped particles (Fig. 1c), which occurred with the use of a different zinc salt precursor (to a nitrate salt), not only the

specific surface area decreased to  $14 \text{ m}^2\text{g}^{-1}$ , [23] but also the percentage of zinc termination since the assembly of the larger particles relied primarily on merging the 100% zinc enriched basal planes along c-axis during synthesis [19] (Fig. 1d). The surface of star-shaped particles were therefore terminated by both zinc and oxygen atoms and the fraction of zinc representation decreased to 67% of the measured  $14 \text{ m}^2\text{g}^{-1}$ . A large portion of this surface was however embedded inside the porous star-shaped particles (Fig. 1c and d), since the specific surface area of  $2 \mu\text{m}$  particles (Fig 1c) can only be expected to be within the range of  $0.4\text{-}0.6 \text{ m}^2\text{g}^{-1}$ , considering the diameters of the entire particles. This was further confirmed by nitrogen sorption experiments (BET), which showed an average pore size of  $3.5 \text{ nm}$  for the star-shaped particles.

Fig. 1e and f show the scanning electron micrograph of hexagonal rod ZnO particles (average length:  $1 \mu\text{m}$ ) with ca. 20 in aspect ratio, obtained by a modified zinc nitrate precipitation. The high aspect ratio rod particles (Fig. 1f) exhibits dominantly  $\{100\}$  crystal planes parallel to c-axis;  $(100)$  and  $(010)$  faces were terminated with zinc atoms, however,  $(\bar{1}\bar{1}0)$  face was terminated with both zinc and oxygen atoms [22] resulting in a total zinc termination of 83% of a calculated total surface area of  $14 \text{ m}^2 \text{ g}^{-1}$ .

The more complex hierarchical microstructure of the ball-like morphology ZnO particles that rely on the assembly of  $25 \text{ nm}$  thick interleaving sheets with dominant crystal plane of  $(\bar{2}\bar{1}0)$  [24] are shown in Fig. 1g. The interconnected sheets are characterized by 33% zinc occupancy in their lattice (Fig. 1h), which was present on a measured surface area (BET) of  $17 \text{ m}^2\text{g}^{-1}$ . The nature of the interconnected surfaces inside the particles are, however, presently unknown.

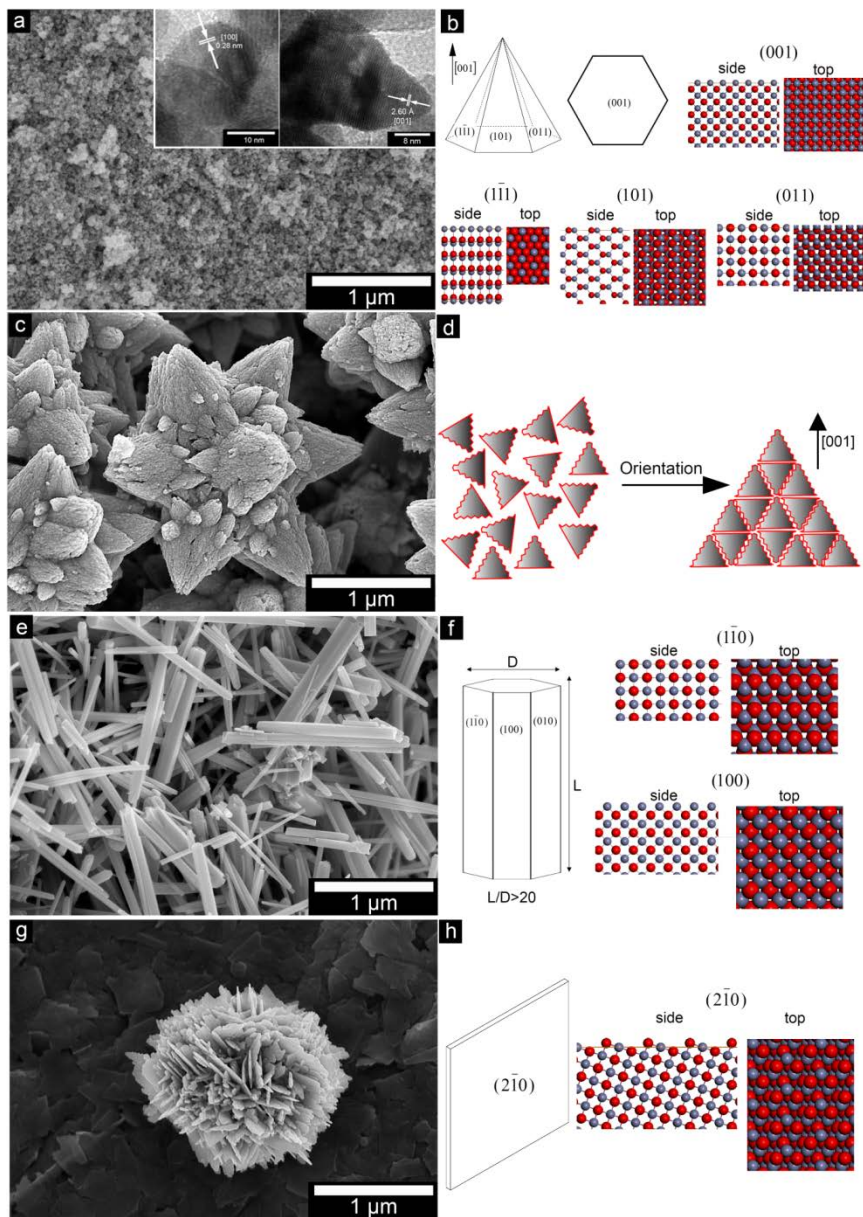


**Figure 1.** SEM micrographs of ZnO particles and crystal model of different planar terminations. (a-b) P-ZnO, (c-d) S-Zn, (e-f) R-ZnO, (g-h) B-ZnO.

X-ray diffractograms of the ZnO particles all showed a single phase ZnO with clear diffraction peaks corresponding to the lattice planes in the wurzite with a hexagonal cell structure, and crystallographic parameters of  $a = b = 3.254 \text{ \AA}$ ,  $c = 5.210 \text{ \AA}$ ,  $\alpha = \beta = 90^\circ$ ;  $\gamma = 120^\circ$  (inorganic crystal structure database; collection code # 067849). The absence of any amorphous halo and the sharpness of the peaks characteristic of ZnO indicated high purity for all the particles (data not reported).

### 3.2 Antimicrobial activity of ZnO particles

In the first part of this work, the antimicrobial activity of ZnO particles against two of the most common pathogenic bacteria (*Salmonella enterica* and *Listeria monocytogenes*) involved in foodborne outbreaks was evaluated. Figure 2 reflects the viability of the tested bacteria when incubated in TSB medium. While control samples without ZnO particles allow an increase of more than 2.5 log units of the bacterial population after 24h, in all tested tubes containing ZnO particles, both bacteria were unable to grow or even decreased in number. An inhibition of growth during 24 h incubation (defined as bacteriostatic effect) occurred in *S. enterica* and *L. monocytogenes* tests for S-ZnO, R-ZnO and B-ZnO particles while a noticeable bactericidal effect (with a reduction of >6 log units) against *L. monocytogenes* was achieved for 750 ppm of P-ZnO. The differences in the antimicrobial performance of the four ZnO morphologies could be related, on the one hand, to a larger particle effective surface area which enhanced the surface reactivity, and on the other hand, to the different configuration of the zinc ions in the lattice of the crystals [10]. In the present work, the antibacterial activity of ZnO seemed to improve when the particle size decreased to the nanosize, which means that the surface area increased being the P-ZnO nanoparticles which resulted in the highest antibacterial effect. As commented above, the toxicity mechanism of ZnO particles is currently controversial and although

## Chapter VI

several studies have been carried out to better understand the antimicrobial activity of ZnO particles against different Gram-positive and Gram negative bacteria, the antibacterial mechanism of ZnO is still a matter of intensive research. In general, it can be assumed that the different behavior of the two types of bacteria used in the present work could be also ascribed to the different structural and chemical composition of the cell surfaces of Gram-negative and Gram-positive bacteria. As an example, Figure 3 shows representative images of the cell damage caused by P-ZnO on *L. monocytogenes* after 24 h of incubation. As can be seen in Figure 3a, untreated bacteria had an intact cell structure while no integral cells were observed in the P-ZnO sample (*cf* Fig 3b). In the treated cells, an electron-light region appeared in the cytoplasm (indicated by asterisk in Fig 3b) which was not present in the untreated cells. These differences suggest an impact in the lumping and lysis of the cytoplasm cell. Similar effects of ZnO nanoparticles on *E. coli* and *B. subtilis* were previously shown by Brayner et al. [25] and by Vidic et al. [26], respectively.

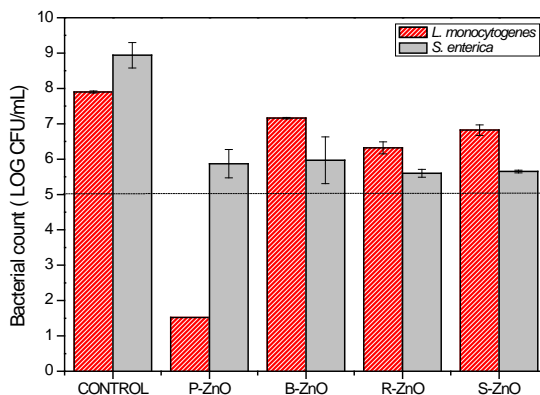


**Figure 2.** Antimicrobial activity of ZnO particles against *Salmonella enterica* and *Listeria monocytogenes* after 24h exposure. The dashed line depicts the initial inoculum size of 5 log CFU/mL. The detection limit was 33 CFU/mL.

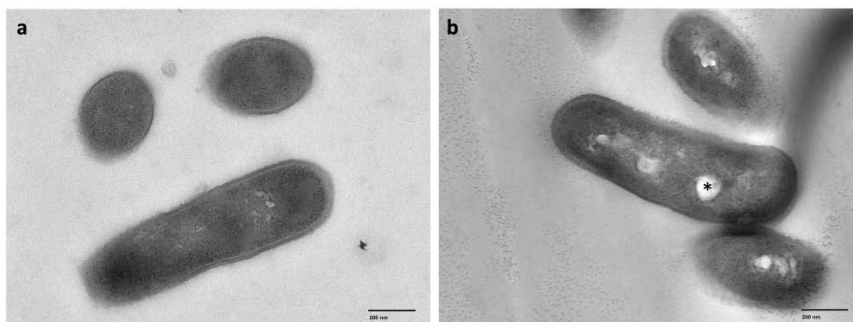


**Figure 3.** TEM images of *Listeria monocytogenes* after 24 h of incubation. (a) Untreated cells, (b) Cells treated with 750 ppm of P-ZnO nanoparticles. The electron-light region indicated by asterisk in Fig 4b shows the morphological changes in the cytoplasm of treated cells.

### 3.3 Development of active PHBV films

Once the antibacterial performance of each type of ZnO particles was determined, P-ZnO nanoparticles were selected as the most effective antimicrobial morphology to prepare antimicrobial PHBV/P-ZnO films in three different forms described above: (i) direct melt-mixing, (ii) melt-mixing of preincorporated ZnO into PHBV18 (18 mol % valerate) fiber mats made by electrospinning, and, (iii) as a coating of the annealed electrospun PHBV18/ZnO fiber mats over compression molded PHBV. The physicochemical and antimicrobial properties of the resulting films are presented below.

#### 3.3.1 Morphology and optical properties

In order to characterize the morphology of the PHBV18 composite structures obtained by electrospinning, the fibers mat was observed by SEM. Figure 4 shows the surface morphology of the electrospun PHBV18 without and with P-ZnO nanoparticles (*cf.* Fig 4a and 4b, respectively), where no substantial differences were observed between the samples. The presence of ZnO in the electrospun mat was confirmed by EDAX analysis (*cf.* Fig 4c) and the dispersion of P-ZnO nanoparticles

## Chapter VI

within the fibers was assessed by SEM-mapping. Figure 4b and its inset show a representative and detailed picture of the PHBV18 fibers containing 6 wt.-% P-ZnO.

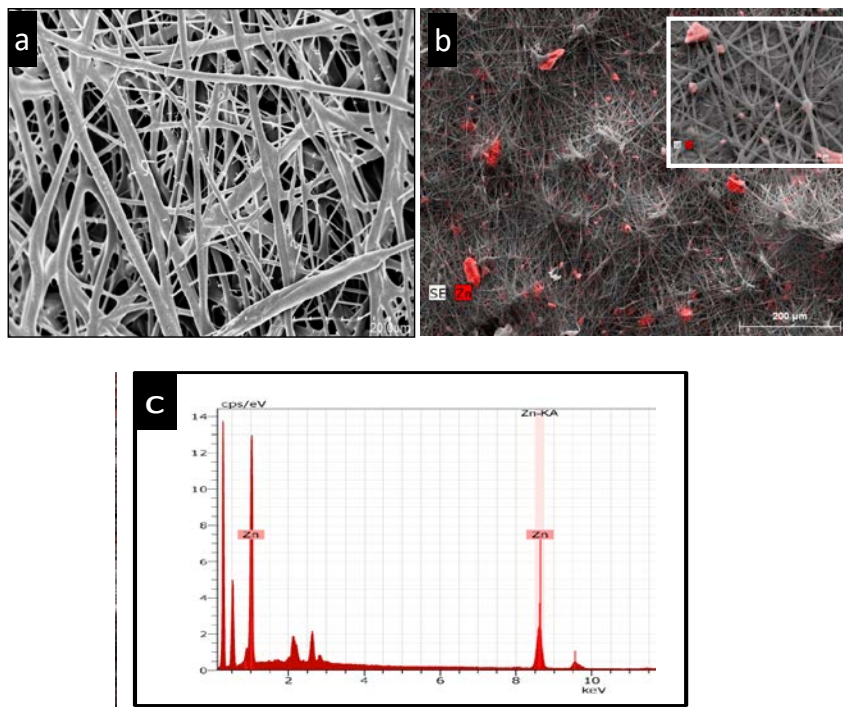


**Figure 4.** SEM micrographs of electrospun PHBV18: (a) PHBV18 without ZnO. (b) PHBV18 with P-ZnO incorporated by electrospinning. An elemental map analysis for zinc was carried out using EDAX on SEM micrographs, the results of mapping are shown in red. The inset shows a detailed image of fibres containing P-ZnO. (c) EDAX spectra of PHBVs and ZnO-based film.

Although some agglomerates can be discerned from the SEM micrographs, most of the P-ZnO nanoparticles are thought to be properly dispersed and distributed within the PHBV18 fibers as it will be later confirmed by examination of the morphology of the PHBVs/P-ZnO nanocomposites. It is worth noting that for the nanocomposites prepared by direct melt mixing, big agglomerates can be clearly discerned in both visual examination (*cf.* Fig 5a) and SEM micrographs (*cf.* Fig 5b),

hence indicating that this method led to a poorer dispersion of the nanoparticles within the biopolymer matrix. However, when nanocomposites were prepared by means of the preincorporation method (*cf.* Fig 5c), better contact transparency was observed, in turn suggesting a better dispersion of the P-ZnO into the PHBV's matrices. This was further suggested by SEM micrographs (*cf.* 5d) where ZnO particles were found to be highly dispersed into the polymeric matrix. Concerning the coating system, it can be easily distinguished a laminate-like structure in which the PHBV18/P-Zn-O fibrous layer (*cf.* Fig. 5e and 5f) formed a continuous coating of ca. 80  $\mu\text{m}$  of thickness onto the top side of the PHBV3 layer, showing good adhesion between them. It is also worth highlighting that although some P-ZnO aggregates could be still detected in the PHBV's-P and PHBV-C films, they were smaller than those observed in the PHBV's-D films. The optical images support the best dispersion and distribution of the ZnO nanoparticles in the PHBV's-P and PHBV-C systems (see contact transparency images, Figure 5).

The transparency of the films is a highly desirable property in many applications, especially in food packaging where the visual appeal of foods results in a key factor for the consumer demand and market trends. According to Hutchings (1999), transparency is the best optical property to assess the appearance of the films and it has been quantified by means of the internal transmittance ( $T_i$ ) spectra. In general, high  $T_i$  values are related to more homogeneous and transparent films, while a decrease in these values implies films with greater opacity and thus more heterogeneous matrices. As observed, all tested films presented a similar pattern over the wavelength considered (*cf.* Fig. 6), although  $T_i$  values of the nanocomposite and coating films were significantly lower (less transparent) than the neat PHBV3 matrix. This decrease in transparency is of course associated to the presence of several compounds with different refractive index such as PHBV18, ZnO nanoparticles and agglomerates.

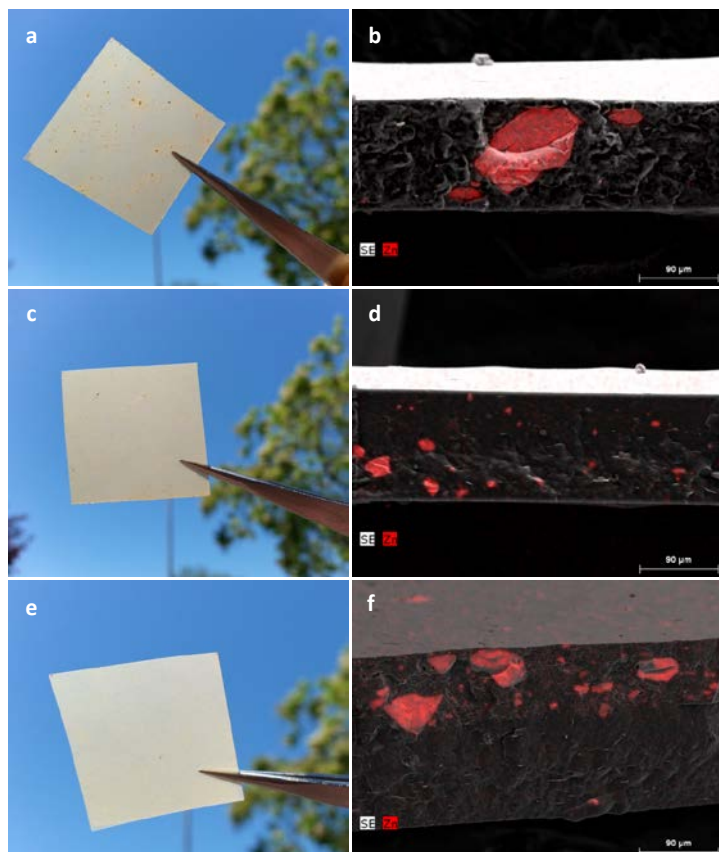


**Figure 5.** Contact transparency pictures of PHBV<sub>s</sub>-ZnO films (right column) and their SEM micrographs (left column) showing the elemental mapping for zinc (in red). (a-b) PHBV<sub>s</sub>-D, (c,d) PHBV<sub>s</sub>-P, (e) PHBV<sub>s</sub>-C.

As can be deduced from Figure 6, the film's surface morphology and thus the type of film (nanocomposites vs. coating form), played a major role on the transparency of the films than the presence of some agglomerates of ZnO nanoparticles. In fact, when nanocomposites prepared by both direct and preincorporation methods were compared, no significant differences were observed between them. However, Ti values of the coating films (PHBV<sub>s</sub>-C) were significantly lower, fact that could be

ascribed to an increase in the light scattering caused by the PHBV18/P-ZnO fibrous coating. As opposed to this, in the nanocomposite films a greater confinement of the PHBV18/P-ZnO into the homogeneous PHBV3 matrix was produced during the melt compounding and thus the transparency of the nanocomposites were affected to a lesser extent.

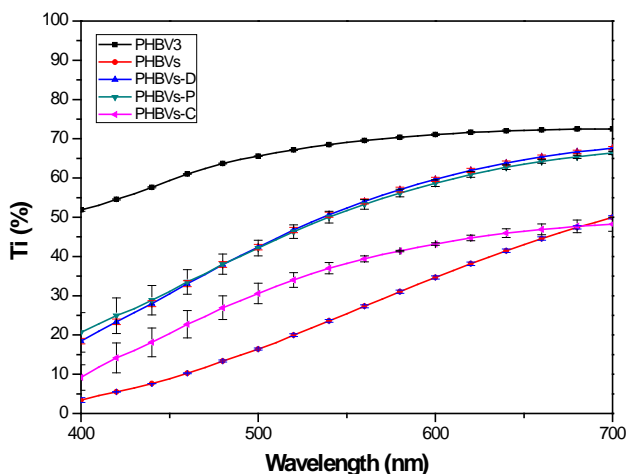


**Figure 6.** Spectral distribution of internal transmittance (Ti) of PHBV3, PHBVs and their ZnO nanocomposites.

From the reflectance spectra of an infinite thickness film, lightness ( $L^*$ ), hue ( $h_{ab}^*$ ) and Chroma ( $C_{ab}^*$ ) were obtained (Table 1). As deduced from Table 1 and contact transparency images (Figure 6), the first thing to highlight is that PHBV18 degraded during the melt-mixing process and the appearance of the heat pressed PHBVs films (without ZnO nanoparticles) were darker (lower  $L^*$ ) and less vivid (lower  $C_{ab}^*$ ) with a brown hue indicating rather deficient optical properties. This was supported by the highest total difference values ( $\Delta E$ ) obtained for these films when they were compared to the neat PHBV3 film. The thermal instability has been ascribed to impurities from the fermentation process (close to 30 wt. % . [27]) which are thought to undergo

## Chapter VI

Maillard reactions between amide groups and residual reducing sugars during the melt mixing process. Interestingly, the addition of ZnO improved the appearance of the developed nanocomposite and coating films and the negative effect of the unpurified PHBV18 was mitigated, as it can be easily observed in Figure 7.  $L^*$  and  $h_{ab}^*$  decreased whereas  $C_{ab}^*$  values increased for nanocomposite and coating films containing ZnO nanoparticles as compared to the neat PHBV3 film which means that these samples were slightly darker, less vivid and with a yellow-brown color but these changes were significantly lower than those obtained for PHBVs film (without ZnO nanoparticles). Accordingly, the PHBVs-D and PHBVs-P nanocomposites displayed a very similar coloration pattern between them, while PHBVs-C presented the lowest color difference ( $\Delta E$ ) as compared to the neat PHBV3. These results suggest that well dispersed and distributed ZnO nanoparticles may exert a stabilizing role for the unpurified PHBV18 during the melt mixing.

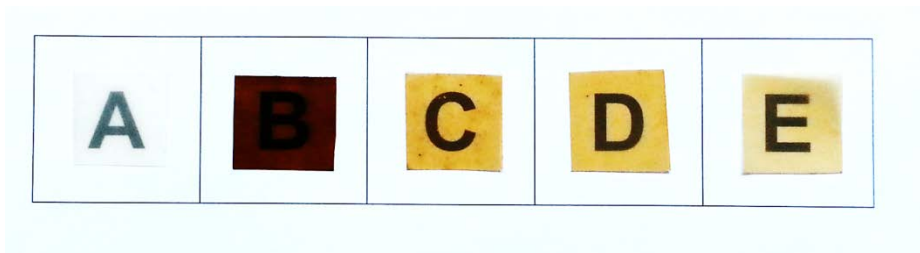


**Figure 7.** Detailed contact transparency pictures of PHBV3 (a), PHBVs (b) and their ZnO nanocomposites and coating structure: (c) PHBVs-D, (d) PHBVs-P, (e) PHBVs-C.

**Table 1.** Colour parameters of the neat PHBV3, PHBVs and their ZnO-based nanocomposites

Sample	L*	a*	b*	C <sub>ab</sub> *	h <sub>ab</sub> *	ΔE
PHBV3	82.3 ± 0.4 <sup>a</sup>	1.4 ± 0.1 <sup>a</sup>	17.7 ± 0.0 <sup>a</sup>	17.8 ± 0.1 <sup>a</sup>	85.5 ± 0.7 <sup>a</sup>	-
PHBVs	32.7 ± 0.5 <sup>b</sup>	6.7 ± 0.1 <sup>b</sup>	10.2 ± 0.1 <sup>b</sup>	12.2 ± 0.5 <sup>b</sup>	57.0 ± 1.4 <sup>b</sup>	50.5 ± 0.9 <sup>a</sup>
PHBVs-D	56.9 ± 0.4 <sup>c</sup>	9.0 ± 0.1 <sup>c</sup>	25.3 ± 0.1 <sup>c</sup>	26.9 ± 0.1 <sup>c</sup>	70.0 ± 0.0 <sup>c</sup>	27.7 ± 0.8 <sup>b</sup>
PHBVs-P	58.4 ± 0.2 <sup>c</sup>	8.5 ± 0.1 <sup>c</sup>	25.1 ± 0.4 <sup>c</sup>	26.5 ± 0.4 <sup>c</sup>	71.0 ± 0.0 <sup>c</sup>	26.1 ± 0.4 <sup>b</sup>
PHBVs-C	72.5 ± 2.4 <sup>d</sup>	3.8 ± 0.6 <sup>d</sup>	24.7 ± 2.8 <sup>c</sup>	24.9 ± 2.8 <sup>c</sup>	79.0 ± 2.8 <sup>d</sup>	12.3 ± 3.3 <sup>c</sup>

Mean values ± standard deviation. Mean values with different letters in the same column represent significant differences ( $p < 0.05$ ) among the samples according to ANOVA and Tukey's multiple comparison tests.

### 3.3.2 Thermal properties

Thermal properties of the PHBV and its active films were investigated by DSC analyses. The first heating DSC thermogram is illustrated in Figures 8 and the corresponding data are gathered in Table 2. The neat PHBV3 and PHBVs mixture presented a two-step melting behavior. The appearance of multiple melting peaks of PHBV copolymer has been previously ascribed to an effect of the melting-recrystallization process occurring during subsequent heating [27, 28], which means that more defective or smaller crystals are able to recrystallize after melting forming more perfect crystals which subsequently melt at higher temperatures. This statement agreed with the differences observed between the PHBV3 and PHBVs mixtures.

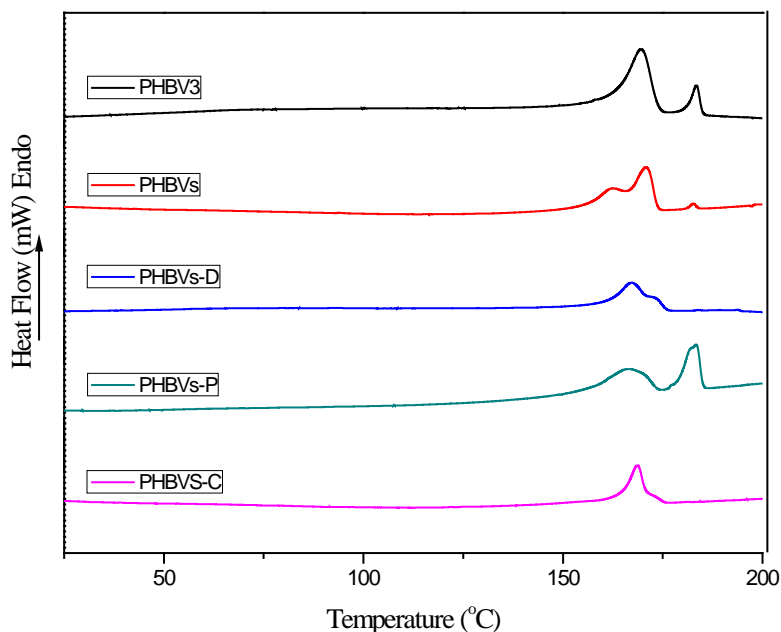


**Figure 8.** DSC thermograms of first heating run of the neat PHBV3, PHBVs and their ZnO-based nanocomposites.

The presence of PHBV18 in the mixture reduced the melting enthalpy and most likely impairs crystallinity development, since there is a sharp reduction in the second melting peak and a small shoulder in the first melting peak. The PHBV18 hinders the crystallization of the PHBV3 polymer matrix probably due to both the higher hydroxyvalerate content [29] and the presence of impurities as previously reported by Martinez-Abad et al. [18] and Castro Mayorga et al. [27].

The incorporation of ZnO nanoparticles by direct melt mixing (PHBVs-D) also changes the melting behavior of the PHBVs matrix in a way that suggests that ZnO particles hinder the recrystallization during heating. A similar melting pattern was observed between nanocomposites prepared by means of the preincorporation method and the neat PHBV3 films suggesting that this methodology does not alter the

melting behavior of the PHBV3 matrix. However, it was found that the estimated crystallinity degree of the nanocomposites decreased most likely as a result of the lower crystallinity brought in by the PHBV18 polymer and also a potential antinucleation of the blending systems involved [18].

The incorporation of ZnO nanoparticles as a coating (PHBVs-C) led to a drop in the melting enthalpy with a subsequent decrease in the crystallinity degree (*cf.* Table 2) attributed to the lower crystallinity brought in by the PHBV18. Regarding the crystallization process, a decrease in the crystallization temperature ( $T_c$ ) for the PHBVs composites as compared to PHBV3 matrix was registered in agreement with previous results reported by Martínez-Abad et al., 2015 [18], supporting the antinucleation effect discussed above. On the other hand, for the coating the crystallization temperature was seen to increase but very slightly.

The thermal stability of the neat PHBV3, PHBVs and their nanocomposites and coating films was evaluated through TGA. Table 3 and Figure 9 show the TGA parameters of the tested films and the P-ZnO nanoparticles, measured under nitrogen conditions. The ZnO nanoparticles display a small weight loss (~9.4%) below 400°C likely ascribed to the elimination of physically and chemically adsorbed water on their surface. In regard to the films, all of them exhibited a similar thermal decomposition process, with a single degradation stage that started at around ~260°C. However, some differences were observed at the temperature of maximum rate of degradation ( $T_d$ ) of PHBVs containing ZnO nanoparticles, which showed lower temperature than that of the pristine PHBV3. This could be attributed to the high heat conductivity and catalytic properties of ZnO nanoparticles. Furthermore, the residual material of P-ZnO composites at 400°C (R400) was around 15% while its amount was approximately 5% for neat PHBV3 and PHBVs. Thus the char residue could be related both to the ZnO content (*ca.* 6%) and to undecomposed material from PHBV complexed with ZnO. This latter subject is in accordance with the positive effect of zinc oxide on optical

## Chapter VI

properties showing reduced early thermal degradation in the films. In any case, TGA analyses do not match the environmental conditions occurring during melt mixing and therefore the colour changes observed after melting at 180°C, especially those presented by the PHBV3/PHBV18 blend, must involve small degradation steps that take place without significant mass changes at the processing temperatures which are not necessarily detected by the TGA measurements.

**Table 2.** DSC melting point ( $T_m$ ), melting enthalpy ( $\Delta H_m$ ), crystallization temperature ( $T_c$ ) and degree of crystallinity ( $X$ ) of the neat PHBV3, PHBVs and their ZnO-based composites.

Sample	$T_{m1}$ (°C)	$T_{m2}$ (°C)	$T_c$ (°C)	$\Delta H_m$ (J/g PHBVs)	$X$ (%)
PHBV3	168.7 ± 1.0 <sup>abc</sup>	181.8 ± 0.2 <sup>a</sup>	114.7 ± 0.0 <sup>a</sup>	72 ± 1 <sup>a</sup>	66 ± 1 <sup>a</sup>
PHBVs	170.9 ± 0.1 <sup>c</sup>	182.6 ± 0.1 <sup>ab</sup>	101.0 ± 0.3 <sup>b</sup>	68 ± 2 <sup>a</sup>	63 ± 2 <sup>a</sup>
PHBVs-D	166.9 ± 0.5 <sup>ab</sup>	-	112.1 ± 0.2 <sup>c</sup>	56 ± 3 <sup>b</sup>	50 ± 2 <sup>b</sup>
PHBVs-P	166.5 ± 0.4 <sup>a</sup>	183.8 ± 0.7 <sup>b</sup>	111.6 ± 0.3 <sup>c</sup>	58 ± 1 <sup>b</sup>	51 ± 1 <sup>b</sup>
PHBVs-C	169.0 ± 0.5 <sup>bc</sup>	-	118.0 ± 0.6 <sup>d</sup>	39 ± 1 <sup>c</sup>	35 ± 1 <sup>c</sup>

Mean values ± standard deviation. Mean values with different letters in the same column represent significant differences ( $p < 0.05$ ) among the samples according to ANOVA and Tukey's multiple comparison tests

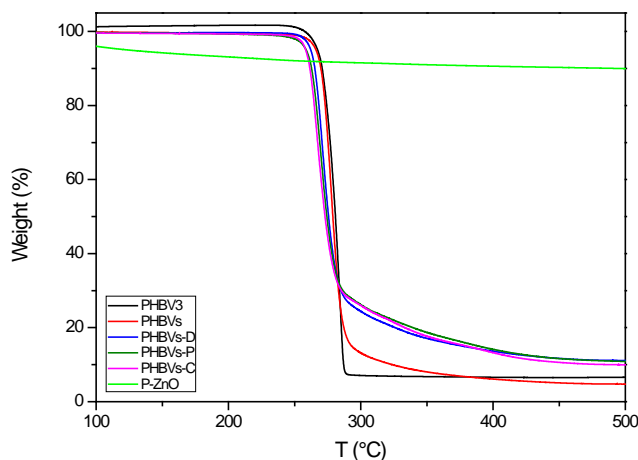


**Figure 9.** TGA curves of the neat PHBV3, PHBVs and their ZnO-based nanocomposites

**Table 3.** TGA decomposition temperatures ( $T_d$ ) and the corresponding peak onset values ( $T_{\text{onset}}$ ) and the residue at 400 °C ( $R_{400}$ ) for the neat PHBV3, PHBVs and their ZnO-based nanocomposites.

Sample	$T_{\text{onset}}$ (°C)	$T_d$ (°C)	$R_{400}$
PHBV3	269.0 ± 8.9 <sup>a</sup>	290.8 ± 3.8 <sup>a</sup>	5.1 ± 2.1 <sup>a</sup>
PHBVs	270.1 ± 7.8 <sup>a</sup>	283.1 ± 6.5 <sup>ab</sup>	5.3 ± 1.1 <sup>a</sup>
PHBVs-D	256.9 ± 2.0 <sup>a</sup>	271.3 ± 0.9 <sup>b</sup>	15.9 ± 3.2 <sup>b</sup>
PHBVs-P	256.6 ± 2.1 <sup>a</sup>	270.3 ± 0.4 <sup>b</sup>	14.8 ± 0.9 <sup>b</sup>
PHBVs-C	251.8 ± 0.2 <sup>a</sup>	270.8 ± 3.7 <sup>b</sup>	13.3 ± 0.1 <sup>b</sup>

Mean values ± standard deviation. Mean values with different letters in the same Column represent significant differences ( $p < 0.05$ ) among the samples according to ANOVA and Tukey's multiple comparison tests.

### 3.3.3 Mass transport properties

Water vapour permeability and oxygen permeability are important properties which can determine the potential application of a packaging material in food preservation. Table 4 gathers the results for the neat PHBV3, the PHBVs mixture and nanocomposites/coating structures containing ZnO nanoparticles. The first observation to highlight is that, although the water and oxygen permeability values increase was very small (not statistically significant), a higher permeability increase was clearly expected from simple application of the rule of mixture, since the blending element (PHBV18) has higher water and oxygen permeability values. This inconsistency between the expected and the experimental results suggests that the blending element when confined into the more hydrophobic matrix is restricted to swell [30]. As can be seen from Table 4, the incorporation of ZnO nanoparticles into PHBVs matrix led to a significant barrier decrease which can be mainly attributed to the decreased crystallinity as well as to the higher hydrophilic character of the ZnO as compared to the neat PHBV[31].

## Chapter VI

**Table 4.** Water vapor permeability measured at 100% RH and oxygen permeability measured at 80% RH for PHBV3, PHBVs their ZnO-based composites. Values between brackets represent calculations obtained by applying the simple rule of mixtures for the PHBV3/PHBV18 composites containing 24% of PHBV18.

Sample	WVP (Kg m/ Pa. s. m <sup>2</sup> )	PO <sub>2</sub> (m <sup>3</sup> m/ m <sup>2</sup> . s. Pa) 80% RH
PHBV3	1.10 ± 0.02 e-15 <sup>a</sup>	2.06 ± 0.09 e-19 <sup>a</sup>
PHBV <sub>s</sub>	2.50 ± 0.06 e-15 <sup>a</sup> (5.61 e-15)	3.09 ± 0.01 e-19 <sup>a</sup> (3.68 e-19)
PHBV <sub>s</sub> -D	1.13 ± 0.07 e-14 <sup>ab</sup>	1.34 ± 0.26 e-15 <sup>d</sup>
PHBV <sub>s</sub> -P	1.94 ± 0.01 e-15 <sup>a</sup>	1.80 ± 0.07 e-18 <sup>e</sup>
PHBV <sub>s</sub> -C	3.17 ± 0.73 e-14 <sup>c</sup>	2.85 ± 0.05 e-18 <sup>f</sup>
PHBV18*	1.88 ± 0.03 e-14 <sup>b</sup>	8.43 ± 0.44 e-19 <sup>b</sup>

Mean values ± standard deviation. Mean values with different letters in the same column represent significant differences ( $p < 0.05$ ) among the samples according to ANOVA and Tukey's multiple comparison tests. \*PHBV18 values were used to calculate the mix ruler (between brackets).

This study is not in agreement with previous works reporting on PHBV and metallic nanoparticles composites where the addition of commercial ZnO increased the crystallinity and barrier properties [15, 31]. However, this negative effect on barrier properties was limited by the good dispersion and distribution achieved with the electrospinning preincorporation method, showing no significant differences in water vapor permeability when PHBV<sub>s</sub>-P nanocomposites were compared to the neat PHBV<sub>s</sub> films. As opposed to this, the big size of agglomerates present in the PHBV-D disrupted the continuity of the PHBV<sub>s</sub> matrix causing a detrimental effect on water vapor and oxygen barrier of the nanocomposites.

In spite of the fact that the most efficient technology to improve barrier properties is a multilayer display, the coating structures did not improve barrier performance of the PHBV<sub>s</sub> which could be explained by the more hydrophilic character of the electrospun coating prepared with PHBV18/ZnO, as compared to the neat PHBV3 film

used as substrate. In fact, great differences were observed in the water uptake values when the neat PHBV18 ( $32.1 \pm 1.2\%$ ) and the neat PHBV3 ( $9.8 \pm 0.6$ ) were compared [30].

### 3.3.4 Mechanical properties

Mechanical properties of the neat and zinc oxide containing films are summarized in Table 5. From these results, it may be deduced that the mechanical properties were mainly affected by the presence of ZnO nanoparticles and the methodology used, but not so greatly by valerate content. Thus, PHBVs films showed similar rigidity and brittleness than the neat PHBV3 but lower strength. The small differences between the unfilled matrices (without ZnO nanoparticles) can be explained by the presence of a high concentration of non-polymeric impurities, derived from the fermentation process of PHBV18 that could act as stress concentration moieties (Martínez-Abad et al., 2015). In fact, Martínez-Abad et al., 2015 reported that EAB values of samples containing more than 15wt. % of the PHBV18 did not significantly differ from the neat PHBV3 although the tensile strength slightly decreased.

**Table 5.** Tensile parameters of the neat PHBV3, PHBVs their ZnO-based nanocomposites.

Sample	Elastic modulus (GPa)	Elongation at break (%)	Tensile strength (MPa)
PHBV3	$2.6 \pm 0.1^a$	$1.5 \pm 0.2^a$	$33.9 \pm 6.9^a$
PHBV <sub>s</sub>	$2.2 \pm 0.2^{ab}$	$1.3 \pm 0.1^a$	$18.5 \pm 1.0^b$
PHBV <sub>s</sub> -D	$1.5 \pm 0.2^c$	$6.5 \pm 1.4^b$	$12.5 \pm 1.8^b$
PHBV <sub>s</sub> -P	$2.1 \pm 0.0^b$	$2.3 \pm 0.2^a$	$34.8 \pm 0.5^a$
PHBV <sub>s</sub> -C	$1.4 \pm 0.1^c$	$6.2 \pm 0.5^b$	$22.6 \pm 1.8^{ab}$

Mean values  $\pm$  standard deviation. Mean values with different letters in the same column represent significant differences ( $p < 0.05$ ) among the samples according to ANOVA and Tukey's multiple comparison tests.

## Chapter VI

Considering the data corresponding to the methodology used during films preparation, the greater ductility of the PHBVs-D and PHBVs-C structures was evidenced by their significantly reduced Young's modulus and increased elongation at break. Besides, the addition of PHBV18 and ZnO nanoparticles directly in the melt mixing step or in a coating form, led to a decrease in the energy absorbed by the material at break (i.e. toughness). However, the electrospinning preincorporation method did not modify the elongation and stiffness of the neat PHBV3 probably due to the higher dispersion of the PHBV18/ZnO fibers into the PHBV3 matrix, fact that also explained the small differences observed in thermal and water vapor barrier properties. It is known that the mobility of the filler within the polymeric matrix together with the nanoparticles alignment under an applied tensile stress is essential for energy dissipation and, thus, the toughness [15, 31]. Hence, once again, it appears that a greater dispersion and distribution of the nanoparticles was achieved in the PHBVs-P system.

### 3.3.5 Antimicrobial activity of active PHBV films

Given that the P-ZnO nanoparticles demonstrated high antimicrobial performance against *Listeria monocytogenes* in liquid media, they were incorporated in PHBV films following the methodology described above. In order to ascertain if the release of ZnO nanoparticles may be sufficiently sustained as to allow a continuous effect, the antimicrobial activity of the obtained films was assessed after successively washing and the zinc concentration in the washing solution was quantified by ICP-OES.

As indicated by Figure 10, before the washes, a bactericidal effect, that is, a reduction of 3 CFU log units compared to the initial inoculum was recorded for active films prepared by preincorporation and coating systems while, for films prepared by direct addition, a lower bacterial reduction of 1 log CFU was achieved. This indicates the potential of antimicrobial ZnO nanoparticles is being more efficiently exploited

when incorporated in the electrospun fibers, which promotes improved dispersion and distribution of the nanoparticles in the polymer matrix.

After successively washes, the antimicrobial efficacy of PHBV<sub>s</sub>-D and PHBV<sub>s</sub>-P decreased gradually as a consequence of the zinc release from the film surface to the water washing. These results were in line with the zinc concentration profile obtained by ICP-OES where a burst release regime was registered in the fifth wash (Figure 11). Interestingly, no viable cells were detected in PHBV<sub>s</sub>-C films even after 15 washes. These results demonstrate that the zinc oxide containing fibers mat placed as coating in the outer layer of the coating structure increased the zinc availability and, thus, its antimicrobial performance.

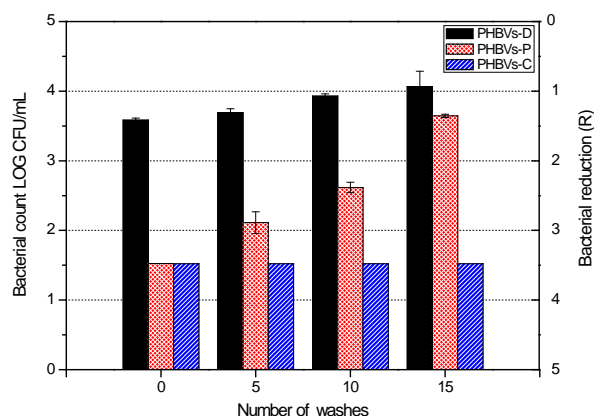


**Figure 10.** Antimicrobial activity of PHBV<sub>s</sub>-ZnO films against *Listeria monocytogenes* after successive washes. The initial inoculum size was 5 log CFU/mL and the detection limit was 33 CFU/mL.

## Chapter VI

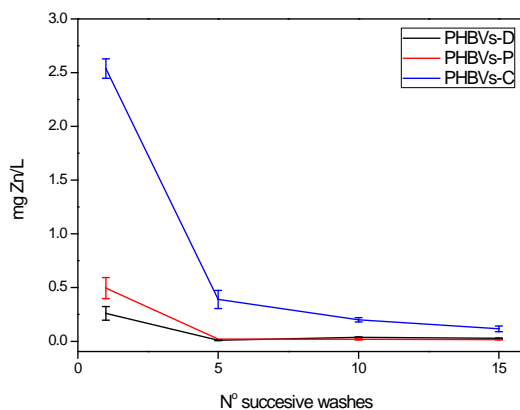


**Figure 11.** Release profile of zinc of PHBV<sub>s</sub>-ZnO films after successive washes.

On the other hand, from the ICP-OES results it is important to highlight that the released zinc detected in the washing water after 15 washes for all tested films was very low as compared to the 6% initial load. Therefore, it can be also concluded that the zinc oxide nanoparticles incorporated into the bulk of PHBV3 matrix (i.e. those films prepared by direct melt mixing or preincorporation method) could not migrate to the surface in contact with the bacterial suspension. Once the zinc available at the surface of PHBV<sub>s</sub>-D and PHBV<sub>s</sub>-P films was released along the first five washes, it was not replaced and its bactericidal effect was lost. In the case of the coating system (PHBV<sub>s</sub>-C), although the burst release also occurred in the first five washes, the amount of zinc available in the film surface was enough to lead a prolonged and effective antimicrobial activity.

Considering the specific migration limit imposed by European Union Guidelines on Regulation (EU) No 10/2011 on plastic materials and articles intended to come into contact with food for zinc (25mg/kg food), under the test washing conditions, even when the burst release took place, the zinc release from in any of the assessed films did not surpass the current restriction limits. However, additional research on the behaviour of these active films in other food simulants or food matrices according to

current legislation is required to ascertain its ultimate implementation in food packaging applications.

## 4. Conclusions

---

Nanotechnology is an interesting field of science offering materials exhibiting unique properties such as enhanced antimicrobial activity against food borne pathogens. The present work shows the great potential of the nanostructured ZnO as antimicrobial material for active food packaging applications. In the first part of this study, it was observed that the antibacterial effect of ZnO particles was significantly improved when the specific surface area of particles increased, being the hexagonal-pyramid nanoparticles (P-ZnO) those that presented the highest antibacterial effect. Moreover, these nanoparticles maintained their antimicrobial activity even when they were incorporated in coating PHBV structures. In addition to their antimicrobial properties, ZnO nanoparticles presented a positive effect on thermal stability and optical properties of active films avoiding their browning after thermal processing. Although some research works have previously demonstrated the reinforcing effect of ZnO nanoparticles in terms of barrier and mechanical properties when they are incorporated into biopolymeric matrices, the high amounts of the PHBV18/ZnO required to obtain a bactericide effect against *L. monocytogenes*, negatively affected the performance of the material. It is important to highlight that barrier properties depend on the product features and the intended end-used application. For instance, in packages for fresh fruits and vegetables, high barrier to oxygen diffusion are undesirable and modified atmosphere packaging should have a high oxygen barrier. Finally, the results show that aqueous prepared inorganic metal oxide nanoparticles

with desirably exposed crystal surfaces' provides an efficient tool for the making of functional antimicrobial nanocomposites within food packaging.

## 5. Acknowledgements

---

The authors are thankful to Dr. Maria Reis from Universidade Nova de Lisboa, and Dr. Catarina Oliveira, from Centro de Quimica fina e Biotecnologia, for the synthesis of PHBV18 and Dr. Luis Cabedo, from Universitat Jaume I for his support with mechanical testing. This work was financially supported by the Spanish Ministry of Economy and Competitiveness (MAT2012-38947-C02-01 and AGL2015-63855-C2-1-R). J.L. Castro-Mayorga is supported by the Administrative Department of Science, Technology and Innovation (Colciencias) of Colombian Government. M. J. Fabra is recipient of a Ramon y Cajal contract from the Spanish Ministry of Economy and Competitiveness.

## 6. References

---

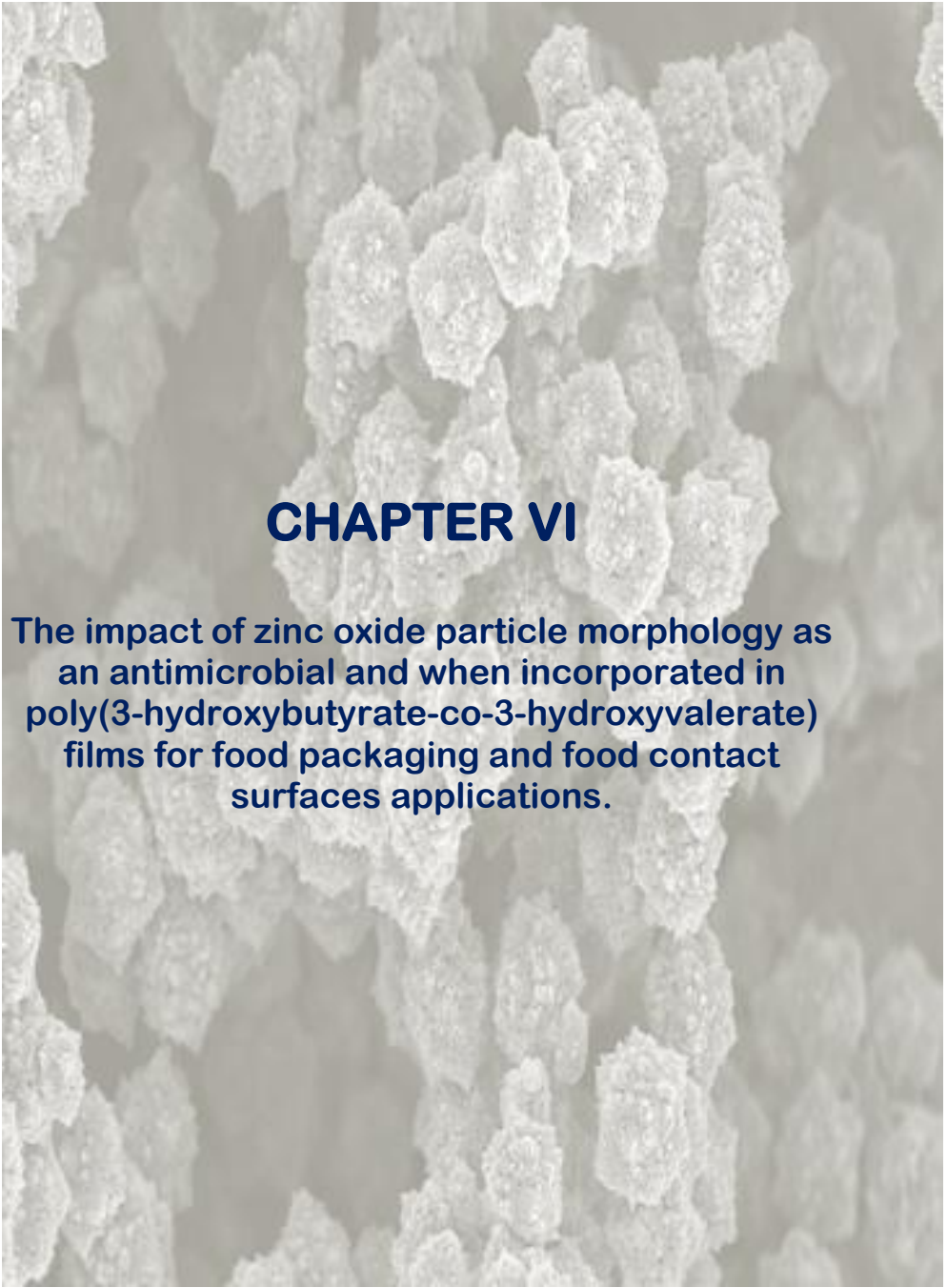
1. M. Ozdemir and J. D. Floros, "Active food packaging technologies," *Critical Reviews in Food Science and Nutrition*, vol. 44, no. 3, pp. 185-193, 2004.
2. J. H. Han, "Antimicrobial Food Packaging," *Food Technology*, vol. 54, no. 3, pp. 56-65, 2000.
3. Z. Huang, P. C. Maness, D. M. Blake, E. J. Wolfrum, S. L. Smolinski and W. A. Jacoby, "Bactericidal mode of titanium dioxide photocatalysis," *Journal of Photochemistry and Photobiology A: Chemistry*, vol. 130, no. 2-3, pp. 163-170, 2000.
4. J. Sawai, S. Shoji, H. Igarashi, A. Hashimoto, T. Kokugan, M. Shimizu and H. Kojima, "Hydrogen peroxide as an antibacterial factor in zinc oxide powder slurry," *Journal of Fermentation and Bioengineering*, vol. 86, no. 5, pp. 521-522, 1998.

5. J. Sawai, H. Kojima, H. Igarashi, A. Hashimoto, S. Shoji, T. Sawaki, A. Hakoda, E. Kawada, T. Kokugan and M. Shimizu, "Antibacterial characteristics of magnesium oxide powder," *World Journal of Microbiology and Biotechnology*, vol. 16, no. 2, pp. 187-194, 2000.
6. J. Sawai, H. Shiga and H. Kojima, "Kinetic analysis of death of bacteria in CaO powder slurry," *International Biodeterioration and Biodegradation*, vol. 47, no. 1, pp. 23-26, 2001.
7. P. K. Stoimenov, R. L. Klinger, G. L. Marchin and K. J. Klabunde, "Metal oxide nanoparticles as bactericidal agents," *Langmuir*, vol. 18, no. 17, pp. 6679-6686, 2002.
8. P. Espitia, N. d. Soares, J. d. Coimbra, N. de Andrade, R. Cruz and E. Medeiros, "Zinc Oxide Nanoparticles: Synthesis, Antimicrobial Activity and Food Packaging Applications," *Food and Bioprocess Technology*, vol. 5, no. 5, pp. 1447-1464, 2012.
9. A. B. Djurišić, Y. H. Leung, A. M. C. Ng, X. Y. Xu, P. K. H. Lee, N. Degger and R. S. Wu, "Toxicity of metal oxide nanoparticles: Mechanisms, characterization, and avoiding experimental artefacts," *Small*, vol. 11, no. 1, pp. 26-44, 2015.
10. N. Talebian, S. M. Amininezhad and M. Douidi, "Controllable synthesis of ZnO nanoparticles and their morphology-dependent antibacterial and optical properties," *Journal of Photochemistry and Photobiology B: Biology*, vol. 120, pp. 66-73, 2013.
11. M. Arakha, M. Saleem, B. C. Mallick and S. Jha, "The effects of interfacial potential on antimicrobial propensity of ZnO nanoparticle," *Sci. Rep.*, vol. 5, 2015.
12. FDA, "PART 182—SUBSTANCES GENERALLY RECOGNIZED AS SAFE," Ed., Food and Drug Administration, 2011.
13. A. Emamifar, M. Kadivar, M. Shahedi and S. Soleimani-Zad, "Evaluation of nanocomposite packaging containing Ag and ZnO on shelf life of fresh orange juice," *Innovative Food Science & Emerging Technologies*, vol. 11, no. 4, pp. 742-748, 2010.
14. D. Plackett and I. Siró, "Polyhydroxyalkanoates (phas) for food packaging," in *Multifunctional and Nanoreinforced Polymers for Food Packaging*, Ed., pp. 498-526, 2011.
15. A. M. Díez-Pascual and A. L. Díez-Vicente, "Poly(3-hydroxybutyrate)/ZnO bionanocomposites with improved mechanical, barrier and antibacterial properties," *International Journal of Molecular Sciences*, vol. 15, no. 6, pp. 10950-10973, 2014.
16. W. Yu, C.-H. Lan, S.-J. Wang, P.-F. Fang and Y.-M. Sun, "Influence of zinc oxide nanoparticles on the crystallization behavior of electrospun poly(3-hydroxybutyrate-co-3-hydroxyvalerate) nanofibers," *Polymer*, vol. 51, no. 11, pp. 2403-2409, 2010.
17. R. Naphade and J. Jog, "Electrospinning of PHBV/ZnO membranes: Structure and properties," *Fibers and Polymers*, vol. 13, no. 6, pp. 692-697, 2012.

## Chapter VI

18. A. Martínez-Abad, L. Cabedo, C. S. S. Oliveira, L. Hilliou, M. Reis and J. M. Lagarón, "Characterization of polyhydroxyalkanoate blends incorporating unpurified biosustainably produced poly(3-hydroxybutyrate-co-3-hydroxyvalerate)," *Journal of Applied Polymer Science*, 2015.
19. A. M. Pourrahimi, D. Liu, L. K. H. Pallon, R. L. Andersson, A. Martínez Abad, J. M. Lagarón, M. S. Hedenqvist, V. Ström, U. W. Gedde and R. T. Olsson, "Water-based synthesis and cleaning methods for high purity ZnO nanoparticles-comparing acetate, chloride, sulphate and nitrate zinc salt precursors," *RSC Advances*, vol. 4, no. 67, pp. 35568-35577, 2014.
20. M. J. Fabra, A. Lopez-Rubio and J. M. Lagaron, "High barrier polyhydroxyalkanoate food packaging film by means of nanostructured electrospun interlayers of zein," *Food Hydrocolloids*, vol. 32, no. 1, pp. 106-114, 2013.
21. M. Scandola, M. L. Focarete, G. Adamus, W. Sikorska, I. Baranowska, S. Świerczek, M. Gnatowski, M. Kowalczyk and Z. Jedliński, "Polymer Blends of Natural Poly(3-hydroxybutyrate-co-3-hydroxyvalerate) and a Synthetic Atactic Poly(3-hydroxybutyrate). Characterization and Biodegradation Studies," *Macromolecules*, vol. 30, no. 9, pp. 2568-2574, 1997.
22. A. Gurlo, "Nanosensors: Towards morphological control of gas sensing activity. SnO<sub>2</sub>, In<sub>2</sub>O<sub>3</sub>, ZnO and WO<sub>3</sub> case studies," *Nanoscale*, vol. 3, no. 1, pp. 154-165, 2011.
23. A. M. Pourrahimi, D. Liu, V. Ström, M. S. Hedenqvist, R. T. Olsson and U. W. Gedde, "Heat treatment of ZnO nanoparticles: new methods to achieve high-purity nanoparticles for high-voltage applications," *Journal of Materials Chemistry A*, vol. 3, no. 33, pp. 17190-17200, 2015.
24. B. Li and Y. Wang, "Facile synthesis and enhanced photocatalytic performance of flower-like ZnO hierarchical microstructures," *Journal of Physical Chemistry C*, vol. 114, no. 2, pp. 890-896, 2010.
25. R. Brayner, R. Ferrari-Iliou, N. Brivois, S. Djediat, M. F. Benedetti and F. Fiévet, "Toxicological Impact Studies Based on Escherichia coli Bacteria in Ultrafine ZnO Nanoparticles Colloidal Medium," *Nano Letters*, vol. 6, no. 4, pp. 866-870, 2006.
26. J. Vidic, S. Stankic, F. Haque, D. Ciric, R. Le Goffic, A. Vidy, J. Jupille and B. Delmas, "Selective antibacterial effects of mixed ZnMgO nanoparticles," *Journal of Nanoparticle Research*, vol. 15, no. 5, pp. 1595, 2013.
27. J. L. Castro-Mayorga, A. Martínez-Abad, M. J. Fabra, C. Olivera, M. Reis and J. M. Lagarón, "Stabilization of antimicrobial silver nanoparticles by a polyhydroxyalkanoate obtained from mixed bacterial culture," *International Journal of Biological Macromolecules*, vol. 71, pp. 103-110, 2014.

28. M. Martínez-Sanz, M. Villano, C. Oliveira, M. G. E. Albuquerque, M. Majone, M. Reis, A. Lopez-Rubio and J. M. Lagaron, "Characterization of polyhydroxyalkanoates synthesized from microbial mixed cultures and of their nanobiocomposites with bacterial cellulose nanowhiskers," *New Biotechnology*, vol. 31, no. 4, pp. 364-376, 2014.
29. L. S. Serafim, P. C. Lemos, C. Torres, M. A. M. Reis and A. M. Ramos, "The influence of process parameters on the characteristics of polyhydroxyalkanoates produced by mixed cultures," *Macromolecular Bioscience*, vol. 8, no. 4, pp. 355-366, 2008.
30. J. L. Castro-Mayorga, M. J. Fabra and J. M. Lagaron, "Stabilized nanosilver based antimicrobial poly(3-hydroxybutyrate-co-3-hydroxyvalerate) nanocomposites of interest in active food packaging," *Innovative Food Science & Emerging Technologies*.
31. A. M. Díez-Pascual and A. L. Díez-Vicente, "ZnO-Reinforced Poly(3-hydroxybutyrate-co-3-hydroxyvalerate) Bionanocomposites with Antimicrobial Function for Food Packaging," *ACS Applied Materials & Interfaces*, vol. 6, no. 12, pp. 9822-9834, 2014.

The background of the page is a scanning electron microscope (SEM) image showing numerous irregular, porous, and interconnected zinc oxide particles. The particles vary in size and shape, creating a complex, textured surface. The image is in grayscale, with the particles appearing as lighter, more detailed structures against a darker background.

## CHAPTER VI

**The impact of zinc oxide particle morphology as an antimicrobial and when incorporated in poly(3-hydroxybutyrate-co-3-hydroxyvalerate) films for food packaging and food contact surfaces applications.**

J. L. Castro Mayorga, M. J. Fabra, A.M. Pourrahimi, R. Olsson . "The impact of zinc oxide particle morphology as an antimicrobial and when incorporated in Poly(3-hydroxybutyrate-co-3-hydroxyvalerate) films for food packaging and food contact surfaces applications". Food and Bioproducts Processing, vol. 101, pp. 32-44, 2017.



## Abstract

---

Active biodegradable poly(3-hydroxybutyrate-co-3-hydroxyvalerate) (PHBV) melt mixed nanocomposites and bilayer structures containing copper oxide (CuO) nanoparticles were developed and characterized. The bilayer structures consisted of a bottom layer of compression molded PHBV3 (3% mol valerate) coated with an active electrospun fibers mat made with microbial mixed culture derived PHBV18 (18 % valerate) and CuO nanoparticles. The results showed that the oxygen barrier properties were slightly enhanced by the addition of 0.05% CuO nanoparticles to nanocomposite films but a negligible effect was registered for the bilayer structures. Neither the water vapor permeability nor the mechanical properties were modified by the addition of CuO. Interestingly, by incorporating highly dispersed and distributed CuO nanoparticles in a coating by electrospinning, a lower metal oxide loading was required to exhibit significant bactericidal and virucidal performance against the food-borne pathogens *Salmonella enterica*, *Listeria monocytogenes* and murine norovirus. The biodegradation tests of the samples under composting conditions showed that even the 0.05% CuO coated structures biodegraded within 35 days.

## Keywords

---

Metal nanoparticles, polyhydroxyalkanoates, antimicrobial, electrospinning, biodegradable.

## **1. Introduction**

---

Among the different kinds of nanoparticles applied in many fields of human life, which range from energy production to industrial production processes and biomedical applications, those having antimicrobial activity are highlighted as they can be incorporated into a variety of polymer matrices used in daily life, producing novel biocide materials. Metal and metal oxide nanoparticles based on gold, zinc, silver and copper have been reported to exhibit a wide antimicrobial spectrum against different species of microorganisms, including virus, fungi and bacteria [1].

In the specific case of copper, it has been used for centuries as biocide compound to disinfect liquids, solids and human tissues and more recently used as an antifouling agent, water purifier, algacide, fungicide, and bactericide for different biomedical applications [2]. In the food area, metallic copper sheets have been studied as antimicrobial surfaces to inhibit the growth of enteropathogens [3]. Copper and copper oxide bulk materials (micro-sized) has been physically and chemically characterized and investigated as antimicrobial agents [4, 5], counting with added advantages such as that they are easily mixed with polar liquids and polymers, relatively stable in terms of chemical and physical properties and cheaper and less toxic for living organism than silver [6, 7]. However, the antimicrobial use of copper could be successfully extended by using it in the nano-sized form and by embedding into polymeric matrices.

The incorporation of antimicrobials in a polymer matrix allows the gradual release of the biocide substance from package, controlling the microbial contamination during the transport and storage phase of food distribution at the same time reducing the amount of preservatives added within the bulk of food [8].

Because of the intrinsic characteristics of electrospun fibres such as very high specific surface and porosity [9] and the suitability of the technique to encapsulate active substances within the fibres, the electrospun materials provide excellent candidates for many applications [17]. Biopolymers constitute ideal carriers for antimicrobials in active packaging applications because of their adaptable capacity for controlled release and the possibility of development of blends and multilayers [10].

One of the most promising biopolymers are the polyhydroxyalkanoates (PHAs) family which has been attracting much attention in recent years as biocompatible and biodegradable thermoplastics with potential applications [11]. The most extensively studied polymer from the PHAs group is the poly(3-hydroxybutyrate), PHB. PHB is partially crystalline with a high melting temperature and high degree of crystallinity and high rigidity [12, 13]. To overcome these aspects, the copolymer obtained with the insertion of 3-hydroxyvalerate (HV) units, known as poly(3-hydroxybutyrate-co-3-hydroxyvalerate), PHBV, is usually employed to improve the handling properties of PHB films.

To the best of our knowledge, there is no existing literature on the incorporation of CuO nanoparticles in bio-based matrices and, in particular, in PHAs matrices. Therefore, the main goal of this work was to develop and characterize the antimicrobial performance and physicochemical properties of PHBV nanocomposites and bilayer films containing CuO nanoparticles. Concretely, melt mixed nanocomposites of commercial PHBV3 (3% mol valerate) and mixed microbial cultures derived PHBV18 (18% mol valerate) with different CuO loadings were prepared and the effect of adding an electrospun PHBV18/CuO coating over compression molded PHBV3 films on the mechanical, thermal, barrier, biodegradation properties and more interestingly on the antibacterial and antiviral activity against the food-borne pathogens *Salmonella enterica*, *Listeria monocytogenes* and murine norovirus were studied.

## 2. Materials and methods

---

### 2.1 Materials

Copper oxide (CuO) nanoparticles were kindly supplied by Hefei Quantum Quelle Nano Science & Technology Co., Ltd (Hefei, China). PHBV3 (3 mol % valerate content) purchased from Tianan Biopolymer (Ningbo, China) and unpurified PHBV18 (18 mol % valerate) synthesized from mixed microbial cultures fed with cheese whey, according to the method described by Martinez-Abad *et al.*, 2015 [14], were used as polymer matrix. 2,2,2-Trifluoroethanol (TFE,  $\geq 99$  wt.%, Sigma Aldrich) was used as a solvent for the PHBV18.

### 2.2 CuO particle size

The particle size distribution, weight mean diameter ( $D_{4,3}$ ) and volume-surface mean diameter ( $D_{3,2}$ ) were determined in triplicate with a dynamic light scattering (DLS) instrument (Malvern Mastersizer, Malvern Instruments, Worcestershire, U.K.). In order to avoid agglomeration/clustering of the nanoparticles in the water suspension, a small amount of Sodium hexametaphosphate (Sigma Aldrich, St. Louis, USA) was incorporated to the water and ultrasound stirring was applied prior to the DLS measurement.  $D_{4,3}$  is the average size based on the unit weight of particles, whereas  $D_{3,2}$  represents the average size based on the specific surface per unit volume. These parameters are described by equations 1 and 2, where  $n_i$  is the number of droplets of a determined size range and  $d_i$  is the droplet diameter.

$$D_{4,3} = \frac{\sum n_i d_i^4}{\sum n_i d_i^3} \quad (\text{Eq. 1})$$

$$D_{3,2} = \frac{\sum n_i d_i^3}{\sum n_i d_i^2} \quad (\text{Eq. 2})$$

## 2.3 Development of active PHBV films

Active films based on CuO nanoparticles and PHBV were developed using two different methods of preparation and two different loading. The samples code and composition are summarized in Table 1.

**Table 1.** Samples code and composition of the developed materials.

Sample code	Composition
PHBVs	86% PHBV3 + 14% PHBV18
0.1%	PHBVs + 0.1% CuO
0.05%	PHBVs + 0.05% CuO
0.05% ES	Bottom layer: PHBV3, coating: 14% electrospunPHBV18+0.05% CuO

### 2.3.1 Preparation of nanocomposites

PHBV3 pellet (86 wt.%), unpurified PHBV18 powder (14 wt.%) and the CuO powder (0.05 and 0.1 wt.%) were directly melt mixed in an internal mixer (Brabender Plastograph, Germany) during 5 minutes at 60 rpm and 180°C. Neat PHBV3/PHBV18 (sample code: PHBVs) blends prepared by melt mixing were used as control for comparative purposes. The batches were subsequently processed into thin sheets (thickness of 130  $\mu\text{m}$ ) by compression molding, using a hot-plate hydraulic press (Carver 4122, U.S.) at 180°C, 1.8 MPa and 3 min.

### 2.3.2 Preparation of the coated systems

In a second approach, PHBV3 films were coated with PHBV18/CuO ultrathin fibers mats containing 0.05 wt.% of CuO which were produced by means of the electrospinning technique according to the above description (sample code: 0.05% ES).

For the PHBV18/CuO ultrathin fibers mats preparation, polymer solutions contained a total solids content of 6 wt.% was prepared as follow: First, the unpurified PHBV18 at 99.95 wt.% was dissolved in TFE under magnetic stirring for 4 h at 50°C

## ***Chapter VII***

and cooled down at room temperature. Then, CuO nanoparticles were incorporated at the remaining 0.05 wt. % and stirred for 2 more hours. After this time, the mixture was homogenized for 2 min using a high shear speed homogenizer (Model T25, *Ultra-Turrax*, IKA, Germany). Thereafter, the solution was transferred to a 5 mL glass syringes, connected through PTFE tubes to a stainless steel needle (0.9 mm of inner diameter) and processed using a Fluidnatek® LE-10 electrospinning equipment (Valencia, Spain). Processed samples were collected on a rotational stainless-steel drum spinning at 200 rpm connected to the cathode of the power supply and oriented in parallel at the syringe. The injector was motorized to scan along the width of the drum collector to homogenously deposit the fibers. The distance between the needle and the collector was 12 cm and the voltage was maintained at 10 kV. All experiments were carried out at room temperature under a steady flow-rate of 7 mL/h. After electrospinning, the fibers mats were dried at 60°C under vacuum for 24 h to completely remove the solvent and were subsequently used to prepare the coating. Later, a post-annealing step was applied to form a continuous film by fibers coalescence. Fibers mats (14 wt.%) of *c.a.* 40 µm of thickness were placed onto PHBV3 films prepared by compression moulding as described above. This assembly was put in between hot plates hydraulic press (Carver 4122, USA) at 150 °C during 2 min (without pressing).

### **2.4 Characterization of CuO and active films**

#### **2.4.1 Morphology**

The morphology of the electrospun fibers and the active films were studied by Scanning Electron and Transmission Microscopy, SEM and TEM respectively. For SEM observations, the films were cryo-fractured after immersion in liquid nitrogen and subsequently sputtered with a gold- palladium mixture under vacuum. The SEM

was conducted on a Hitachi microscope (Hitachi S-4800) at an accelerating voltage of 5 kV and a working distance of 8-10 mm. The TEM analysis was performed on previously ultra-microtomed (Leica EM UC6) samples using a Jeol 1010 (Hitachi) transmission electronic microscope with an accelerating voltage of 80kV.

To obtain an accurate estimation of the average fiber and nanoparticles diameter, 200 to 300 measurements were done by means of the Adobe Photoshop CS4 software from the SEM and TEM micrographs in their original magnification.

### **2.4.2 Optical properties**

Transparency of the neat PHBV3 film and coated systems was determined through the surface reflectance spectra in a spectrophotometer CM-3600d (Minolta Co., Tokyo, Japan) with a 10 mm illuminated sample area. The internal transmittance (Ti) of the samples was determined by applying the Kubelka-Munk theory [19] for multiple scattering to the reflection spectra where an increase in the spectral distribution of transmittance is associated with more homogeneous and transparent samples. Measurements were taken in triplicate for each sample by using both a white and black background.

Moreover, CIE-L\* a\* b\* coordinates (CIE, 1986) were obtained by the infinite reflection spectra of the samples, using D65 illuminant/10 observer. Samples were evaluated per duplicate and three measurements were taken at random locations on each of the studied films.

### **2.4.3 Wide Angle X-Ray Diffraction Analysis (WAXD)**

X-ray diffractograms of the CuO powder samples and films were recorded at room temperature using a Bruker AXSD4 Endeavour diffractometer with a Cu-K $\alpha$  source (wavelength = 1.54178 Å). Peak fitting was carried out using IgorPro software

## ***Chapter VII***

package (Wavemetrics, Lake Oswego, Oregon). Gaussian function was used to fit the experimental diffraction profiles obtained. The crystallinity degree ( $X_c$ ) of the films was taken as the ratio of the sum of areas under the crystalline diffraction peaks to the total area under the curve between  $2\theta = 5^\circ$  and  $40^\circ$ .

### **2.4.4 Differential Scanning Calorimetry (DSC)**

Thermal properties of the neat PHBVs films and its active nanocomposites were evaluated by DSC using a Perkin-Elmer DSC 8000 thermal analysis system under nitrogen atmosphere. The sample treatment consisted of a first heating step from  $0^\circ\text{C}$  to  $200^\circ$ , a subsequent cooling down to  $-50^\circ\text{C}$  and a second heating step up to  $200^\circ\text{C}$ . The heating and cooling rates for the runs were  $10^\circ\text{C}/\text{min}$  and the typical sample weight was  $\sim 3$  mg. The first melting endotherm, and the controlled crystallization at  $10^\circ\text{C}/\text{min}$  from the melt, was analysed. To ensure reliability of the data obtained, heat flow and temperature were calibrated using indium as a standard. The tests were done, at least, in triplicate.

### **2.4.5 Mechanical properties**

Tensile tests were performed according to ASTM Standard D638 using a Universal Testing Machine (Shimadzu AGS-X 500N). Before testing, the samples were allowed to reach the equilibrium under ambient conditions ( $25^\circ\text{C}$  and 50% R.H. for 24 h) and cut in dumbbell shaped specimen. Elastic modulus, tensile strength, and elongation at break were determined from the stress-strain curves, estimated from force–distance data obtained for the different films. At least, three specimens of each film were tensile tested as to obtain statistically meaningful results.

### **2.4.6 Water Vapour Permeability (WVP)**

Water vapour permeability (WVP) was determined according to the ASTM E96 (ASTM 2011) gravimetric method, using Payne permeability cups (Elcometer SPRL,

Hermelle/s Argenteau, Belgium). Cells containing distillate water were placed inside a desiccator at 0% RH and 24°C and the water weight loss through a film area of 0.001 m<sup>2</sup> was monitored. WVP was calculated from the steady-state permeation slopes obtained from the regression analysis of weight loss data over time. All measurements were performed in triplicate.

#### **2.4.7 Oxygen transmission rate (OTR) measurements**

The oxygen permeability coefficient was derived from oxygen transmission rate (OTR) measurements recorded using an Oxygen Permeation Analyzer M8001 (Systech Illinois, UK). Experiments were carried out at 23°C and 80% RH. The samples were previously purged with nitrogen in the humidity equilibrated samples, before exposure to an oxygen flow of 10 mL min<sup>-1</sup>. The exposure area during the test was 5 cm<sup>2</sup> for each sample. In order to obtain the oxygen permeability, film thickness and gas partial pressure were considered in each case. The measurements were done in triplicate.

### **2.5 Antibacterial activity of active films**

The antibacterial activity experiments were performed with the foodborne pathogens, *Salmonella enterica* CECT 4300 and *Listeria monocytogenes* CECT 7467. All the strains were obtained from the Spanish Type Culture Collection (CECT: Valencia, Spain) and stored in phosphate buffered saline (PBS, Sigma Aldrich) with 10 wt.-% tryptic soy broth (TSB, Conda Laboratories) and 10 wt.-% glycerol at -80°C until needed. The stock culture was maintained by regular subculture to tryptone soy agar (TSA) slants at 4°C and transferred monthly. Previous to each antimicrobial assay, a loopful of bacteria was transferred to 10 mL of TSB and incubated at 37°C overnight

## *Chapter VII*

and an aliquot was again transferred to TSB and grown at 37°C and 120 rpm to the mid-exponential phase of growth and this cultured was used as inoculum.

The antibacterial activity of the active films was evaluated according to the Japanese Industrial Standard JIS Z 2801 (ISO 22196:2011) with some modifications. Film samples (3 x 3 cm) sterilized by UV treatment were placed into sterile Petri dishes. A microorganism suspension containing about  $5 \times 10^5$  CFU/mL was put onto film samples. Then inoculated film samples were covered with an inert piece of UV sterilized Low-Density Polyethylene (LDPE) of 2.5 x 2.5 cm. Petri dishes containing the inoculated film samples were incubated at 25°C under relative humidity (RH) of above 95% for 24 h. After the incubation time, microorganisms were recovered from film samples and inoculated onto TSA plates for conventional microbiological counts. The PHBVs films (without CuO) were used as a control. The value of the bacterial reduction (R) was calculated by determining  $\log_{10} (N_0/N_t)$ , where  $N_0$  is the average of the number of viable cells of bacteria on the untreated test piece after 24 h and  $N_t$  is the average of the number of viable cells of bacteria on the antimicrobial test piece after 24 h. Three replicate experiments were performed for each sample.

### **2.6 Virucidal activity of active films**

Murine norovirus, MNV-1 strain, was propagated and assayed in RAW 264.7 cells (kindly provided by Prof. H. W. Virgin, Washington University School of Medicine, USA). Semi-purified viral stocks were harvested 2 days post infection by three freeze-thaw cycles of infected cells followed by centrifugation at  $660 \times g$  for 30 min to remove cell debris. Infectious viruses were enumerated by determining the 50% tissue culture infectious dose (TCID<sub>50</sub>) with eight wells per dilution and 20 µl of inoculum per well using the Spearman-Kärber method [16].

The virucidal activity of copper based films was also evaluated based on the JIS Z 2801 (ISO 22196:2011) standard. Briefly, a suspension of MNV diluted in PBS buffer (6 log TCID<sub>50</sub>/ml) was placed onto the test films of 3×3 cm and covered by an inert piece of Low-Density Polyethylene (LDPE) of 2.5×2.5 cm and 10 μm thickness. Samples were overnight incubated at 25 °C and 95% RH. Subsequently, the top film was lifted, and the virus droplet-exposed sides were recovered. Ten-fold dilutions of the samples were inoculated into confluent RAW monolayers in 96-well plates. Then, infectious viruses were enumerated by cell culture assays as described above. Each experimental condition was done in triplicate. Positive controls were virus inoculated in PHBVs films. The decay of MNV titers was calculated as  $\log_{10} (N_0/N_t)$ , where  $N_0$  is the infectious virus titer for PHBVs films and  $N_t$  is the infectious virus titer for active films containing CuO.

## **2.7 Biodisintegration in composting conditions**

Disintegrability of the films was assessed by means of a disintegration test under lab-scale composting conditions according to the ISO 20200 standard, “Determination of the degree of disintegration of plastic materials under simulated composting conditions in a laboratory-scale test”. For the preparation of solid synthetic waste, 10% of activated mature compost (Vigorhumus H-00, purchased from Burás Profesional, S.A., Girona, Spain) was mixed with 30 wt. % rabbit food, 10 wt. % starch, 5 wt. % sugar, 1wt. % urea, wt. 4% corn oil and 40wt. % sawdust. The water content of the substrate was around 55 wt. % and the aerobic conditions were guaranteed by gently mixing the compost and periodically adding water according to the standard requirements. The samples were cut from the films (10 × 10 × 0.1 mm<sup>3</sup>) and buried inside plastic mesh bags to simplify their extraction and allow the contact of the compost with the specimens, and were incubated at 58°C for 41 days. At different

## Chapter VII

composting times samples were recovered for analysis, washed with distilled water, dried at 40°C under vacuum for 24 h, and weighed. The degree of disintegration was calculated by normalising the sample weight, at different days of incubation, to the initial weight with Equation (3), where  $m_i$  is the initial dry mass of the test material and  $m_f$  is the dry mass of the test material recovered at different incubation stages.

$$D = \frac{m_i - m_f}{m_i} \times 100 \quad (\text{Eq. 3})$$

### 2.8 Statistical analysis

The statistical analysis was carried out by means of StatGraphics Plus version 5.1 (Statistical Graphics Corp.) through the analysis of variance (ANOVA). Homogeneous sample groups were obtained by using Tukey's Honestly Significant Difference (HSD) (95% significant level).

## 3. Results and discussion

---

In the present work, commercial CuO nanoparticles were incorporated into PHBV by direct melt-mixing at two different concentrations (0.05 and 0.1% CuO) and, the lower loading (0.05%) was also used for the formation of an annealed coating of electrospun PHBV18/CuO fibers mats put over compression molded PHBV3 films for comparison purposes. The physicochemical properties of both systems were determined and are shown below. .

### 3.1 Morphology and optical properties of CuO nanoparticles and active films

Firstly, the morphology and the particle size of the commercial CuO nanoparticles were characterized. From Figure 1, the morphology of the particles appears to be rather flaky (Figure 1a) and their particle size distribution shows (Figure 1b) a bimodal distribution with a mean weight size  $D_{4,3}$  of 191nm.

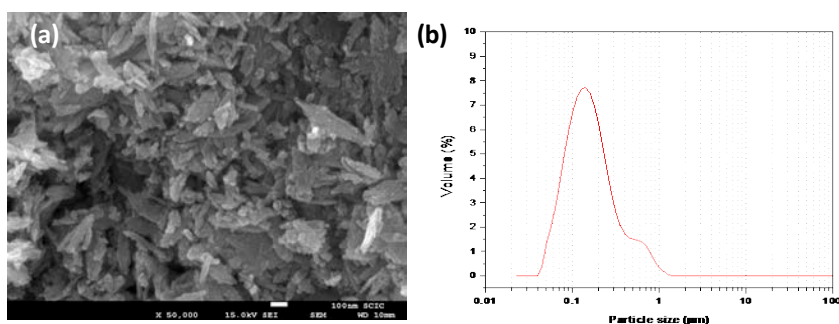


**Figure 1.** CuO morphology. (a) SEM images, (b) particle size distribution.

Once the CuO nanoparticles were incorporated into the PHBV films, a microstructural analysis by means of electronic microscopy was carried out in order to obtain information about the arrangement of films components and CuO nanoparticles dispersion. Representative SEM micrographs of cryo-fractured sections of the nanocomposites films are displayed in Figure 2. PHBVs films showed a compacted structure (*cf.* Fig 2a) which was not significantly altered by the addition of 0.05% CuO by melt-mixing (*cf.* Fig 2b). However, the incorporation of CuO at 0.1% promoted some changes in the morphology of the PHBVs matrix since a rough surface was observed in the cross-section of films (*cf.* Fig 2c) and a marked agglomeration pattern in the TEM images of the ultrathin sections (*cf.* Fig 2d). Moreover, it is noteworthy to remark that all samples shows the presence of some flaky elements in

## Chapter VII

the morphology of the cross section (see Figures 2a, 2b and 2c) that could be ascribed to the presence of a nucleating additive (see later the WAXD data in further support of this argument).

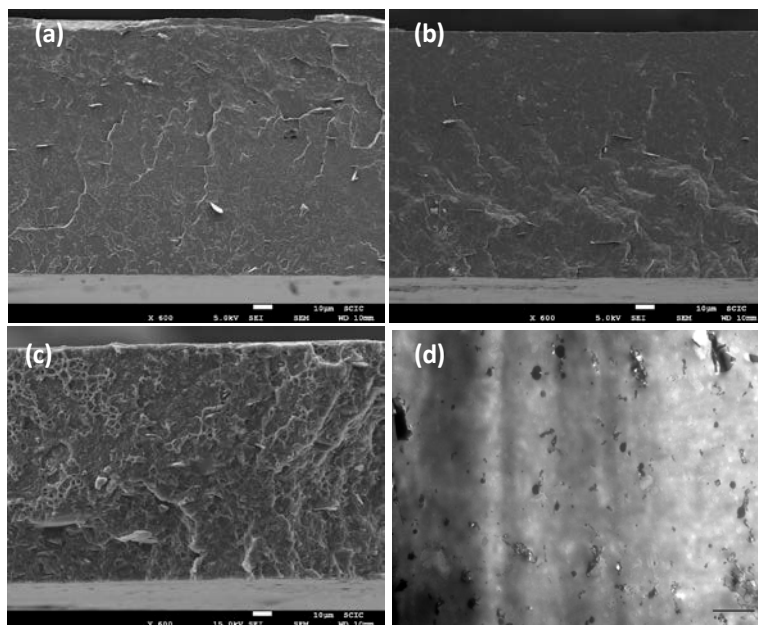


**Figure 2.** Micrograph of the neat PHBVs and its active nanocomposites obtained by melt mixing. **(a)** SEM image of PHBVs, **(b)** SEM image of PHBVs 0.1%, **(c)** SEM image of PHBVs 0.05%, **(d)** TEM image of an ultrathin section of 0.01% CuO film.

The fibers mats used as coating in the 0.05% ES films were also observed by SEM, Figure 3 shows representative images of electrospun PHBV18/CuO fibers before the annealing step (*cf.* Fig 3a) exhibiting an average diameter of  $1.01 \pm 0.2 \mu\text{m}$ . After the thermal annealing, the electrospun fibers formed a continuous layer (*cf.* Fig 3b) which was strongly adhered to the surface of PHBV3 (*cf.* Fig 3c). Moreover, CuO nanoparticles appeared well dispersed and distributed within the polymer matrix, having a diameter of around  $182 \pm 5 \text{ nm}$  as it can be seen in the ultrathin section of TEM images of the coated structure TEM images (*cf.* Fig 3d). This value matches with

the CuO nanoparticles mean weight size ( $D_{4,3} = 191\text{nm}$ ) observed for CuO nanoparticles before their incorporation into the PHBV film and is an indication of the effective prevention of nanoparticles agglomeration resulted from the application of electrospinning coating technique.

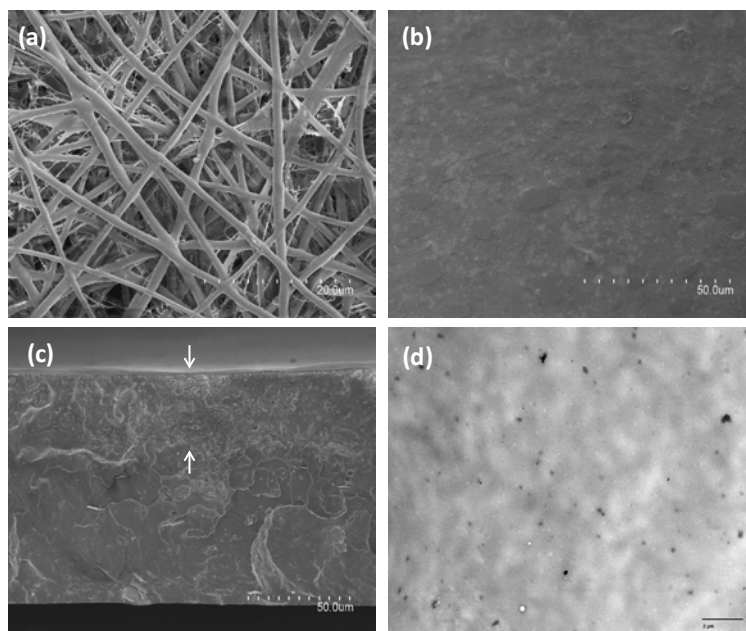


**Figure 3.** Microscopic pictures of the electrospun fibers and the active 0.05% ES film. **(a)** SEM image of the PHBV18/CuO fibers, **(b)** top view of the 0.05% ES film. **(c)** cross-section of the 0.05% ES film. **(d)** TEM image of the ultrathin section of the 0.05% ES film. The white arrows in figure 3c highlight the thickness of the active coating layer

Optical properties (transparency and color parameters) are relevant for the packaging application, since it is desirable that the packaging contents can be inspected through the film. Changes in transparency are related with their internal structure since CuO nanoparticles might affect the optical properties. Figure 4 shows the contact transparency images of the neat PHBV3, the PHBVs mixture and the active systems. In principle, the neat PHBV3 and coating structures preserved a good contact

## Chapter VII

transparency but it was slightly compromised in nanocomposite films prepared by melt-mixing (with and without CuO), in turn suggesting some level of degradation of the PHBV18 during the melt-mixing process.

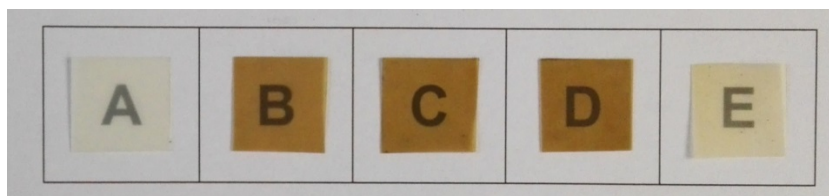


**Figure 4.** Contact transparency pictures of films. (A) PHBV3, (B) PHBVs, (C) 0.1%, (D) 0.05%, (E) 0.05% ES.

The transparency was also quantitatively assessed by means of internal transmittance ( $T_i$ ) measurements. This parameter is directly related to the arrangement of film's components and thus, linked to the light transmission/dispersion behavior of nanocomposites/coating structures. As observed, the neat PHBV3 and the coating structure (0.05% ES) showed a similar pattern over the wavelength considered (*cf.* Fig. 5), although  $T_i$  values of the coating structure were significantly lower (less transparent) than the neat PHBV3 matrix which can be associated to the presence of several compounds with different refractive index (i.e. PHBV18 and CuO). Interestingly, a different pattern was observed for active PHBVs melt compounded nanocomposites, being also less transparent (lower  $T_i$  values) than the neat PHBVs and the coated structures. Therefore, the surface morphology and thus, the strategy followed to develop the films (nanocomposites or coating) play an important role on their optical properties. The lower  $T_i$  values observed in nanocomposite films, implies a greater light dispersion, greater opacity and thus, more heterogeneous matrices probably due to the presence of PHBV18 which seems to be thermally degraded to some extent during the melt-mixing process,

making the film darker with a brown hue as it can also be deduced from the contact transparency images (*cf.* Fig. 4).

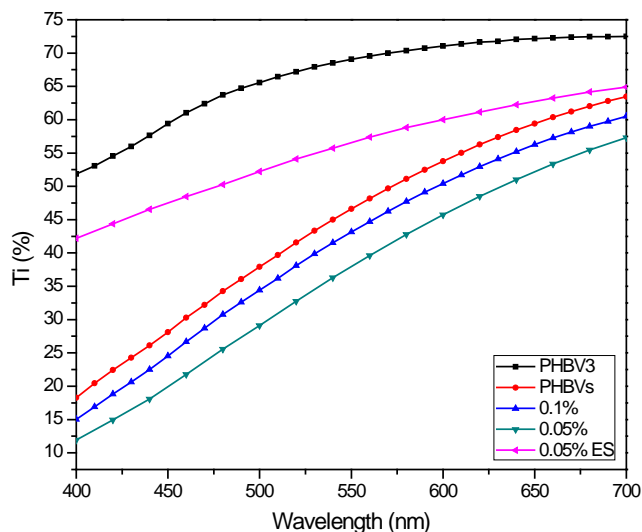


**Figure 5.** Internal transmittance (Ti) of PHBV3, PHBVs and their CuO nanocomposites.

Color differences were also quantitatively assessed by means of lightness ( $L^*$ ), hue ( $h_{ab}^*$ ) and Chroma ( $C_{ab}^*$ ), obtained from the reflectance spectra of an infinity thickness film and the results are gathered in Table 2. The first thing to highlight is that the degraded PHBV18 in nanocomposite films (with and without CuO) made the films darker (lower  $L^*$ ), less vivid (higher  $C_{ab}^*$ ) and with a brown hue indicating rather deficient optical properties, as compared to the neat PHBV3 and the coated films. This was supported by the highest total difference values ( $\Delta E$ ) obtained for the PHBVs and nanocomposites films; whereas the coating structures presented the lowest color difference as compared to the neat PHBV3. As previously reported by Castro-Mayorga et al. [17], this color differences can be ascribed to PHBV18 impurities from the fermentation process (close to 30 wt.%, Castro-Mayorga et al. [18]), which

## Chapter VII

induce Maillard reactions between amide groups and residual reducing sugars during the melt-mixing process. Interestingly, while the addition of ZnO mitigated the effect of the unpurified PHBV18, improving the appearance of the melt-mixed nanocomposite films [19], this seems not to occur for CuO nanoparticles as it can be observed in Figure 4.

**Table 2.** Color parameters of PHBV3, PHBVs and their CuO nanocomposite/coating systems.

Sample	L	C <sub>ab</sub>	h <sub>ab</sub>	ΔE
PHBV3	82.4 ± 0.4 <sup>a</sup>	17.8 ± 0.1 <sup>a</sup>	85.5 ± 0.7 <sup>a</sup>	
PHBVs	48.4 ± 1.1 <sup>b</sup>	19.2 ± 0.4 <sup>a</sup>	68.5 ± 0.7 <sup>b</sup>	34.5 ± 0.8 <sup>a</sup>
0.1%	45.4 ± 1.3 <sup>bc</sup>	19.4 ± 0.3 <sup>a</sup>	68.5 ± 0.7 <sup>b</sup>	37.4 ± 1.6 <sup>ab</sup>
0.05%	42.8 ± 0.4 <sup>c</sup>	16.9 ± 0.0 <sup>a</sup>	66.0 ± 0.0 <sup>b</sup>	40.1 ± 0.7 <sup>b</sup>
0.05%ES	73.0 ± 0.8 <sup>d</sup>	19.5 ± 1.9 <sup>a</sup>	82.5 ± 0.7 <sup>c</sup>	9.7 ± 0.8 <sup>c</sup>

Mean values ± standard deviation. Mean values with different superscript letters in the same column represent significant differences ( $p < 0.05$ ) among the samples according to ANOVA and Tukey's multiple comparison tests.

### 3.2 Thermal properties

Differential Scanning Calorimetry (DSC) assays were carried out to evaluate how the CuO nanoparticles affected the thermal properties of the PHBVs matrix. Table 3 gathers thermal parameters (melting/crystallization temperature and melting enthalpy) of the developed samples which were determined from the first heating run, offering information related to the thermal characteristics of the so obtained material. Figure 6 shows representative first heating thermograms for each sample. The first clear observation is that the method of CuO incorporation, either by melt-mixing or as an electrospun coating, affected the thermal behavior of the PHBVs films. Thus, when CuO nanoparticles were directly added in the melt mixing process, the

DSC curves of the first heating scan showed two distinguishable melting peaks, which occurred between 165°C and 172°C. Multiple melting peaks occurring during the DSC first heating scan of PHBV and PHBV containing metal nanoparticles have been previously interpreted as a result of a melting-recrystallization process during the thermal run [19-21]. Nevertheless, compared to the neat PHBVs, the active films prepared by melt compounding, i.e. 0.1% and 0.05% films, did not present any significant difference in their melting enthalpy ( $\Delta H_m$ ) or crystallization temperature ( $T_c$ ) suggesting that the nanoparticles do not interfere with crystallization.

In contrast, the addition of CuO within the coated structures led to a significant decrease in the melting enthalpy with regard to the neat PHBVs and their nanocomposites. This agrees with the results reported earlier by Castro-Mayorga et. al. [22] which ascribed the thermal behavior variations to the more homogeneous melting of the fibers due to the high surface to volume ratio of the electrospun materials as compared to a thicker continuous film. These results do not necessarily translate into crystallinity due to the differential behavior during melting of the materials and the crystallinity development observed during the DSC run.

**Table 3.** DSC maximum of melting ( $T_m$ ) and melting enthalpy ( $\Delta H_m$ ) obtained from the first heating scan of the neat PHBVs film and their CuO nanocomposite/coated systems. \* The degree of crystallinity ( $X_c$ ) was determined by WAXD.

Sample	$T_{m1}$ (°C)	$T_{m2}$ (°C)	$T_c$ (°C)	$\Delta H_m$	$X_c^*$
				(J/g PHBVs)	(WAXD)
PHBVs	169.6 ± 2.4 <sup>a</sup>	173.2 ± 1.0 <sup>a</sup>	107.1 ± 1.0 <sup>a</sup>	74 ± 2 <sup>a</sup>	66 ± 1 <sup>a</sup>
0.10%	165.3 ± 0.9 <sup>a</sup>	171.5 ± 0.5 <sup>a</sup>	104.9 ± 0.3 <sup>a</sup>	75 ± 2 <sup>a</sup>	66 ± 1 <sup>a</sup>
0.05%	165.1 ± 0.7 <sup>a</sup>	171.4 ± 0.5 <sup>a</sup>	103.8 ± 0.7 <sup>a</sup>	77 ± 2 <sup>a</sup>	64 ± 1 <sup>a</sup>
0.05% ES	169.9 ± 2.7 <sup>a</sup>		107.6 ± 2.5 <sup>a</sup>	69 ± 1 <sup>b</sup>	57 ± 1 <sup>b</sup>

Mean values with different superscript letters in the same column represent significant differences ( $p < 0.05$ ) among the samples according to ANOVA and Tukey's multiple comparison tests

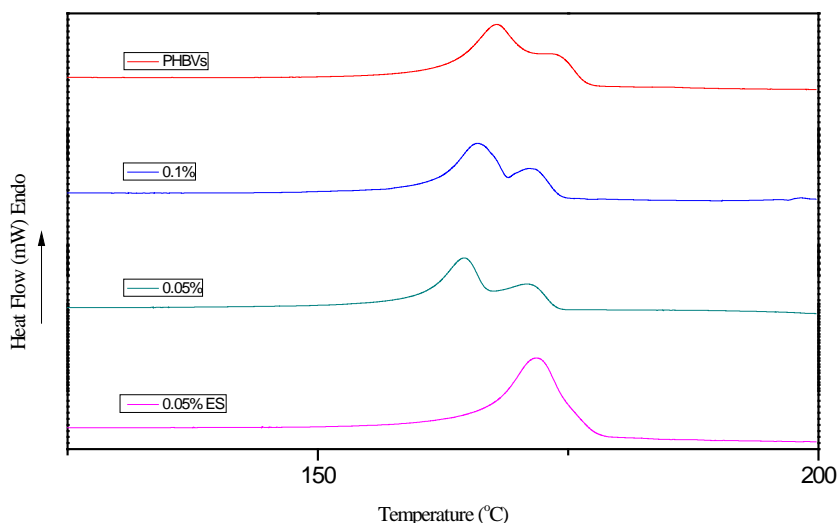


**Figure 6.** DSC thermograms of the first heating run of the neat PHBV films and their CuO nanocomposite/coated systems.

In order to have a more reliable source of crystallinity information, the effect of the CuO addition and the processing type on the PHBVs crystallinity was also analyzed by WAXD (Fig. 7). The X-Ray patterns of all samples showed the typical peaks at  $2\theta$  angles of  $13.6^\circ$ ,  $17.1^\circ$  and  $22.6^\circ$ , corresponding to the (0 2 0), (1 1 0) and (1 0 1) lattice planes of the orthorhombic unit cell of PHBV [23, 24]. A more intense peak at  $2\theta = 26^\circ$  was found and associated to the (0 2 2) reflection of boron nitride, which has been recently reported by Sanchez-Safont et al. [25] as a nucleating agent used in the commercial PHBV3 grade used as matrix. No significant differences in the diffraction peak positions were observed between the neat and the active film. This suggests that the crystal morphology of the PHBVs did not noticeably change with the CuO addition neither with the processing type. However, the lower intensity of the diffraction peaks of 0.05% coated films pointed out a lower crystallinity degree for the electrospun coating layer (also supported by the DSC results shown in the Table 3).

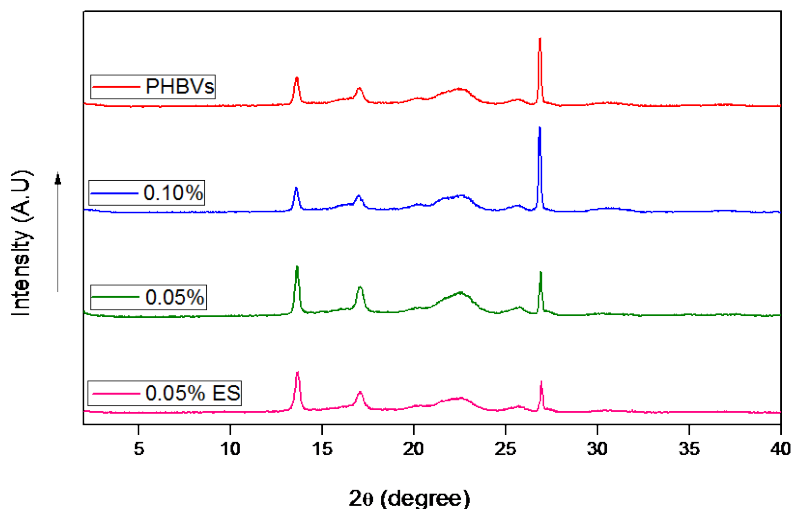


**Figure 7.** WAXD diffractograms of the neat PHBVs films and their CuO nanocomposite/coated systems.

### 3.3 Mechanical properties

Elastic modulus (E), elongation at break (EAB) and tensile strength (TS) were measured for the different specimens and the results are shown in Table 4. In general, mechanical properties were not significantly altered by the addition of CuO either by the melt-mixing process or by the coating methodology. The negligible impact of CuO on mechanical properties of the active films could be explained mainly by the low CuO loading and the high nanoparticles dispersion. These results were in line with the previous observations by Castro-Mayorga et al. [17, 22] and Jeong et al. [26] in which highly dispersed silver nanoparticles did not present a significant effect on PHBV melt compounded nanocomposites.

**Table 4.** Tensile parameters (E: Elastic modulus, EAB: Elongation at break and TS: Tensile strength and) of the neat PHBVs films and their CuO nanocomposite/coated systems.

Sample	E (GPa)	EAB (%)	TS (MPa)
PHBVs	2.4 ± 0.0 <sup>a</sup>	1.7 ± 0.2 <sup>a</sup>	35.8 ± 4.0 <sup>a</sup>
0.10%	2.4 ± 0.1 <sup>a</sup>	1.9 ± 0.1 <sup>a</sup>	39.3 ± 2.6 <sup>a</sup>
0.05%	2.3 ± 0.1 <sup>a</sup>	2.1 ± 0.2 <sup>a</sup>	41.9 ± 2.5 <sup>a</sup>
0.05% ES	2.3 ± 0.2 <sup>a</sup>	1.8 ± 0.2 <sup>a</sup>	34.2 ± 4.4 <sup>a</sup>

Mean values with different superscript letters in the same column represent significant differences ( $p < 0.05$ ) among the samples according to ANOVA and Tukey's multiple comparison tests

### 3.4 Barrier properties

The barrier properties are key for the application use of the materials in food packaging. The water vapour permeability (WVP) and oxygen permeability (OP) of the nanocomposite and coated systems are summarized in Table 5. As the table shows, the WVP of the obtained films increased with the addition of CuO, more especially when the fibers mats were put as an antimicrobial active coating onto PHBV3 matrix. This behavior might be related with the more hydrophilic character of the electrospun fibers mats prepared with PHBV18/CuO as compared to the neat PHBV3 film used as substrate in the coated system. In fact, Castro-Mayorga et. al [17] determined that the water uptake values of the neat PHBV18 ( $32.1 \pm 1.2\%$ ) is significantly greater than that for the neat PHBV3 ( $9.8 \pm 0.6\%$ ). Moreover, some authors reported on the superhydrophilic behavior of CuO-based surfaces [27, 28].

**Table 5.** Water vapor permeability and oxygen permeability of the neat PHBV<sub>s</sub> films and their CuO nanocomposite/coating systems.

Sample	WVP (Kg m/ Pa. s. m <sup>2</sup> )	OP (m <sup>3</sup> .m/m <sup>2</sup> . s .Pa) 80% RH
PHBV <sub>s</sub>	1.36 ± 0.17 e <sup>-15</sup> a	1.90 ± 0.11 e <sup>-19</sup> ac
0.10%	2.20 ± 0.31 e <sup>-15</sup> b	1.45 ± 0.11 e <sup>-19</sup> ab
0.05%	2.57 ± 0.07 e <sup>-15</sup> bc	1.25 ± 0.06 e <sup>-19</sup> b
0.05% ES	3.04 ± 0.27 e <sup>-15</sup> c	2.00 ± 0.14 e <sup>-19</sup> c

Mean values with different superscript letters in the same column represent significant differences ( $p < 0.05$ ) among the samples according to ANOVA and Tukey's multiple comparison tests

The addition of 0.05% CuO to the nanocomposites reduced the OP of the PHBV<sub>s</sub> mixture by *ca.* 34.2 % which is more likely explained by the additional tortuous path created by the well dispersed and distributed nanoparticles. However, an increase in the CuO loading did not improve the oxygen barrier properties of the PHBV<sub>s</sub> mixture. The oxygen permeability of the coated system (0.05%ES) was higher than its counterpart prepared by melt-compounding (0.05%), which might be associated with its lower crystallinity degree.

### 3.5 Antimicrobial properties

In this work, the antibacterial activity of the nanocomposites films and the coating structures containing CuO nanoparticles was explored against two food-borne pathogens: the Gram-negative *Salmonella enterica* and the Gram-positive *Listeria monocytogenes*, and the results are gathered in Table 6. As can be observed, PHBV<sub>s</sub> mixture (without CuO) did not exhibit antibacterial activity, whereas, after 24 h of exposure, a reduction of *ca.* 5 log CFU/mL of *Salmonella enterica* was recorded for those films prepared with 0.05% CuO by melt-mixing and no viable count of bacteria were recorded either for nanocomposites films containing 0.1% CuO or the 0.05% ES coating structure. Interestingly, after 24 h of exposure, no viable counts of

## *Chapter VII*

*L. monocytogenes* were recorded in any of the samples. The more effective inactivation of *L. monocytogenes* should be attributed to structural and chemical compositional differences between cell surfaces of Gram-positive and Gram-negative bacteria [17, 29].

The virucidal activity against murine norovirus was also recorded in these films and reductions in the infectious titers of MNV inoculated in nanocomposites and coated structures are shown in Table 5. Accordantly to the bacterial results, coating structures seem to be more effective against murine norovirus than nanocomposite films. Results show that MNV titers decreased by more than 2 logs TCID<sub>50</sub>/ml when in contact with nanocomposite films containing 0.05 and 0.1 wt.% CuO while no infectious MNV were recovered when in contact with the coated structure.

Therefore, it was demonstrated how by incorporating CuO into an electrospun coating form, it can be reduced the CuO loading, improve the nanoparticles dispersion and still achieve a significant bactericidal and virucidal performance. This could be of great interest for antimicrobial food packaging applications since the coating structure containing 0.05 wt.% CuO (0.05%-ES) is below the permitted migration limit (5mg Cu/Kg food) established by the current EU regulation (Commission Regulation (EU) No 10/2011 of 14 January 2011) for a hypothetical package surface of 6 dm<sup>2</sup>/Kg food, although there is not a specific regulation for nanoparticles.

**Table 6.** Antibacterial and virucidal microbial activity of the neat PHBVs films and their CuO nanocomposites/coating systems. against *S. enterica*, *L.* and murine Norovirus after 24h of exposure. The detection limit were 20 CFU/mL and 1.15 TCID50/mL. \* One negative samples out of three

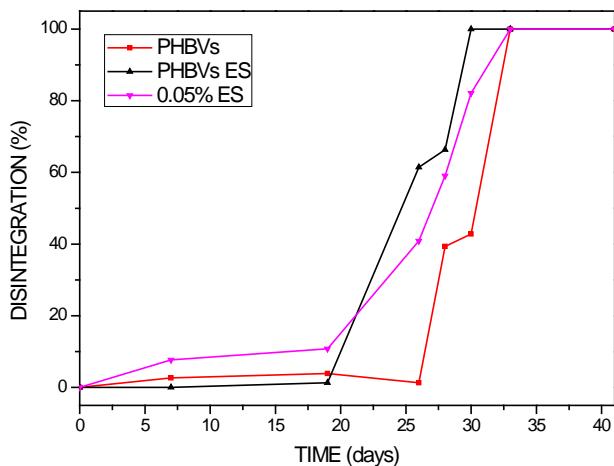
	<i>Salmonella enterica</i>			<i>Listeria monocytogenes</i>		
	CFU/mL	LOG (CFU/mL)	R	CFU/mL	LOG (CFU/mL)	R
<b>Control</b>	$(2.25 \pm 0.79) \times 10^7$	$7.33 \pm 0.14$	-	$(1.95 \pm 0.8) \times 10^5$	$5.26 \pm 0.21$	-
<b>0.1%</b>	ND	-	> 6.23	ND	-	> 4.16
<b>0.05%</b>	$(2.25 \pm 1.42) \times 10^2$	$2.30 \pm 0.29$	5.03	ND	-	> 4.16
<b>0.05% ES</b>	ND	ND	> 6.23	ND	-	> 4.16

	murine norovirus		
	TCID50/mL	LOG (TCID50/mL)	R
<b>Control</b>	$(5.83 \pm 1.17) \times 10^5$	$5.95 \pm 0.35$	-
<b>0.1%</b>	$(5.13 \pm 1.19) \times 10^2$	$2.76 \pm 0.09$	3.19
<b>0.05%</b>	$(1.39 \pm 0.52) \times 10^4$	$4.12 \pm 1.91$	1.83
<b>0.05% ES</b>	ND	ND	>4.81

### 3.6 Biodegradability

PHBV is known to undergo biodegradation in composting conditions within a short time, being this one of the main advantages of these materials for short time applications, such as packaging. However, in this work an antimicrobial agent has been introduced in the PHBV which may potentially interfere in its biodegradation; thus, the disintegrability of the most effective antimicrobial materials and their counterpart (without CuO) were assessed by measuring the weight loss over composting time according to the ISO 20200 standard. Figure 8 shows the evolution of the disintegration (%) over time for the PHBVs films, 0.05% ES films and bilayer PHBVs systems consisting of a PHBV3 matrix coated with electrospun PHBV18 fibers mat (PHBVs-ES) prepared for comparatives purposes.



**Figure 8.** Disintegration of the blends over time under composting conditions.

Weight loss remained practically unchanged until the 19th day of composting for the three compositions studied. This induction time has been already reported for the same PHBV3 grade [25, 30]. However, there is a difference in the onset time for the PHBV depending on the surface: PHBVs-ES samples start the degradation before melt compounded PHBVs. This difference in biodegradation onset time for PHBV can be ascribed to a different accessibility of the microorganism involved in the biodegradation to the amorphous fraction in the surface of the polymer, since biodegradation takes place in the first place on the amorphous fraction. Therefore, the higher surface crystallinity of the melt compounded PHBVs sample would explain this trend. Nevertheless, once the biodegradation has started, the biodegradation rate is similar for all the samples and the final disintegration is reached almost at the same time. Full biodegradation has occurred for all the samples in a period of 35 days. Therefore, the presence of 0.05% of CuO, although having an antimicrobial effect, did not affect the biodegradability of the final material.

## 4. Conclusions

---

Antimicrobial PHBV nanocomposites and coated structures containing CuO nanoparticles were developed and characterized. It was confirmed that the antimicrobial activity increase when the CuO is loaded into electrospun fibers mats and deposited as a coating onto PHBV3 films. For instance, the antiviral activity against of the nanocomposites *vs.* the coated structures, both containing 0.05% of CuO improved by more than 225%; the bacterial reduction against *S. enterica* by at least 23%; and no viable cells of *L. monocytogenes* were detected in either of them. It was furthermore demonstrated that the CuO addition by means of electrospinning enhanced the nanoparticles dispersion and did not modify significantly the oxygen permeability, mechanical or optical properties. Instead, the water vapour permeability increased due to the more hydrophilic character of the PHBV18 coating and the poor dispersion of the higher nanoparticles loading. Interestingly, biodegradation tests showed that the coated structures were fully biodegraded in a period of 35 days at composting condition.

## 5. Acknowledgements

---

The authors would like to thank Prof. Maria Reis from Universidade Nova de Lisboa, and Dr. Catarina Oliveira, from Centro de Quimica fina e Biotecnologia, for the synthesis of PHBV18. This work was financially supported by the Spanish Ministry of Economy and Competitiveness (project AGL2015-63855-C2-1-R). J.L. Castro-Mayorga is supported by the Administrative Department of Science, Technology and Innovation (Colciencias) of Colombian Government. M. J. Fabra is

recipient of a Ramon y Cajal contract from the Spanish Ministry of Economy and Competitiveness.

## 6. References

---

1. M. Moritz and M. Geszke-Moritz, "The newest achievements in synthesis, immobilization and practical applications of antibacterial nanoparticles," *Chemical Engineering Journal*, vol. 228, pp. 596-613, 2013.
2. M. S. Usman, M. E. E. Zowalaty, K. Shamel, N. Zainuddin, M. Salama and N. A. Ibrahim, "Synthesis, characterization, and antimicrobial properties of copper nanoparticles," *International Journal of Nanomedicine*, vol. 8, pp. 4467-4479, 2013.
3. G. Faúndez, M. Troncoso, P. Navarrete and G. Figueroa, "Antimicrobial activity of copper surfaces against suspensions of *Salmonella enterica* and *Campylobacter jejuni*," *BMC Microbiology*, vol. 4, pp. 19-19, 2004.
4. M. Vincent, P. Hartemann and M. Engels-Deutsch, "Antimicrobial applications of copper," *International Journal of Hygiene and Environmental Health*, vol. 219, no. 7, Part A, pp. 585-591, 2016.
5. G. Grass, C. Rensing and M. Solioz, "Metallic Copper as an Antimicrobial Surface," *Applied and Environmental Microbiology*, vol. 77, no. 5, pp. 1541-1547, 2011.
6. R. P. Allaker, M. A. Vargas-Reus and G. G. Ren, "Nanometals as Antimicrobials," in *Antimicrobial Polymers*, Ed., pp. 327-350, 2011.
7. O. Bondarenko, K. Juganson, A. Ivask, K. Kasemets, M. Mortimer and A. Kahru, "Toxicity of Ag, CuO and ZnO nanoparticles to selected environmentally relevant test organisms and mammalian cells in vitro: a critical review," *Archives of Toxicology*, vol. 87, no. 7, pp. 1181-1200, 2013.
8. P. Appendini and J. H. Hotchkiss, "Review of antimicrobial food packaging," *Innovative Food Science and Emerging Technologies*, vol. 3, no. 2, pp. 113-126, 2002.
9. A. Frenot and I. S. Chronakis, "Polymer nanofibers assembled by electrospinning," *Current Opinion in Colloid and Interface Science*, vol. 8, no. 1-2, pp. 64-75, 2003.
10. Y. Echegoyen, M. J. Fabra, J. L. Castro-Mayorga, A. Cherpinski and J. M. Lagaron, "High throughput electro-hydrodynamic processing in food encapsulation and food packaging applications: Viewpoint," *Trends in Food Science and Technology*, vol. 60, pp. 71-79, 2017.

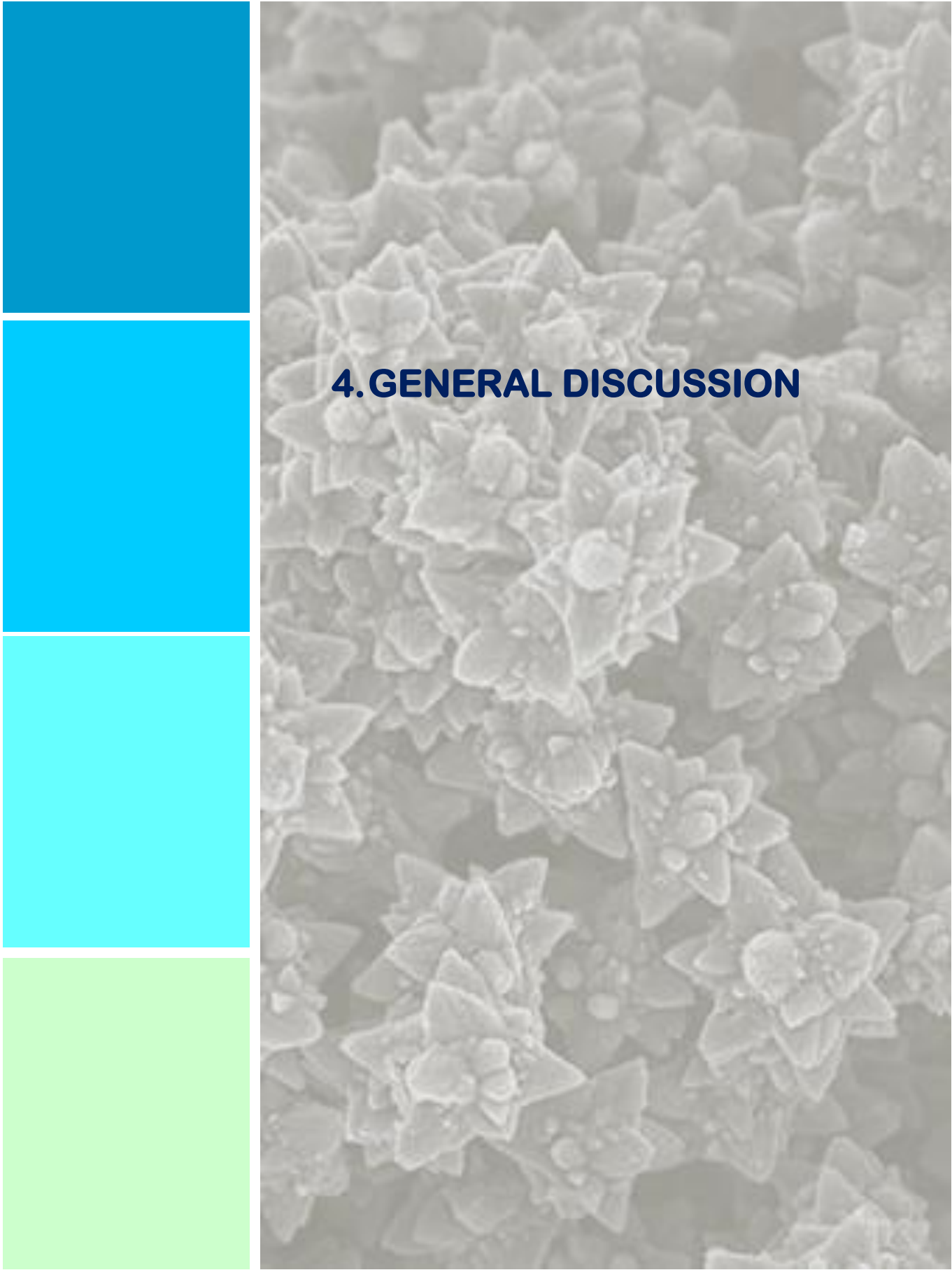
11. D. Plackett and I. Siró, "Polyhydroxyalkanoates (phas) for food packaging," in *Multifunctional and Nanoreinforced Polymers for Food Packaging*, Ed., pp. 498-526, 2011.
12. M. Erceg, T. Kovačić and I. Klarić, "Thermal degradation of poly(3-hydroxybutyrate) plasticized with acetyl tributyl citrate," *Polymer Degradation and Stability*, vol. 90, no. 2, pp. 313-318, 2005.
13. E. Bugnicourt, P. Cinelli, A. Lazzeri and V. Alvarez, "Polyhydroxyalkanoate (PHA): Review of synthesis, characteristics, processing and potential applications in packaging," *Express Polymer Letters*, vol. 8, no. 11, pp. 791-808, 2014.
14. A. Martínez-Abad, L. Cabedo, C. S. S. Oliveira, L. Hilliou, M. Reis and J. M. Lagarón, "Characterization of polyhydroxyalkanoate blends incorporating unpurified biosustainably produced poly(3-hydroxybutyrate-co-3-hydroxyvalerate)," *Journal of Applied Polymer Science*, 2015.
15. M. J. Fabra, A. López-Rubio and J. M. Lagaron, "On the use of different hydrocolloids as electrospun adhesive interlayers to enhance the barrier properties of polyhydroxyalkanoates of interest in fully renewable food packaging concepts," *Food Hydrocolloids*, vol. 39, pp. 77-84, 2014.
16. F. X. Abad, R. M. Pinto, J. M. Diez and A. Bosch, "Disinfection of human enteric viruses in water by copper and silver in combination with low levels of chlorine," *Applied and Environmental Microbiology*, vol. 60, no. 7, pp. 2377-2383, 1994.
17. J. L. Castro-Mayorga, M. J. Fabra and J. M. Lagaron, "Stabilized nanosilver based antimicrobial poly(3-hydroxybutyrate-co-3-hydroxyvalerate) nanocomposites of interest in active food packaging," *Innovative Food Science and Emerging Technologies*, vol. 33, pp. 524-533, 2016.
18. J. L. Castro-Mayorga, A. Martínez-Abad, M. J. Fabra, C. Olivera, M. Reis and J. M. Lagarón, "Stabilization of antimicrobial silver nanoparticles by a polyhydroxyalkanoate obtained from mixed bacterial culture," *International Journal of Biological Macromolecules*, vol. 71, pp. 103-110, 2014.
19. J. L. Castro-Mayorga, M. J. Fabra, A. M. Pourrahimi, R. T. Olsson and J. M. Lagaron, "The impact of zinc oxide particle morphology as an antimicrobial and when incorporated in poly(3-hydroxybutyrate-co-3-hydroxyvalerate) films for food packaging and food contact surfaces applications," *Food and Bioproducts Processing*, vol. 101, pp. 32-44, 2017.
20. M. Martínez-Sanz, M. Villano, C. Oliveira, M. G. E. Albuquerque, M. Majone, M. Reis, A. Lopez-Rubio and J. M. Lagaron, "Characterization of polyhydroxyalkanoates synthesized from microbial mixed cultures and of their nanobiocomposites with bacterial cellulose nanowhiskers," *New Biotechnology*, vol. 31, no. 4, pp. 364-376, 2014.

## Chapter VII

21. J. Ambrosio-Martin, M. J. Fabra, A. López-Rubio, G. Gorrasi, A. Sorrentino and J. M. Lagaron, "Assessment of Ball Milling as a Compounding Technique to Develop Nanocomposites of Poly(3-Hydroxybutyrate-co-3-Hydroxyvalerate) and Bacterial Cellulose Nanowhiskers," *Journal of Polymers and the Environment*, vol. 24, no. 3, pp. 241-254, 2016.
22. J. L. Castro-Mayorga, M. J. Fabra, L. Cabedo and J. M. Lagaron, "On the use of the electrospinning coating technique to produce antimicrobial polyhydroxyalkanoate materials containing in situ-stabilized silver nanoparticles," *Nanomaterials*, vol. 7, no. 1, 2017.
23. L. N. Carli, J. S. Crespo and R. S. Mauler, "PHBV nanocomposites based on organomodified montmorillonite and halloysite: The effect of clay type on the morphology and thermal and mechanical properties," *Composites Part A: Applied Science and Manufacturing*, vol. 42, no. 11, pp. 1601-1608, 2011.
24. J. Li, C. R. Sun and X. Q. Zhang, "Preparation, thermal properties, and morphology of graft copolymers in reactive blends of PHBV and PPC," *Polymer Composites*, vol. 33, no. 10, pp. 1737-1749, 2012.
25. E. L. Sanchez-Safont, J. Gonzalez-Ausejo, J. Gamez-Perez, J. M. Lagaron and L. Cabedo, "Poly(3-Hydroxybutyrate-co-3-Hydroxyvalerate)/ purified cellulose fiber composites by melt blending: characterization and degradation in composting conditions," *Journal of Renewable Materials*, vol. 4, no. 2, pp. 123-132, 2016.
26. S. Jeong, S. Yeo and S. Yi, "The effect of filler particle size on the antibacterial properties of compounded polymer/silver fibers," *Journal of Materials Science*, vol. 40, no. 20, pp. 5407-5411, 2005.
27. Z. Qiao bao, X. Daguo, H. Tak Fu and Z. Kaili, "Facile synthesis, growth mechanism and reversible superhydrophobic and superhydrophilic properties of non-flaking CuO nanowires grown from porous copper substrates," *Nanotechnology*, vol. 24, no. 6, pp. 065602, 2013.
28. G. Fan and F. Li, "Effect of sodium borohydride on growth process of controlled flower-like nanostructured Cu<sub>2</sub>O/CuO films and their hydrophobic property," *Chemical Engineering Journal*, vol. 167, no. 1, pp. 388-396, 2011.
29. A. Grigor'Eva, I. Saranina, N. Tikunova, A. Safonov, N. Timoshenko, A. Rebrov and E. Ryabchikova, "Fine mechanisms of the interaction of silver nanoparticles with the cells of Salmonella typhimurium and Staphylococcus aureus," *BioMetals*, vol. 26, no. 3, pp. 479-488, 2013.

30. A. Martínez-Abad, J. González-Ausejo, J. M. Lagarón and L. Cabedo, "Biodegradable poly(3-hydroxybutyrate-co-3-hydroxyvalerate)/thermoplastic polyurethane blends with improved mechanical and barrier performance," *Polymer Degradation and Stability*, vol. 132, pp. 52-61, 2016.





## **4. GENERAL DISCUSSION**



## 4. General discussion

---

With increasing concerns regarding foodborne illnesses and consumer preferences towards minimally processed, easily prepared and ready-to-eat 'fresh' products, the use of alternative technologies as active packaging and particularly, metal nanoparticles, exhibiting antimicrobial activity has emerged as a great promise for food preservation and on the overall for the development of antimicrobial food contact surfaces. In addition, the lack of biodegradability and renewability of most plastics being currently commercialized and their environmental concerns have driven the research for economically viable, biodegradable and bio-based polymers. In response to these needs, the present work deals with the *development of biotechnological routes for the synthesis of polyhydroxyalkanoates based on nanometals for antimicrobial applications and in particular for antimicrobial active food packaging.*

In recent years, metal and metal oxide nanoparticles based on silver [1, 2], gold [3], copper [4], copper oxide [5], zinc oxide [6], maghemite [7, 8], and magnetite have been increasingly applied in medicine, dentistry, pharmacy, and biology. As before mentioned in the introduction, the wide interest in metal nanoparticles bioapplications is due to their excellent antimicrobial activity [9] and their improved stability and safety in comparison with their organic antimicrobial counterparts [10]. However, the preparation of highly dispersed and distributed metal nanoparticles systems, particularly based on silver, exhibiting sufficient stability in time and resistance to external factors remained a challenge.

Regarding the silver, which is one of the strongest antimicrobial agents, several works have investigated the effects of adding ionic silver and silver containing

## *General discussion*

nanofillers into different polymer matrices such as poly(vinyl alcohol) [11-13] and poly(lactic acid) [14, 15], but none of the existing technologies addressed the idea of developing the *in situ* AgNPs synthesis and stabilization into biodegradable polymers when generally speaking, and into microbial derived polyhydroxyalkanoates in particular.

In this dissertation first chapter, the stability of the *in situ* produced AgNPs by chemical reduction into PHBV suspensions was compared to the AgNPs prepared by mixing AgNPs with the PHBV suspension and to aqueous AgNPs suspension without polymer. The unique capacity of PHBV derived from microbial mixed cultures to retain and to stabilize AgNPs prepared *in situ* within the biopolymer suspension was demonstrated. FTIR analysis suggested a possible interaction between the protein residues of the unpurified PHBV and the AgNPs which promoted their stabilization during the synthesis and storage (at least for 40 days). Thus, the particles in the *in situ* samples were considerably smaller and better distributed ( $7 \pm 3$  nm) than in the physically mixed ( $23 \pm 10$  nm) and aqueous AgNPs samples ( $17 \pm 14$  nm). Furthermore, it was also demonstrated that the dispersion and size distribution of AgNPs affects their antimicrobial performance, for instance, the *in situ* prepared materials had a stronger and more long-lasting antibacterial activity against *Salmonella enterica* (more than 8 LOG CFU/mL of bacterial reduction at 0.5 ppm after 40 days of aging compared to the 2 LOG CFU/mL of reduction for the materials prepared by mixing). It should be also highlighted that the polymer used in these experiments (PHBV18, 18 mol% valerate) was obtained by an innovative bioprocess developed within a European cooperating project with Prof. M. Reis and collaborators, which allowed the production of low cost polyhydroxyalkanoates by using microbial mixed cultures and cheese whey as feedstock.

The AgNPs stability achieved by the *in situ* method developed in this work was higher than or similar to those reported for other stabilizing agents [16-18] counting

on the extra advantage of avoiding the use of synthetic surfactants as stabilizer. Moreover, the incorporation of the AgNPs into PHBV prevented their agglomeration and likely their migration, which in return, increase their potential for application as packaging material. In fact, AgNPs-PHBV nanocomposites were subsequently prepared by melt compounding of the enriched masterbatch form of the *in situ* synthesized AgNPs (PHBV18/AgNPs) and a commercial PHBV (PHBV3, 3 mol% valerate, Tianan, Ningbo, China). The so-obtained materials presented good thermal stability and excellent and stable upon aging optical properties. The high dispersed and distributed AgNPs, whose diameter ranges between 10 and 60 nm, with a maximum frequency at around 41-50 nm and with a small percentage of agglomerates, acted as a tortuosity element, providing improved barrier properties. Furthermore, the developed nanocomposites exhibited a strong and prolonged (ever after seven months) bactericidal activity (of more than 5 log CFU/mL) against pathogens such as *L. monocytogenes* and *S. enterica* at the low silver content of  $0.04 \pm 0.002$  wt.%.

In spite of the previous progress beyond the art, and especially taking into account that the application of these materials in the restrictive food legislation frames could be severely limited because of the use of AgNPs and the possible health and environmental risks, the aim of the further work described in the third chapter was the development of a new strategy based on the development of a coating design to reduce the silver loading in the packaging while keeping the antibacterial performance. For this purpose, a bilayer system of PHBV3 and nanostructured silver-based coating of PHBV3/PHBV18 made by means of the electrospinning coating technique was developed and characterized. The electrospinning process favored the proper AgNPs dispersion and entrapment and avoided the agglomeration that typically occurs when the nanocomposites are processed by conventional melt compounding methods [19-21]. Accordingly, the coated systems, containing

## *General discussion*

0.002 ± 0.0005 wt.% of silver content (20 times lower than the previously cited nanocomposites of chapter I), presented a bactericidal effect against *S. enterica* (i.e. a bacterial reduction of 5 log CFU/mL) and did not significantly modified the physicochemical properties of the neat PHBV3 polymer.

The route explored above also led to generate more efficient active heterogeneous-across-thickness films for antiviral applications. Throughout the fourth chapter, the effect of silver nitrate and AgNPs on norovirus surrogates was investigated. It was found that both chemical forms significantly decreased the Murine norovirus (MNV) and Feline calicivirus (FCV) infectivity in a dose-dependent manner between concentration of 2.1 and 21 ppm and that, as in the case of antibacterial, the virucidal performance was found to depend on the type of virus and mainly on the silver stabilization degree. In this case, bilayer films were also prepared by electrospinning, but this time the active layer was made from the AgNPs-based masterbatch (without dilution with virgin polymer). These films showed a complete reduction of FCV infectivity and a reduced antiviral effect of 0.86 log TCID<sub>50</sub> against MNV when the tests were performed at 37°C, while not significantly virucidal effect were detected at 25°C. These results are in agreement with previous works carried out in the group that already reported the effect of temperature on silver antiviral activity [22] and hence the need to design a custom made antimicrobial material adapted for the final intended use.

Once the effectiveness of the silver-based polyhydroxyalkanoates nanocomposites was deeply explored and achieved, the challenge of developing an integrated bioprocess for the biological synthesis of AgNPs and polyhydroxybutyrate (PHB) was undertaken. To do so, the traditional fermentation process from *Cupriavidus necator* and sodium gluconate as carbon source was used a starting point. First, a comparative study of the chemical and biological synthesis of AgNPs during the fermentation at shake flask-scale was carried out and secondly the process was scaled-up to 10 liters

bioreactor. This work led to a patent application P201630829, which protected the unknown capacity of *C. necator* to reduce silver salts and produce polyhydroxyalkanoates and AgNPs without the need for adding a synthetic reducing or capping agent. Through these experiments it was also observed that the method of synthesis (with or without reducing agent) affected the dispersion of the AgNPs and therefore their antimicrobial performance, being the biosynthesized nanoparticles the most effective method for killing *S. enterica* and *L. monocytogenes* food pathogens. Moreover, the incorporation of AgNPs by means of this method did not cause any detrimental effects on the thermal degradation and the optical properties of the polymer, although a slight reduction in crystallinity was seen. Thus, the procedure here developed allows the production of bio-based material for antimicrobial applications, which is suitable industrial scale uses.

Despite the substantial progress in the research and production of silver ions and AgNPs based materials and their undeniable antimicrobial effectiveness against a wide range of microorganisms, there are still some difficulties in the opinion of some legislation bodies in characterizing, detecting and measuring the possible risks for the human health and for the environment, which currently limit the applications of silver-based technologies in the food and feed area. Indeed, as commented in the introduction section, the regulatory standards have been and -continue to be- a topic of debate across legislation bodies in Europe, US, Japan or Australia. Therefore, in addition to the silver studies, two non-silver antimicrobial systems, i.e. ZnO, CuO-based systems, were also developed and characterized in the sixth and seventh chapters of this PhD thesis.

The sixth chapter dealt with the study of the effect of ZnO particles size and morphology on the antimicrobial activity, thermal and barrier properties of PHBV/ZnO nanocomposites prepared by the previously developed strategies. In that work, ZnO micron and nano sized-particles with different morphologies were

## *General discussion*

synthesized by aqueous precipitation and evaluated as an antibacterial agent. The results showed that, like others metal compounds, the antibacterial activity of ZnO, depends on the type of bacteria but also on the surface reactivity of the particle, which improved by decreasing particle size to the nanorange as expected. Subsequently, the most effective bactericide system (i. e the smallest ZnO nanoparticles, with 25 nm of diameter), was used to prepare active PHBV films by three different methods: (i) direct melt-mixing, (ii) melt-mixing of preincorporated ZnO into electrospun fibers mats, and, (iii) as a coating system. The method of preparation and the ZnO loading both noticeable affected the barrier properties of the materials, resulting in a decrease in water vapour and oxygen permeability. On the other hand, the ZnO successfully improved the thermal stability of the melt mixed nanocomposites and exerted a strong and prolonged bactericide effect against *L. monocytogenes* (even after 15 water washing) when it was incorporated as electrospun coating.

Finally, active PHBV nanocomposites and coating structures containing CuO nanoparticles were developed and characterized. Once again, it was confirmed that the antimicrobial activity increases when the active agent is loaded into electrospun fibers mats and deposited as a coating onto PHBV3 films. In this work, the antiviral activity of the nanocomposites *vs.* the coated structures, both containing 0.05% of CuO, improved by more than 133%, the bacterial reduction against *S. enteric*, by at least 23% and no viable cells of *L. monocytogenes* were detected in either of them. It was furthermore demonstrated that the CuO addition by means of electrospinning enhanced the nanoparticles dispersion and did not modify significantly the oxygen permeability, mechanical or optical properties. Instead, and in a similar way as the ZnO- based materials, the water vapour permeability increased due to the more hydrophilic character of the PHBV18 coating and the poor dispersion of the higher nanoparticles loading required for achieving a good antimicrobial performance in the

blends. Interestingly, biodisintegration tests showed that the CuO active coating structures were fully biodegraded in a period of 35 days at composting condition.

Regarding metals migration, neither the zinc release from the coated structures containing 6 wt.% of ZnO (after several washing cycles) nor the Cu in composites containing 0.05 wt.% of CuO surpassed the current restriction limits (25mg Zn/kg and 5mg Cu/kg of food) established by the European legislation (Commission Regulation (EU) No 10/2011 of 14 January 2011). Nevertheless, additional migration work carried out in food simulants and further cytotoxicity assays need be performed from a risk management view point.

In summary, the results presented in this PhD thesis demonstrated how by incorporating stable and well dispersed metal nanoparticles in PHAs by the developed methods, it is possible to attain strong biocide nanocomposites and packaging structures that can be useful for antimicrobial active packaging applications.

## References

---

1. W. Zhou, Y. Ma, H. Yang, Y. Ding and X. Luo, "A label-free biosensor based on silver nanoparticles array for clinical detection of serum p53 in head and neck squamous cell carcinoma," *International Journal of Nanomedicine*, vol. 6, pp. 381-386, 2011.
2. R. Arunachalam, S. Dhanasingh, B. Kalimuthu, M. Uthirappan, C. Rose and A. B. Mandal, "Phytosynthesis of silver nanoparticles using *Coccinia grandis* leaf extract and its application in the photocatalytic degradation," *Colloids and Surfaces B: Biointerfaces*, vol. 94, pp. 226-230, 2012.
3. D. A. Giljohann, D. S. Seferos, W. L. Daniel, M. D. Massich, P. C. Patel and C. A. Mirkin, "Gold nanoparticles for biology and medicine," *Angewandte Chemie - International Edition*, vol. 49, no. 19, pp. 3280-3294, 2010.

## *General discussion*

4. J. Luo, S. Jiang, H. Zhang, J. Jiang and X. Liu, "A novel non-enzymatic glucose sensor based on Cu nanoparticle modified graphene sheets electrode," *Analytica Chimica Acta*, vol. 709, pp. 47-53, 2012.
5. J. Ping, S. Ru, K. Fan, J. Wu and Y. Ying, "Copper oxide nanoparticles and ionic liquid modified carbon electrode for the non-enzymatic electrochemical sensing of hydrogen peroxide," *Microchimica Acta*, vol. 171, no. 1, pp. 117-123, 2010.
6. X. Zhao and L. Qi, "Rapid microwave-assisted synthesis of hierarchical ZnO hollow spheres and their application in Cr(VI) removal," *Nanotechnology*, vol. 23, no. 23, pp. 235604, 2012.
7. A. Afkhami and R. Moosavi, "Adsorptive removal of Congo red, a carcinogenic textile dye, from aqueous solutions by maghemite nanoparticles," *Journal of Hazardous Materials*, vol. 174, no. 1-3, pp. 398-403, 2010.
8. M. Magro, G. Sinigaglia, L. Nodari, J. Tucek, K. Polakova, Z. Marusak, S. Cardillo, G. Salviulo, U. Russo, R. Stevanato, R. Zboril and F. Vianello, "Charge binding of rhodamine derivative to OH<sup>-</sup> stabilized nanomaghemite: Universal nanocarrier for construction of magnetofluorescent biosensors," *Acta Biomaterialia*, vol. 8, no. 6, pp. 2068-2076, 2012.
9. W. R. Li, X. B. Xie, Q. S. Shi, S. S. Duan, Y. S. Ouyang and Y. B. Chen, "Antibacterial effect of silver nanoparticles on Staphylococcus aureus," *BioMetals*, vol. 24, no. 1, pp. 135-141, 2011.
10. R. K. Dutta, B. P. Nenavathu, M. K. Gangishetty and A. V. R. Reddy, "Studies on antibacterial activity of ZnO nanoparticles by ROS induced lipid peroxidation," *Colloids and Surfaces B: Biointerfaces*, vol. 94, no. 0, pp. 143-150, 2012.
11. E. Fortunati, F. Luzi, D. Puglia, A. Terenzi, M. Vercellino, L. Visai, C. Santulli, L. Torre and J. M. Kenny, "Ternary PVA nanocomposites containing cellulose nanocrystals from different sources and silver particles: Part II," *Carbohydrate Polymers*, vol. 97, no. 2, pp. 837-848, 2013.
12. A. N. Krklješ, M. T. Marinović-Cincović, Z. M. Kačarević-Popović and J. M. Nedeljković, "Dynamic thermogravimetric degradation of gamma radiolytically synthesized Ag-PVA nanocomposites," *Thermochimica Acta*, vol. 460, no. 1-2, pp. 28-34, 2007.
13. Z. H. Mbhele, M. G. Salemane, C. G. C. E. Van Sittert, J. M. Nedeljković, V. Djoković and A. S. Luyt, "Fabrication and Characterization of Silver-Polyvinyl Alcohol Nanocomposites," *Chemistry of Materials*, vol. 15, no. 26, pp. 5019-5024, 2003.

14. A. Martínez-Abad, J. M. Lagarón and M. J. Ocio, "Antimicrobial beeswax coated polylactide films with silver control release capacity," *International Journal of Food Microbiology*, vol. 174, pp. 39-46, 2014.
15. M. A. Busolo and J. M. Lagaron, "Antimicrobial biocomposites of melt-compounded polylactide films containing silver-based engineered clays," *Journal of Plastic Film and Sheeting*, vol. 29, no. 3, pp. 290-305, 2013.
16. K. P. Bankura, D. Maity, M. M. R. Mollick, D. Mondal, B. Bhowmick, M. K. Bain, A. Chakraborty, J. Sarkar, K. Acharya and D. Chattopadhyay, "Synthesis, characterization and antimicrobial activity of dextran stabilized silver nanoparticles in aqueous medium," *Carbohydrate Polymers*, vol. 89, no. 4, pp. 1159-1165, 2012.
17. M. Mukherjee and A. Mahapatra, "Catalytic effect of silver nanoparticle on electron transfer reaction: Reduction of  $[\text{Co}(\text{NH}_3)_5\text{Cl}](\text{NO}_3)_2$  by iron(II)," *Colloids and Surfaces A: Physicochemical and Engineering Aspects*, vol. 350, no. 1-3, pp. 1-7, 2009.
18. P. Phukon, J. P. Saikia and B. K. Konwar, "Enhancing the stability of colloidal silver nanoparticles using polyhydroxyalkanoates (PHA) from *Bacillus circulans* (MTCC 8167) isolated from crude oil contaminated soil," *Colloids Surf B Biointerfaces*, vol. 86, no. 2, pp. 314-318, 2011.
19. S. Jeong, S. Yeo and S. Yi, "The effect of filler particle size on the antibacterial properties of compounded polymer/silver fibers," *Journal of Materials Science*, vol. 40, no. 20, pp. 5407-5411, 2005.
20. J. L. Castro-Mayorga, M. J. Fabra and J. M. Lagaron, "Stabilized nanosilver based antimicrobial poly(3-hydroxybutyrate-co-3-hydroxyvalerate) nanocomposites of interest in active food packaging," *Innovative Food Science and Emerging Technologies*, vol. 33, pp. 524-533, 2016.
21. C. Radheshkumar and H. Münstedt, "Morphology and mechanical properties of antimicrobial polyamide/silver composites," *Materials Letters*, vol. 59, no. 14-15, pp. 1949-1953, 2005.
22. A. Martínez-Abad, M. J. Ocio, J. M. Lagarón and G. Sánchez, "Evaluation of silver-infused polylactide films for inactivation of *Salmonella* and feline calicivirus in vitro and on fresh-cut vegetables," *International Journal of Food Microbiology*, vol. 162, no. 1, pp. 89-94, 2013.





## **5. CONCLUSIONS**



## 5. Conclusions

---

- I. PHBV18 produced from mixed microbial cultures fed with by-products was found to stabilize AgNPs prepared *in situ* within the biopolymer suspensions. A masterbatch enriched material containing well dispersed and distributed AgNPs with a high antimicrobial performance was developed without the need for surfactants or synthetic polymers as stabilizer or capping agents.
- II. The incorporation of AgNPs by means of melt compounding of the PHBV18/AgNPs masterbatch into PHBV3 resulted in materials with improved optical and barrier properties. The developed nanocomposites showed a strong and sustained (even after seven-months) antibacterial activity against the food borne-pathogens *Salmonella enterica* and *Listeria monocytogenes*.
- III. The electrospinning coating technique allowed the development of bilayer structures with improved nanometal dispersion and, thus, with a higher antibacterial and antiviral performance against *Salmonella enterica* and Norovirus surrogates at very low nanoparticles loadings.
- IV. The high dispersion and distribution of AgNPs, ZnO and CuO nanoparticles achieved by means of the electrospinning coating technique improved the thermal stability and optical properties of the PHAs films, despite the fact that some decreases in crystallinity and barrier properties were observed.
- V. An integrated bioprocess for the biological synthesis of AgNPs and PHB from the fermentation process with *Cupriavidus necator* was developed and scaled-up to fully automated 10 liters bioreactor. The inherent capacity of *C. necator* to reduce the silver salt and produce AgNPs without the need for adding a

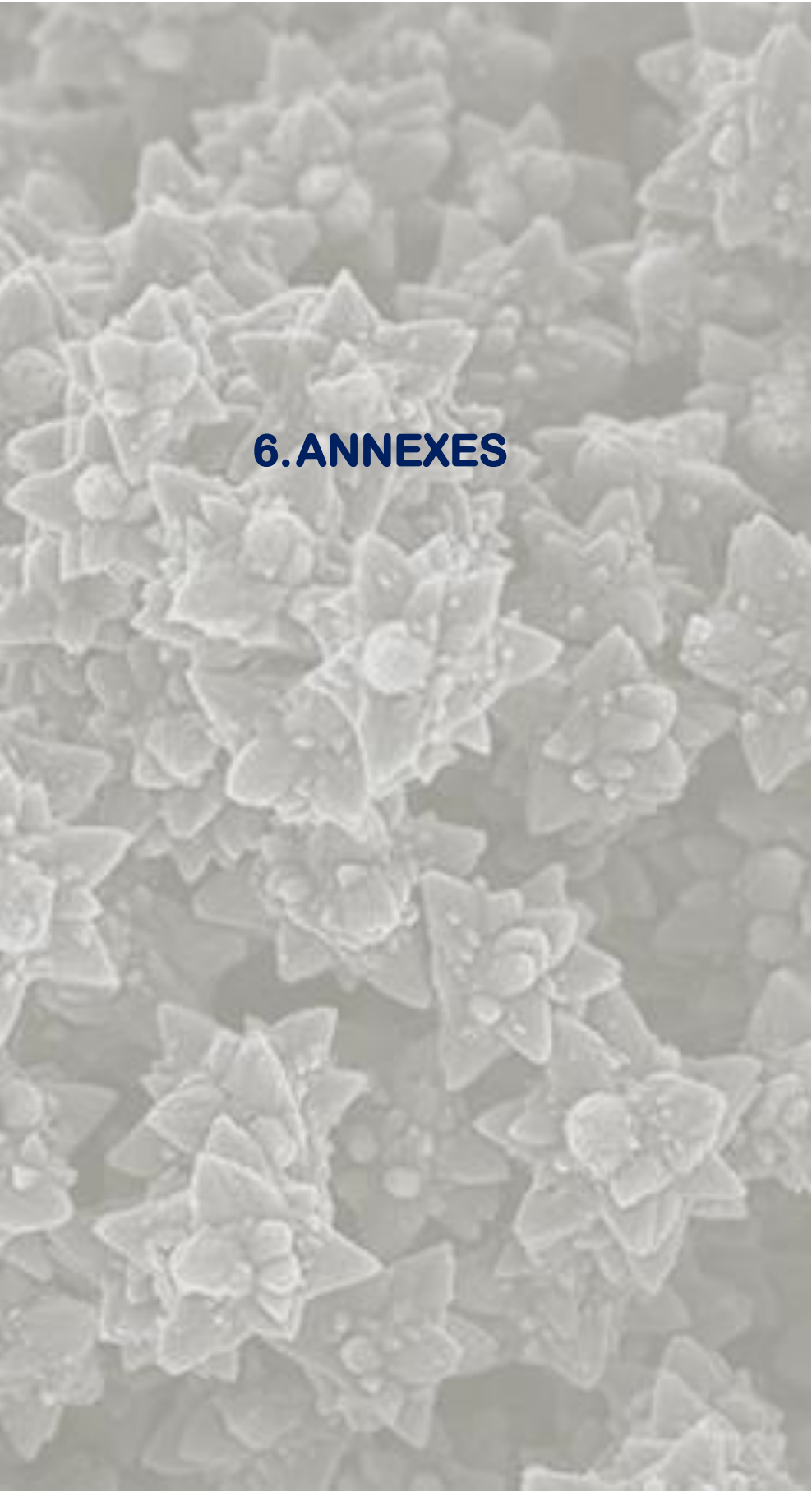
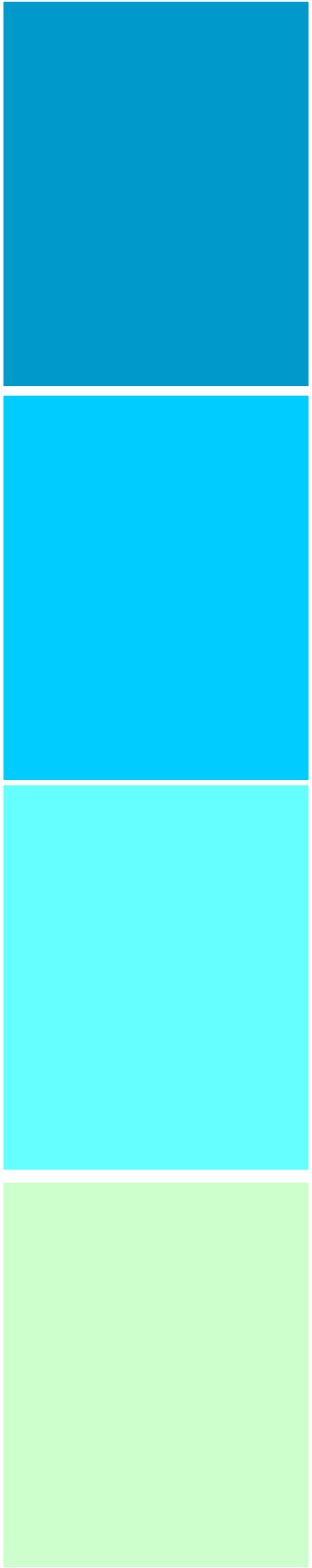
## *Conclusions*

reducing agent was demonstrated for the first time as well as the suitability of the so-obtained materials for antibacterial applications.

- VI. It was demonstrated that the antibacterial activity of ZnO particles depends on their morphology, especially on size and surface to volume ratios. The smaller size particles, i.e. those in the nanorange, with the larger effective surface area, resulted in the highest antibacterial effect against *Listeria monocytogenes*.
- VII. The metal nanoparticles analyzed had an antimicrobial effect against the food borne pathogens *L. monocytogenes*, *S. enterica* and the norovirus surrogates (Murine Norovirus and Feline Calicivirus) in a dose-dependent manner. Furthermore, their antimicrobial activity was also found to depend on the type of microorganism, on their stabilization degree and their availability in the surface of the active films.
- VIII. The incorporation of CuO into PHBV3/PHBV18 films did not impair the biodegradability of the active films, which fully biodegraded over a period of 35 days at composting condition.
- IX. The zinc release from the coated structures containing 6 wt.% of ZnO after several water-washing cycles or the total Cu in nanocomposites and coated structures containing 0.05 wt.% of CuO did not surpassed the current restriction limits established by the European Food Safety Authority for Zn and Cu. However, additional research on the migration and cytotoxicity of the nano-metal based materials should be carried out to do a correct food contact compliancy and safety assessment.
- X. The stabilization of nanometals as well as a dispersion/distribution of them into the biopolymer matrices are key aspects to successfully improve the bactericidal and virucidal properties of the nanocomposite films at low nanometal contents.

- XI. The technologies developed in this PhD thesis have shown significant potential in antimicrobial applications but more specifically in the development of efficient antimicrobial active biopackaging.





## 6. ANNEXES



## **ANNEX A**

---

---

### **LIST OF PUBLICATION**





## Stabilization of antimicrobial silver nanoparticles by a polyhydroxyalkanoate obtained from mixed bacterial culture

J.L. Castro-Mayorga<sup>a</sup>, A. Martínez-Abad<sup>a</sup>, M.J. Fabra<sup>a</sup>, Catarina Olivera<sup>b</sup>, M. Reis<sup>b</sup>, J.M. Lagarón<sup>a,\*</sup>

<sup>a</sup> Novel Materials and Nanotechnology Laboratory, Institute of Agrochemistry and Food Technology (IATA), CSIC, 46980 Valencia, Spain  
<sup>b</sup> REQUIMTE/CQFB, Chemistry Department, FCT/Universidade Nova de Lisboa, 2829-516 Caparica, Portugal



### ARTICLE INFO

**Article history:**  
 Received 10 March 2014  
 Received in revised form 6 June 2014  
 Accepted 23 June 2014  
 Available online 18 July 2014

**Keywords:**  
 Polyhydroxyalkanoates  
 Silver nanoparticles  
 Antimicrobial properties

### ABSTRACT

The incorporation of antimicrobials into polymer matrices is a promising technology in the food packaging and biomedical areas. Among the most widely used antimicrobials, silver nanoparticles (AgNPs) have emerged as one of the most researched technologies to prevent microbial outbreaks. However, it is known that AgNPs are rather unstable and present patterns of agglomeration that might limit their application. In this work, AgNPs were produced by chemical reduction in suspensions of an unpurified poly(3-hydroxybutyrate-co-3-hydroxyvalerate) (PHBV) which was previously obtained from a mixed culture fermentation using a synthetic medium mimicking fermented cheese whey. The synthesis of AgNPs was carried out within the unpurified PHBV suspension (*in situ*) and by physical mixing (*mix*). The stability of crystalline and spherical nanoparticles (7 ± 3 nm) obtained *in situ* was found to be stable during at least 40 days. The results suggest that the unpurified PHBV appears to be a very efficient capping agent, preventing agglomeration and, thereby, stabilizing successfully the silver nanoparticles. The *in situ* obtained AgNP-PHBV materials were also found to exhibit a strong antibacterial activity against *Salmonella enterica* at low concentration (0.1–1 ppm).

© 2014 Elsevier B.V. All rights reserved.

### 1. Introduction

Polyhydroxyalkanoates (PHA's) are a family of naturally occurring storage biopolyesters synthesized by more than 300 species of Gram-positive and Gram-negative bacteria [1]. Among the various biodegradable polymers, PHA's provide a good alternative to fossil-fuel based plastics as they possess thermoplastic properties similar to conventional polyolefins, such as polypropylene, with the advantage of being 100% biodegradable and compostable and being produced from renewable resources [2–5]. Production of PHA's usually involves fermentation, isolation and purification processes, which imply higher production costs as compared to polyolefins. Therefore, much efforts and improvements have been developed to reduce the costs of the fermentation and downstream processes [4,6]. As an example, the use of open mixed cultures avoids the need for sterility in the reactor and makes easier the use of low cost agricultural or industrial waste feedstock in the production of PHA's [4,7]. Guriëff and Lant [8] performed a lifecycle assessment

and financial analysis and proved that PHA production by mixed cultures from renewable resources is financially and environmentally attractive. Moreover, it is a greener alternative to the pure culture processes since less CO<sub>2</sub> is produced [8].

The good biocompatibility and slow hydrolytic degradation of PHA's have prompted their implementation in packaging as well as in medical applications [9]. In the areas of food and cosmetic packaging, PHA's are already commercialized as cosmetic containers, shampoo bottles, covers, milk cartons and films, moisture barriers in nappies and sanitary towels, pens, and combs, among others (reviewed by [10]). More recently, attention has been also focused on the medical applications of PHA's, such as in bone plates, surgical sutures and blood vessel replacements [5,11], or as biodegradable carriers for long-term dosage of drugs, medicines, hormones, insecticides and herbicides [5,12].

In this sense, the incorporation of antimicrobial substances into PHA's might allow the production of biodegradable materials which could be used for the targeted release of the antimicrobials in active food packaging, food contact surfaces or medical applications.

Silver nanoparticles (AgNPs) are highly effective against a wide spectrum of bacteria, fungi and viruses, possess anti-inflammatory properties and promote epithelisation and scarring [13–16]. Owing to the growing concern about resistance to antibiotics, the

\* Corresponding author at: IATA-CSIC, Avda. Agustín Escardino, 7, Paterna, 46980 Valencia, Spain. Tel.: +34 96 3900022; fax: +34 96 3636301.  
 E-mail address: [lagaron@iata.csic.es](mailto:lagaron@iata.csic.es) (J.M. Lagarón).

<http://dx.doi.org/10.1016/j.ijbiomac.2014.06.059>  
 0141-8130/© 2014 Elsevier B.V. All rights reserved.





Contents lists available at ScienceDirect

Innovative Food Science and Emerging Technologies

journal homepage: [www.elsevier.com/locate/ijfset](http://www.elsevier.com/locate/ijfset)

## Stabilized nanosilver based antimicrobial poly(3-hydroxybutyrate-co-3-hydroxyvalerate) nanocomposites of interest in active food packaging

J.L. Castro-Mayorga, M.J. Fabra, J.M. Lagaron\*

Novel Materials and Nanotechnology Group, Institute of Agrochemistry and Food Technology (IATA), CSIC, 46980, Valencia, Spain



### ARTICLE INFO

#### Article history:

Received 26 August 2015

Received in revised form 28 October 2015

Accepted 30 October 2015

Available online 12 November 2015

#### Keywords:

Polyhydroxyalkanoates

Silver nanoparticles

Antimicrobials

Active packaging

### ABSTRACT

Antimicrobial silver based nanocomposites of poly(3-hydroxybutyrate-co-3-hydroxyvalerate) were successfully synthesized and characterized. For the synthesis, a masterbatch of *in situ* stabilized silver nanoparticles (AgNPs) produced into a mixed microbial cultures based poly(3-hydroxybutyrate-co-18 mol% 3-hydroxyvalerate) (PHBV18) was used, which was diluted by melt compounding with a commercial poly(3-hydroxybutyrate-co-3 mol% 3-hydroxyvalerate) (PHBV3) material. The incorporated AgNPs (0.04 wt.%) led to a surprising oxygen permeability drop of ca. 56% compared to the neat polymer. The thermal stability and optical properties of the nanocomposites were not significantly modified as compared to the neat PHBV3. Moreover, the antimicrobial performance of the PHBVs-AgNPs films against two of the most common food borne pathogens, *Salmonella enterica* and *Listeria monocytogenes*, showed a strong and sustained (even after seven-months) antibacterial activity. This study provides an innovative route to generate fully renewable and biodegradable antimicrobial nanocomposites that could potentially be of interest in film and coating applications such as active food packaging.

**Industrial relevance:** As a response to the consumers for more safety foodstuffs and ecofriendly packaging materials, this work presents a novel methodology to develop antimicrobial packaging by using biodegradable materials obtained from industrial food by-products in combination of an industrially meaningful melt blending process. The methodology here applied allows the use of low doses of stabilized silver nanoparticles in the polymer matrix, without additives, which exhibits prolonged antimicrobial activity against food borne pathogens and enhanced oxygen barrier properties. These materials are of great interest in the development and design of biodegradable active food packaging materials and antibacterial food contact surfaces with the additional advantage that they can be easily scale-up.

© 2015 Elsevier Ltd. All rights reserved.

### 1. Introduction

With a continuous growth for more than 50 years and a worldwide production of more than 250 million tonnes per year, plastics are the base of many products typically used, being packaging the largest sector of application for the plastics industry (Association of Plastics Manufacturers). Most plastics are primarily synthesized from petroleum derived compounds. However, these finite petroleum reserves will progressively decline. The eventually growing gap between supply and demand as well as the greenhouse gas emissions, and the saturation of landfill sites with plastic waste has steered research toward the development of green polymeric materials.

Polyhydroxyalkanoates (PHA) have recently attracted much attention as an alternative to petroleum-based materials. PHA are polymers synthesized by a wide range of microorganisms as carbon storage material (Reddy, Ghai, Rashmi, & Kalia, 2003). Nowadays, PHA have still

economic shortcomings that limit their use. The major drawbacks of PHA production are the high cost of raw materials (mainly carbon source), low yield, low productivity and the high cost of the downstream process (Heinrich, Madkour, Al-Ghamdi, Shabbaj, & Steinbüchel, 2012; Patwardhan & Srivastava, 2008). To reduce cost production, researchers have targeted the synthesis of PHA through fermentation from by-products and wastes. In fact, low cost processes, such as the use of mixed microbial cultures, have recently been developed. Their use offers several advantages compared with the pure-cultures fermentation, as sterile conditions are not required and cheap or even free substrates, like industrial waste material or by-products, may be used (Gurieff & Lant, 2007).

One of the most extensively studied polymers from the PHA group is poly(3-hydroxybutyrate), PHB. However, PHB is partially crystalline with a high melting temperature, high degree of crystallinity and high rigidity. To overcome these aspects, the copolymer obtained with the insertion of 3-hydroxyvalerate (HV) units, known as poly(3-hydroxybutyrate-co-3-hydroxyvalerate), PHBV, is usually used to improve handling properties of PHB films. PHBV has greater flexibility and reduced melting temperature without reducing the thermal

\* Corresponding author. IATA-CSIC, Avda. Agustín Escardino, 7, 46980, Paterna, Valencia, Spain.

E-mail address: [lagaron@iata.csic.es](mailto:lagaron@iata.csic.es) (J.M. Lagaron).





Article

# On the Use of the Electrospinning Coating Technique to Produce Antimicrobial Polyhydroxyalkanoate Materials Containing In Situ-Stabilized Silver Nanoparticles

Jinneth Lorena Castro-Mayorga <sup>1</sup>, Maria Jose Fabra <sup>1</sup>, Luis Cabedo <sup>2</sup> and Jose Maria Lagaron <sup>1,\*</sup>

<sup>1</sup> Novel Materials and Nanotechnology Group, IATA-CSIC, 46980 Valencia, Spain; jincasma@iata.csic.es (J.L.C.-M.); mjfabra@iata.csic.es (M.J.F.)

<sup>2</sup> Polymers and Advanced Materials Group (PIMA), Universitat Jaume I, 12071 Castellón, Spain; lcabedo@uji.es

\* Correspondence: lagaron@iata.csic.es; Tel.: +34-963-900-022

Academic Editor: Mikael S. Hedenqvist

Received: 24 October 2016; Accepted: 15 December 2016; Published: 29 December 2016

**Abstract:** Electro-hydrodynamic processing, comprising electrospinning and electrospinning techniques, has emerged as a versatile technology to produce nanostructured fiber-based and particle-based materials. In this work, an antimicrobial active multilayer system comprising a commercial polyhydroxyalkanoate substrate (PHA) and an electrospun PHA coating containing in situ-stabilized silver nanoparticles (AgNPs) was successfully developed and characterized in terms of morphology, thermal, mechanical, and barrier properties. The obtained materials reduced the bacterial population of *Salmonella enterica* below the detection limits at very low silver loading of  $0.002 \pm 0.0005$  wt %. As a result, this study provides an innovative route to generate fully renewable and biodegradable materials that could prevent microbial outbreaks in food packages and food contact surfaces.

**Keywords:** electro-hydrodynamic processing; foodborne pathogens; metal nanoparticles; biopolyesters

## 1. Introduction

Electro-hydrodynamic processing comprising electrospinning and electrospinning techniques is a broadly used and efficient technology that uses electrical forces to produce ultrathin fibers and nanocapsules, respectively [1,2]. Electrospinning has recently gained much attention not only because of its versatility in processing a wide range of polymer and biopolymer materials, but also because of its ability to produce fiber diameters within the submicro and nano range that is otherwise not viable to achieve by using conventional-generating technologies. The intrinsic characteristics of electrospun fibers, like very high specific surface and porosity [3] and the suitability of the technique to encapsulate active substances within the fibers, have prompted their use in a wide range of applications [4–8]. With the expansion of this technology, several researchers have used electrospinning to improve physicochemical and functional properties of biopolymer based materials by means of a controlled release of active compounds or by enhancing the dispersion of nano-additives into the biopolymer matrices [9–11].

Of particular interest is the generation of fiber-based systems for antimicrobial food packaging and food contact surface applications given that the direct application of biocide compounds onto the food surface can be inefficient because of their rapid diffusion within the bulk of food [12]. In this way, the incorporation of antimicrobial fiber-base mats as coating of the packaging material, leading to antimicrobial films, could improve their activity in maintaining an optimal effect during the food





Contents lists available at ScienceDirect

LWT - Food Science and Technology

journal homepage: [www.elsevier.com/locate/lwt](http://www.elsevier.com/locate/lwt)

## Antiviral properties of silver nanoparticles against norovirus surrogates and their efficacy in coated polyhydroxyalkanoates systems



J.L. Castro-Mayorga<sup>a</sup>, W. Randazzo<sup>a, b</sup>, M.J. Fabra<sup>a</sup>, J.M. Lagaron<sup>a</sup>, R. Aznar<sup>a, b</sup>, G. Sánchez<sup>a, b, \*</sup>

<sup>a</sup> Food Safety and Preservation Department, Institute of Agrochemistry and Food Technology (IATA-CSIC), Avda. Agustín Escardino 7, 46980 Paterna, Valencia, Spain

<sup>b</sup> Microbiology and Ecology Department, University of Valencia, Av. Dr. Moliner, 50, 46100 Burjassot, Valencia, Spain

### ARTICLE INFO

#### Article history:

Received 26 July 2016

Received in revised form

20 January 2017

Accepted 23 January 2017

Available online 27 January 2017

#### Keywords:

Noroviruses

Silver nanoparticles

Active packaging

Polyhydroxyalkanoates

Electrospinning

### ABSTRACT

Silver nanoparticles (AgNP) have strong broad-spectrum antimicrobial activity and gained increased attention for the development of AgNP based products, including medical and food applications. Initially, the efficacy of AgNP and silver nitrate (AgNO<sub>3</sub>) was evaluated for inactivating norovirus surrogates, the feline calicivirus (FCV) and the murine norovirus (MNV). These norovirus surrogates were exposed to AgNO<sub>3</sub> and AgNP solutions for 24 h at 25 °C and then analyzed by cell-culture assays. Both AgNP and silver ions significantly decreased FCV and MNV infectivity in a dose-dependent manner between concentrations of 2.1 and 21 mg/L. Furthermore, poly (3-hydroxybutyrate-co-3-hydroxyvalerate) (PHBV) films were prepared by depositing a coating of thermally post-processed electrospun PHBV18/AgNP fiber mats over compression moulded PHBV3 films. After 24 h exposure at 37 °C and 100% RH, no infectious FCV were recovered when in contact with the AgNP films while MNV titers decreased by 0.86 log. The morphology of the PHBV18 and PHBV18/AgNP fibers studied by SEM showed smooth and continuous fibers in both cases and the EDAX analysis confirmed the homogeneously distribution of AgNP into the coating and onto the PHBV3/PHBV18 layer. This study showed, for the first time, the suitability of the PHBV18/AgNP electrospun coating for antiviral surfaces.

© 2017 Elsevier Ltd. All rights reserved.

### 1. Introduction

Human norovirus (family *Caliciviridae*) are reported as the leading causes of viral gastroenteritis in industrialized countries, and worldwide constituting a high public health concern. Norovirus gastroenteritis is self-limiting but extremely infectious with a low infectious dose (10–100 particles). This non-enveloped, single-stranded, positive-sense RNA virus is responsible for over 90% cases of non-bacterial and approximately half of all cases of gastroenteritis. Recently, the World Health Organization has estimated the global burden of foodborne diseases, reporting that infectious agents that cause diarrhoeal diseases accounted for the vast majority (550 million cases per year), in particular human norovirus (120 million cases per year) (WHO, 2015).

Moreover human norovirus is responsible for many outbreaks,

especially in closed environments e.g. health-care facilities and cruise ships, whereas the contribution of contaminated surfaces in the spread of infection has a key role (Lopman et al., 2012). To effectively prevent norovirus outbreaks, the scientific community has been working to develop strategies for treating and preventing norovirus infection. The use of antimicrobial surfaces in food, clinical and community environments may help to reduce the spread of norovirus infection. Among them, the use of silver has emerged as a very efficient technology to prevent microbial proliferation on medical and food-contact surfaces (Kuorwel, Cran, Orbell, Buddhadasa, & Bigger, 2015) and, more concretely, silver nanoparticles (AgNP) have received considerable attention due to their attractive physico-chemical and antimicrobial properties (Moritz & Geszke-Moritz, 2013; Rai, Yadav, & Gade, 2009) such as the high surface-to-volume ratio, nanosize diameter and enhanced surface reactivity, making them able to inactivate microorganisms more effectively than their micro- or macro-scale counterparts. For instance, Castro-Mayorga and collaborators (Castro-Mayorga, Fabra, & Lagaron, 2016a) have demonstrated that poly (3-

\* Corresponding author. Institute of Agrochemistry and Food Technology (IATA-CSIC), Avda. Agustín Escardino, 7, Paterna, Valencia, Spain.  
E-mail address: [gloriasanchez@iata.csic.es](mailto:gloriasanchez@iata.csic.es) (G. Sánchez).

<http://dx.doi.org/10.1016/j.lwt.2017.01.065>

0023-6438/© 2017 Elsevier Ltd. All rights reserved.





Contents lists available at ScienceDirect

Food and Bioproducts Processing

journal homepage: [www.elsevier.com/locate/fbp](http://www.elsevier.com/locate/fbp)

## The impact of zinc oxide particle morphology as an antimicrobial and when incorporated in poly(3-hydroxybutyrate-co-3-hydroxyvalerate) films for food packaging and food contact surfaces applications

J.L. Castro-Mayorga<sup>a</sup>, M.J. Fabra<sup>a</sup>, A.M. Pourrahimi<sup>b</sup>, R.T. Olsson<sup>b</sup>,  
J.M. Lagaron<sup>a,\*</sup>

<sup>a</sup> Novel Materials and Nanotechnology Group, Institute of Agrochemistry and Food Technology (IATA), CSIC, 46980 Valencia, Spain

<sup>b</sup> KTH Royal Institute of Technology, School of Chemical Science and Engineering, Fibre and Polymer Technology, SE-100 44 Stockholm, Sweden

### ARTICLE INFO

#### Article history:

Received 11 January 2016

Received in revised form 12 October 2016

2016

Accepted 16 October 2016

Available online 24 October 2016

#### Keywords:

ZnO

PHBV

Antimicrobial activity

Electrospinning

Active Packaging

Food contact surfaces

### ABSTRACT

In this work, zinc oxide (ZnO) micron and nano sized-particles with different morphologies were synthesized by aqueous precipitation and evaluated as antimicrobial agents against foodborne pathogens. The most effective bactericide system was selected to prepare active poly(3-hydroxybutyrate-co-3-hydroxyvalerate) (PHBV) films by three different methods (i) direct melt-mixing, (ii) melt-mixing of preincorporated ZnO into PHBV18 (18 mol% valerate content) fiber mats made by electrospinning, and, (iii) as a coating of the annealed electrospun PHBV18/ZnO fiber mats over compression molded PHBV. Results showed that ZnO successfully improved the thermal stability of the PHBV18, being the preincorporation method the most efficient in mitigating the negative impact that the PHBV18 had on the thermal stability, barrier and optical properties of the PHBV films. Similar behavior was found for the coating structure although this film showed effective and prolonged antibacterial activity against *Listeria monocytogenes*. This study highlights the suitability of the PHBV/ZnO nanostructures for active food packaging and food contact surface applications.

© 2016 Institution of Chemical Engineers. Published by Elsevier B.V. All rights reserved.

### 1. Introduction

Over the last decades, polymer nanocomposites have become key materials in many nanotechnology applications. In this area, polymers reinforced by metal-based nanoparticles are advanced functional materials which have gained considerable attention specifically for the development of active materials containing metal-based nanoparticles. Active materials of particular interest in for instance food packaging involve components that release or absorb substances, from or into the packaged food, or the surrounding environment,

thus extending the shelf life of foods (e.g. inhibiting the growth of pathogenic and spoilage microorganism), preventing and/or indicating the migration of contaminants while maintaining or even improving their nutritional quality and ensuring food safety (Ozdemir and Floros, 2004). Recently, the interest in antimicrobial packaging has been increased considerably owing to their ability to eliminate food borne pathogens and to reduce the risks of various food poisoning outbreaks and illnesses (Han, 2000). Inorganic agents, such as TiO<sub>2</sub>, ZnO, MgO and CaO (Huang et al., 2000; Sawai et al., 1998, 2000, 2001) in the form of bulk materials or nanoparticles are being applied in antimicrobial applica-

\* Corresponding author at: IATA-CSIC, Avda. Agustín Escardino, 7, Paterna 46980, Valencia, Spain.

E-mail address: [lagaron@iata.csic.es](mailto:lagaron@iata.csic.es) (J.M. Lagaron).

<http://dx.doi.org/10.1016/j.fbp.2016.10.007>

0960-3085/© 2016 Institution of Chemical Engineers. Published by Elsevier B.V. All rights reserved.



## **ANNEX B**

---

---

### **ADDITIONAL WORKS**





Justificante de presentación electrónica de solicitud de patente

Este documento es un justificante de que se ha recibido una solicitud española de patente por vía electrónica, utilizando la conexión segura de la O.E.P.M. Asimismo, se le ha asignado de forma automática un número de solicitud y una fecha de recepción, conforme al artículo 14.3 del Reglamento para la ejecución de la Ley 11/1986, de 20 de marzo, de Patentes. La fecha de presentación de la solicitud de acuerdo con el art. 22 de la Ley de Patentes, le será comunicada posteriormente.

Número de solicitud:	P201630829	
Fecha de recepción:	20 junio 2016, 11:46 (CEST)	
Oficina receptora:	OEPM Madrid	
Su referencia:	2016-0025 P	
Solicitante:	JINNETH LORENA CASTRO MAYORGA	
Número de solicitantes:	5	
País:	ES	
Título:	PROCEDIMIENTO PARA LA OBTENCIÓN DE BIOPOLÍMEROS ANTIMICROBIANOS QUE COMPRENDEN POLIHIDROXIALCANOATOS Y NANOPARTÍCULAS METÁLICAS	
Documentos enviados:	Descripción.pdf (24 p.) Reivindicaciones.pdf (3 p.) Resumen.pdf (1 p.) Dibujos.pdf (3 p.) OLF-ARCHIVE.zip POWATT.pdf (2 p.)	package-data.xml es-request.xml application-body.xml es-fee-sheet.xml feesheet.pdf request.pdf
Enviados por:	CN=ENTIDAD UNGRIA PATENTES Y MARCAS SA - CIF A28378578 - NOMBRE UNGRIA LOPEZ JAVIER - NIF 05211582N,OU=703015232,OU=FNMT Clase 2 CA,O=FNMT,C=ES	
Fecha y hora de recepción:	20 junio 2016, 11:46 (CEST)	
Codificación del envío:	C6:E6:F2:F3:02:6B:3E:94:25:A3:02:0D:C3:43:E5:3F:60:B7:5E:BF	



# Silver-Based Antibacterial and Virucide Biopolymers: Usage and Potential in Antimicrobial Packaging

J.L. Castro-Mayorga\*, A. Martínez-Abad\*, M.F. Fabra\*, J.M. Lagarón\*, M.J. Ochoa<sup>†</sup> and G. Sánchez<sup>†</sup>

*\*Institute of Agrochemistry and Food Technology (IATA-CSIC), Valencia, Spain, †University of Valencia, Valencia, Spain*

## 32.1 BIOPOLYMERS IN FOOD PACKAGING

Plastics are a family of materials whose use has been increased in many applications since the late 1930s. The most rapidly adopting area of applications for plastics has been packaging. To the extent that nowadays, plastic packaging is the largest application for plastics (about 40% in Europe, [www.plasticseurope.org](http://www.plasticseurope.org)), and within the packaging niche, food packaging amounts to the largest plastics-demanding application.

More recently there has been a current trend to substitute petroleum-based materials by renewable biobased-derived plastics, which will reduce the oil dependence, facilitate the afterlife of the packaging (by composting, for instance), and reduce the carbon footprint of the food packaging industry. Regarding biodegradable (renewable and non-renewable) materials, three families are usually considered: (1) polymers directly extracted from biomass, such as the polysaccharides (chitosan, starch, cellulose, etc.) and proteins (caseinates, soy protein, whey protein, gluten, zein, etc.); (2) synthetic polymers from oilbased or biomass-derived monomers such as polycaprolactones, polyvinyl-alcohol, ethylene-vinyl alcohol copolymers and polylactic acid (PLA) (Arvanitoyannis et al., 1997; Haugaard et al., 2001; Petersen et al., 1999); (3) polymers produced by natural or genetically modified microorganisms such as polyhydroxyalkanoates (PHA) or bacterial cellulose (Fabra et al., 2013, 2014a,b; Martínez-Sanz et al., 2012; Plackett and Siro, 2011).

The bioplastics more commercially viable at the moment are some biodegradable polyesters, which can be processed by conventional processing equipment and are being used in several monolayers and multilayer applications already, particularly in the food packaging and biomedical fields. The most widely researched thermoplastic sustainable biopolymers for monolayer packaging applications are starch, PHA, and PLA. Of these, starch and PLA biopolymers are without a doubt the most interesting families of biodegradable materials, because they have become commercially available (by, for instance, companies such as Novamont and Natureworks), are produced on a large industrial scale, and present an interesting balance of properties. Of particular interest in food packaging is the case of PLA due to its excellent transparency and relatively good water resistance. The challenge for these specific biomaterials is to improve their properties so they perform (in terms of barrier and thermal properties) like polyethylene terephthalate. There are also other materials extracted from biomass resources, such as proteins (e.g., zein), polysaccharides (e.g., chitosan), and lipids (e.g., waxes), with excellent potential as gas and aroma barriers.

The main drawbacks of these families of materials are their inherently high rigidity, difficulty of processing in conventional equipment and, for proteins and polysaccharides, the very strong water sensitivity arising from their hydrophilic character, which leads to a strong plasticization, deteriorating the excellent oxygen barrier characteristic (in dry state) as relative humidity and water sorption in the material increase. This low water resistance of proteins and polysaccharides strongly handicaps their use in food packaging applications. From an application point of view, it is of great relevance to diminish the water sensitivity of proteins and polysaccharides, and to enhance the gas barrier properties and overall functionalities of thermoplastic biopolyesters to make them more adequate for food packaging applications.





## Use of Electrospinning to Develop Antimicrobial Biodegradable Multilayer Systems: Encapsulation of Cinnamaldehyde and Their Physicochemical Characterization

Miguel A. Cerqueira<sup>1,2</sup> · María José Fabra<sup>3</sup> · Jinneth Lorena Castro-Mayorga<sup>3</sup> · Ana I. Bourbon<sup>1</sup> · Lorenzo M. Pastrana<sup>2</sup> · António A. Vicente<sup>1</sup> · Jose M. Lagaron<sup>3</sup>

Received: 19 February 2016 / Accepted: 4 July 2016 / Published online: 15 July 2016  
© Springer Science+Business Media New York 2016

**Abstract** In this work, three active bio-based multilayer structures, using a polyhydroxybutyrate-co-valerate film with a valerate content of 8 % (PHBV8) as support, were developed. To this end, a zein interlayer with or without cinnamaldehyde (CNMA) was directly electrospun onto one side of the PHBV8 film and the following systems were developed: (1) without an outer layer; (2) using a PHBV8 film as outer layer; and (3) using an alginate-based film as outer layer. These multilayer structures were characterized in terms of water vapour and oxygen permeabilities, transparency, intermolecular arrangement and thermal properties. The antimicrobial activity of the active bio-based multilayer systems and the release of CNMA in a food simulant were also evaluated. Results showed that the presence of different outer layers reduced the transport properties and transparency of the multilayer films. The active bio-based multilayer systems showed antibacterial activity against *Listeria monocytogenes* being the multilayer structure prepared with CNMA and PHBV outer layers (PHBV + zein/CNMA + PHBV) the one that showed the greater antibacterial activity. The release of CNMA depended on the multilayer structures, where both Fick's and

Case II transport—polymer relaxation explained the release of CNMA from the multilayer systems.

Overall, the deposition of electrospun CNMA-loaded zein fibres on a PHBV8 layer is a promising methodology for the development of active bio-based multilayer systems, with a great potential for food packaging applications.

**Keywords** Biodegradable polymers · Electro-hydrodynamic processing · Electrospinning · Active packaging · Multilayers · Polyhydroxyalkanoates

### Introduction

Packaging materials based on bio-based and biodegradable materials have received great attention for the development of innovative packaging systems. Their biodegradability is considered to be a promising solution to environmental issues, but also their properties (e.g. solubility and transport properties) are considered unique when a controlled release of functional compounds is aimed at (Pinheiro et al. 2013; Souza et al. 2015). The development of active materials through the incorporation of antimicrobial and antioxidant compounds and their controlled release has attracted attention for several applications, such as active packaging and surface treatment of medical devices (Cerqueira et al. 2014; De Azeredo 2012; Kujawa et al. 2007; Tran et al. 2015).

Some of the drawbacks of bio-based and biodegradable active packaging materials are, according to the materials used, their hydrophilicity (i.e. polysaccharides and proteins), inadequate transport and thermal properties (i.e. polyhydroxyalkanoates—PHAs and poly(3-hydroxybutyrate—PHB)) (Bordes et al. 2009; Cerqueira et al. 2010), the influence of added functional compounds in film's properties (e.g. transport and mechanical properties) and the decrease of the functional activity of the active compounds during processing.

✉ Miguel A. Cerqueira  
miguelribeirocerqueira@gmail.com

✉ María José Fabra  
mjfabra@iata.csic.es

<sup>1</sup> Centre of Biological Engineering, University of Minho, Campus de Gualtar, 4710-057 Braga, Portugal

<sup>2</sup> INL—International Iberian Nanotechnology Laboratory, Av. Mestre José Veiga, 4715-330 Braga, Portugal

<sup>3</sup> Novel Materials and Nanotechnology Group, IATA-CSIC, Av. Agustín Escardino 7, 46980 Paterna (Valencia), Spain





## Efficacy of Cinnamaldehyde Against Enteric Viruses and Its Activity After Incorporation Into Biodegradable Multilayer Systems of Interest in Food Packaging

M. J. Fabra<sup>1</sup> · J. L. Castro-Mayorga<sup>1</sup> · W. Randazzo<sup>2,3</sup> · J. M. Lagarón<sup>1</sup> · A. López-Rubio<sup>1</sup> · R. Aznar<sup>3,4</sup> · G. Sánchez<sup>3,4</sup>

Received: 7 January 2016 / Accepted: 14 March 2016 / Published online: 23 March 2016  
© Springer Science+Business Media New York 2016

**Abstract** Cinnamaldehyde (CNMA), an organic compound that gives cinnamon its flavor and odor, was investigated for its virucidal activity on norovirus surrogates, murine norovirus (MNV) and feline calicivirus (FCV), and hepatitis A virus (HAV). Initially, different concentrations of CNMA (0.1, 0.5 and 1 %) were individually mixed with each virus at titers of ca.  $6\text{--}7 \log_{10}$  TCID<sub>50</sub>/ml and incubated 2 h at 4 and 37 °C. CNMA was effective in reducing the titers of norovirus surrogates in a dose-dependent manner after 2 h at 37 °C, while HAV titers were reduced by 1  $\log_{10}$  after treatment with 1 % of CNMA. When incubation time was extended, HAV titers were reduced by 3.4 and 2.7  $\log_{10}$  after overnight incubation at 37 °C with 1 and 0.5 % of CNMA, respectively. Moreover, this paper analyzed, for the first time, the antiviral activity of adding an active electrospun interlayer based on zein and CNMA to a polyhydroxybutyrate packaging material (PHB) in a multilayer form. Biodegradable multilayer systems prepared with 2.60 mg/cm<sup>2</sup> (~9.7 %) of CNMA completely inactivated FCV according to ISO 22196:2011, while MNV titers were

reduced by 2.75  $\log_{10}$ . When the developed multilayer films were evaluated after one month of preparation or at 25 °C, the antiviral activity was reduced as compared to freshly prepared multilayer films evaluated at 37 °C. The results show the excellent potential of this system for food contact applications as well as for active packaging technologies in order to maintain or extend food quality and safety.

**Keywords** Enteric viruses · Cinnamaldehyde · Active packaging · Multilayer structures

### Introduction

Enteric viruses are viruses that are primarily transmitted by the fecal–oral route, either by person-to-person contact or by ingestion of contaminated food or water. For most food products, handling is often the source of contamination, while shellfish is most commonly contaminated by fecally polluted water in the harvesting area.

Moreover, enteric viruses, in particular human norovirus (NoV), are the leading causes of foodborne illnesses in industrialized countries (Anonymous 2013; EFSA and ECDC 2015), while hepatitis A virus (HAV) has recently been considered as a re-emerging foodborne public health threat in Europe due to the number of foodborne outbreaks associated to imported foods (Sprenger 2014).

Cinnamaldehyde (CNMA) is the major component in cassia and cinnamon bark oils. CNMA is Generally Recognized As Safe (GRAS) by the Flavoring Extract Manufacturers' Association and is approved for food use (21 CFR 182.60) by the Food and Drug Administration (FDA) to impart a cinnamon flavor in numerous foods.

Furthermore, CNMA is known to have anti-inflammatory (Youn et al. 2008), antioxidant, and antimicrobial

✉ G. Sánchez  
gloriasanchez@iata.csic.es

<sup>1</sup> Food Preservation and Food Quality Department, Institute of Agrochemistry and Food Technology (IATA-CSIC), Avda. Agustín Escardino 7, 46980 Paterna, Valencia, Spain

<sup>2</sup> Department of Agricultural and Forest Science, University of Palermo, Palermo, Italy

<sup>3</sup> Biotechnology Department, IATA-CSIC, Avda. Agustín Escardino 7, 46980 Paterna, Valencia, Spain

<sup>4</sup> Microbiology and Ecology Department, University of Valencia, Avda. Dr. Moliner, 50, 46100 Burjassot, Valencia, Spain





Contents lists available at ScienceDirect

## Trends in Food Science &amp; Technology

journal homepage: <http://www.journals.elsevier.com/trends-in-food-science-and-technology>

## Review

## High throughput electro-hydrodynamic processing in food encapsulation and food packaging applications: Viewpoint

Y. Echegoyen<sup>a, b</sup>, M.J. Fabra<sup>a</sup>, J.L. Castro-Mayorga<sup>a</sup>, A. Cherpinski<sup>a</sup>, J.M. Lagaron<sup>a, \*</sup><sup>a</sup> Novel Materials and Nanotechnology Group, Institute of Agrochemistry and Food Technology (IATA), CSIC, 46980, Valencia, Spain<sup>b</sup> Science Education Department, Facultat de Magisteri, Universitat de València, 46022, Valencia, Spain

## ARTICLE INFO

## Article history:

Received 19 April 2016

Accepted 28 October 2016

Available online 8 November 2016

## Keywords:

Electrospinning

Nanostructured layers

Nanoencapsulation

Barrier biopackaging

Active surfaces

Oxygen scavengers

Antimicrobial packaging

## ABSTRACT

Looking genuinely at nature, nanofibers often serve as a basic platform where either organic or inorganic components are built upon. The fiber structure exhibits, from a structural point of view, the intrinsic ability to mechanically reinforce materials but also the less well-known property of enhancing the barrier performance of polymer matrices when applied smartly. To reproduce and tailor this extraordinary nature's design, a reliable technology that is able to fabricate fiber nanostructures from a variety of materials with size and size distribution control and composition flexibility is highly desirable. In addition, if this technology could allow nanofiber shortening to achieve nanodrop size materials, then this technology could also be used to obtain powders for encapsulation purposes. The electrohydrodynamic processing, a voltage-driven technology, comprising electrospinning and electro-spraying to dry and conform materials, is such unique technology. Up until recently this processing tech largely remained to a laboratory scale, however, recent developments in instrumentation and process aid design have allowed this process to be scaled to achieve the production volumes required in certain industrial commodity applications such as fortified foods and active packaging. The current overview highlights some recent advances carried out by electro-hydrodynamic processing in these food-related fields.

© 2016 Elsevier Ltd. All rights reserved.

## 1. Introduction

Electro-hydrodynamic processing (EHDP) is a cost-effective technique that uses a uniform electro-hydrodynamic force to break up the liquids into fine jets. The atomiser nozzle, usually made in the form of metal capillary, is biased by a high voltage. The shear stress on the liquid surface, due to the established electric field, causes elongation of a jet producing fibers or droplets, whose size and morphology can be adjusted by changing the process parameters. There are two main processing techniques in the electro-hydrodynamic processing: electrospinning and electro-spraying. Electrospinning is a process that produces continuous polymer fibers with diameters generally in the submicrometer range through the action of an external high-voltage electric field imposed on a polymer solution or melt. The electrospun nanostructures morphology is affected by the solution properties (mainly by the

viscosity, surface tension and conductivity of the polymer solution) and by the process (Doshi & Reneker, 1995).

For certain materials, capsules in the nanoscale range can be obtained by adjusting the solution properties and the process parameters (e.g. increasing the tip-to-collector distance and/or lowering the polymer concentration). The term electro-spraying or electro-hydrodynamic atomization (EHDA) is applied in those cases where non-continuous structures are obtained (Chen, Pui, & Kaufman, 1995; Lagaron, López-Rubio, Fabra, & Pérez-Masiá, 2014; Yurteri, Hartman, & Marijnissen, 2010). In both cases the basic setup consists of three components: a high-voltage power supply, a spinneret (a metallic needle) and a collector surface (a single piece of conductive substrate).

Food packaging is one of the fields where the development of functional films can provide an added value to the final product. Recently, much research has been focused in the development of water and/or oxygen barriers that provide the package with enhanced properties, thus increasing the food shelf life. Micro- and nanostructured layers including nanocomposites have demonstrated a great potential to improve those properties. EHDP is an efficient technique to develop nanostructured surfaces and

\* Corresponding author. IATA-CSIC, Avda, Agustín Escardino, 7, 46980, Paterna, Valencia, Spain.

E-mail address: [lagaron@iata.csic.es](mailto:lagaron@iata.csic.es) (J.M. Lagaron).

<http://dx.doi.org/10.1016/j.tifs.2016.10.019>

0924-2244/© 2016 Elsevier Ltd. All rights reserved.





Contents lists available at ScienceDirect

## Trends in Food Science &amp; Technology

journal homepage: <http://www.journals.elsevier.com/trends-in-food-science-and-technology>

## Review

## High throughput electro-hydrodynamic processing in food encapsulation and food packaging applications: Viewpoint

Y. Echegoyen<sup>a, b</sup>, M.J. Fabra<sup>a</sup>, J.L. Castro-Mayorga<sup>a</sup>, A. Cherpinski<sup>a</sup>, J.M. Lagaron<sup>a, \*</sup><sup>a</sup> Novel Materials and Nanotechnology Group, Institute of Agrochemistry and Food Technology (IATA), CSIC, 46980, Valencia, Spain<sup>b</sup> Science Education Department, Facultad de Magisteri, Universitat de València, 46022, Valencia, Spain

## ARTICLE INFO

## Article history:

Received 19 April 2016

Accepted 28 October 2016

Available online 8 November 2016

## Keywords:

Electrospinning

Nanostructured layers

Nanoencapsulation

Barrier biopackaging

Active surfaces

Oxygen scavengers

Antimicrobial packaging

## ABSTRACT

Looking genuinely at nature, nanofibers often serve as a basic platform where either organic or inorganic components are built upon. The fiber structure exhibits, from a structural point of view, the intrinsic ability to mechanically reinforce materials but also the less well-known property of enhancing the barrier performance of polymer matrices when applied smartly. To reproduce and tailor this extraordinary nature's design, a reliable technology that is able to fabricate fiber nanostructures from a variety of materials with size and size distribution control and composition flexibility is highly desirable. In addition, if this technology could allow nanofiber shortening to achieve nanodrop size materials, then this technology could also be used to obtain powders for encapsulation purposes. The electrohydrodynamic processing, a voltage-driven technology, comprising electrospinning and electro-spraying to dry and conform materials, is such unique technology. Up until recently this processing tech largely remained to a laboratory scale, however, recent developments in instrumentation and process aid design have allowed this process to be scaled to achieve the production volumes required in certain industrial commodity applications such as fortified foods and active packaging. The current overview highlights some recent advances carried out by electro-hydrodynamic processing in these food-related fields.

© 2016 Elsevier Ltd. All rights reserved.

## 1. Introduction

Electro-hydrodynamic processing (EHDP) is a cost-effective technique that uses a uniform electro-hydrodynamic force to break up the liquids into fine jets. The atomiser nozzle, usually made in the form of metal capillary, is biased by a high voltage. The shear stress on the liquid surface, due to the established electric field, causes elongation of a jet producing fibers or droplets, whose size and morphology can be adjusted by changing the process parameters. There are two main processing techniques in the electro-hydrodynamic processing: electrospinning and electro-spraying. Electrospinning is a process that produces continuous polymer fibers with diameters generally in the submicrometer range through the action of an external high-voltage electric field imposed on a polymer solution or melt. The electrospun nanostructures morphology is affected by the solution properties (mainly by the

viscosity, surface tension and conductivity of the polymer solution) and by the process (Doshi & Reneker, 1995).

For certain materials, capsules in the nanoscale range can be obtained by adjusting the solution properties and the process parameters (e.g. increasing the tip-to-collector distance and/or lowering the polymer concentration). The term electro-spraying or electro-hydrodynamic atomization (EHDA) is applied to those cases where non-continuous structures are obtained (Chen, Pui, & Kaufman, 1995; Lagaron, López-Rubio, Fabra, & Pérez-Masiá, 2014; Yurteri, Hartman, & Marijnissen, 2010). In both cases the basic setup consists of three components: a high-voltage power supply, a spinneret (a metallic needle) and a collector surface (a single piece of conductive substrate).

Food packaging is one of the fields where the development of functional films can provide an added value to the final product. Recently, much research has been focused in the development of water and/or oxygen barriers that provide the package with enhanced properties, thus increasing the food shelf life. Micro- and nanostructured layers including nanocomposites have demonstrated a great potential to improve those properties. EHDP is an efficient technique to develop nanostructured surfaces and

\* Corresponding author. IATA-CSIC, Avda. Agustín Escardino, 7, 46980, Paterna, Valencia, Spain.

E-mail address: [lagaron@iata.csic.es](mailto:lagaron@iata.csic.es) (J.M. Lagaron).

<http://dx.doi.org/10.1016/j.tifs.2016.10.019>

0924-2244/© 2016 Elsevier Ltd. All rights reserved.







